Table of Content

APPLICATION FIELDS OF NMR SPECTROSCOPY

High-resolution NMR spectroscopy

Analytics
- "small" molecules
  - determination of the covalent structure
  - determination of the purity

Elucidation of the 3D structure
- "small" molecules
  - determination of the stereochemistry: cis,trans isomerism,
  - determination of optical purity
- Biopolymers up to about 20-30 kDa
  - determination of the 3D solution structure *provided the primary sequence is known!*
  - investigation of the interaction of molecules (complexes)
  - investigation of the dynamics of proteins
    - ^{1}H, ^{13}C or ^{15}N relaxation measurements
    - ^{1}H,^{1}H oder ^{1}H,^{15}N NOE measurements

Determination of the kinetics of reactions

Solid-state NMR spectroscopy

insoluble compounds (synthetic polymers)
very large compounds (requires specific labels)
determination of the structure in the solid-state (vs. liquid-state)
determination of the dynamics in the solid-state

Imaging techniques

spin tomography

"In vivo" NMR spectroscopy

distribution of metabolites in the body

1. THE PHYSICAL BASIS OF THE NMR EXPERIMENT

Imagine a charge travelling circularily about an axis. This is similar to a current that flows through a conducting loop:

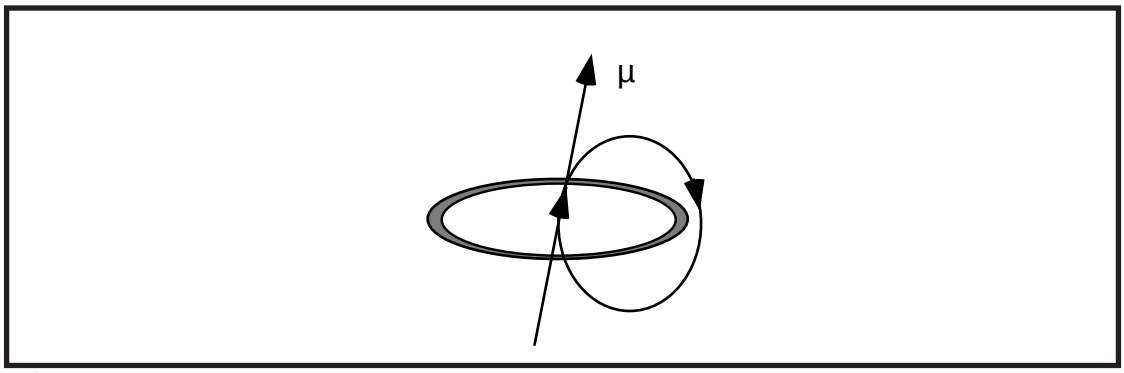

FIGURE 1.

Such a circular current builds up a magnetic moment μ whose direction is perpendicular to the plane of the conducting loop. The faster the charge travels the stronger is the induced magnetic field. In other words, a magnetic dipole has been created.

Such dipoles, when placed into a magnetic field, are expected to align with the direction of the magnetic field. In the following we will look at a mechanical equivalent represented by a compass needle that aligns within the gravitational field:

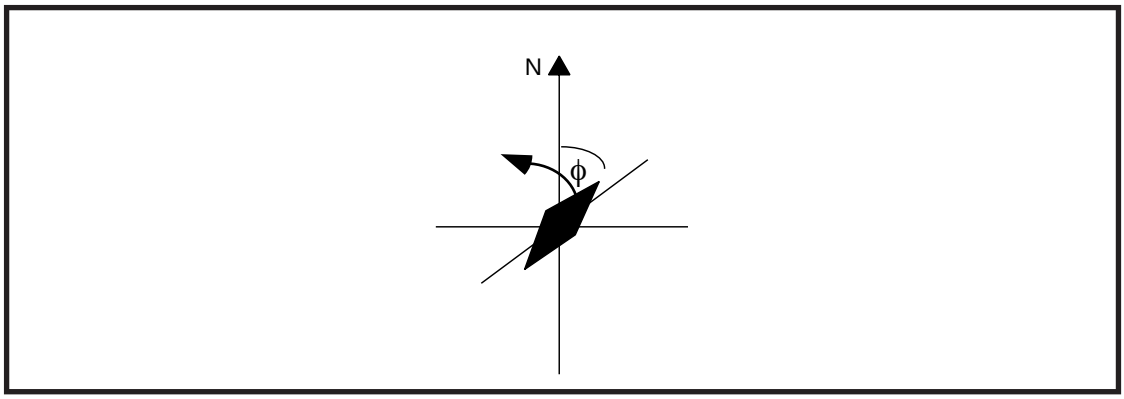

FIGURE 2.

When such a compass needle is turned away from the north-pole pointing direction to make an angle ϕ a force acts on the needle to bring it back. For the case of a dipole moment that has been created by a rotating charge this force is proportional to the strength of the field (**B**) and to the charge (**m**).

The *torque* that acts to rotate the needle may be described as

$$\mathbf{T} = \frac{\partial \mathbf{J}}{\partial t} = \mathbf{r} \times \mathbf{F}$$

in which **J** is defined as the *angular momentum* which is the equivalent for rota-

tional movements of the linear momentum.

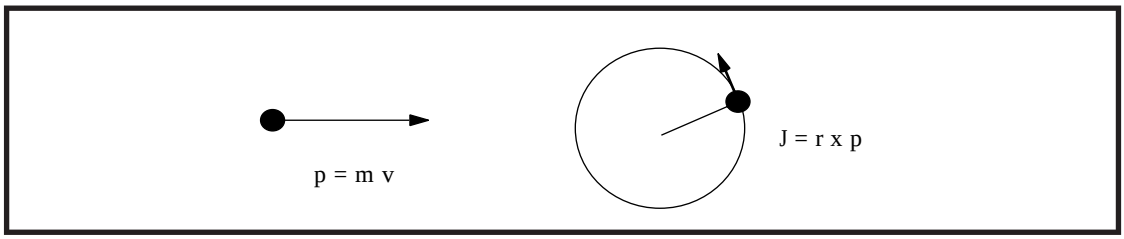

FIGURE 3. Left: linear momentum. Right: angular momentum

Excurse: Corresponding parameter for translational and rotational movements

	PureTranslation (fixed direction)	*Pure Rotation (fixed axis)*
Position	x	θ
Velocity	v = dx / dt	ω =dθ / dt
Acceleration	a = dv / dt	α = dω / dt
Translational (Rot.) Inertia	m	I
Force (Torque)	**F**	**T** = **r** x **F**
Momentum	**p** = m**v**	**J** = **r** x **p**
Work	W = Int **F** dx	W = Int **T** dθ
Kinetic energy	K = 1 / 2 mv^2	K = 1/2 $I\omega^2$
Power	P = F v	P = T ω

Note that the direction of the momentum is tangential to the direction along which the particle moves. The torque is formed by the vector product between the radius and the momentum (see additional material) and is described by a vector which is perpendicular to both radius and momentum. In fact, it is the axis of rotation which is perpendicular to the plane. The corresponding potential energy is

$$E_{pot} = -\int_0^{\varphi} T d\varphi$$

In contrast to the behaviour of a compass needle the nuclear spin does not exactly align with the axis of the external field:

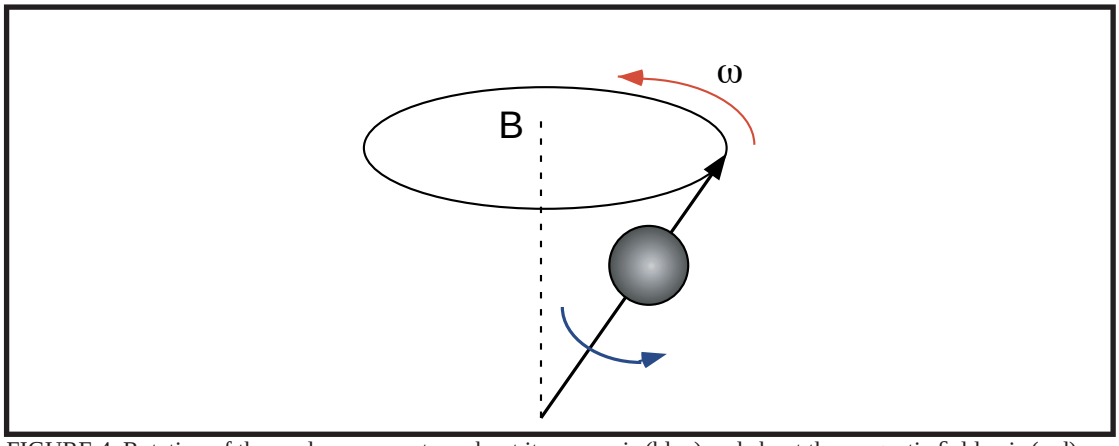

FIGURE 4. Rotation of the nuclear momentum about its own axis (blue) and about the magnetic field axis (red).

This is a consequence of its rotation about its own axis. This property is called spin. It rotates (spins) about its own axis (the blue arrow) and **precesses** about the axis of the magnetic field B (the red arrow). The frequency of the precession is proportional to the strength of the magnetic field:

$$\omega = \gamma \mathbf{B}$$

The proportionality constant is called the **gyromagnetic ratio**.

Excurse: *The movement of a classical gyroscope*

Imagine a wheel fixed to a shaft. When the this gyroscope is placed with the shaft perpendicular to the ground and released it will fall down (see Fig. below, left side). However, when the wheel *spins* about the axis of the shaft, the gyroscope precesses about the axis perpendicular to the ground with a frequency ω that is called the precession frequency (right side) and takes a well-defined angle ϕ with respect to the rotation axis:

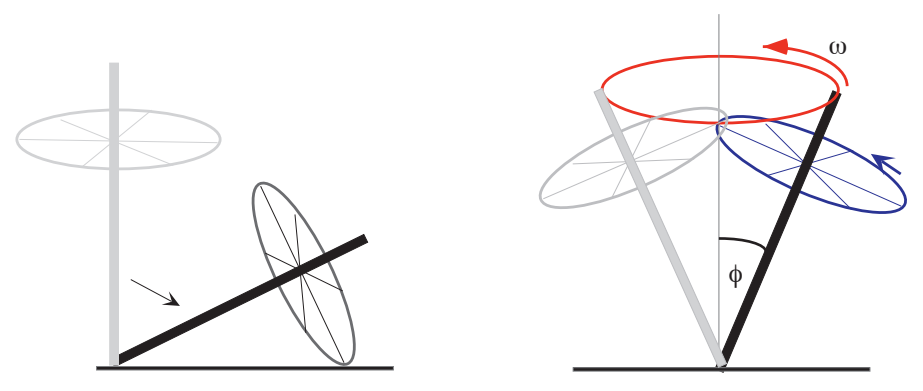

The frequency ω is expressed in terms of a angular velocity (see additional material). It is specific for the kind of nucleus and therefore has a different value for ^{1}H,^{13}C,^{19}F etc. The precession frequency

$$\omega_0 = \nu_o 2\pi$$

is called the **Lamor frequency**. In contrast to a compass needle which behaves "classically" in the way that it can adopt a continous band of energies depending only on the angle ϕ it makes with the field the corresponding angle ϕ of the nuclear dipole moment is quantitized. Hence, we will later introduce the quantum-mechanical treatment shortly.

Of course, we do not observe single molecules but look at an ensemble of molecules (usually a huge number of identical spins belonging to different molecules). The sum of the dipole moments of identical spins is called **magnetization**:

$$M = \sum_j \mu_i$$

1.1 The Bloch equations:

The Bloch's equations describe the fate of magnetization in a magnetic field. We have stated before that a force (a torque) acts on a dipole moment when it is placed inside a mgnetic field such that the dipole moment will be aligned with the direction of the static magnetic field. Mathematically this is decribed by forming the vector product between dipole moment and magnetic field (see add. material for the mathematics involved):

$$\mathbf{T} = \mathbf{M} \times \mathbf{B}$$

Considering that (see page 2)

$$\mathbf{T} = \frac{\partial \mathbf{J}}{\partial t}$$

and that

$$\mathbf{M} = \sum_i \mu_i = \sum_i \gamma \mathbf{J}_i$$

we find that

$$\frac{\partial \mathbf{M}}{\partial t} = \gamma \frac{\partial}{\partial t}\mathbf{J} = \gamma \mathbf{T} = \gamma(\mathbf{M} \times \mathbf{B})$$

which describes the time-evolution of the magnetization.

In the absence of an additional B_1 field the components of the field along the cartesian axes are:

$$B_x = 0$$
$$B_y = 0$$
$$B_z = B_o$$

which leads to the following set of coupled differential equations:

$$\frac{\partial}{\partial t}M_x(t) = \gamma M_y B_0 - M_x / T_2$$
$$\frac{\partial}{\partial t}M_y(t) = -\gamma M_x B_0 - M_y / T_2$$
$$\frac{\partial}{\partial t}M_z(t) = -(M_z - M_0) / T_1$$

In order to drive the system into the equilibrium state (no transverse coherence, relative population of the α/ β states according to the Boltzmann distribution) additional terms have been phenomenologically introduced such as M_x / T_2 for the M_x component.

The solutions to these equations are given by:

$$M_x(t) = [M_x(0)\cos\omega t - M_y(0)\sin\omega t]e^{(-t/T2)}$$
$$M_y(t) = [M_x(0)\sin\omega t + M_y(0)\cos\omega t]e^{(-t/T2)}$$
$$M_z(t) = M_{eq} + [M_z(0) - M_{eq}]e^{(-t/(T1))}$$

The first two equations describe mathematically a vector that precesses in a plane (see add. mat.) and hence give the correct description for what we will be looking at in a rather pictorial way in the following.

1.2 Quantum-mechanical treatment:

The dipole moment μ of the nucleus is described in quantum-mechanical terms as

$$\mu = \gamma J$$

Therein, J is the **spin angular momentum** and γ the gyromagnetic ratio of the spin. When looking at single spins we have to use a quantum-mechanical treatment. Therein, the z-component of the angular momentum J is **quantitized** and can only take **discrete values**

$$\langle J_z \rangle = m\frac{h}{2\pi}$$

where **m** is the magnetic quantum number. The latter can adopt values of m = -I, -I+1, …,0,...,I-1, I with I being the **spin quantum number**.

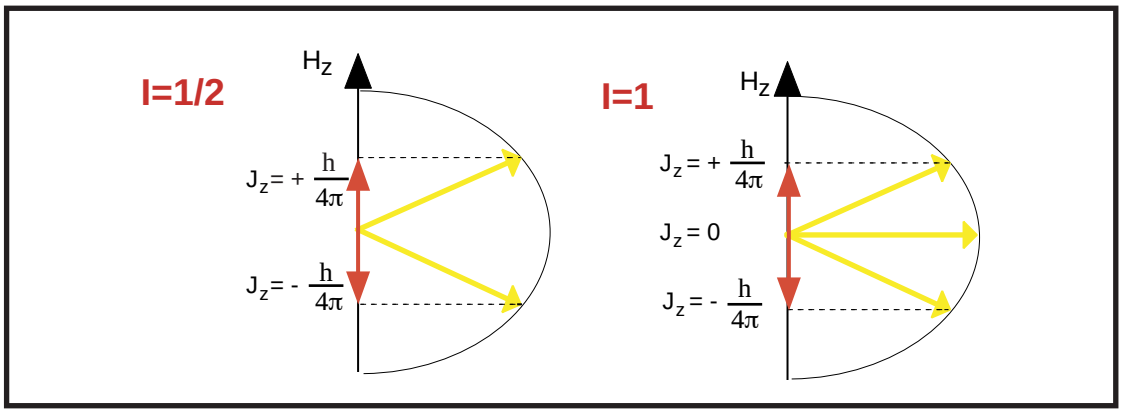

FIGURE 5. Vectorial representation of the z-component of the angular momentum for a spin I=1/2 (left) and spin I=1 (right) nucleus.

For I=1/2 nuclei, **m** can only be +1/2 or -1/2, giving rise to two distinct energy levels. For spins with I=1 nuclei three different values for J_z are allowed:

$$E_{pot} = \mu_z B = \gamma J B$$

The energy difference ΔE_{pot}, which corresponds to the two states with m=±1/2, is then

$$E_{pot} = \gamma \frac{h}{2\pi} B$$

(the quantum-mechanical selection rule states, that only transitions with Δm=±1 are allowed):

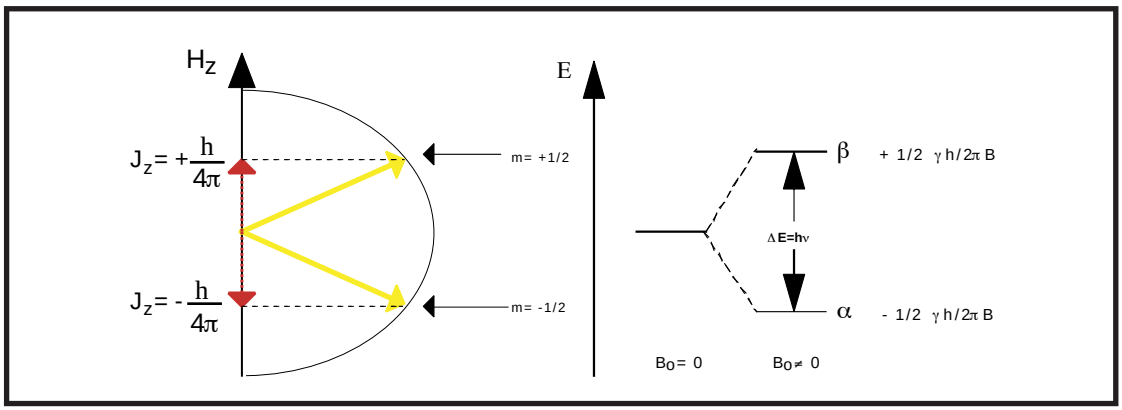

FIGURE 6. Energy levels of the α- and β- states of I=1/2 nuclei

1.3 The macroscopic view:

The NMR experiment measures a large **ensemble of spins** derived from a huge number of molecules. Therefore, we now look at the macroscopic bevaviour. The sum of the dipole moments of all nuclei is called **magnetization.** In equilibrium the spins of I=1/2 nuclei are either in the α- or β-state and precess about the axis of the static magnetic field. However, their phases are *not correlated*. For each vector pointing in one direction of the transverse plane a corresponding vector can be found which points into the *opposite* direction:

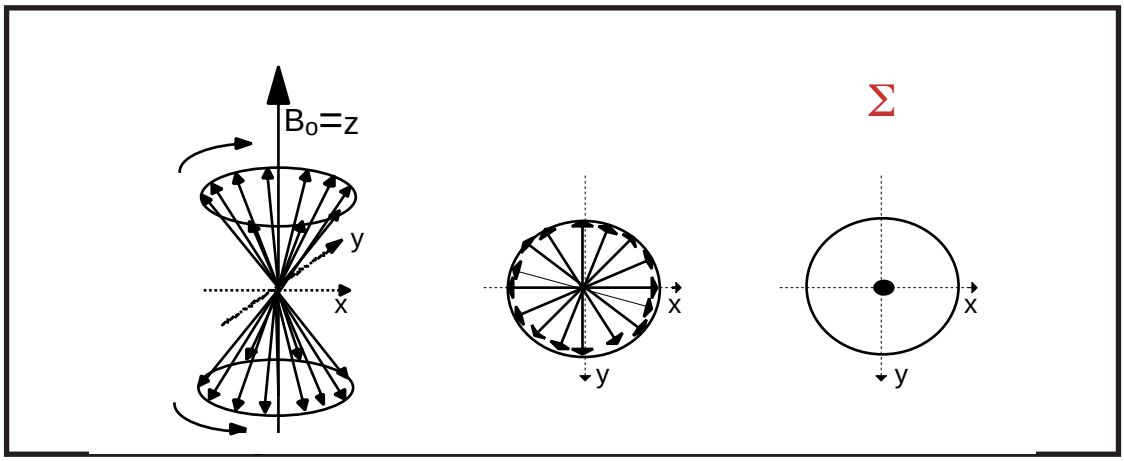

FIGURE 7. Equilibrium state with similarily populated α- and β-states (left), uncorrelated phases (middle) and no net phase coherence (right).

Therefore, the projection of all vectors onto the x,y plane (the vector sum of the transverse components) is vanishing provided that the phases of the spins are uncorrelated.

However, application of a radiofrequency (RF) field *perpendicular* to the magnetic field (e.g. along the x- or y-axis), the so-called B_1 field, creates a state in which the phases of the spins are *partially* correlated. This state is called **coherence.** When projecting the vectors onto the x,y plane the resulting transverse magnetization is non-vanishing giving rise to a signal in the detection coil. When the motions of spins are described in vector diagrams most frequently only the vector sum of the spins is shown in order to simplify it.

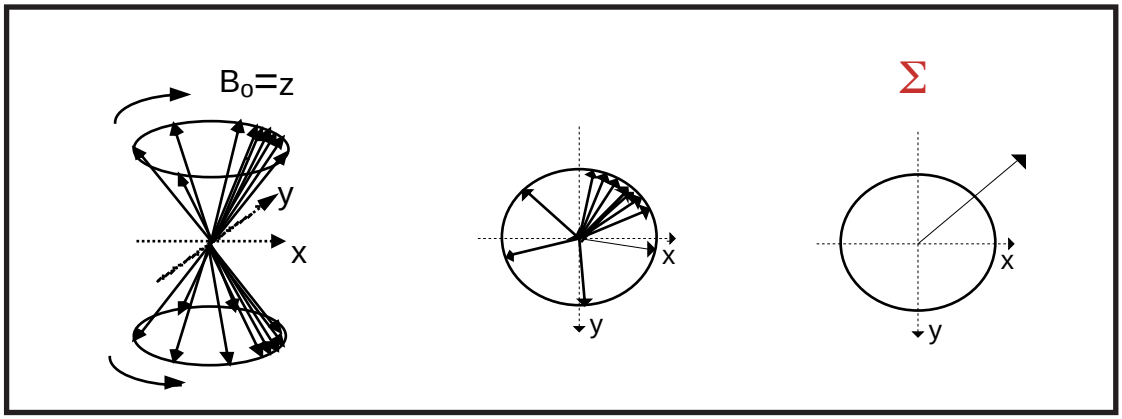

FIGURE 8. Coherent state of spins in α- or β(left) states and the projection onto the x,y plane(middle) and sum vector of the x,y component.

The magnitude and direction of the magnetization vector can be calculated by vectorial addition of the separate dipole moments.

This is shown in the following figure in which the vector sum of longitudinal (blue) and transverse (yellow) magnetization of uncorrelated spins which are only in the α-state (A) or in both states (B) is displayed as well as for correlated states (C and D): It is evident that only for correlated states transverse magnetization (magnetization in the x,y plane) is observed. Only transverse magnetization leads to a detectable signal in the receiver coil and hence contributes to the NMR signal. Therefore, only the vector sum of the transverse component is

shown to describe the relevant part of the spins:

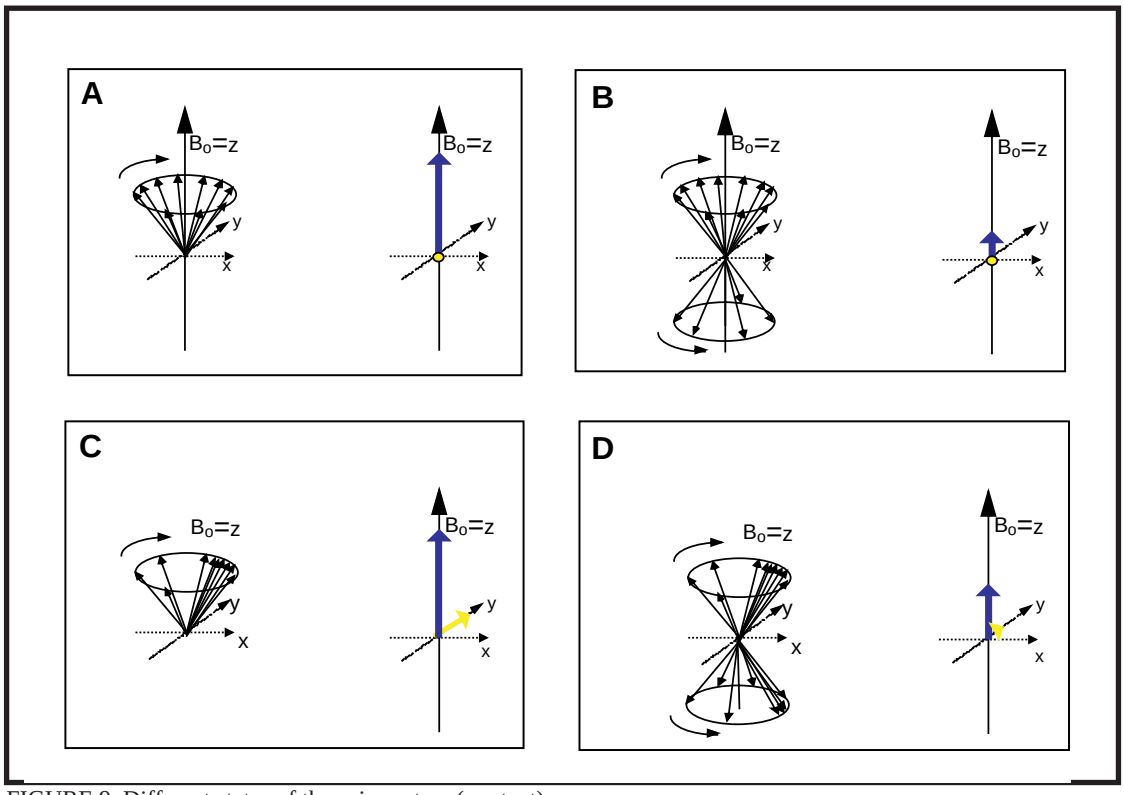

FIGURE 9. Different states of the spin system (see text).

The experiment setup of the spectrometer includes a radiofrequency coil, which delivers the orthogonal B_1 field. Simultaneously this coil serves to pick up the NMR signal. To understand how the magnetization that rotates in the transverse (x,y) plane induces the NMR signal it is convenient to look at the vector sum of the transverse components which present a magnetic field that rotates in space:

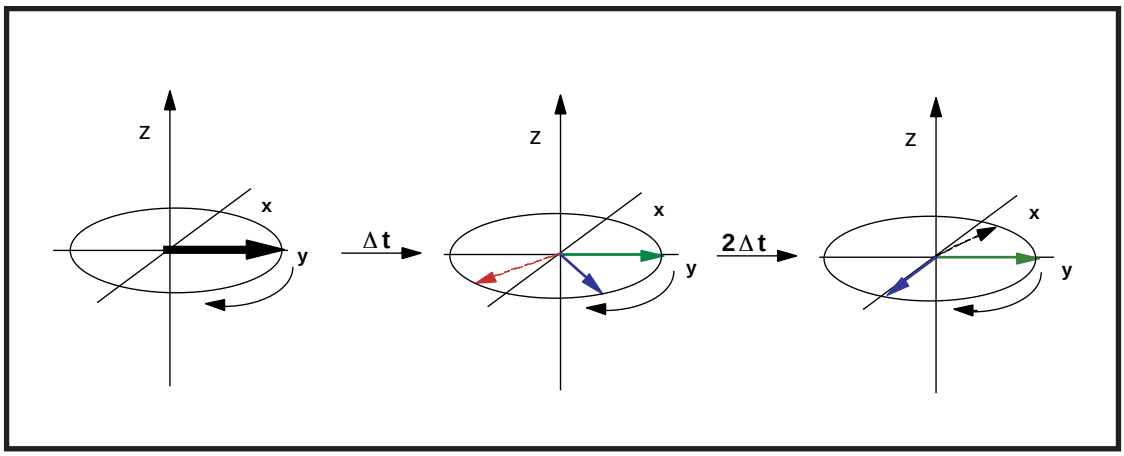

FIGURE 10. Spins precessing at different velocities (and hence have different chemical shifts) are color coded.

The magnitude of the current that is induced in the receiving coil depends on the orientation of the magnetization vector with respect to the coil. When the

magnetization is pointing towards the coild the induced current is at maximum. Because the magnetization rotates the induced current follows a sine (or cosine) wave (see additional material). Spins with different chemical shift, different larmor frequencies, precess at different rates and hence the frequency of the current is the larmor frequency, e.g. the frequency of the precessing spins: .

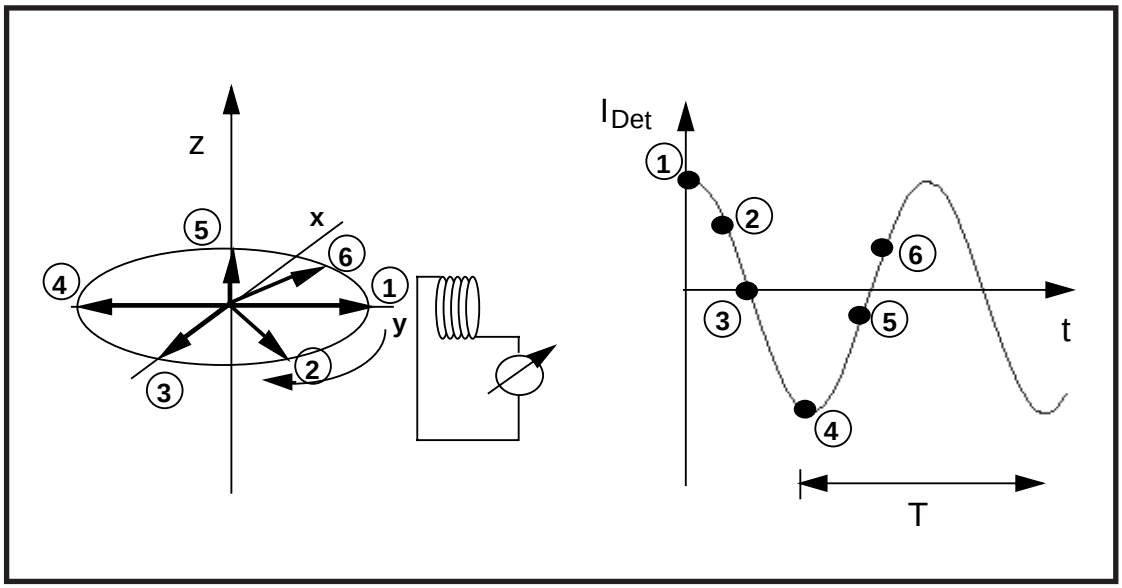

FIGURE 11. Left:Rotating spin with its position at certain time intervals 1-6 are marked. Right: Corresponding signal in the receiver coil.

In the picture above the induced current is shown for different orientations of the transverse magnetization.
This situtation is very similar to a conducting loop that rotates in a magnetic field as encountered in a generator:

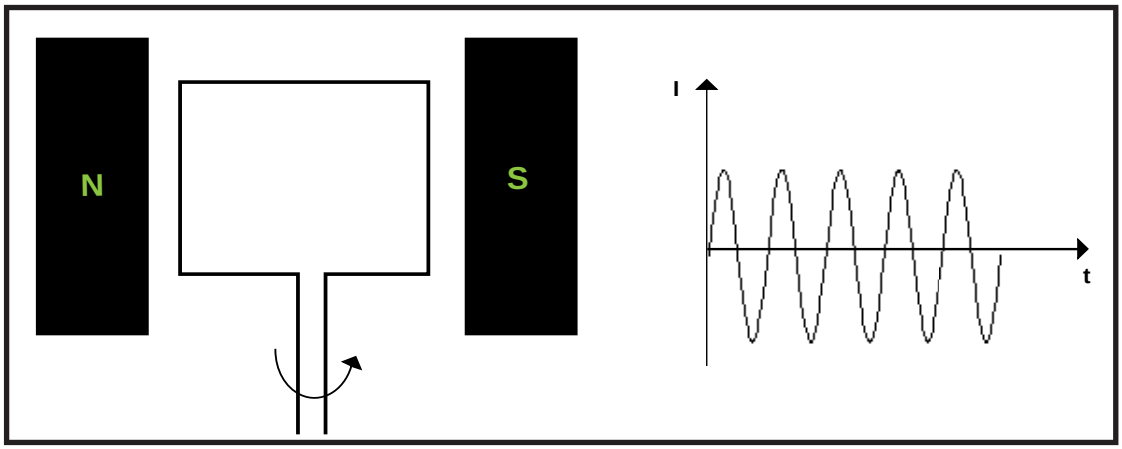

FIGURE 12. Left: Conducting loop rotating in a magnetic field with corresponding current induced (right).

However, in the generator the (coil) loop is rotating and the magetic field is stationary, opposite to the situation in a NMR experiment. The amplitude of the induced current is following a (co) sine wave. Similarily, the rotating dipoles in NMR create a sine-modulated current.

1.4 Fourier Transform NMR:

Spins that belong to nuclei with different chemical environment precess with different frequencies. For more complex compounds that contain many different spins the signal in the receiver coil is a superposition of many different frequencies. The *Fourier Transformation* is a convenient mathematical tool for simultaneous extraction of all frequency components. It allows to transform data from the time into the frequency domain:

$$I(t) \xrightarrow{FT} I(\nu)$$

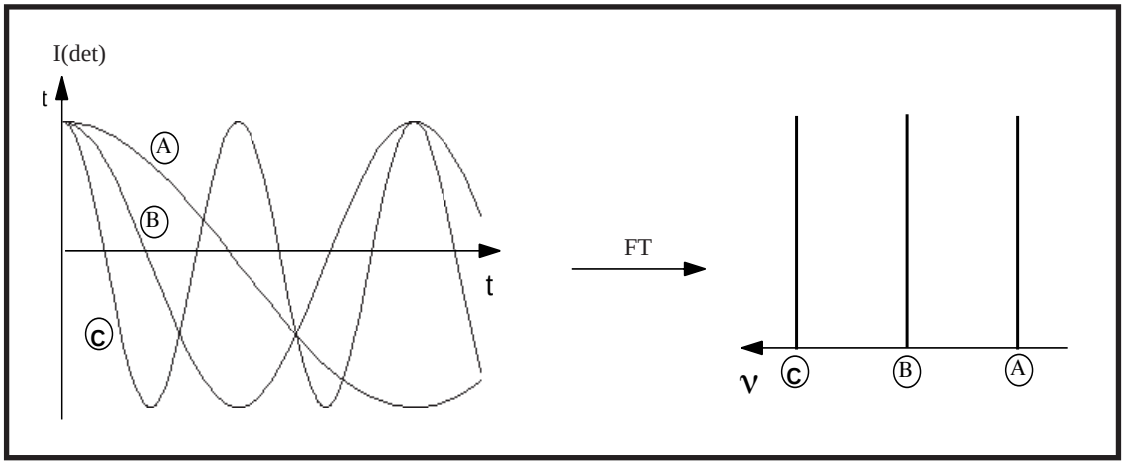

FIGURE 13. Signals from 3 spins with different precession frequencies (left) and their corresponding Fourier transforms (right)

In reality, the magnetization does not precess in the transverse plane for infinite times but returns to the z-axis. This phenomenon is called *relaxation* and leads to decreasing amplitude of signal in the detector with time.

1.5 The interaction between the magnetization and the additonal RF (B_1) field:

When only the static B_0 field is present the spins precess about the z-Axis (the axis of the B_0 field). To create spin-coherence an additional RF field is switched on, that is perpendicular to the axis of the static field (the so-called B_1 field). To emphazise that this field is turned on for only a very short period of time usually it is called a (RF) pulse. During the time where B_0 and B_1 field are both present the magnetization rotates about the axis of the resulting effective field.

This effective field is calculated by taking the vector sum of the B_0 and B_1 field:

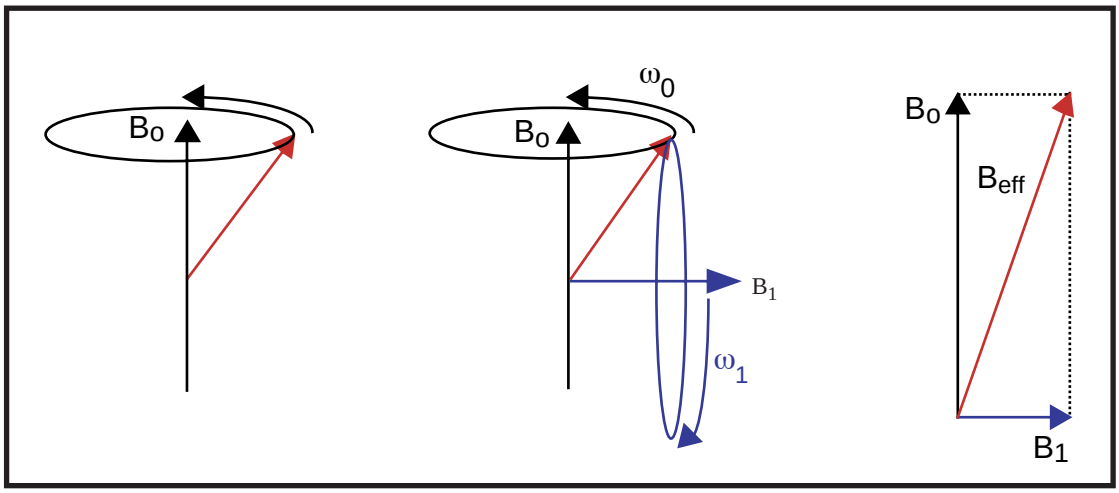

FIGURE 14. Movement of spins in the presence of only the B_0 field (left), B_o and B_1 field (middle) and vector additon to calculate the effective field formed by B_o and B_1

Now, the B_0 field is larger than the B_1 field by many orders of magnitude (for protons, the B_0 field corresponds to precession frequencies of hundreds of MHz whereas the B_1 field is about 1-20 KHz). If the B_1 field would be applied fixed along the x-axis all the time it would have an negligible influence onto the spins. However, the B_1 field is not static but rotates about the z-axis (the axis of the static field) with a frequency that is very similar to the precession frequency of the spins about the z-axis. To understand the effect of the rotating B_1 field, it is very convenient to transform into a coordinate system that rotates with the precession frequency ω_o of the B_0 field (in the picture above that means that the small "blue" man jumps onto a platform that rotates with the larmor frequency of the spin. This operation transforms from the laboratory frame to a rotating frame, e.g. a frame in which the coordinate system is not fixed but rotates with ω_o):

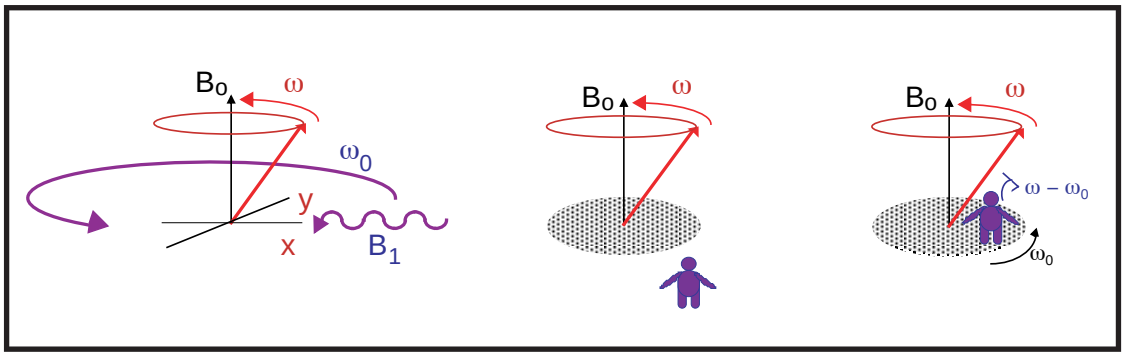

FIGURE 15. left: Static B_o field and rotating B_1 field. middle: Laboratory frame frequencies, right: Rotating frame frequencies.

For those spins whose lamor frequency is exactly ω_o the *effective* B_o field they

experience in such a rotating reference frame is zero. These spins then only feel the effect of the B_1 field and precess about the B_1 axis as long as the B_1 field is turned on. Spins that have a slightly different precession frequency ω the strength of the B_0 field is

$$B' = B_0 - \omega/\gamma$$

(For $\omega=\omega_0$, B' is zero).

During RF pulses spins which are exactly on-resonance (e.g. whose precession frequency is equal to the precession frequency of the B_1 field about the z-axis) only feel the B_1 field. These spins precess about the axis of the B_1 field until the B_1 field is turned off again:

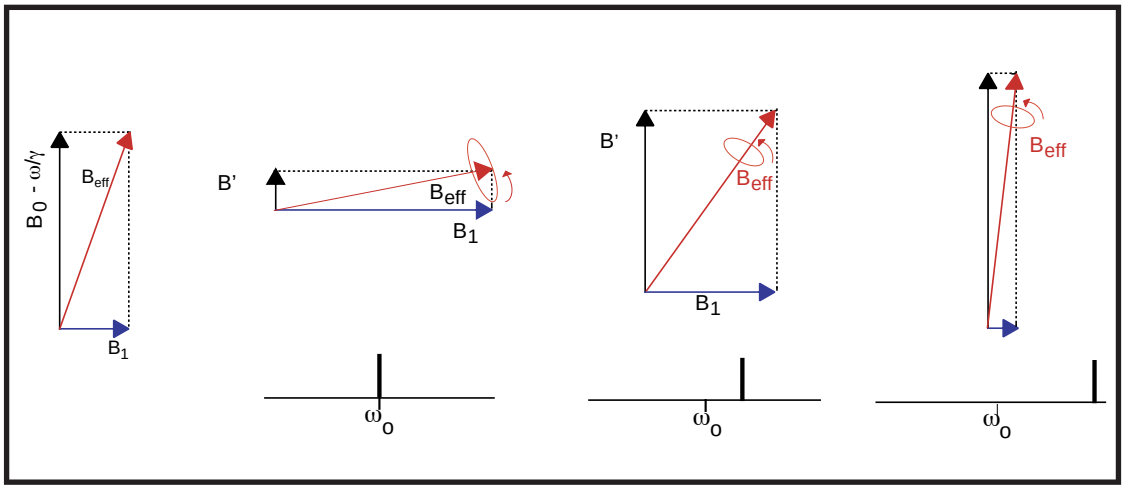

FIGURE 16. 1st : Vectorial addition of B_1 and B_0 field. 2nd: Direction of the effective field for spins exactly on-resonance, 3rd more off-resonance, 4th far off-resonance.

The overall flip-angle they have experienced during that time t_p is

$$\alpha = \gamma B_1 t_p$$

Usually the pulse lengths t_p are choosen such that the flip angle α is 90 or 180 degrees. As stated above the effect of the B_1 field is to create phase coherence amongst the spins. The macroscopic effect of coherent spins is transverse magnetization.

1.6 Description of the effect of the B_1 field on transverse and longitudinal magnetization using the Bloch equations:

We have seen before that

$$\frac{\partial \mathbf{M}}{\partial t} = \gamma(\mathbf{M} \times \mathbf{B})$$

Now,

$$B_x = B_1 \cos\omega_0 t$$

$$B_y = B_1 \sin\omega_0 t$$
$$B_z = B_o$$

and hence

$$\frac{\partial}{\partial t}M_x(t) = \gamma(M_y B_0 + M_z B_1 \sin\omega_0 t) - (M_x / T_2)$$
$$\frac{\partial}{\partial t}M_y(t) = -\gamma(M_x B_0 - M_z B_1 \cos\omega_0 t) - (M_y / T_2)$$
$$\frac{\partial}{\partial t}M_z(t) = -\gamma(M_x B_1 \sin\omega_0 t + M_y B_1 \cos\omega_0 t) - (M_z - M_0) / T_1$$

To solve these equations they are conveniently transformed into a reference frame that rotates at the frequency ω_0 about the z-axis. Therein

$$M_x' = M_x \cos\omega_0 t - M_y \sin\omega_0 t$$
$$M_y' = M_x \sin\omega_0 t + M_y \cos\omega_0 t$$

In this "primed" coordinate system the equations become:

$$\frac{\partial M_x'}{\partial t} = (\omega_0 - \omega)M_y' - (M_x' / T_2)$$
$$\frac{\partial M_y'}{\partial t} = -(\omega_0 - \omega)M_x' + \gamma B_1 M_z - M_y' / T_2$$
$$\frac{\partial M_z'}{\partial t} = -\gamma B_1 M_y' - (M_z - M_0) / T_1$$

The solutions are rather involved and will not presented here since the signals are usually recorded when only the B_0 field is present nowadays. However, it is important to see that in this frame the effect of the B_1 field on transverse magnetization aligned along the y' axis is to rotate it about x' with a frequency of $\omega_1 = \gamma B_1$.

1.7 The excitation profile of pulses:

A pulse is a *poly-chromatic* source of radiofrequency and it covers a broad band of frequencies. The covered band-width is proportional to the inverse of the pulse duration. Short pulses are required for uniform excitation of large band-widths, long (soft) pulses lead to selective excitation. Usually the non-selective (hard) pulses have B_1 fields of the order of 5-20 kHz and pulselengths of 5-20 μs, whereas selective (soft) pulses may last for 1-100 ms with an appropriately

attenuated RF amplitude:

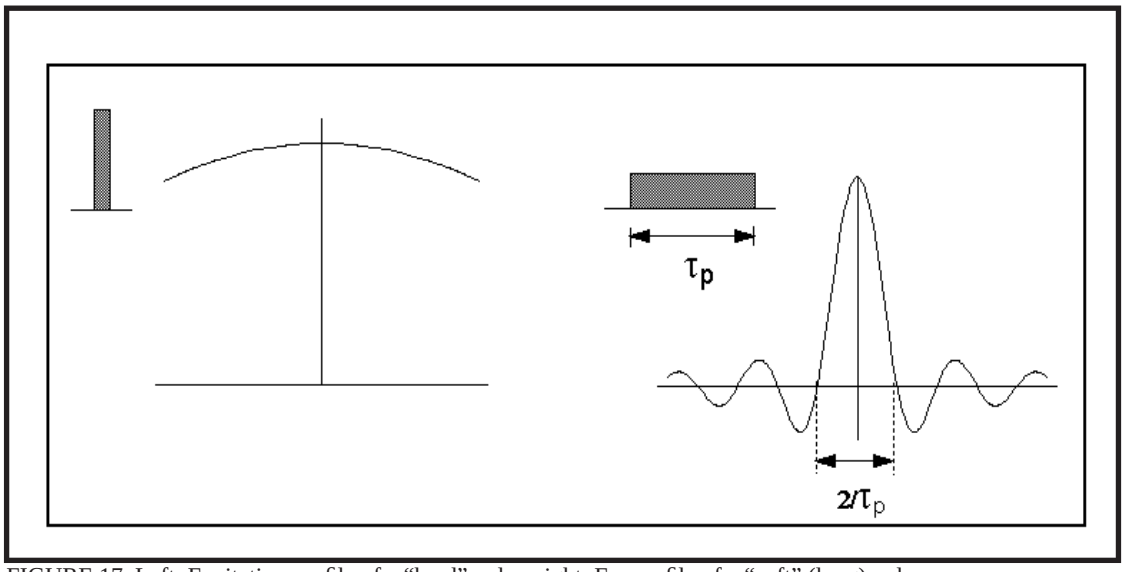

FIGURE 17. Left: Excitation profile of a “hard” pulse, right: Ex. profile of a “soft” (long) pulse

1.8 Relaxation:

The magnetization does not precess infinitely in the transverse plane but turnes back to the equilibrium state. This process is called relaxation. Two different time-constants describe this behaviour:

a) the re-establishment of the equiilibirum α/β state distribution (T1)

b) dephasing of the transverse component (destruction of the coherent state, T2). The T2 constant characterizes the exponential decay of the signal in the receiver coil:

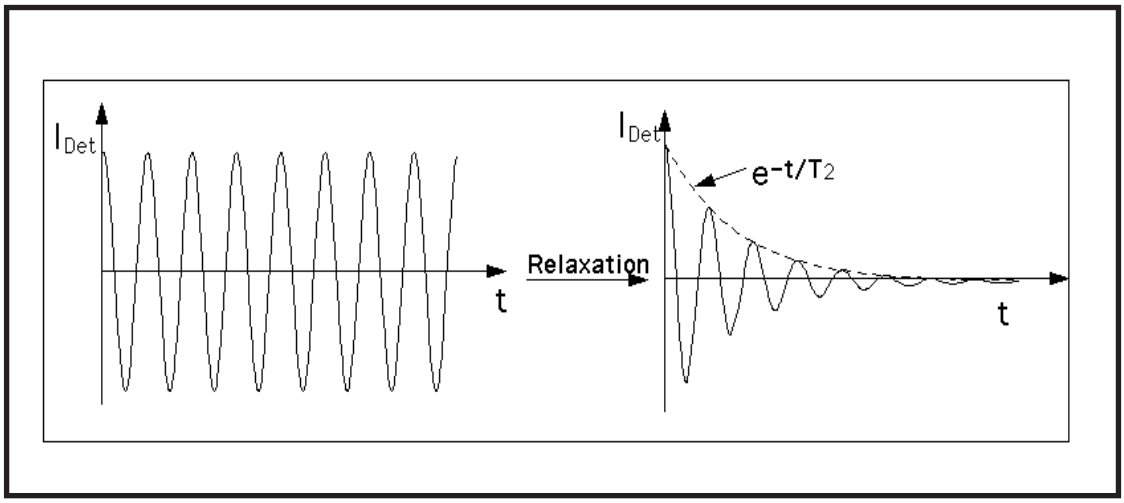

FIGURE 18. Right: Signal in absence of transverse relaxation, right: real FID (free induction decay)

The precessing spins slowly return to the z-axis. Instead of moving circularily in the transverse plane they slowly follow a spiral trajectory until they have

reached their inital position aligned with the +/- z-axis:

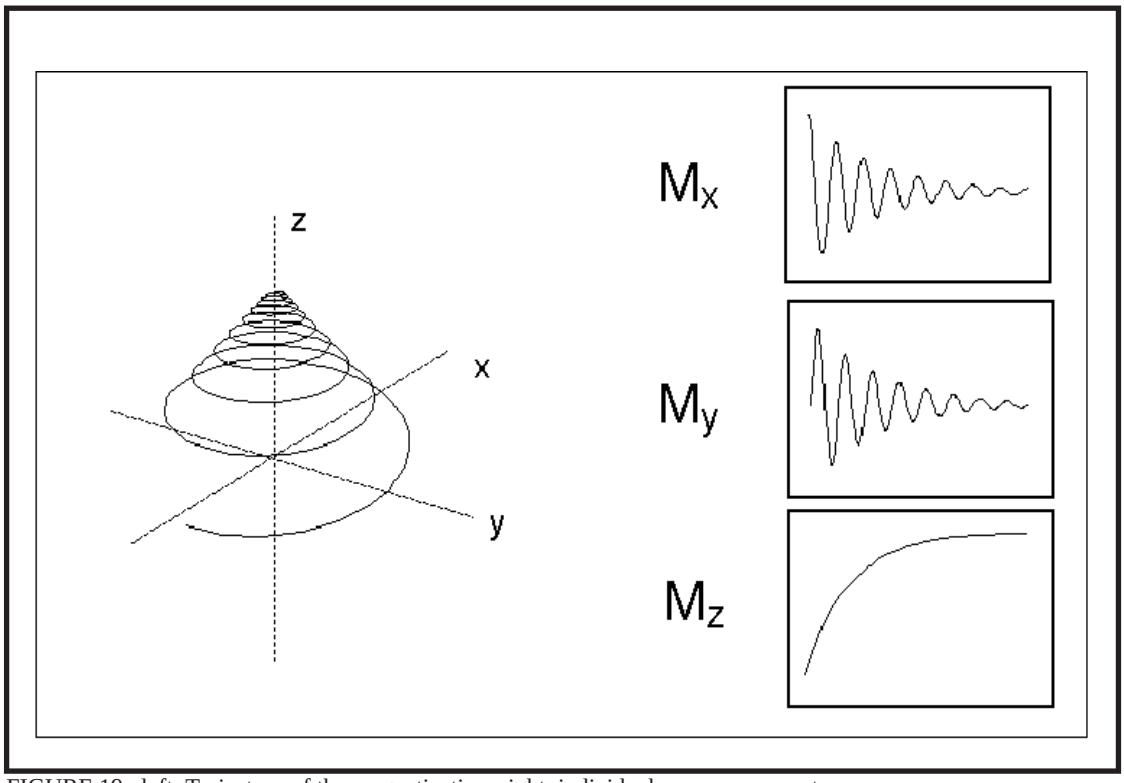

FIGURE 19. left: Trajectory of the magnetization, right: individual x,y,z component

A mechanical equivalent is a spring oscillating in time. The oscillation occurs periodically so that the displacement from the equilibrium position follows a cosine time-dependence. Because of frictional energy loss the oscillation is damped so that after some time the spring is not oscillating anymore:

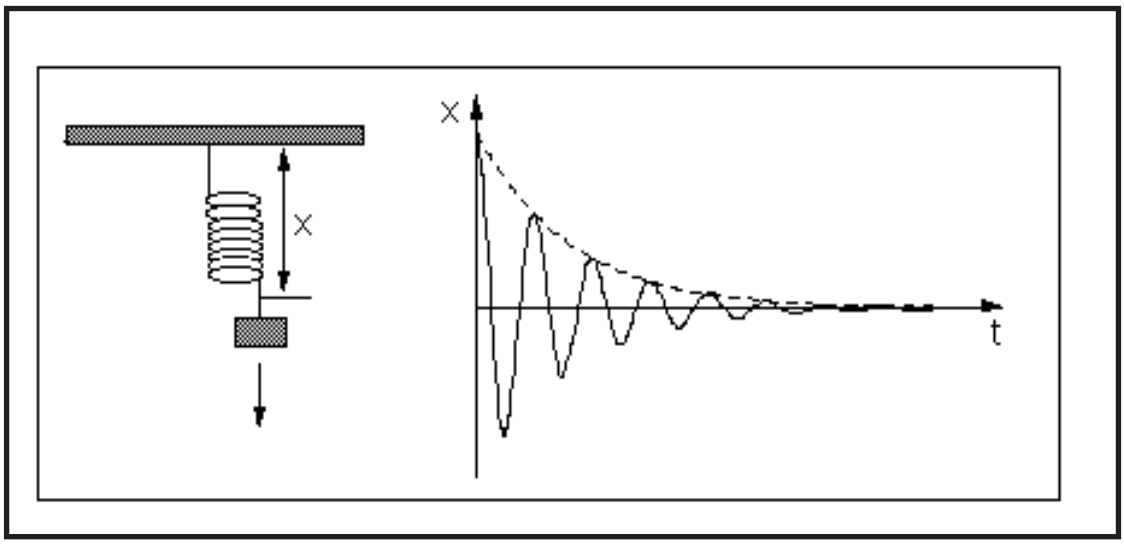

FIGURE 20. Monitoring the position of a weight fixed to a spring depending on the time elapsed after release can be described by an damped oscillation.

The damping time-constant is called T2 or transverse relaxation time. It charac-

terizes the time it takes so that the signal has decayed to 1/e of its original magnitudeThe transverse relaxation constant T_2 is related to the linewidth of the signals. The width of the signal at half height is given by:

$$\Delta\nu_{1/2} = 1/(\pi T_2)$$

Fast decay leads to broad signals, slow decay to sharper lines:

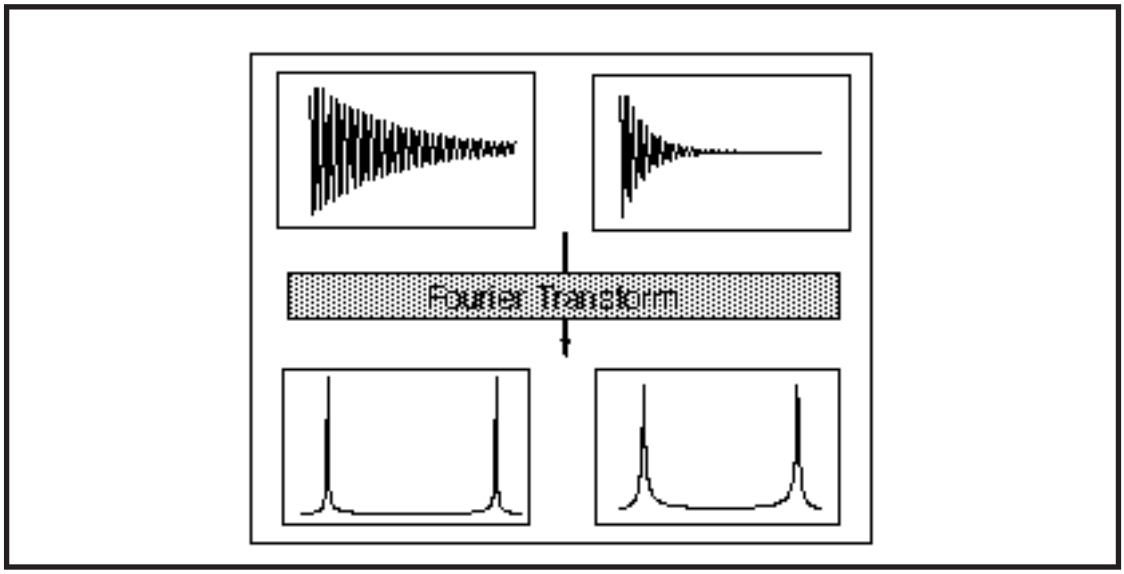

FIGURE 21. Slowly decaying FIDs lead to narrow lines (left), rapidly decaying ones to broad lines (right).

The transverse relaxation constant T_2 of spin I=1/2 nuclei is mainly governed by

- the *homogeneity* of the magnetic field (the "shim")
- the strength of the *dipolar interaction* with other I=1/2 nuclei, depending on the number and the distance of neighbouring nuclei
- the overall *tumbling time* of the molecule which is related to its size.

1.9 The intensity of the NMR signal:

If the α and β states would be populated equally, no netto change in energy could be observed. The signal intensity is proportional to the population difference of the two states.
The relative population of the states can be calculated from the Boltzmann distribution:

$$\frac{N^{\alpha}}{N^{\beta}} = e^{\frac{(E^{\beta}-E^{\alpha})}{kT}}$$

with T being the measuring temperature and k the Boltzmann constant. E^{β}-E^{α}

is the energy difference between the α- and the β-state.

Unfortunately, the energy difference in NMR experiments is very small, much smaller than in IR or UV spectroscopy, and therefore the signal is much weaker. In other words, the required quantities of sample are much larger. The energy difference ΔE depends on the gyromagnetic ratio γ:

$$E = \gamma \frac{h}{2\pi} B_o$$

nucleus	I_N	γ	S_{rel}	Nat. Abd.
		[10^8 $T^{-1}s^{-1}$]		[%]
^{1}H	1/2	2.675	1.00	99.98
^{13}C	1/2	0.673	$1.76\ 10^{-4}$	1.11
^{19}F	1/2	2.517	0.83	100
^{15}N	1/2	-0.2712	$3.85\ 10^{-6}$	0.37
^{31}P	1/2	1.083	0.0665	100

Since γ of ^{1}H is approx. 10 times larger for ^{1}H than for ^{15}N N^{α}/N^{β} is much larger and the signal much more intense. Furthermore, the natural abundance of ^{1}H is 300 times larger than for ^{15}N. Direct observation of ^{15}N nuclei requires high concentrations and long measuring times. ΔE also depends on B_o. Higher fields lead to dramatically reduced measurement times.

To be more precise the signal that is induced in the receiver coil depends on both the gyromagnetic ratio of the excited and detected spin:

$$\text{Int prop } \gamma_{ex} * \gamma_{det}^{3/2}$$

1. THE COMPONENTS OF A NMR INSTRUMENT

The NMR instrument consists mainly of the following parts:

- the magnet
- probehead(s)
- radiofrequency sources
- amplifiers
- analog-digital converters (ADC's)
- the lock-system
- the shim system
- a computer system

1.1 The magnet system:

Usually the static magnetic field nowadays is provided by a superconducting (super-con) magnet. Therein, the main coil that produces the field is placed in a liquid helium bath so that the electric resistance of the coil wire is zero. The helium dewar is surrounded by a liquid nitrogen dewar to reduce loss of the expensive helium:

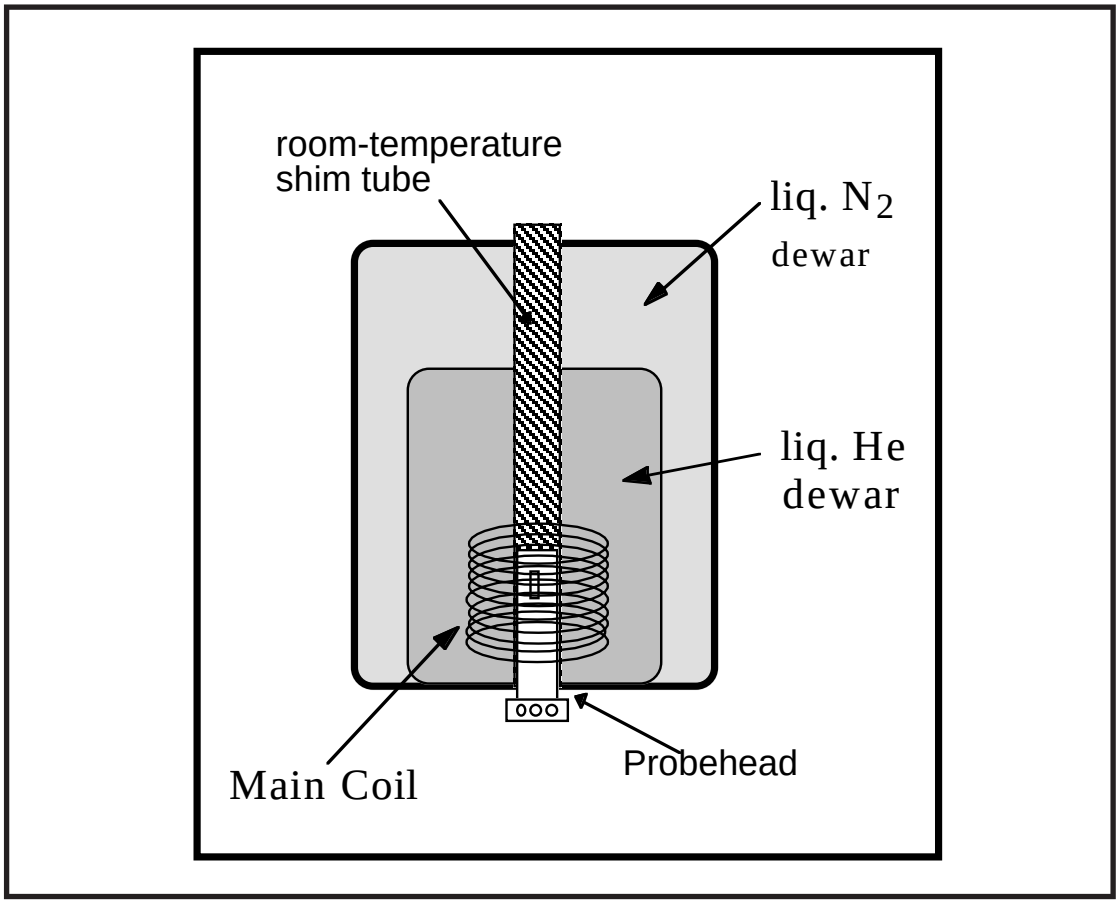

FIGURE 1. Schematic drawing of the magnet, showing He and N2 dewars, coils and probehead

Additional so-called cryo-coils are placed in the He-bath to correct partially for field in homogeneity. The magnet is vertically intersected by the room-temperature shim tube. On its surface the r.t. shim coils are located. These are the ones that have to be adjusted by the user. The sample that is mostly contained in a deuterated solvent inside a 5mm glastube is placed inside a spinner and then lowered through the r.t. shim tube so that it enters the probehead from the top.

1.2 The probehead:

The probehead contains the receiver/transmitter coil (actually only a single coil for both purposes):

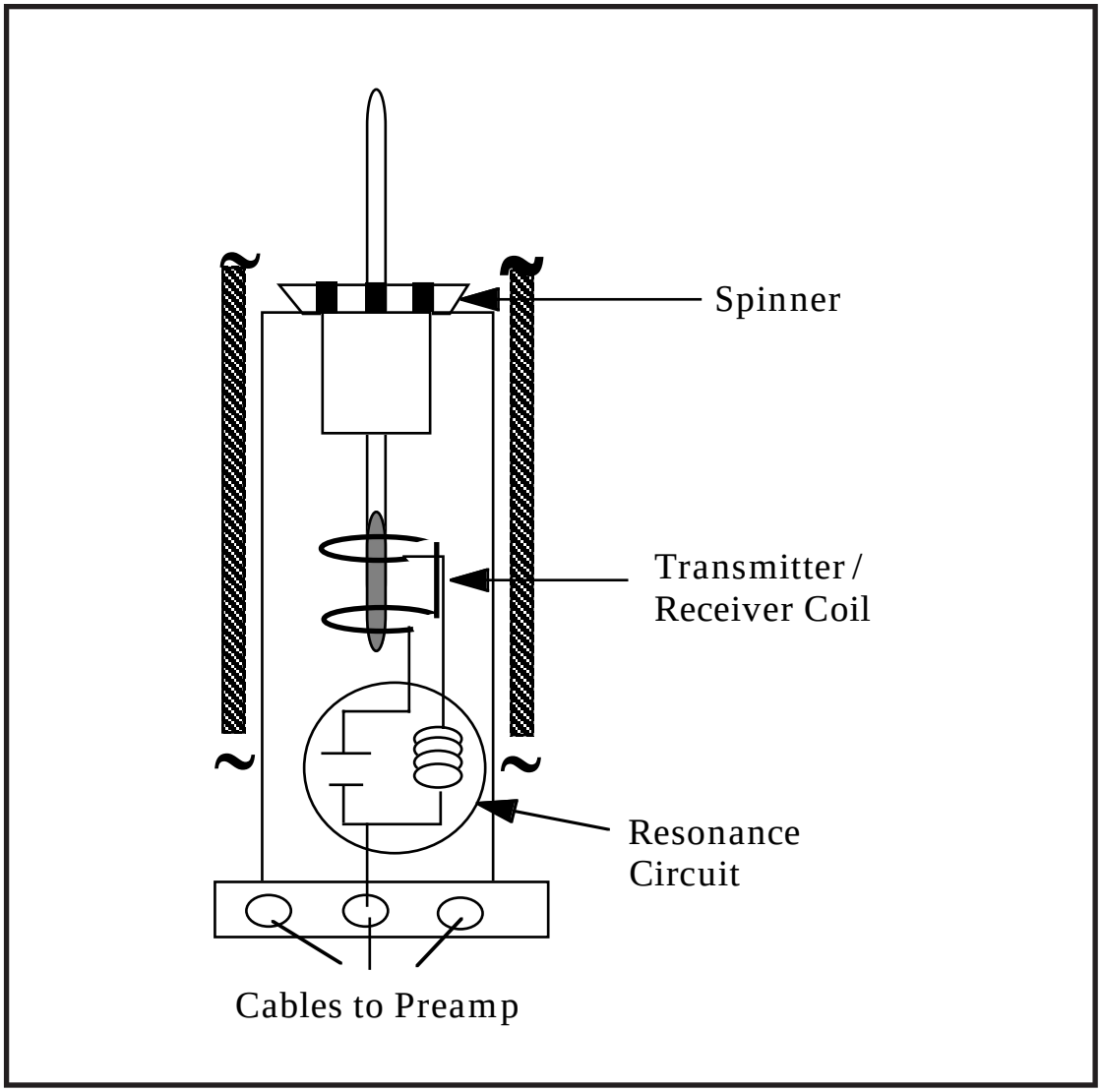

FIGURE 2. View of the spinner with sample tube placed in probehead

However, most probes contain two coils: An inner coil tuned to deuterium (lock) and a second frequency and an outer coil tuned to a third and possibly a fourth frequency. The deuterium channel is placed on most probes on the inner coil. The inner coil is more sensitive (higher S/N) and gives shorter pulselengths. An inverse carbon probe has the inner coil tuned to ^{2}H and ^{1}H and the outer coil to ^{13}C. It has high proton sensi-

tivity and is well-suited for inverse detection experiments like HSQC or HMBC. A carbon dual probe has the inner coil tuned to ^{2}H and ^{13}C and the outer to ^{1}H and is dedicated for carbon experiments with proton decoupling. The resonance circuit inside the probe also contains the capacitors that have to be tuned when changing the sample (especially when the solvent is changed). The receiver coil is in the center of the magnetic field. Once the spinner is lowered the NMR tube is positioned such that the liquid inside is covered by the receiver coil completely. The receiver/transmitter coil should not be confused with the cryo-coils (coils placed in the He bath) that produce the static field. The probehead is then connected to the preamplifier which is usually placed close to the magnet and which performs a first amplification step of the signal. The preamplifier also contains a wobbling unit required for tuning and matching the probe:

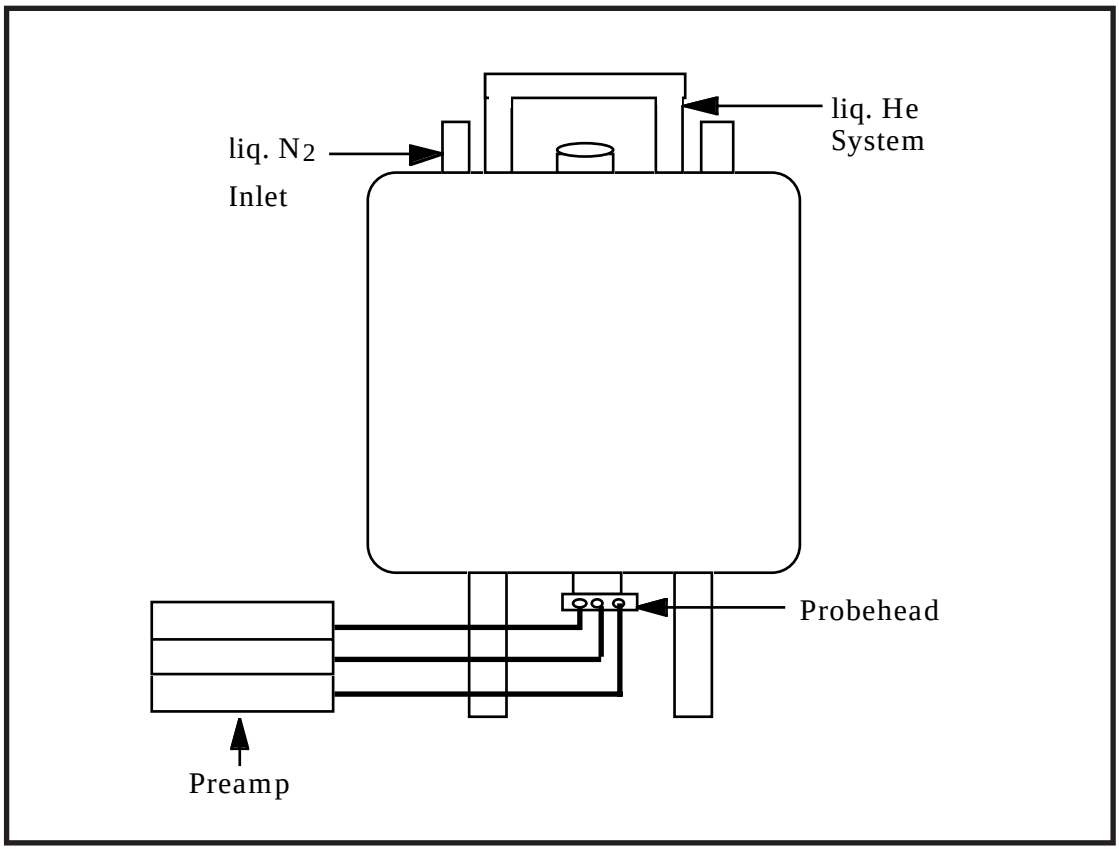

FIGURE 3. Magnet and preamplifier system

The *radiofrequency sources* (frequency synthesizers) are electronic components that produce sine/cosine waves at the appropriate frequencies. Part of them are often *modulaters* and *phase shifters* that change the shape and the phase of the signals. The frequency synthesizers nowadays are completely digital.Frequency resolution is usually better than 0.1 Hz.

The amplifiers are low-noise audio-amplifiers which boost the outgoing and incoming signals. They are in the range of 50-100 Watts for protons and 250-500 Watts for heteronuclei.

The *analog-digital converters* (ADC's) are required because the signal is recorded

in analog form (superposition of various damped harmonic oscillations) but must be in digital form in order to be accessible to Fourier transformation by the computer. In modern nmr spectrometers 16 or 18 bit digitizers are used. This means that the most intensive signal can be digitized as 2^{18}. This has severe consequences for the dynamic range because it implies that signals with less than $1/2^{18}$ of the signal amplitude cannot be distinguished in intensity. Therefore, the receiver gain (the amplification of the signal) should be adjusted such that the most intense signal almost completely fills the amplifier. *However, some care has to be paid in experiments that utilize water suppression: Sometimes the most intense signal in a 2D experiment does not occur in the first increment because the water may be (due to radiation damping) stronger in later increments. It is advisable to set the evolution time to longer values (e.g. 100ms) and observe the intensity of the water signal.*

The computer system is an industry-standard UNIX machine with lots of RAM. However, off-side processing on PCs is also possible and the PC is also started being used as host computers on the spectrometer (unfortunately).

1.3 The shim system:

Considering that the precession frequencies are proportional to the magnetic field strength the magnetic field has to be highly homogenous across the sample volume in order to be able to observe small frequency differences (small couplings). If the field would not be highly homogenous, the effective field strengths in different volume compartments inside the sample would be different and the spins therefore would precess at different rates. This would lead to considerable line-broadening (*inhomogeneous broadening*). The shimsystem is a device that corrects for locally slightly different magnetic fields.

The shimsystem consists of two parts: (A) the cryo-shimsystem and (B) the room-temperature shims. The basic principle behind them is the same. Small coils are supplied with regulated currents. These currents produce small additional magnetic fields which are used to correct the inhomogeneous field created by the main coil. There are a number of such coils of varying geometry producing correction fields in different orientations. In the cryo-shim system the coils are placed in the He bath, they are usually only adjusted by engineers during the initial setup of the instrument. The room-temperature shim system is regulated by the user *whenever a new sample is placed in the magnet* or when the temperature is changed.

The room temperature shim system is grouped into two sets of shims

- the on-axis (spinning) shims ($z,z^2,z^3,z^4..$)
- the off-axis (non-spinning) shims (x,y,xy...)

The on-axis shims only correct for inhomogeneity along the z-axis. They are highly dependent on the solvent and the solvent filling height. At least the lower order gradients (z, z^2 and z^3) should always be adjusted. The z^4 gradient depends very much on the filling height and its adjustment is tedious. Therefore, in order to speed up the shimming process, the filling height should (if possible) always be the same (e.g. 500 or 550 µl) and a shimset for that height and probehead should be recalled from disk. The off-axis shims usually do not have to be adjusted extensively (only x, y, xz and yz routineously). Wrong off-axis shims lead to spinning side-bands when the sample is rotated during measurement. Their contribution to the lineshape is largely removed with spinning but this unfortunately introduces disturbances. It should therefore be avoided during 2D and NOE measurements.

The name of the on-axis shims is derived from the order of the polynomial that needs to be used to correct for the field gradient along the z-axis:

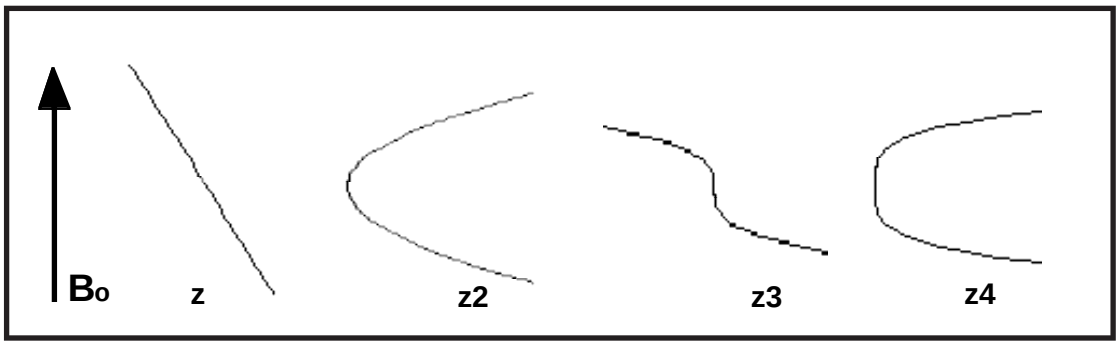

FIGURE 4. Field dependence of on-axis shims

The z-shim delivers an additional field that linearly varies along the sample tube. The z^2 shim has its largest corrections to the field at the top and the bottom of the sample.

For the more experienced spectroscopist the misadjusted on-axis shim can mostly be recognized from the signal lineshape. Misadjusted shims with even exponentials (z^2,z^4,z^6) give asymmetric signals, those with odd exponentials (z^1,z^3,z^5) show up as a symmetrical broadening. This is due to the symmetry of the function needed to correct of it. Z^4 for example increses the field strength at the the top and the bottom of the sample and hence gives only frequencies larger than the correct frequency. Z^3 in contrast increases the freuqnecy at the top and decreases the frequency at the bottom of the sample. Therefore, in the case of z4, there is a proportion of singal shifted to higher frequencies and hence to one side of the signal, whereas z^3 give proportions of the signals shift to lower *and* higher frequencies resulting in asymmetric and symmetric errors for the former and latter, respectively. The closer the bump is to the base of the signal the higher the gradients needs to be to correct for it.

Shimming is usually performed by either observing the intensity of the lock

signal (*vide infra*) or by monitoring the shape of the FID.:

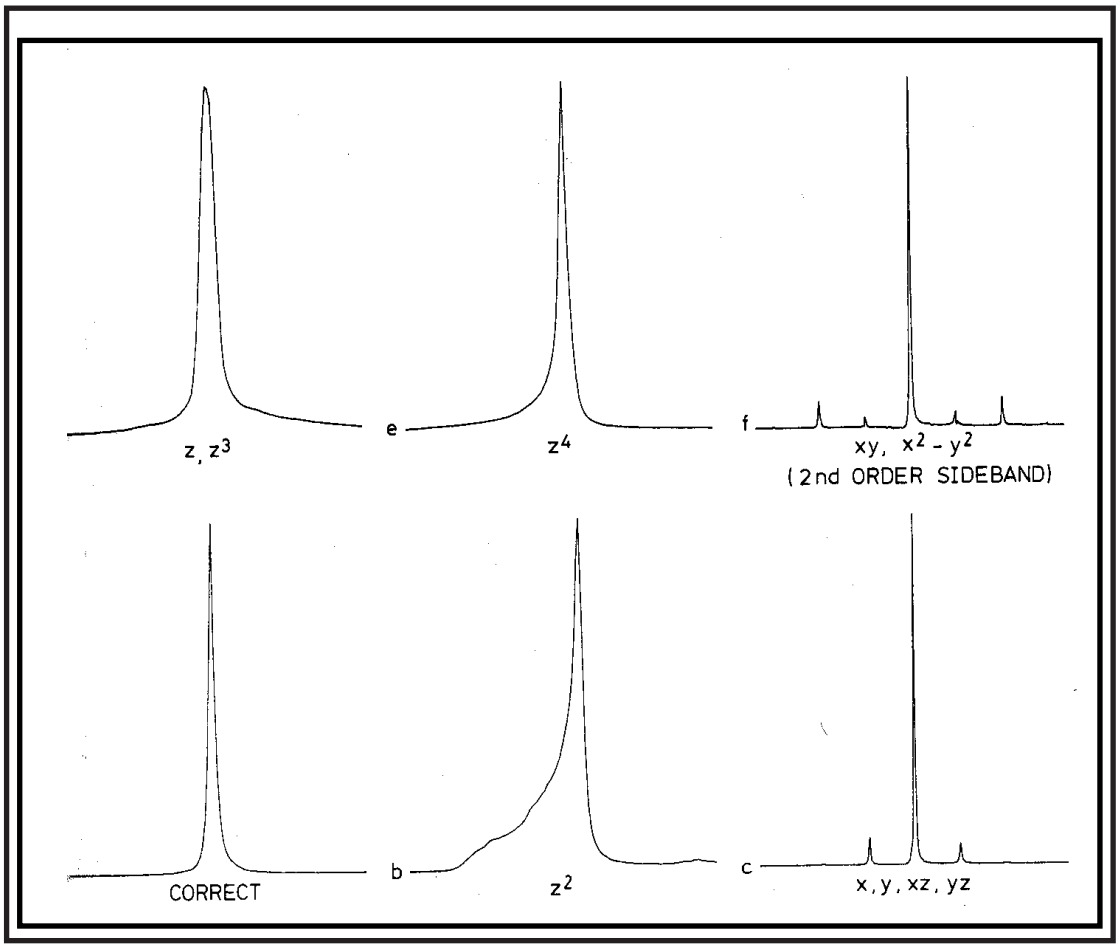

FIGURE 5. Misadjusted shims and appearance of corresponding signals after FT.

Another way of controlling the homogeneity of the magnetic field is to watch the shape of the FID. When the field is highly homogenous, the FID should fall smoothly following an exponential. The resolution of the signal determines how long the FID lasts:

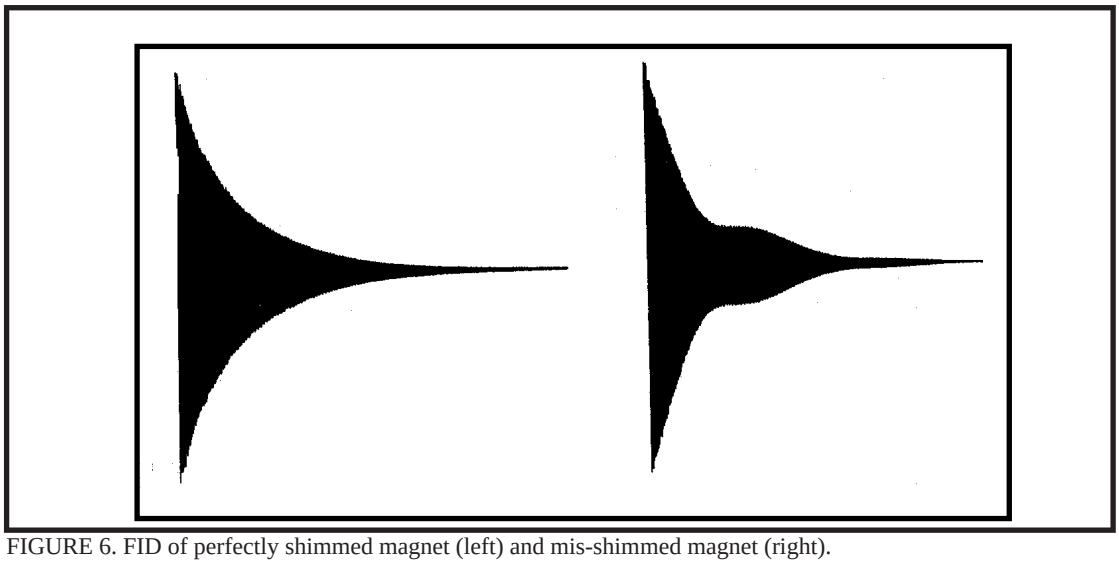

FIGURE 6. FID of perfectly shimmed magnet (left) and mis-shimmed magnet (right).

1.4 The lock-system:

Stability of the magnetic field is achieved by the *deuterium lock* system. The deuterium lock measures the frequency of the deuterium line of the solvent. Hence, deuterated solvents have to be used for FT-NMR. The system has a feedback loop, which generates corrections to the magnetic field strength B_o, such that the resonance frequency of the solvent deuterium line remains constant. This is achieved by delivering a suitable current to the z^0 shim coil. Consequently, all other resonance frequencies are also kept constant. Usually the lock system has to be activated when the sample has been placed in the magnet. When the lock-system is not activated the naturally occurring drift of the magnetic field leads to varying resonance frequencies over time and hence to line-broadening.

The stability of the lock system is critical for many experiments, mostly 2D measurements and even more importantly, NOE measurements. The stability is influenced by many factors of which the temperature instability has the largest influence. To provide good sensitivity of the lock the lock power should be adjusted just below saturation (lock-line must still be stable!).

Modern digital lock system allow to adjust the regulation parameters of the lock channel.Thereby, one can determine how fast the lock circuit reacts (the damping of the lock). For experiments utilizing pulsed-filed gradients the lock should be highly damped in order to avoid that the lock tries to correct each time the field recovers from the gradient!

1.5 The transmitter/receiver system:

It is much more convenient to handle audio-frequencies than handling radiofrequencies. We have seen before that the B_1 field rotates about the axis of the static field with a certain frequency, the carrier frequency, that coincides with the center frequency of the recorded spectrum. Similarly, the received signal is also transformed down to audio frequency. In addition we require *quadrature detection*: A single coil cannot distinguish positive and negative frequencies, that means distinguish frequencies of spins rotating slower than the carrier frequency from those that precess at higher rates:

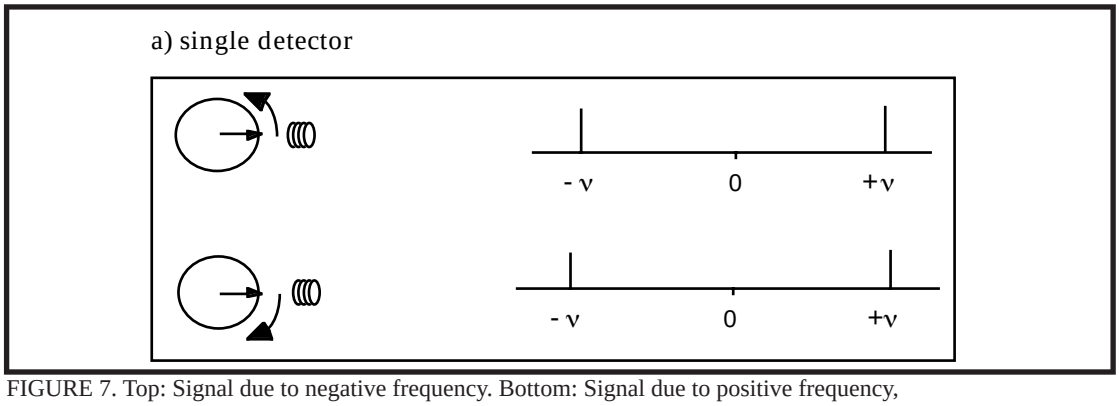

FIGURE 7. Top: Signal due to negative frequency. Bottom: Signal due to positive frequency,

In principle, such a separation could be achieved by using two receiver coils which differ by 90° in phase (a quadrature detector):

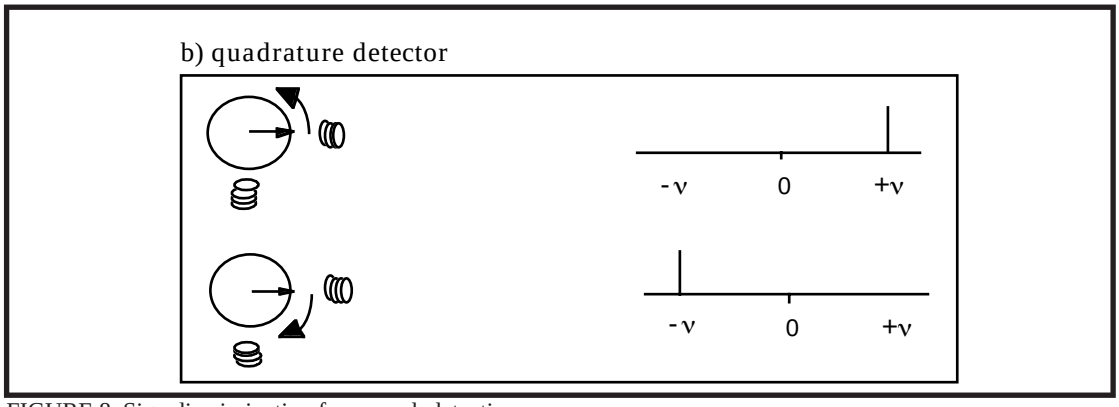

FIGURE 8. Sign discrimination from quad. detection

One could would then detect the cosine- modulated and the other the sine-modulated component of the signal. Adding sine- and cosine modulated components of the signal cancels the “wrong” frequency component:

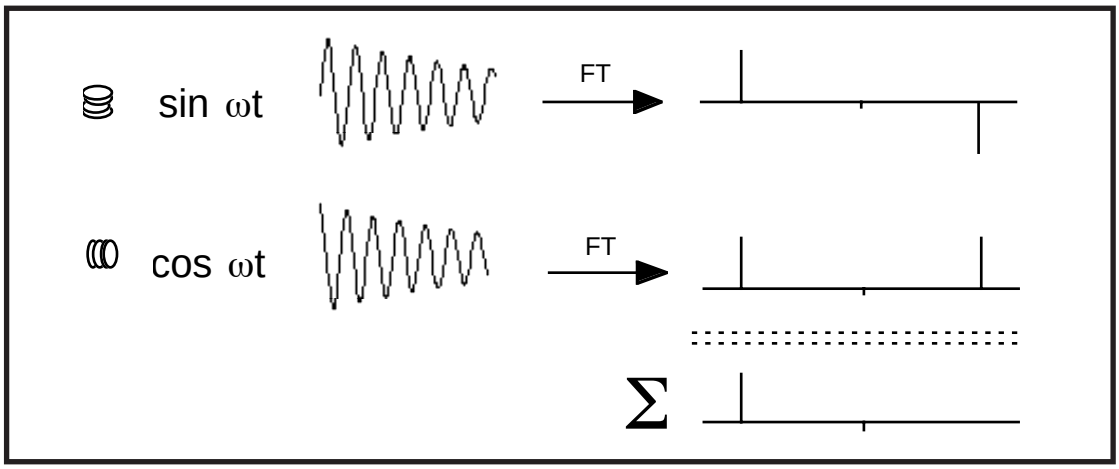

FIGURE 9. Fourier transform of a sin (top) and cosine wave (bottom).

However, probeheads contain only one coil. Sine-and cosine-modulated components of the signal result from a different trick: The signal that comes from the receiver coil (which of course is HF (MHz)) is split into two. Both parts are mixed with the transmitter (carrier) frequency [for Bruker machines: SFO1], the frequency with which the B_1 field rotates. However, the phase of the transmitter frequency that is added differs by 90 degrees for the two parts. Thereby, the radiofrequencies (MHz range) are transformed into audiofrequencies (kHz range). These can be handled in the following electronics much easier. We do see now, that both the transmitter and the receiver system effectively work in the rotating frame. The rotating frame was introduced in the transmitter system by having the B_1 field rotating in the x,y plane and in the receiver system by subtracting the transmitter frequency from the signal. What we actually measure are therefore not MHz-frequencies but frequency-offsets (differences to) the carrier frequency. In addition, we have introduced quadrature detection:

Transmitting and receiving is done on the same coil. The signal coming from

the coil is blanked for a short time after the pulses (the so-called pre-scan delay) and then used for detection. The transmitter / receiver system contains mainly analog parts.

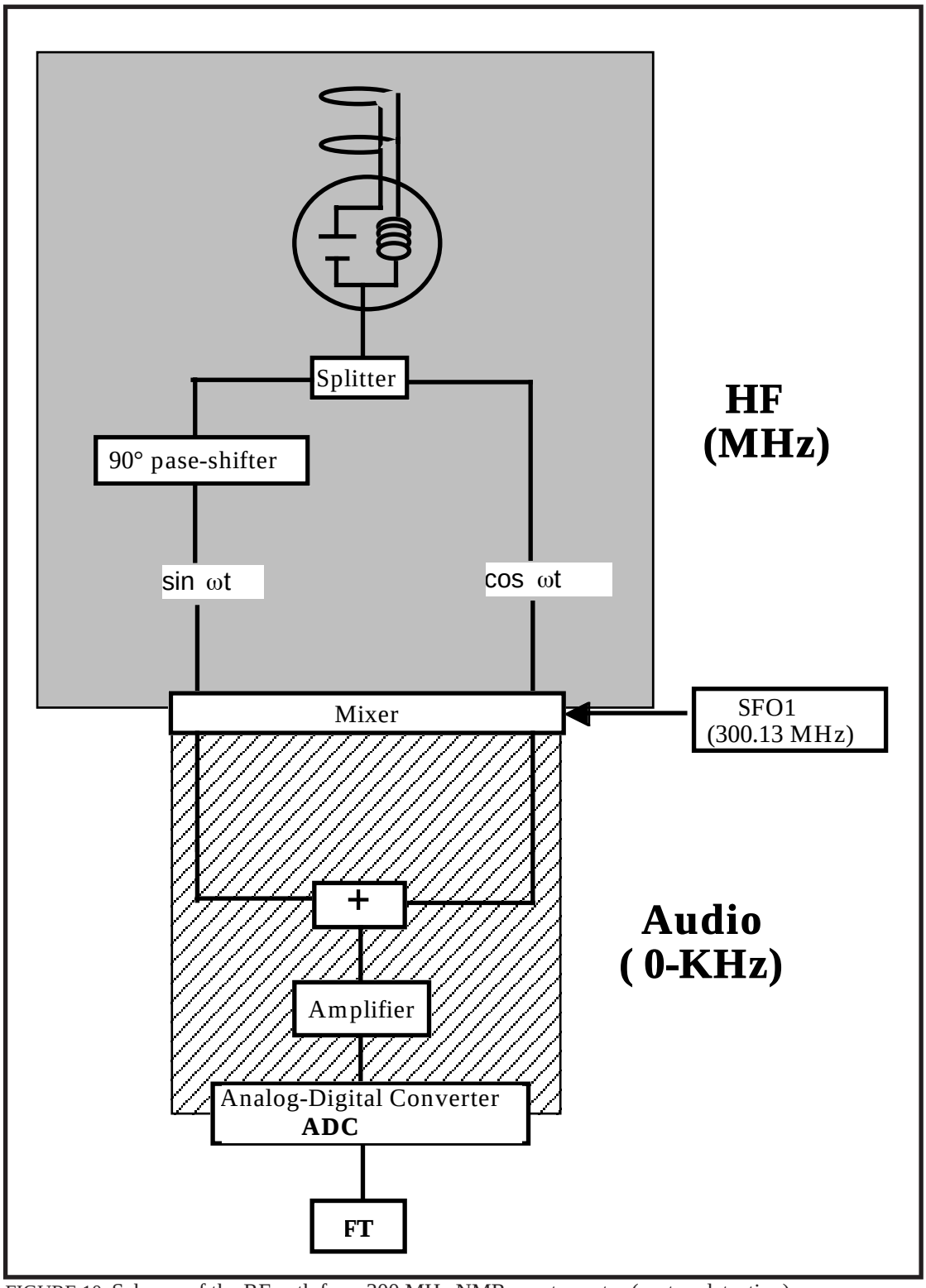

FIGURE 10. Scheme of the RF path for a 300 MHz NMR spectrometer (proton detection).

When cosine and sine-modulated signals are slightly differently amplified so-called quadrature images remain. They are usually observed for intense signals when few scans are recorded and can be easily recognized because they are mirrored about the

zero-frequency (the middle of the spectrum). Therefore, modern instruments utilize "*oversampling*". A much larger spectral width is sampled, such that the quadrature images do not fall into the observed spectrum any longer. Prior to processing the non-interesting part of the spectrum is removed.

2. BASIC DATA ACQUISITION PARAMETER

The following paragraph summarizes the parameters that govern the acquisition of 1D spectra and hence have to be properly adjusted before the measurement.
The 1D spectrum is characterized by the frequency in the center of the spectrum and by its width. Remember that the B_1 field rotates about the axis of the static field with a certain frequency:

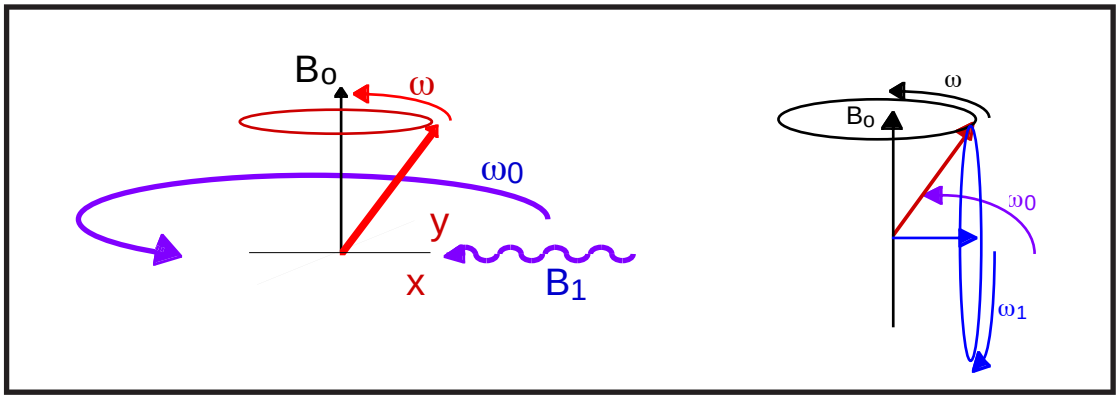

FIGURE 11.

Exactly this frequency is mixed with the signal that comes from the receiver coil and therefore is effectively subtracted from the signal frequency. Hence, the signal is measured in the rotating frame and the frequencies will be audio frequencies (0- kHz). If the precession frequency of a particular spin is exactly the same as the frequency with which the B_1 field rotates it will have zero frequency and appear in the center of the spectrum. The frequency of the rotating B_1 field is called the (transmitter) carrier frequency:

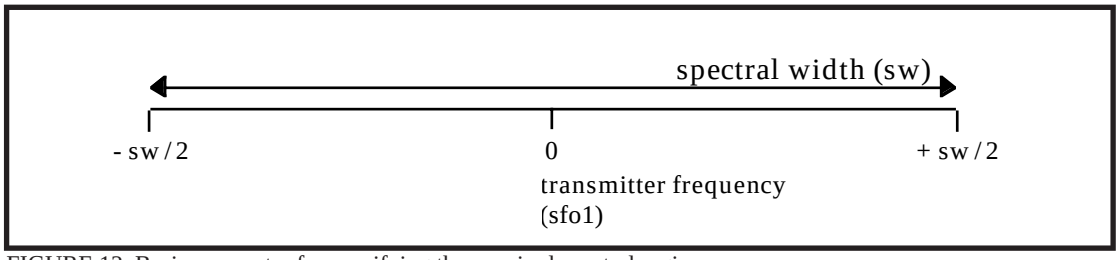

FIGURE 12. Basic parameter for specifying the acquired spectral region

sfo1: *spectrometer frequency offset* of the first (observe) channel
this parameter determines the carrier offset. Frequencies larger than sfo1 will be on the left side of the spectrum, smaller frequencies on the right side. **sfo1** is the absolute frequency (in MHz). If you want to make a small change of the carrier position, you can change the offset **o1**

sfo1 = bf1 + o1
bf1 is the so-called basic-spectrometer frequency, e.g. 500.13 MHz and o1 is the offset, a frequency in the audio (0-> KHz) range.

sfo2: *spectrometer frequency offset* of the second (decoupler) channel
like **sfo1**, required for example for acquisition of proton decoupled carbon spectra. The proton frequency is then defined on the second channel and should correspond to the center of the proton spectrum.

Now, the next question is, how to adjust the spectral width (the width of the spectrum in Hz). This done by proper choice of the dwell time. The signal is sampled stroboscopically and neighboring data points are separated by the dwell time. The Nyquist theorem says that at least one point per period must be sampled in order to characterize the frequency correctly. Since the highest frequency is **sw** (in Hz), the dwell time must be
dw = 1/sw

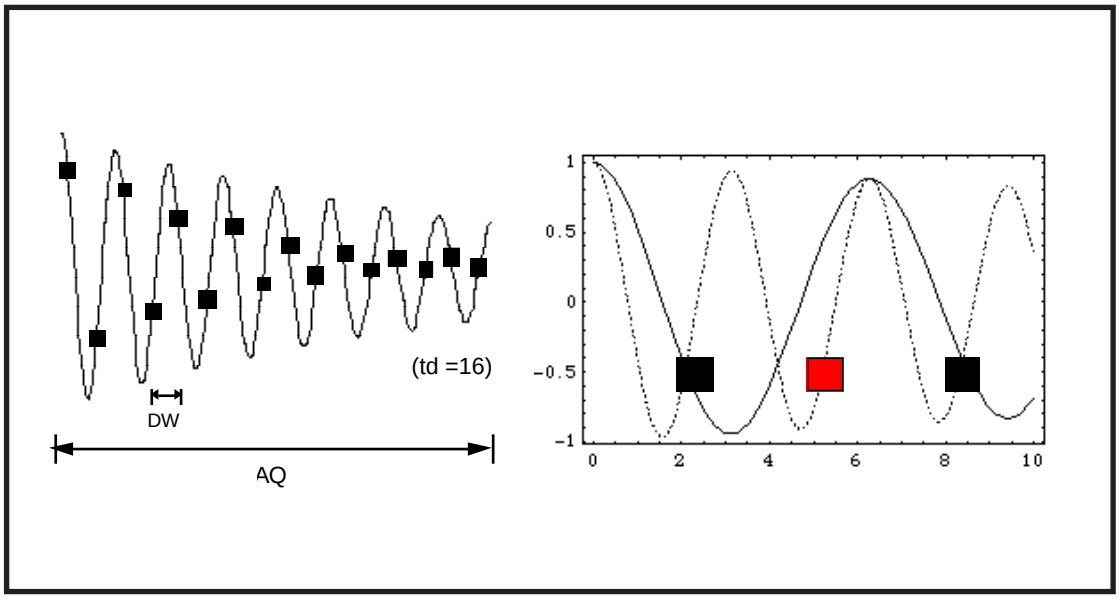

FIGURE 13. Left: Sampled data points. Right: Black: Sampled data points. Red: Missing sampling point for a frequency of twice the nyquist value..

Signals that have a higher frequency have made more than a 360 degree rotation between the sampling points. On older instruments (AMX spectrometers) they are attenuated by the audio-filters. They are recognized from the fact that they cannot be phased properly, usually. On the modern instruments (those with oversampling, DRX series), signals outside the spectral width completely disappear. Therefore, it is always recommended to record the spectrum over a very large spectral width initially to make sure that no signals at unusual places (e.g. OH protons at 20 ppm or signals below 0 ppm) are lost.

sw: *spectral width*

gives the width of the acquired spectrum (on Bruker instruments, **sw** is in units of ppm, **swh** in units of Hz).

dw: *dwell time*

is the time spacing between sampling of two consecutive data points.

dw = 1/**sw** or **dw** = 1/2**sw**

The dwell time is determined by the inverse of the spectral width (or the inverse of twice the spectral width, depending on the quadrature detection mode).

td: *time domain data points*

The number of points that are sampled is called "time domain" data points (td). The longer the FID is sampled the better will be the resolution in the spectrum provided there is still signal in the FID.

aq: *acquisition time*

determines the total time during which a *single* FID is sampled

aq = td * dw

for 1D spectra, aq is set such that the signals have completely decayed towards the end of the FID (which corresponds to the transverse relaxation time T2). If **aq** is set to a shorter value, the resolution is lower, if aq is >> T2, only noise will be sampled at the end of the FID, and therefore the experimental time is unnecessarily prolonged.

The complete measuring time for a simple 1D spectrum is approx.

t_{tot} = ns (RD+aq)

in which ns is the number of scans and RD the relaxation delay (*vide infra*).

ns: *number* $\frac{S}{N} \propto \sqrt{ns}$

the number of FIDs which are co-added. The signal to noise ratio of a measurement increases as

which means that in order to improve the S/N by a factor of two the measurement time must be increased by a factor of 4. Sometimes, the minimum number of **ns** is determined by the phase-cycle of an experiment.

RD: *relaxation delay*

time between end of sampling of the FID and start of the next experiment. On Bruker instruments, the relaxation delay is characterized by the parameter **d1**. The effective time for relaxation is given by the repetition rate

t_r = **aq** + **d1**

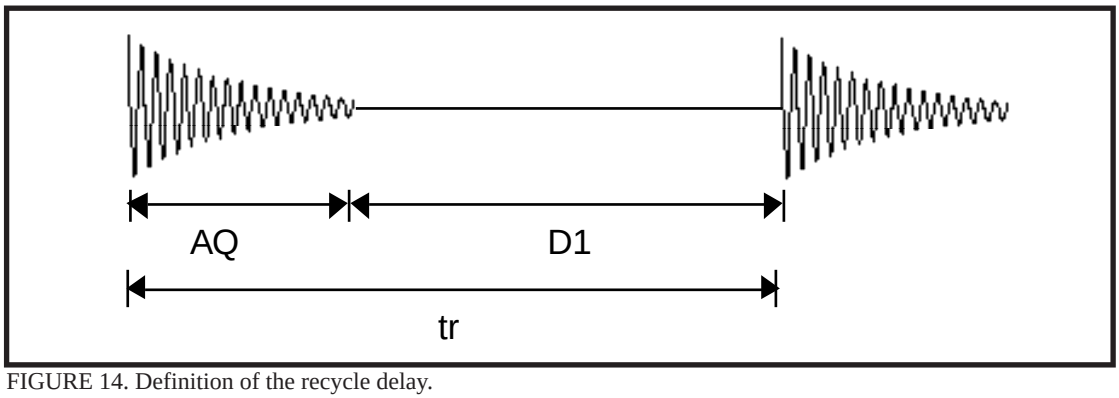

FIGURE 14. Definition of the recycle delay.

rg: *receiver gain*

This is the amplification of the signal. Settings are possible in powers of 2 (e.g. 1,..,128,256,...32k). For automatic adjustment of the receiver gain on spectrometers use **rga**. The receiver gain has to be set such that the maximum intensity of the FID fills the ADC (analog-digital converter). If the receiver setting is too low, the dynamic range of the instrument is not exploited fully and very small signals may be lost. If the receiver gain setting is too high, the first points of the FID are clipped, which will lead to severe baseline distortions.

p1,**p2**,..length of pulses [in µs]

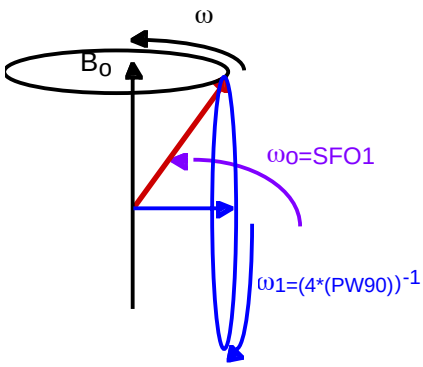

length of pulses in µs. This is the duration that the B_1 field is switched on. The B_1 field rotates about the z-axis with the frequency ω_o. We have seen before that if the frequency ω with which the spin precesses about the z-axis is identical to ω_o it does not feel B_0 in the rotating frame.It will then precess about the axis of the effective field which in that case corresponds to the axis of the B_1 field. However, the precession frequency about the B_1 axis, ω_1, is much smaller, it is in the kHz range (or smaller). The strength of the B_1 field is correlated to the time required for a 360 degree rotation PW_{360} via

$$\omega_1 = \gamma B_1 \; / \; 2\pi = \; 1 / (PW_{360})$$

Usually either 90 or 180 degree rotations are required in NMR. The following conventions are made in pulseprograms:

- p190˚ transmitter pulse length
- p2180˚ transmitter pulse length
- p390˚ decoupler pulse length
- p4180˚ decoupler pulse length

The flip angle of the pulse Φ is determined not only by the length of the pulse τ_p, but also by the power level, at which the B_1 field is applied:

$$\Phi = \tau_p \gamma B_1$$

For proton pulses, the power level is given by the parameters **hl1**,**hl2**,**hl3**,..**hl6** (hl= ^{1}H level). For pulses on the heteronuclei (^{13}C, ^{15}N, ^{31}P ...), power setting parameters are **tl0**,**tl1**,..**tl6** (transmitter level 1,2..) or **dl0**,**dl1**..**dl6** (decoupler level 1,2..) for the low power mode. In the default mode, heteronuclear pulsing is done in the high-power mode and cannot be regulated (always full power). On the newer DRX instruments the power levels are specified as pl1:f1 (power level 1 on channel 1).

1. ACQUISITION OF 1D SPECTRA

Acquisition of simple 1D spectra comprises the following steps

- changing the probehead
- Setting the correct temperature for measurement
- Correct positioning of the tube in the spinner and insertion of the sample into the magnet
- recalling a shimset with approximately correct shims for the solvent and probehead
- activation of the field/frequency lock system
- adjustment of the homogeneity of the magnetic field (shimming)
- recalling a parameter set for the desired experiment
- (tuning of the probehead)
- (calibration of the pulse lengths)
- determination of the correct receiver gain setting
- performing a preliminary scan with large spectral width (^{1}H only, approx. 20 ppm)
- acquisition of the final spectrum with sufficient S/N and optimized spectral width

1.1 Calibration of pulse lengths:

The flip-angle θ of pulses is proportional to the duration (τ_p) and strength of the applied B_1 field:

$$\theta = \gamma B_1 \tau_p$$

It is also obvious that for nuclei with lower γ, higher power setting must be applied (typically for ^{1}H: 50 W, for ^{15}N:300W). The length of the pulses has therefore to be determined for a given power setting. For calibration of proton pulses, a spectrum is acquired with setting the length of the pulse corresponding to a small flip angle, phasing of the spectrum, and then increasing the pulse-length in small steps. When the length of the pulse is set corresponding to a 180˚ pulse, a zero-crossing of the signal is observed, as well as for the 360˚ pulse. The length of the 90˚ pulse can be calculated to be half of the length of

the 180˚ pulse:

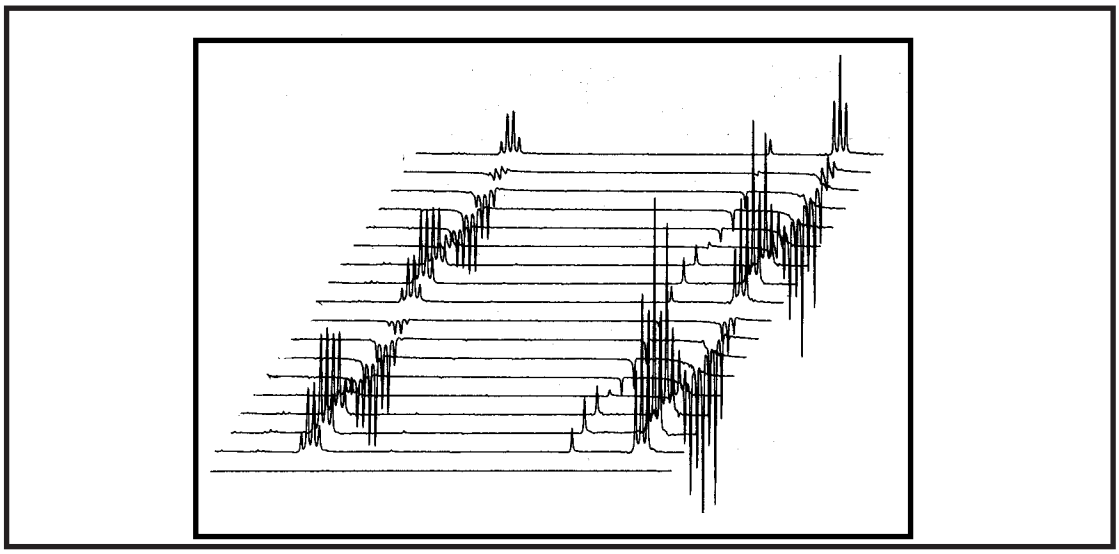

FIGURE 1. Calibration of pulse length. The length of the proton pulse is incremented by a fixed amount for each new spectrum.

^{13}C pulses are most easily determined on a ^{13}C-labeled sample such as an acetate sample (labeled at the Me carbon). Calibration is performed in the so-called inverse-detection mode with the following sequence detecting the proton signal (which is split by the ^{13}C coupling into an anti-phase doublet):

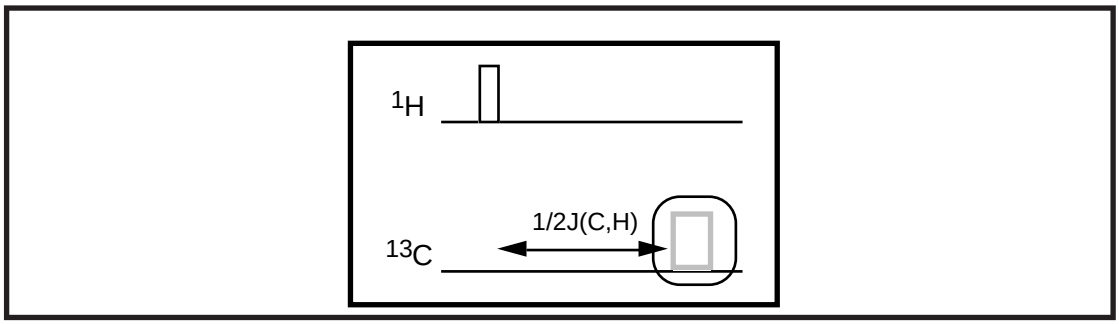

FIGURE 2. Pulse sequence to determine the 90° carbon pulse with proton detection

When the carbon pulse is exactly set to 90˚, all magnetization is converted into multiple-quantum coherences, and no signal is observed:

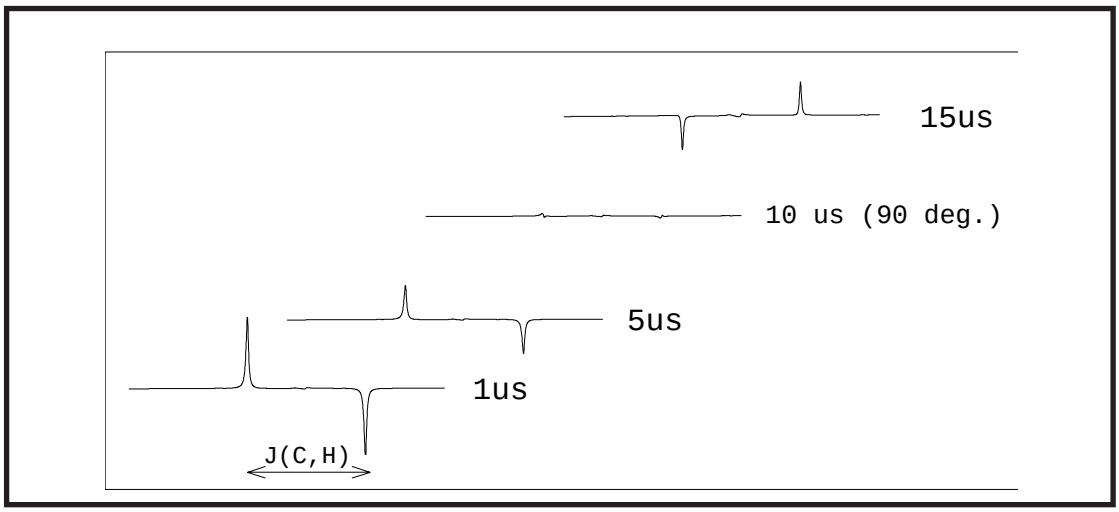

FIGURE 3. Resulting spectra from the sequence of Fig.2.

1.2 Tuning the probehead:

The purpose of the radiofrequency circuit inside the probe is to deliver a rotating B_1 field and to detect the signal. An oscillating electromagnetic field is also part of a radio and hence the resonance circuit inside the probe has much in common with the one found in a radio:

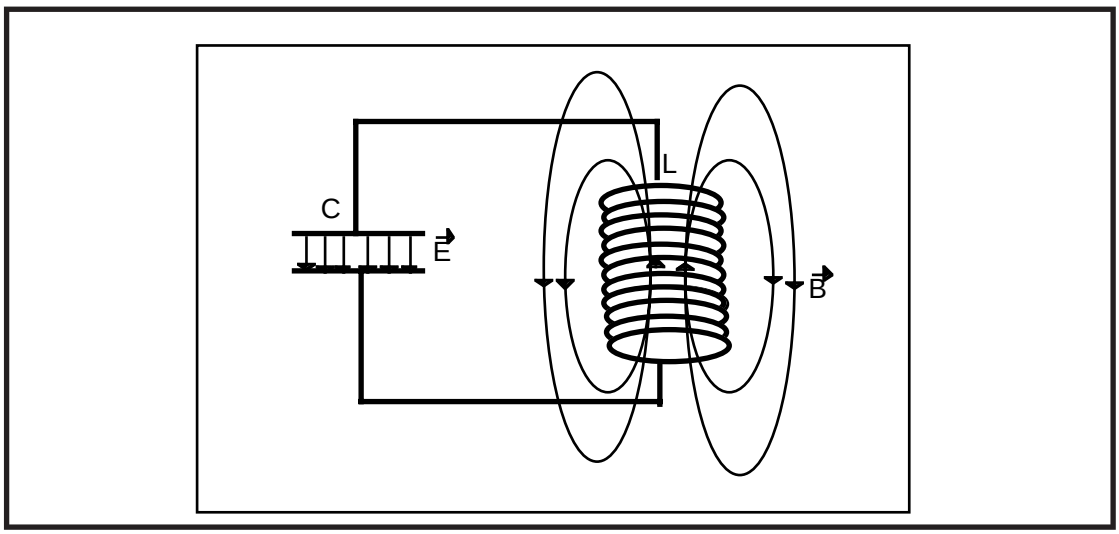

FIGURE 4. Basic principle of the probehead circuit.

A resonance circuit has two basic components: a capacitor (C) and a coil (or inductance, L). The energy is interchangingly stored in form of an electric or magnetic field in the capacitor or in the coil, respectively. The frequency of oscillation is

$$\omega = 1 / (\sqrt{LC})$$

in which L is the inductance of the coil and C the capacity.
In order to get best sensitivity and the shortest pulselengths the probe has to be

- tuned to the transmitter frequency
- the impedance should be matched to 50 Ω.

When properly tuned and matched, the probe has optimum sensitivity and the ^{13}C pulse lengths for example do not have to be measured on the sample but pre-determined values can be used instead. A large influence to the tuning and matching is caused by the dielectric constant of the sample. The reason for this is, that if the sample is introduced into the inner of the coil the dielectric constant in that part and hence the impedance of the coil changes. Care has be taken when solvents with high salt contents are used: Even in the case of perfect matching and tuning the pulselengths can be considerably longer (about 1.5 times for protons when using 150mM NaCl), although this effect largely depends on the nucleus and is most pronounced for proton frequencies. Tuning and matching can be performed in different ways: (A) the reflected power

of the probe during pulsing can be minimized. (B) Nowadays *wobbling* is used during which the frequency is swept continuously through resonance covering a bandwidth of 4-20 MHz:

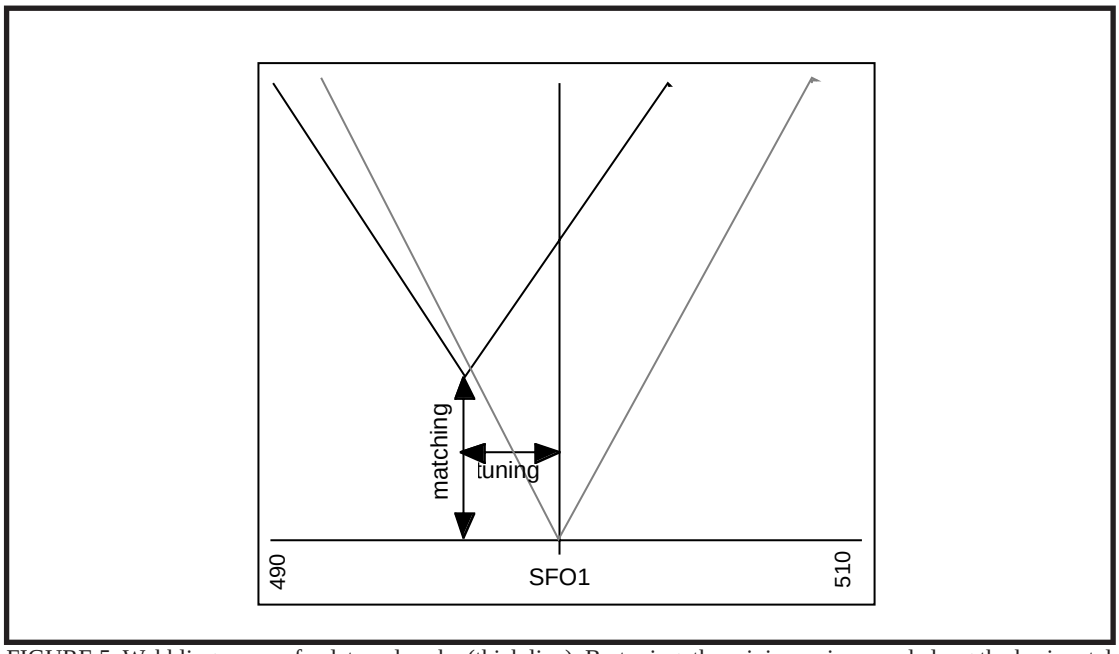

FIGURE 5. Wobbling curve of a detuned probe (thick line). By tuning, the minimum is moved along the horizontal axis and by matching the minimum becomes deeper. The optimum setting is shown as a dotted line.

Modern probes usually have two coils, an inner coil and a outer coil, and the inner one has higher sensitivity. An inverse probe, which is optimized for ^{1}H detection has ^{1}H frequency on the inner and ^{13}C frequency on the outer coil. The dual probe has higher sensitivity for ^{13}C, and consequently, the inner coil is used for 13C:

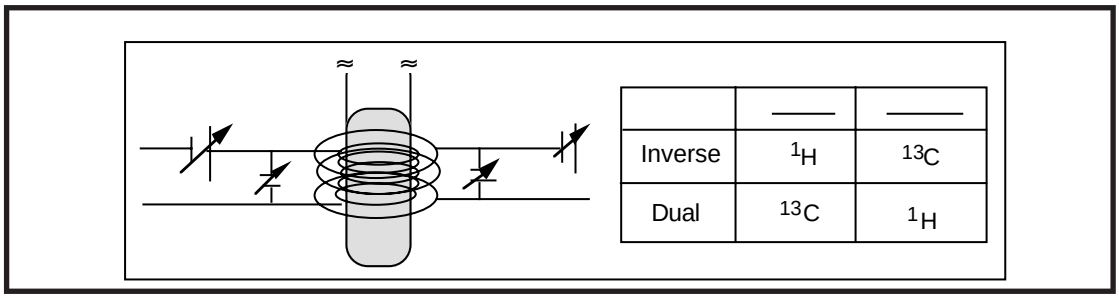

FIGURE 6. Arrangement of coils for inverse and direct carbon detection probeheads

Recently, so-called cryo-probes have been introduced. For these probes the RF-coil and the preamplifier is at He-temperature. Thereby, the thermal noise level is largely reduced (the amount of signal is even a little less than for a conventional probe) and the signal / noise in the absence of salt increased by almost a factor of four.

1.3 Adjusting the bandwidth of the recorded spectrum:

The bandwidth of the spectrum is determined by the dwell time (**dw**), the time spacing between recording of two consecutive data points (*vide supra*).

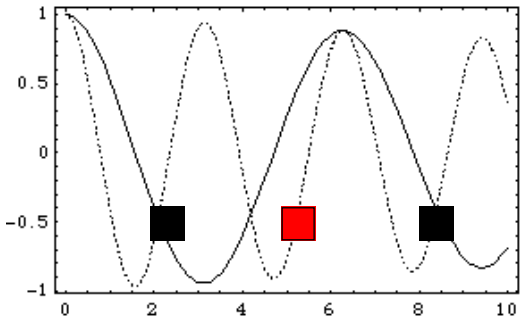

If the sampling rate is too low, the signal will still be sampled but will have a wrong frequency after Fourier transformation. Although analog or digital filter decrease the intensity of folded peaks, they may well be in the spectrum. On the other hand, signals may easily become lost, if the spectral width is set too small. The best way to prevent folding or loosing of signals is to record a preliminary experiment with a very large bandwidth (e.g. 30 ppm for ^{1}H) and then adjusting offset and spectral width to cover all signals. Usually 10% are added to the edges because the audio filters tend to decrease signal intensity of signals close to the edge. Folded peaks can be recognized, because usually they are not in-phase after adjustment of zero and first order phase correction. Alternatively, they change their position in the spectrum, when the offset is varied slightly.

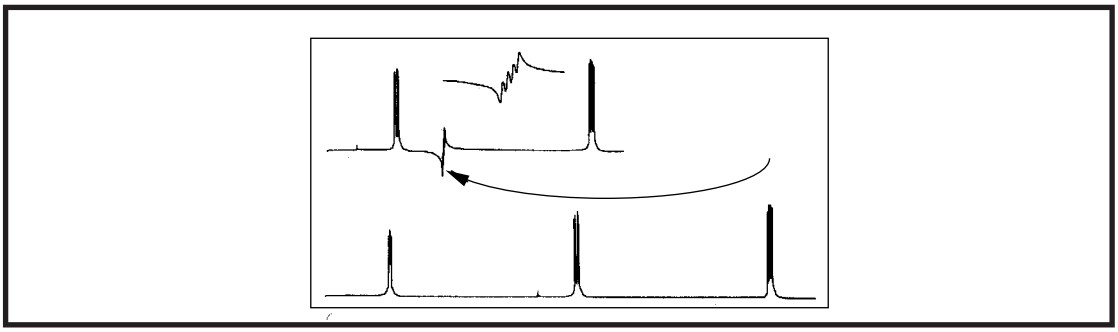

FIGURE 7. Effect of folding (aliasing) of signals.

However, care has to be taken on the newer instruments that use oversampling and digital filters. In this case the frequencies outside the sampled region will be almost completely removed by the digital filters!

1.4 Data processing:

Once the analog signal that comes from the coil has passed the amplifiers, it is converted into a number by the analog-to-digital converter (ADC). The resulting numbers which represent signal intensity *vs.* time [f(t)] are then converted into a spectrum that represents signal intensity *vs.* frequency [f(ω)] by use of the Fourier Transformation.

The Fourier theorem states that every periodic function may be decomposed into a series of sine- and cosine functions of different frequencies:

$$f(x) = a_0/2 + \sum_{n=1}^{\infty} a_n \cos nx + \sum_{n=1}^{\infty} b_n \sin nx$$

The Fourier decomposition therefore tells us which frequencies are present to

which amount (with which intensity). Using the integral form of the equation above

$$f(\omega) = 1/(\sqrt{2\pi}) \int_{-\infty}^{\infty} \lfloor a(t)\cos(\omega t) + b(t)\sin(\omega t) \rfloor dt$$

$$a(t) = 1/(\sqrt{2\pi}) \int_{-\infty}^{\infty} f(x)\cos(tx)dx$$

$$b(t) = 1/(\sqrt{2\pi}) \int_{-\infty} f(x)\sin(tx)dx$$

and utilizing the Euler relation the equation can be re-written as:

$$f(\omega) = 1/\sqrt{2\pi} \int_{-\infty}^{\infty} F(t)e^{-i\omega t}dt$$

This is the recipe to transform the signal function F(t) which for a single resonance is

$$F(t) = e^{-i\omega t} \bullet e^{-t/T2}$$

into the spectrum F(ω). Analogously, the FT can be used to transform from the frequency- into the time-domain:

$$F(t) = 1/(\sqrt{2\pi}) \int_{-\infty}^{\infty} f(\omega)e^{-i\omega t}d\omega$$

Note that this transformation is the *continuous* FT (used for continuous functions). Usually, the integral is split up again into the cosine- and sine terms corresponding to the cosine and sine transforms, so that

$$\int_{-\infty}^{\infty} f(t)e^{i\omega t}dt = Re[f(\omega)] + Im[f(\omega)]$$

$$= \int_{-\infty}^{\infty} f(t)\cos\omega t dt + i\int_{-\infty}^{\infty} f(t)\sin\omega t dt$$

Note that in FT-NMR the signal is sampled as *discrete* points. Hence, the discrete FT has to be utilized, which transforms a N-point time series consisting of values d_k into a N-point spectrum f:

$$f_n = 1/(\sqrt{N}) \sum_{k=0}^{N-1} d_k e^{-2\pi ikn/N}$$

The discrete FT is implemented in form of the very fast Cooley-Tukey algorithm. *The consequence of using this algorithm is, that the number of points the spectrum has must be a power of 2 (2^n).*

The next figure will summarize the FT of some important functions (the so-called Fourier pairs):

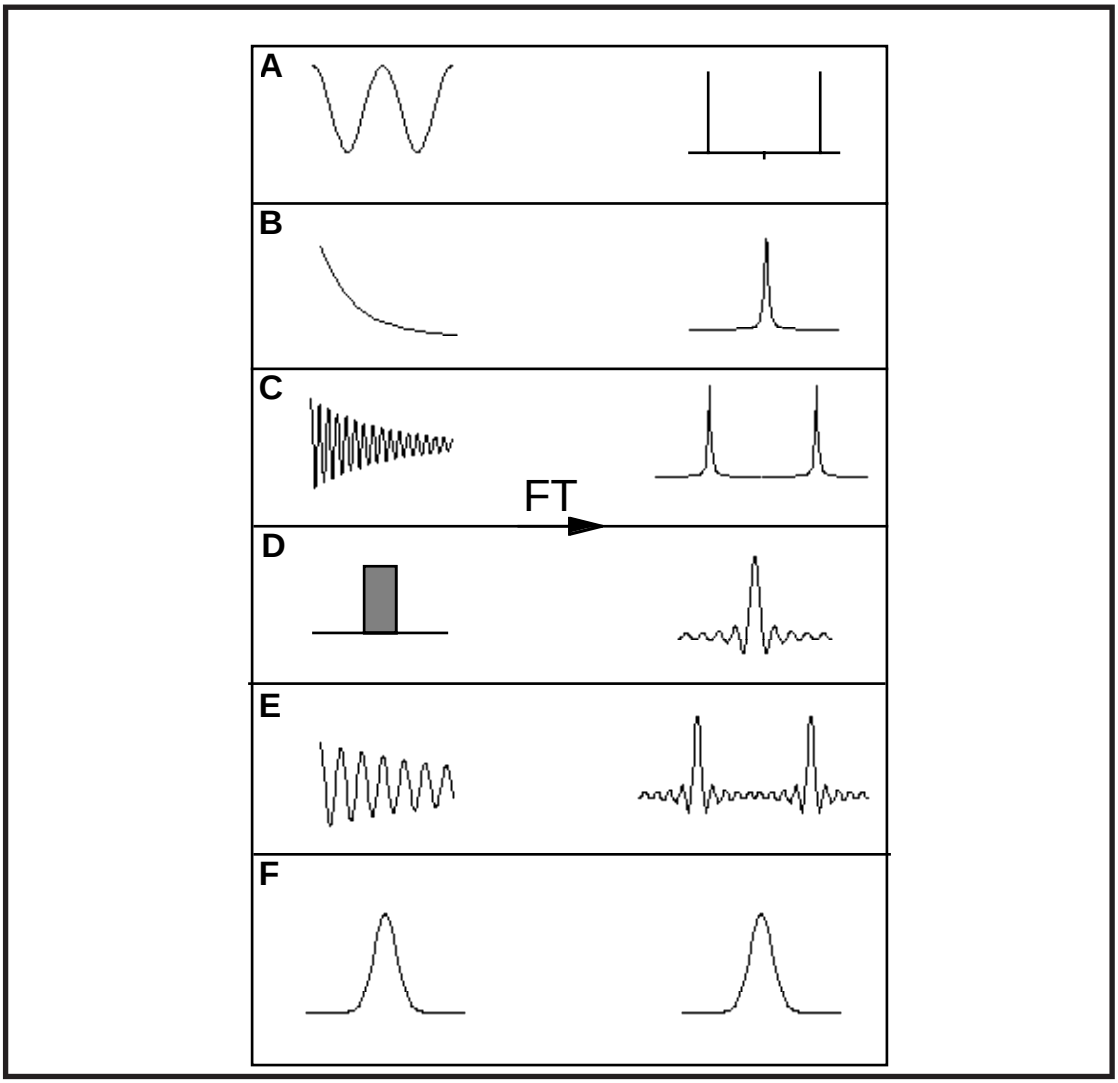

FIGURE 8. Results of different functions after Fourier transformation in frequency space.

The FT of a cosine-wave gives two delta-functions at the appropriate frequency (A). The FT of a decaying exponential gives a lorentzian function with a characteristic shape (B). The FT of a properly shimmed sample containing a single frequency gives two signals at the appropriate frequency with lorentzian lineshape (C). In fact the FT of (C) can be thought of a convolution of (A) and (B). The FT of a step function gives a sinc function

$$\mathrm{sinc}(x) = \sin(x)/x$$

The sinc function has characteristic wiggles outside the central frequency band (D). A FID that has not decayed properly can be thought of as a convolution of a step function with an exponential which is again convoluted with a cosine function. The FT gives a signal at the appropriate frequency but containing the wiggles arising from the sinc function (E). A gaussian function yields a gaussian function after FT. Signals that have not decayed to zero are common in 2D

NMR were the number of data points sampled is restricted. In these cases suitable window functions are used to force the signal to become zero towards the end of the FID.

1.5 Phase Correction

We have seen that the complex Fourier transform can be decomposed into a cosine transform and a sine transform that yield the real and imaginary parts of the signals, respectively. In practice, real and imaginary parts of the signal are stored in separate memory locations. However, the real part that is used for displaying the spectrum does not necessarily need to be purely absorptive:

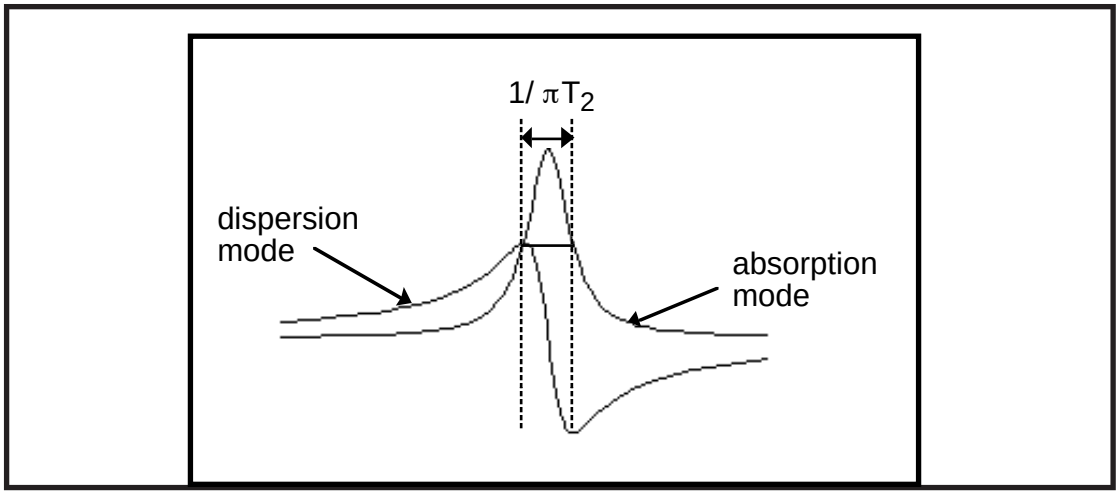

FIGURE 9. Signal in pure absorption or dispersion mode

Purely absorptive signals have a much narrower base, so that differentiation of peaks very close to each other is easier if they have been phased to yield purely absorptive line shape. Therefore, a phase-correction ϕ is needed to yield purely absorptive signals. It will do the following manipulations:

$$\mathrm{Re}(\Delta\Phi) = -\mathrm{Im}(\Delta\Phi = 0)\sin\phi + \mathrm{Re}(\Delta\Phi = 0)\cos\Phi$$
$$\mathrm{Im}(\Delta\Phi) = \mathrm{Re}(\Delta\Phi = 0)\sin\phi + \mathrm{Im}(\Delta\Phi = 0)\cos\Phi$$

with $\mathrm{Re}(\Delta\phi=0)$ and $\mathrm{Re}(\Delta\phi)$ being the real part of each data point before and after the phase correction, respectively.

The phase of the signals after Fourier Transformation depends on the first point of the FID. If the oscillation of the signal of interest is purely cosine-modulated, the signal will have pure absorptive line shape. If the signal starts as a pure sine-modulated oscillation, the line shape will be purely dispersive:

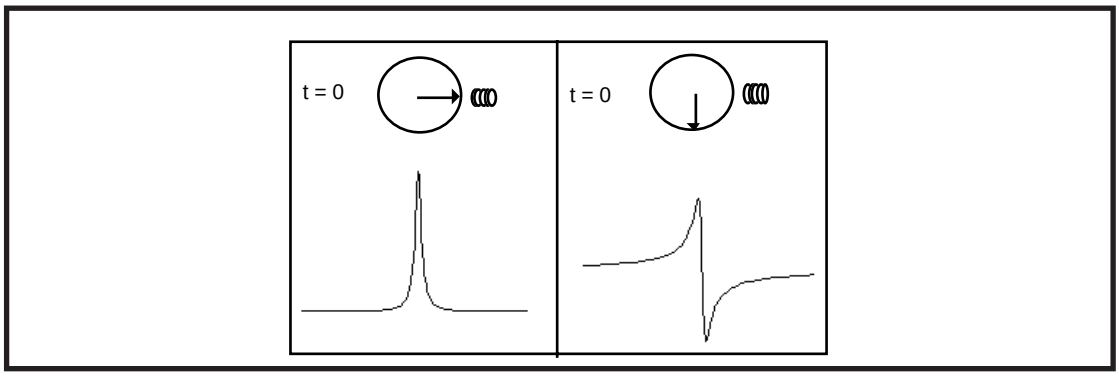

FIGURE 10. The relative phase of the magnetization with respect to the receiver coil determines the phase of the signal after Fourier transformation

There are two different types of phase-correction. The *zero-order phase correction* applies the phase change to all signals in the same way. The *first order phase correction* applies a phase change, whose amount increases linearly with the distance to the reference signal (marked with an arrow in the figure below):

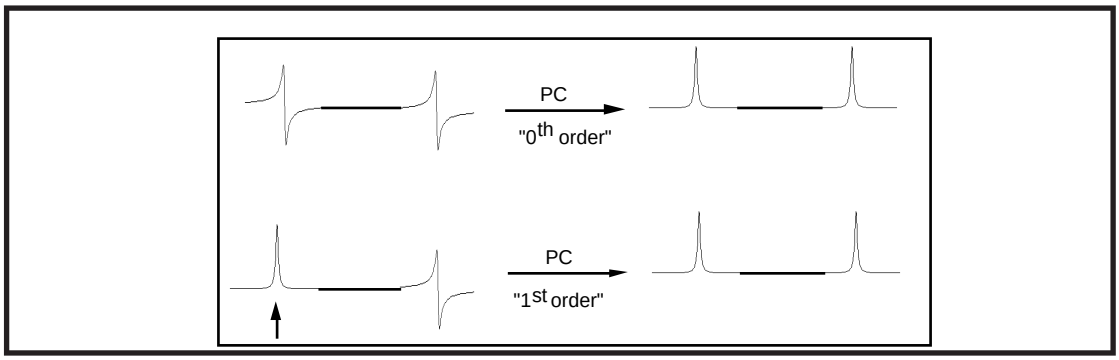

FIGURE 11. Top: The zero order phase correction changes the signal phase for all signals by the same amount. Lower: For the first order phase correction the applied correction depends on the frequency difference to the reference signal (marked by an arrow).

What is the origin of the varying phase in the spectra? The zero-order arises because the absolute phase of the signals at the detector depends on the cable lengths etc. The linear dependence of the phase of the signals has a more complicated reason. In a theoretical 1D experiment, acquisition of the FID would start immediately after application of the pulse. However, in a real experiment there is a protection delay (called **de** on Bruker instruments), to wait for the pulse ring-down (pulsing and detection of the signal is done on the same coil, so that there must be a protection delay after the pulse):

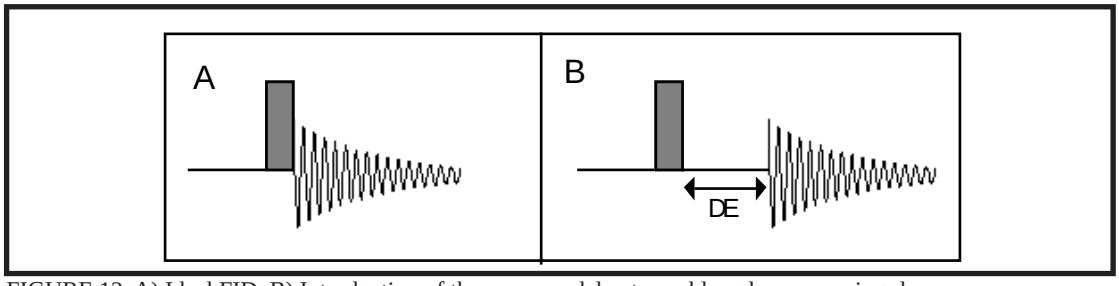

FIGURE 12. A) Ideal FID. B) Introduction of the pre-scan delay to enable pulse power ring-down.

During the protection delay **de**, the spins start to precess. The precession frequency depends on the offset of the signal frequency, e.g. the distance of the signal from the middle of the spectrum. The first-order phase correction reverses the phase change due to shift evolution during **de** and is therefore linearly dependent on the frequency of the signal:

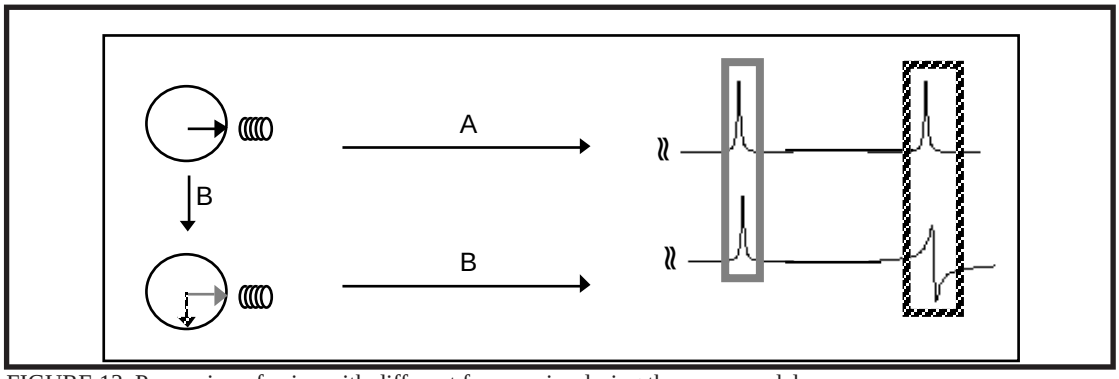

FIGURE 13. Precession of spins with different frequencies during the pre-scan delay.

To adjust the phase, go into the phase correction mode, define a signal at one end of the spectrum as the reference phase, use the zero-order phase correction to phase it to absorption and then use the first order phase-correction to phase the signal at the other edge of the spectrum. All other *but folded signals* will then be in phase.

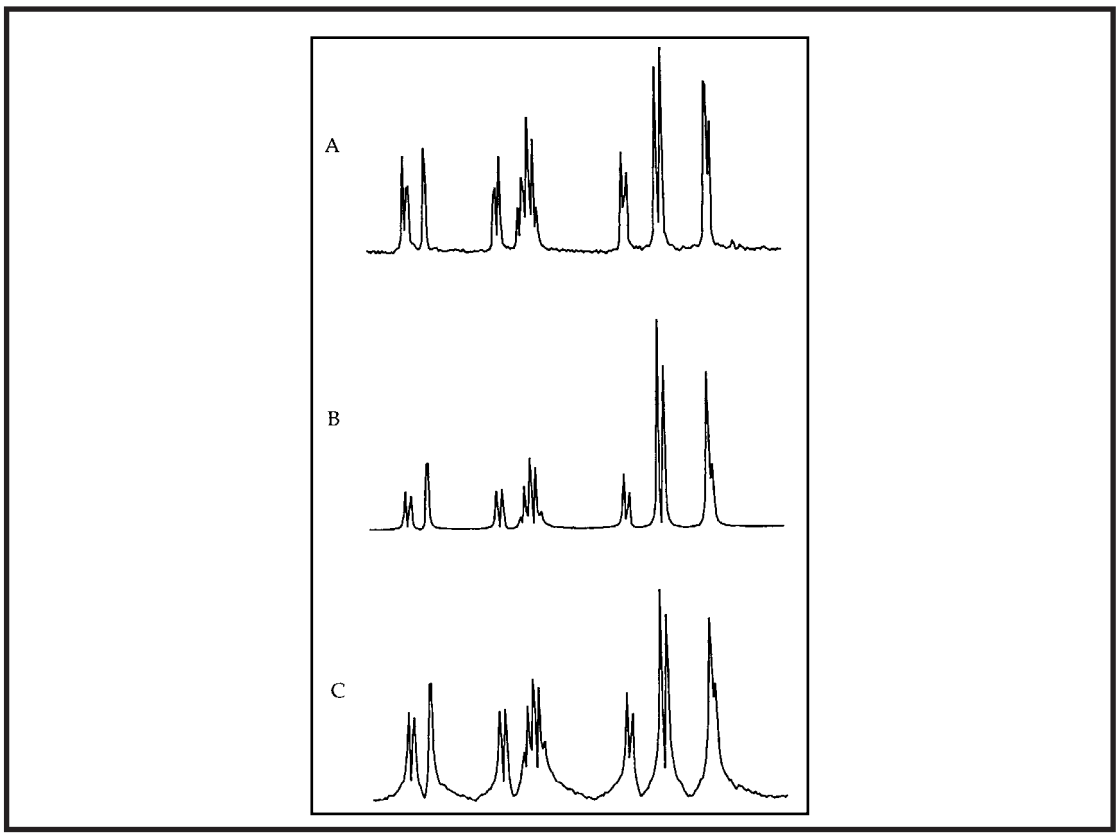

FIGURE 14. (A) normal FT with phase correction.(B) Power spectrum. (C) Magnitude calculation.

When spectra cannot be phased a magnitude calculation or the power spectrum ($PS=M^2$) is used:

$$M = \sqrt{Re^2 + Im^2}$$

The magnitude calculation yields much broader peaks at the base. Both, magnitude and power calculation lead to a severe loss in resolution.

1.6 Zero-filling and the resolution of the spectrum

The resolution that can be obtained from a spectrum is determined by two factors:

- the natural line width that is related to the transverse relaxation time (*homogenous broadening*) and which is due to efficient dipolar coupling of the spins. Fast transverse relaxation may also be caused by field inhomogeneity (*inhomogenous broadening*).
- the number of points which are used to digitize the signal. If the number of points after FT (on Bruker instruments the parameter **SI**) is smaller than the number of acquired data points (on Bruker instruments the parameter **TD**), the signal can not be digitized properly, and the resolution is very low:

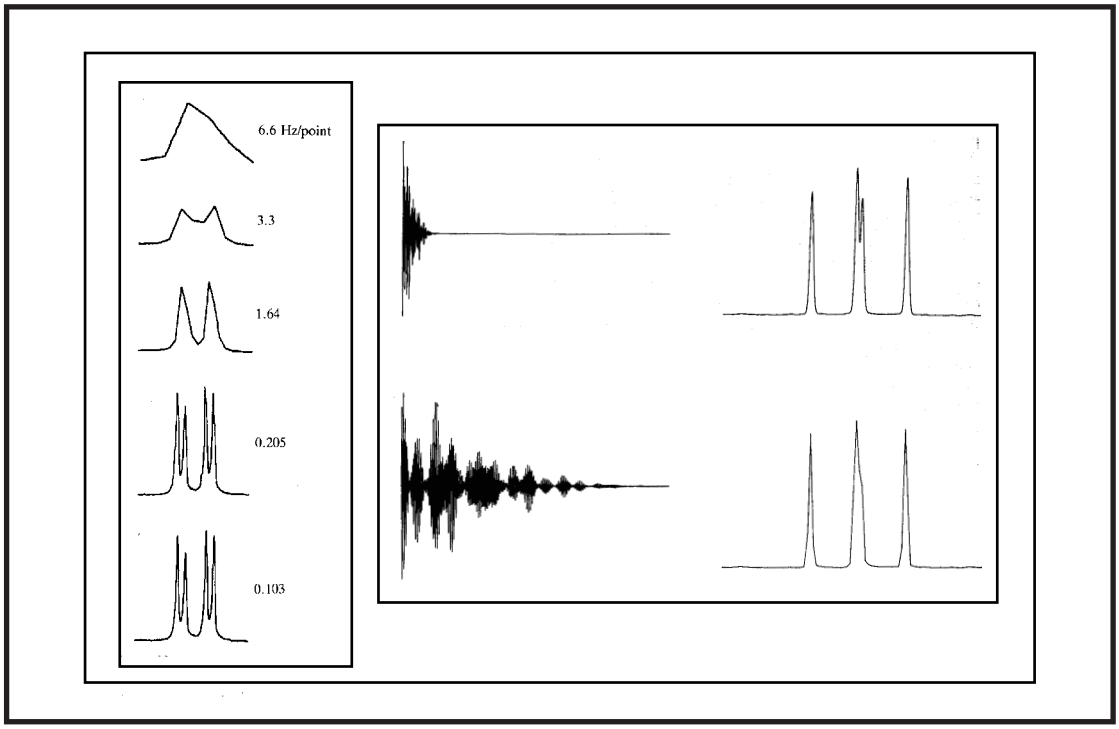

FIGURE 15. Left:Effect of increasing number of data points after FT. Right: Spectrum without zero-filling (lower trace) and after zero filling with 5*TD (upper trace).

The theoretical resolution obtainable from the FID can be calculated as

$$Res = SW (Hz) / TD$$

neglecting relaxation effects.

Provided that the FID has decayed to zero towards its end it is useful to

append zeros to the FID. Adding zeros once (that means making **si** = 2***td**) gives a significant improvement in resolution, adding more zeros gives only cosmetic effects but does not add more information.
When the FID has not decayed to zero, adding zeros introduces a step function that causes sinc-type artifacts (wiggles).

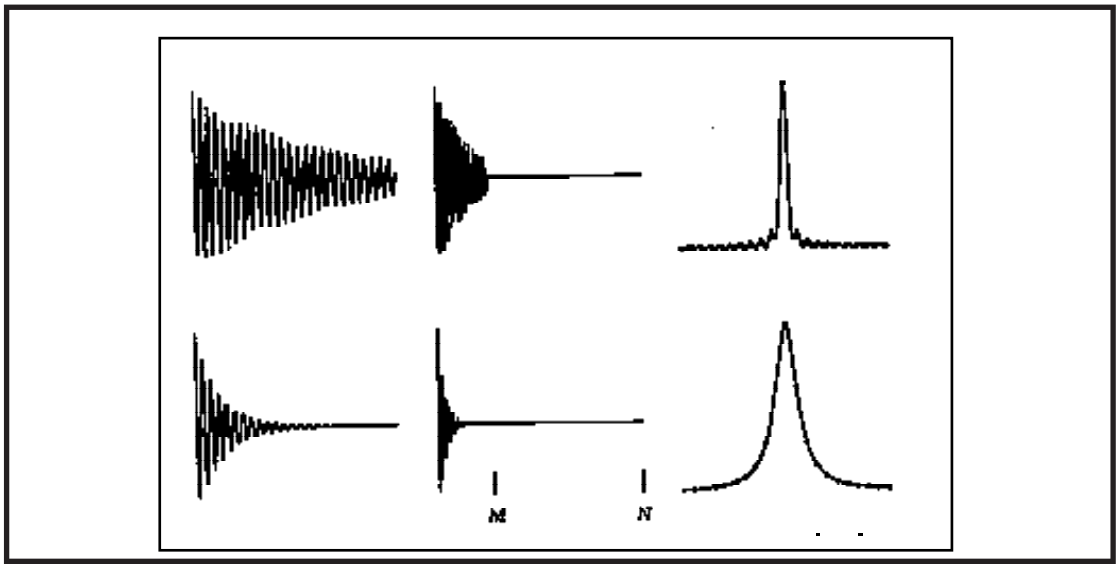

FIGURE 16. Top: Resulting FT of a FID that did not decay to zero in comparison to a fast decaying FID (bottom)

1.7 Resolution enhancement and S/N improvement

The resolution is determined by the transverse relaxation time T2 of the spins. A long transverse relaxation time leads to a slowly decaying, fast relaxation to a quickly decaying FID. Therefore, the resolution is determined by the amount of signal which remains towards the end of the FID. Any data manipulation, e.g. multiplying the FID with a increasing exponential ($e^{t/x}$) will improve the resolution. Conversely, the S/N is determined by the amount of signal at the beginning of the FID. Most manipulations that improve resolution lead to a loss in S/N.
In ^{13}C nmr, S/N is comparably bad, whereas resolution is rarely a problem. Data processing of ^{13}C spectra therefore usually is performed with exponential multiplication with a decaying exponential (**em** with **LB**>=1). In ^{1}H nmr, S/N is rarely a problem, but good resolution is required, and data could be multiplied with an increasing exponential (**em** with **LB**< 0).
Application of the window function amounts to multiplying the FID data point d_k by

$$d_k' = d_k * a_k$$

in which k runs from 0 to TD (the total number of data points).
There are number of so-called window functions that are aimed at either improving resolution or S/N and their effect on a spectrum is shown in the figure below:

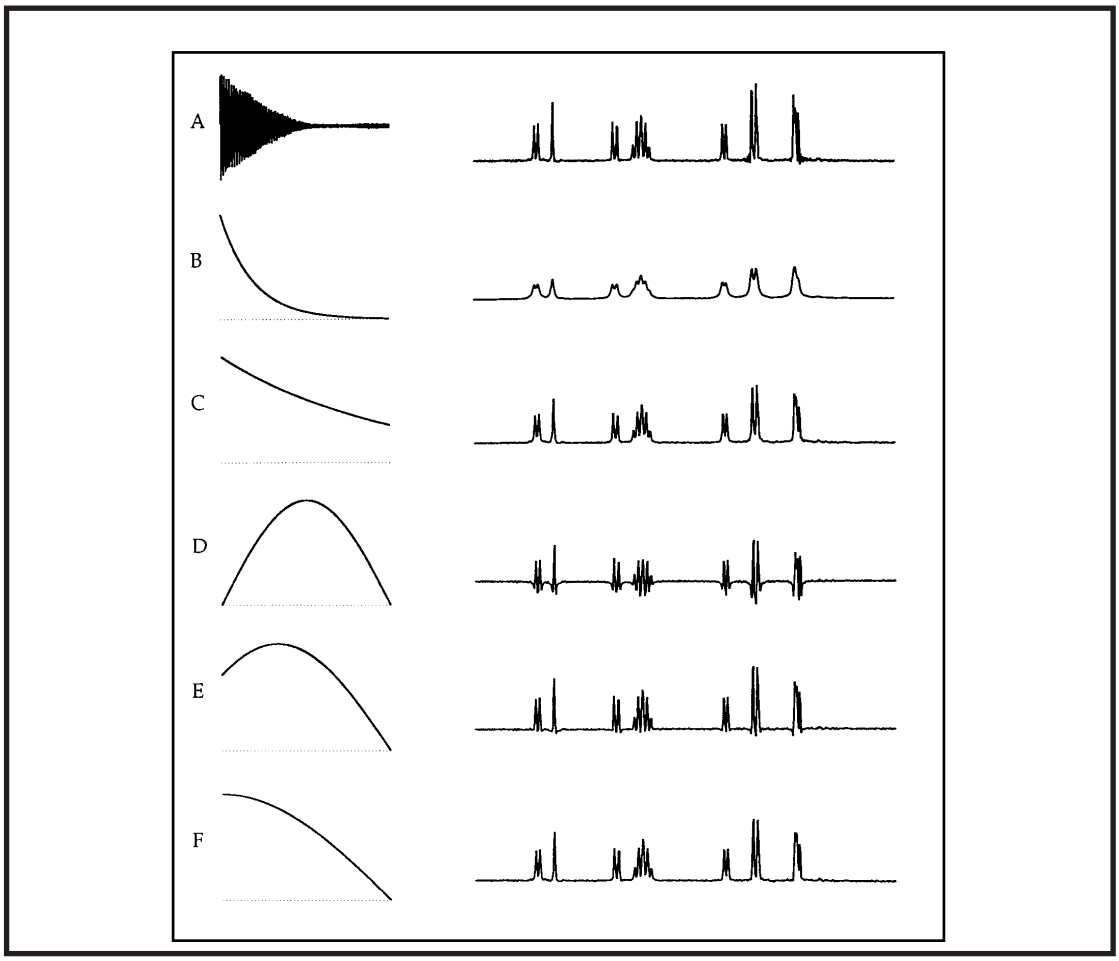

FIGURE 17. (A) raw spectrum after FT. (B)Multiplication with exponential,LB=5.(C) as (B), but LB=1. (D) sine-bell.(E) 45 degree shifted sine-bell.(F)90 degree shifted sine-bell.

Important, frequently used window functions are

1.7.1 Exponential multiplication:

The line broadening constant lb can be positive (sensitivity enhancement) or negative (resolution enhancement). A lorentzian line of width W will have a width of W + LB Hz after apodization. It is mainly used for processing ^{13}C data, for which sensitivity enhancement is desired but where resolution is rarely a problem (use lb = 1-2 Hz).

$$a_k = e^{-\pi lbk\Delta t}$$

1.7.2 Lorentz-to-Gauss transformation:

This a combination of exponential and gaussian multiplication.

$$a_k = e^{\pi lbk\Delta t} \bullet e^{-gb(k\Delta t)^2}$$

The factor lb determines the broadening, whereas gb determines the center of the maximum of the gaussian curve. When gb is set 0.33, the maximum of the

function occurs after 1/3 of the acquisition time.

By this multiplication, the Lorentzian lineshape is converted into a gaussian lineshape, which has a narrower base:

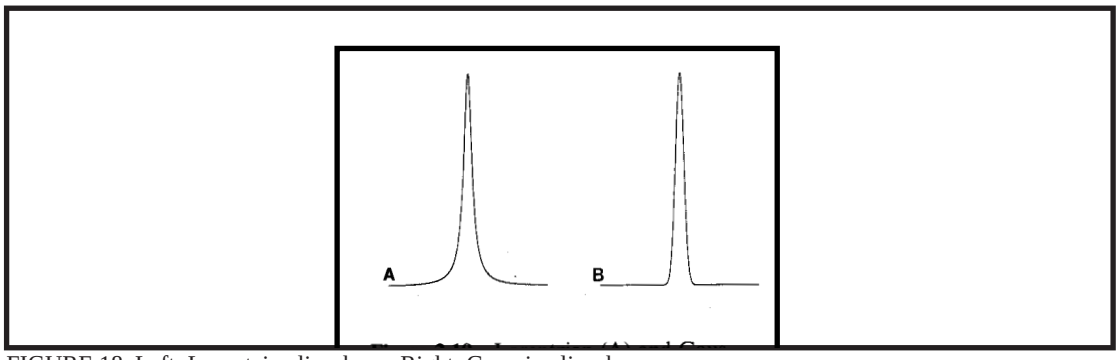

FIGURE 18. Left: Lorentzian lineshape. Right: Gaussian lineshape.

1.7.3 Sine-Bell apodization:

Sine-bell apodization is frequently used in 2D NMR processing. A pure sine-bell corresponds to the first half-lobe of a sine-wave and multiplies the FID such that it brought to zero towards the end. However, such a function also sets the first data points to zero and hence leads to severe loss of S/N and introduces negative wiggles at the bases of the signals in addition to a strong improvement in resolution. Shifting the sine-bell by 90 degrees (a cosine-bell) means that the function used starts of the maximum of the first lobe and extends to zero towards the end of the FID. This is usually used for FIDs that have maximum signal in the first data points (NOESY, HSQC). A pure sine-bell is used for such experiment in which the FID does not have maximum signal in the first points (such as COSY) or for improving magnitude data (HMBC):

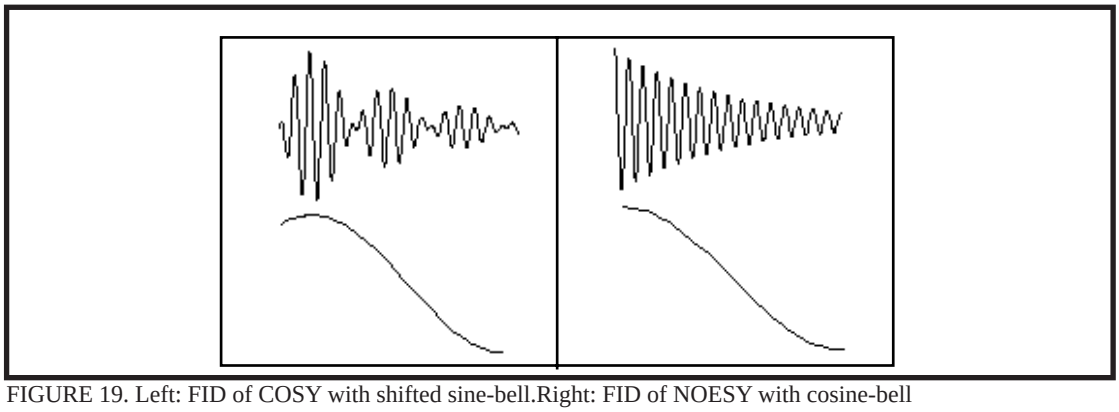

FIGURE 19. Left: FID of COSY with shifted sine-bell.Right: FID of NOESY with cosine-bell

The influence of the parameters on the window functions is shown below:

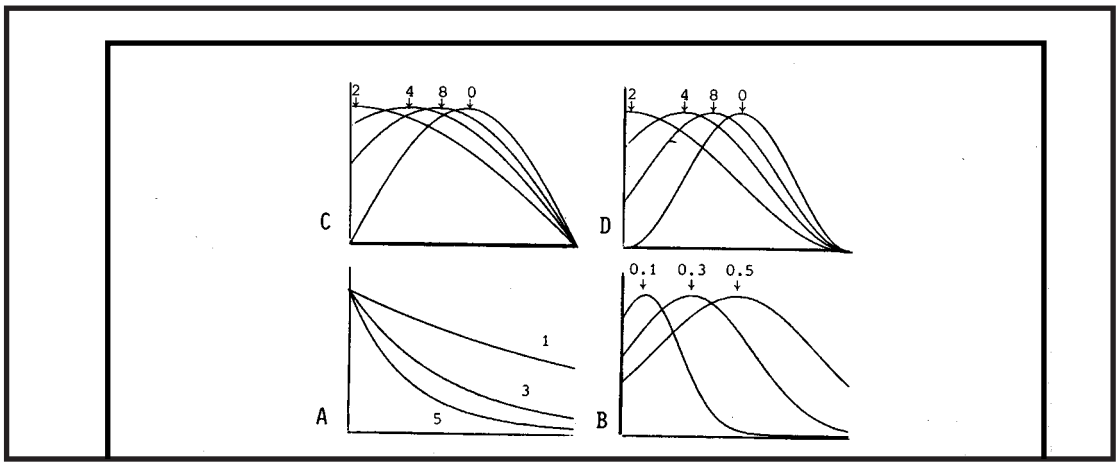

FIGURE 20. Different window functions. A: exponential multiplication with LB=1,3,5Hz. B) Lorentz-Gaussian transformation with LB=-5 and GB =0.1, 0.3, 0.5 Hz. C) Sine-bell shifted by 0, π/2, π/4, π/8. D) Sine-bell squared shifted by 0, π/2, π/4, π/8.

An often encountered problem is truncation of the signal, which means, that the signal is not sampled until it has completely decayed. This is the case, when the data matrices, e.g. the number of data points, must be kept to a reasonable low value, e.g. in 2D NMR, or when one very slowly decaying line is present in the spectrum. Then the signal can be described by a superposition of an oscillation, an exponential and a square function. The contribution from the square function will introduce wiggles at the base of the signals which are originating from the sinc function. Such a problem can be circumvented if the FID is multiplied with a function that decays to zero at the end of the FID, e.g. an decaying exponential or a cosine bell function.

1.8 Baseline Correction

Baselines that are not flat are a major problem in FT-NMR. Firstly, spectra with non-flat baselines give wrong integrals. Secondly, in spectra with baseline roll small signals may not be recognized. Thirdly, those spectra are difficult to phase. Furthermore, peak-picking routines need a threshold for minimal signal intensity and such peak-picking for tiny signals is not possible when the baseline is not flat. There are many reasons for bad baselines. In general, baseline distortions are caused by distortions of the first points of the FID. A frequent source is receiver overload, that means, that the receiver gain has been set too high. The ADC (analog-to-digital converter) can only digitize a certain maximal signal intensity. On the Bruker instruments, that means that the FID must fit into the acquisition window completely. If the signal intensity is larger, the first points of the FID are clipped:

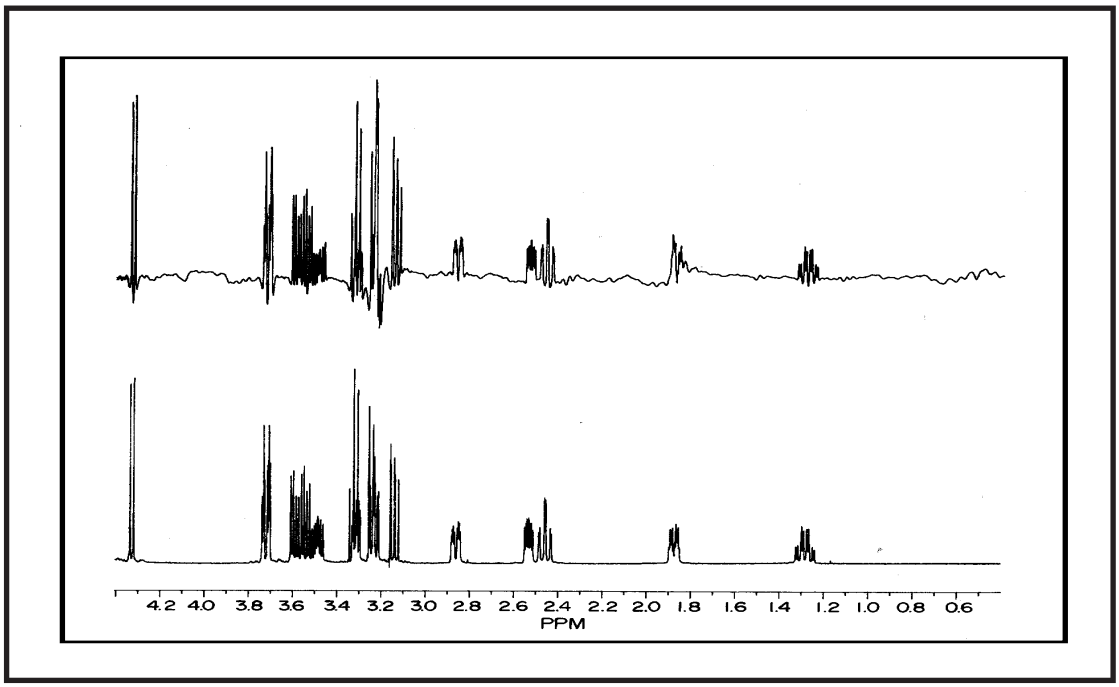

FIGURE 21. lower trace: spectrum after FT of an FID with correctly adjusted receiver gain. Top: Spectrum after FT of a clipped FID.

Such a baseline cannot be corrected, and the measurement must be repeated with a lower receiver gain setting. Other baseline problems, like baseline-drift (non-horizontal but flat baseline) or baseline-curvature can be corrected, on Bruker machines either automatically (with the command **abs**) or manually. Oversampling has shown to reduce baseline problems in the directly sampled frequency dimensions dramatically.

Frequently, one can recognize which data point is distorted from the shape of the baseline. A wrong first data point leads to an offset, a wrong second one to a half-wave, a wrong third one to a full wave, etc. In principle, spectra with (a few) wrong first data points can still be used, if *linear back-prediction* of the first data points is used.

1.9 Linear prediction:

For exponential decaying signals that are sampled at constant spacing (as is usually the case for NMR) new data points can be predicted. The reason behind this is that one can assume that new data points can be represented as a fixed linear combination of immediately preceding values. LP provides a means of fitting a time series to a number of decaying sinusoids. Provided that S/N is good the number of points can be doubled with LP (or the measuring time can be halved to achieve the same resolution). Predicting more points severely changes the lineshape of the signals and is not recommended. LP gives very good results for COSY and HSQC data. Especially in the case of the

COSY, antiphase signals cancel when the resolution is low. Linear prediction in these cases not only increases the resolution but also increases the amount of signal!

With modern computing power it is performed rather quickly and the results can be astonishing good. Remember that in order to double the resolution in the indirect dimension the number of experiments in a 2D spectrum and hence the acquisition time has to be doubled. Linear prediction may achieve the same goal in a few seconds. In the case of constant-time experiments, mirror-image linear prediction may be applied which is capable to predict N points to 4*N points.

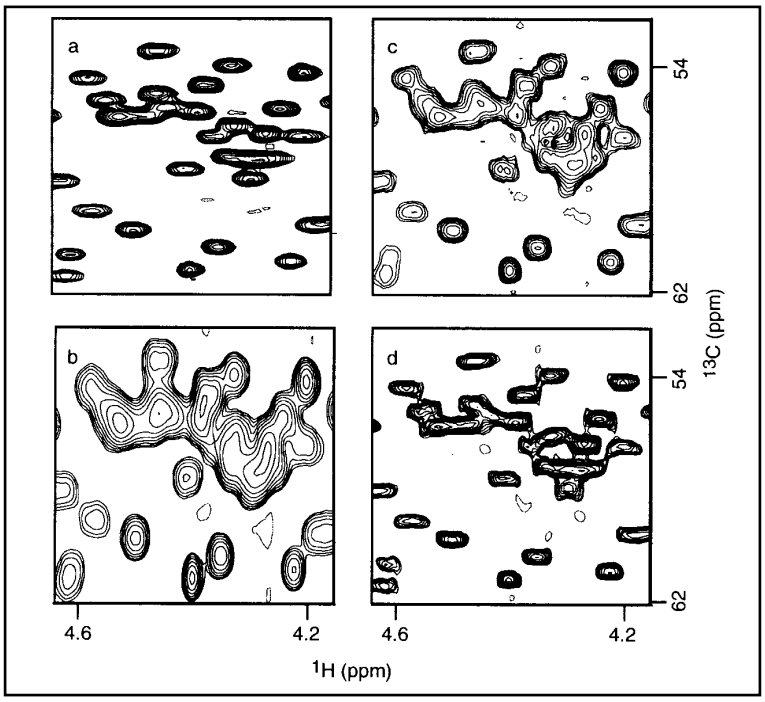

FIGURE 22. ct-HSQC spectra (A) 240 points.(B) 64 points.(C) LP to 128 points.(D) mirror -image LP to 240 points.

1. THE CHEMICAL SHIFT:

Soon after the discovery of the phenomenon of nuclear magnetic resonance scientists realized that more than a single line was observed for protons in a organic molecule such as ethanol. In liquid (isotropic) phase, this splitting of lines is caused by the chemical shift due to the Zeeman interaction and to scalar spin,spin couplings.

As we have seen before, the resonance frequency depends on the strength of the applied static field and on the gyromagnetic ratio of the nucleus:

$$\omega = \gamma B$$

However, the field strength to be considered is not exactly the strength of the applied magnetic field *in vacuo* but is locally modified by the electronic environment of the nucleus. What is really important is the *effective* field strength at the nucleus site. Many different mechanisms are known that may influence the exact strength of field at the nucleus:

$$\sigma = \sigma_{dia}(\text{local}) + \sigma_{para}(\text{local}) + \sigma_m + \sigma_{rc} + \sigma_{ef} + \sigma_{solv}$$

Herein is

- σ_{dia} the diamagnetic contribution
- σ_{para} the paramagnetic contribution
- σ_m the neighbor anisotropy effect
- σ_{rc} the ring-current contribution
- σ_{ef} the electric field effect
- σ_{solv} the solvent effect

1.1 The diamagnetic effect:

The nucleus is surrounded by an electron cloud. The static magnetic field B_o causes the electrons to precess about the axis of the magnetic field. Thereby, a current is created that itself builds up a magnetic field. The direction of the induced field is opposed to the static field and acts to decrease the strength of the latter:

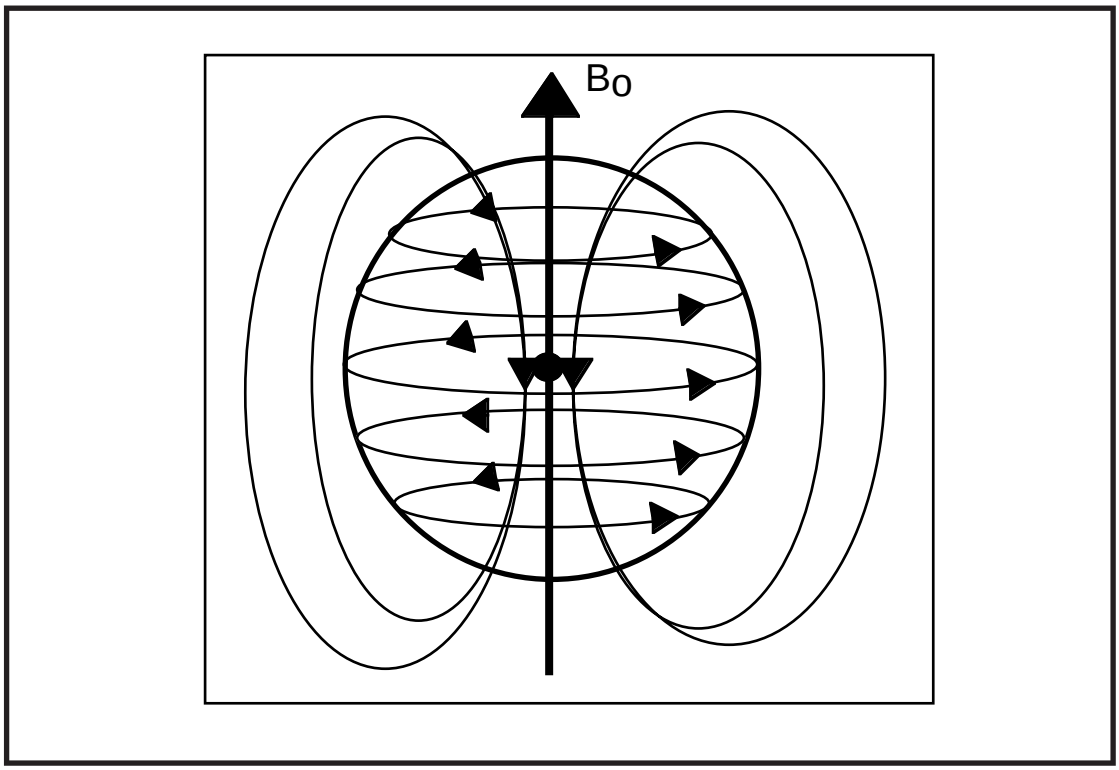

FIGURE 1.

This effect is called the **Lamb Shift**. It can be calculated as

$$\sigma_{iso} = \mu_0 e^2 / 3m_e \bullet \int_0^\infty r\rho(\vec{r})dr$$

in which ρ(r) is the electron density, r the distance of the electron from the nucleus, e the charge and m_e the mass of the electron. One important statement of this so-called **Biot-Savart** Law is that the electron density at larger distances from the nucleus is of importance for the counter-acting field.

The diamagnetic shielding describes the behavior of spherically distributed electrons such as electrons from the s-orbital of protons. It is therefore the dominant term for proton shifts but less important for the heavier nuclei.

1.2 The paramagnetic term:

The paramagnetic term serves to correct for the disturbance of the spherical rotation of electrons. This may be caused by the formation of bonds. Quantum-mechanically speaking, the paramagnetic term may be calculated by finding the way by which the electron wave functions are modified by the magnetic field. Such a modification of the wave function takes place because properties

of exited states (contributions from the LUMO, lowest unoccupied molecular orbital) are mixed into ground state wave (esp. the HOMO, highest occupied molecular orbital) functions through application of the static field. The electron distribution in such an excited state wavefunction is very different from that encountered in the ground state giving rise to a large change in the shielding:

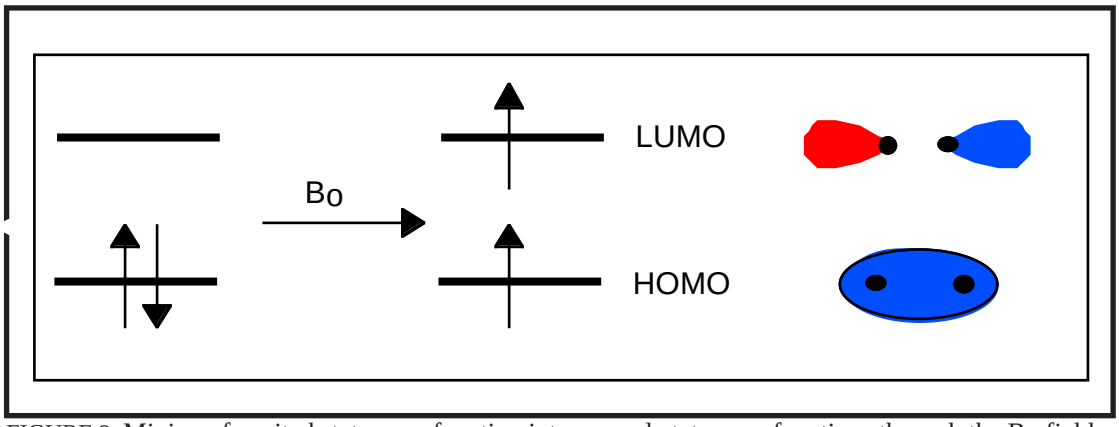

FIGURE 2. Mixing of excited state wavefunction into ground-state wavefunctions through the Bo field.

The calculation of the diamagnetic shift is rather involved and requires the exact knowledge of the excited wave functions. For ^{13}C it is given as

$$\sigma_i^{para} = (\mu_0 \mu_B^2) / 2\pi \Delta E \langle r^{-3} \rangle \left[Q_i + \sum_{i \neq j} Q_j \right]$$

In this formula, ΔE is the energy difference between HOMO and LUMO , r the radius of the 2p orbital and the Q describe electron densities and bond orders. Very low-lying ground-state wavefunctions are usually paired with rather high lying excited state wave functions such that the resulting energy separation is comparably large. Since the paramagnetic shift is inversely proportional to the energy gap, the shift is large when the gap is small. Reactivities of compounds are often related to HOMO/LUMO energy separations and chemical shifts have therefore been successfully used to screen for reactive compounds.

The paramagnetic term requires non-spherical electron distribution (a non-vanishing angular momentum) and can hence only be applied to nuclei that have non-s orbital electrons. It is the dominant term for all nuclei other than protons. The shift range due to the paramagnetic contribution is larger than for the diamagnetic shift. This is obvious from the huge shift ranges (e.g. several thousand ppm for ^{57}Fe compared to approx. 15 ppm for ^{1}H).

Substituents influence the chemical shift because they change the electron den-

sity at the proton nucleus via inductive effects. This is fairly evident from a comparison of a oxygen and a carbon bound proton:

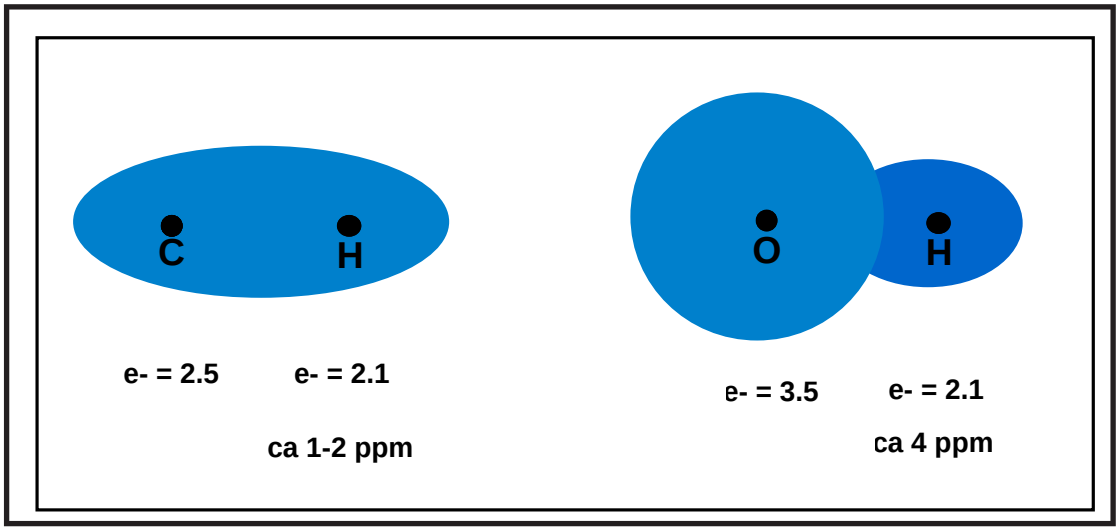

FIGURE 3. Dependence of chemical shielding upon orientation of carbonyl bond toi the external field

1.3 Chemical shift anisotropy:

The distribution of the electrons about the nucleus is usually non-spherically. The magnitude of the shielding therefore depends on the relative orientation of the nucleus with respect to the static field. For sp^3 carbons the nuclei are tetrahedrally coordinated and the electron distribution is almost invariant under rotation. For sp^2 carbons such as aromatic or carbonyl nuclei the shielding highly depends on the orientation of the bond relative to the static field:

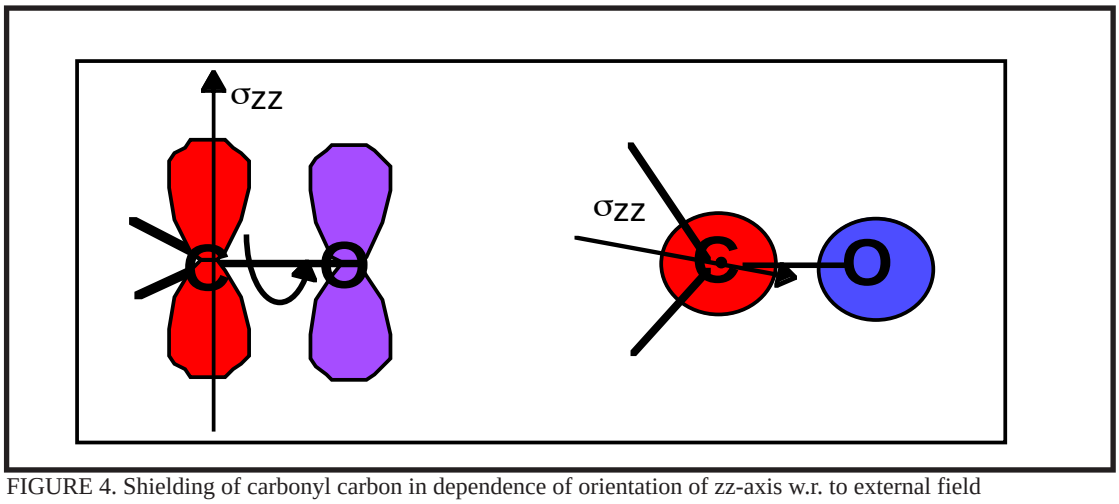

FIGURE 4. Shielding of carbonyl carbon in dependence of orientation of zz-axis w.r. to external field

The chemical shielding is described by the chemical shift *tensor*, which transforms the static field into the effective field (see add. mat.) The zz axis is usually taken as the axis with the largest shielding. Due to the shielding the direction of the effective field B_{eff} may deviate from the direction of the static

field B_o. Since the molecule rotates quickly in solution the observed chemical shift is a average over the shifts coresponding to the different orientations (isotropic chemical shift). However, when rotation is hindered, as is the case in the solid state, the line is significantly broadened. In liquids this effect contributes to relaxation, and is the major relaxation mechanism for non-protonated carbons. Chemical shift anisotropy values can be measured from solid-state NMR.

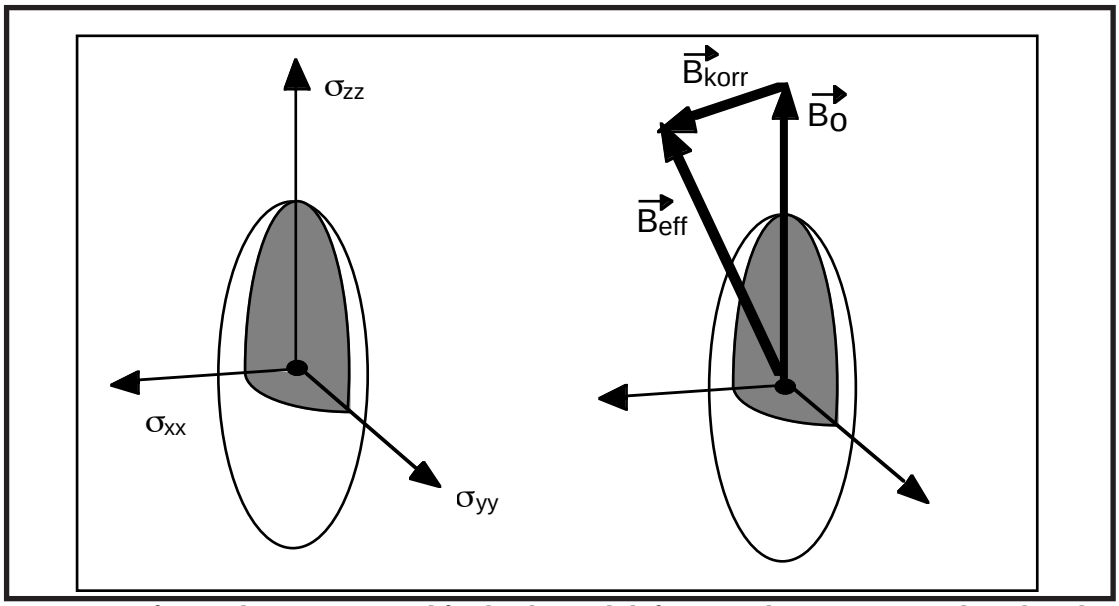

FIGURE 5. Left: Coordinate system used for the chemical shift tensor. The zz axis points along the value of the largest shielding, xx and yy orthogonal to zz. Right: Direction of the static and the effective field.

The value of the chemical shift for the isotropic case can be taken as 1/3 of the trace

$$\sigma_{iso} = 1/3(\sigma_{xx} + \sigma_{yy} + \sigma_{zz})$$

1.4 Magnetic anisotropy of neighboring bonds and ring current shifts:

Some types of neighboring bonds create an additional magnetic field which is anisotropic in space. An example is a triple bond. The π electrons of the triple bond form an electron cloud that extends around the bond axis in form of a tube. The magnetic field forces the electrons to rotate about the bond axis creating a magnetic field whose direction is along the bond axis and which again counteracts the static field. A similar counteracting field is formed in the π-cloud of aromatic systems. Such anisotropies can dramatically change the appearance of proton spectra. They usually increase the dispersion of proton spectra. However, in order to give substantial effects the influenced protons

must be sterically fixed in relative to the anisotropic group. This is the case for folded proteins that do adopt a unique structure. Therefore, one can sometimes judge from the signal dispersion of 1D proton spectra whether a protein is folded or random coil.

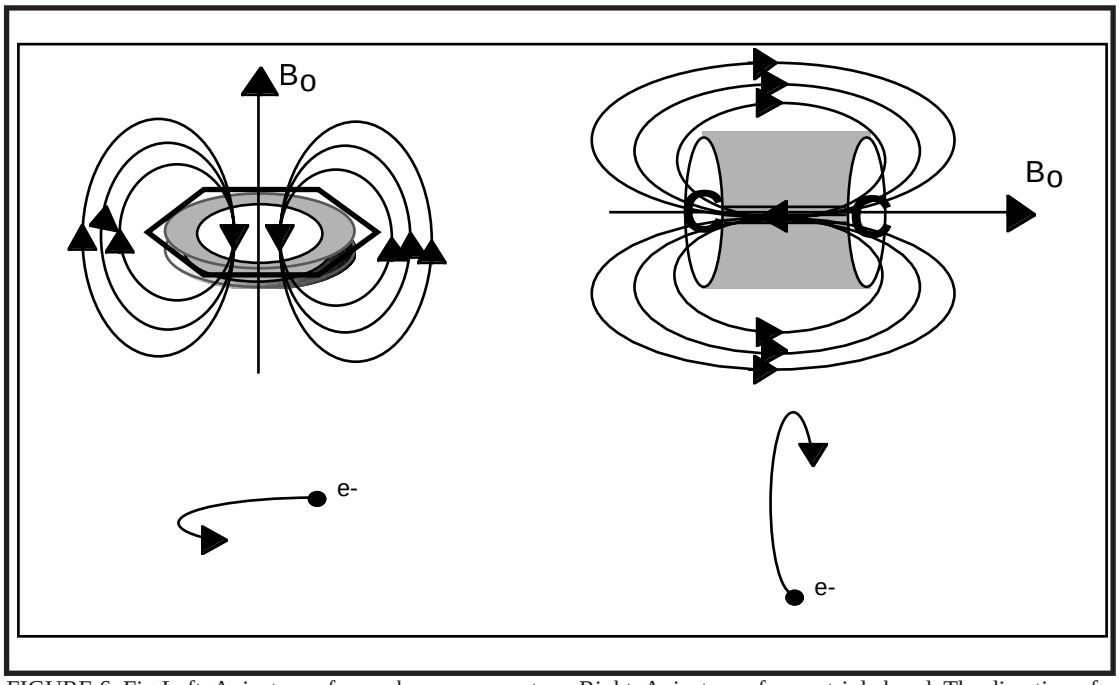

FIGURE 6. Fig:Left: Anisotropy from a benzene π system. Right: Anisotropy from a triple bond. The direction of the induced electron flow is indicated below

The observed shifts can be either up-field or down-field, depending on the exact postion of the proton. The following figure shows regions of increasing (+) or decreasing (-) field:

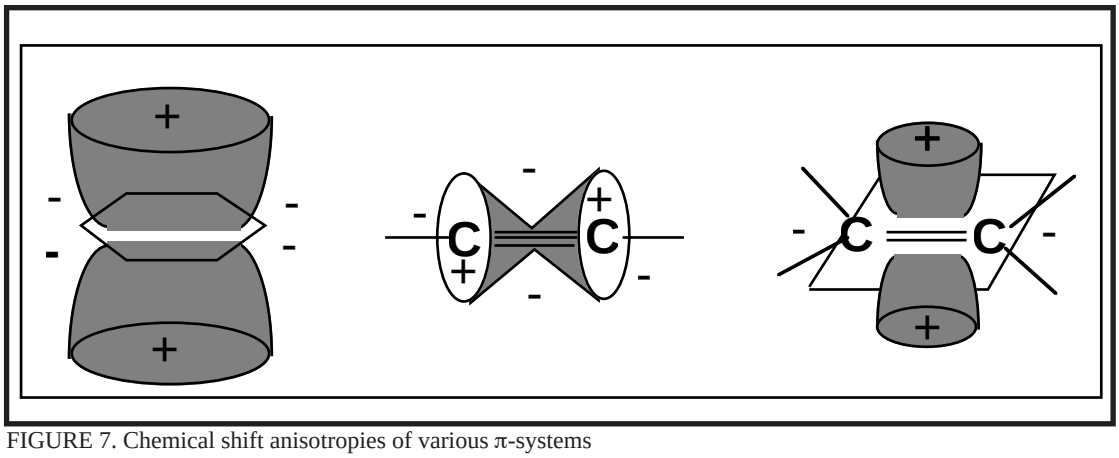

FIGURE 7. Chemical shift anisotropies of various π-systems

These effects can be dramatically. Aliphatic Protons that are fixed in space above the plane of an aromatic ring can be shifted to values below 0 ppm, those in the plane to values higher than 10 ppm.

The chemical shift anisotropy for a triple bond can be calculated as

$$\Delta\sigma = 1/3r^3[(\chi_{II} - \chi_{\perp})(3\cos\theta)]1/(4\pi)$$

where theta is the angle with respect to the bond axis, r the distance to the centre and χ the magnetic susceptibilities parallel and perpendicular to the bond axis. As can be seen from the formula, the effect depends strongly on the distance and orientation.

1.5 Electric field gradients:

Strongly polar groups create intramolecular electric fields. This has the effect of distorting electron density in the rest of the molecule and will hence influence the chemical shifts.

1.6 Hydrogen bonds:

Hydrogen bonds decrease the electron density at the involved proton site and hence leads to a high-frequency shift. The effect is especially pronounced for symmetric hydrogen bonds (those in which the distance of the proton is equal to both acceptors). Protons that are hydrogen bonded usually be easily recognized from their shift. Their shift is highly temperature, concentration and solvent dependent. Protons that are part of hydrogen bonds do exchange much more slowly with labile solvent deuterons and can therefore be differentiated from others. This is used in protein NMR to identify β-sheets or α–helices that display extended hydrogen bond networks.

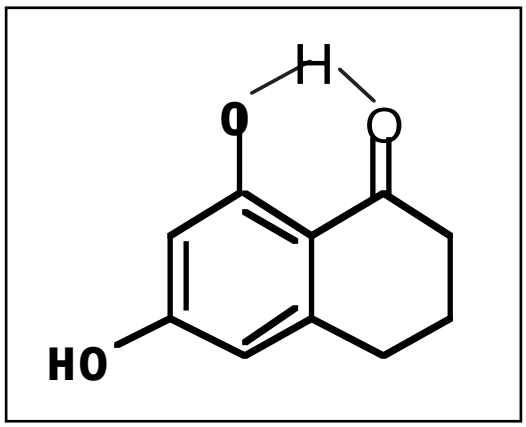

FIGURE 8. The hydroxyl group at the top of the molecule is part of a sym. H-bond and will therefore be down-field shifted.

1.7 Solvent effects:

It is very important to realize that different solvents may have different effects on the chemical shifts. Quite often an overlapping signal can be resolved when changing the solvent. Suitable solvents for causing large changes in chemical shifts are benzene or acetone, which may completely change the appearance of a spectrum that has been acquired in chloroform. This effect is especially pronounced when benzene selectively complexes parts of the molecule due to the ring-current effect from the aromatic ring. Such selective effects may be the case when not all parts of the molecule can be accessed by the solvent.

1.8 Shifts due to paramagnetic species:

Paramagnetic compounds have unpaired electrons. When paramagnetic impurities are contained in the sample, the lines are usually considerably broadened for solvent excessible protons. However, the chemical shift can also be influenced. The mechanism is Fermi-contact interaction (see section scalar couplings) between the nuclear spin and the unpaired electron. This effect is moderate, since electron density of the unpaired electron at the observed nucleus (which is usually not in the same molecule) is required. Since relaxation times of electrons are very short, the splitting due to the electron,proton coupling is removed rapidly (self-decoupling), so that comparably sharp lines can be observed. Paramagnetic reagents, also known as shift reagents, serve to disperse proton spectra. Thereby, a 2 ppm shift range for aliphatic protons can be dispersed over 6 ppm after addition of the shift reagent.

2. SCALAR COUPLINGS:

Two types of interaction between spins are known:

- dipolar coupling
- scalar coupling

The contributions from dipolar coupling usually cannot be observed in isotropic (liquid) phase. This is so because the dipolar coupling depends on the orientation of the connecting vector to the static field. This orientation rapidly changes in solution due to molecular tumbling and the dipolar coupling there-

fore averages to zero. However, it can be observed in the solid state or in liquid crystals.

The scalar coupling leads to a splitting of resonance lines. The effect is mediated via the electrons and its magnitude therefore rapidly decreases when the number of intervening bonds increases.

The basic mechanism that propagates the coupling is the **Fermi-contact** interaction. This effect describes the coupling between the nuclear and the electron spin:

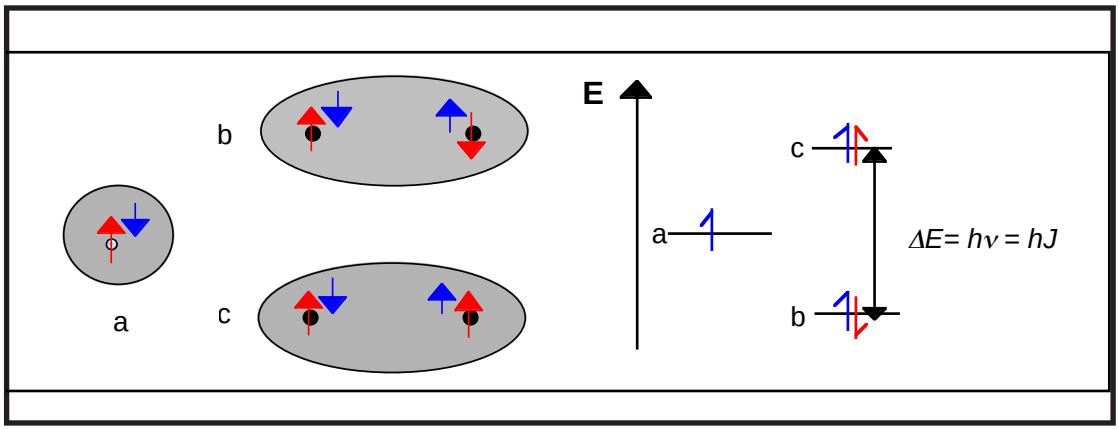

FIGURE 9. Spin states of nuclear (red) and electron (blue) spins for hydrogen atom (a) and singlet hydrogen molecule (b) and triplet hydrogen (c) with corresponding energy diagram.

Electrons that occupy an orbital that has a non-vanishing electron density at the nucleus (such as s-electrons) have the electron spin antiparallel to the nuclear spin (Hund's rule). Is the atom bonded to another atom, then the two s-orbitals of the separate atoms form a σ-orbital, which is occupied by two electrons with *antiparallel* spin (Pauli principle). The second nuclear spin can now have its spin parallel or antiparallel to the spin of the second electron depending on whether it is in the α- or β- state. The antiparalell alignment is energetically favourable and hence gives a signal at lower frequency. The magnitude of the coupling is expressed as the scalar coupling constant and can be calculated as:

$$J = (2\mu_0 g_e \mu_B /3)^2 \gamma_A \gamma_B |\Psi_A(0)|^2 |\Psi_B(0)|^2 c_A^2 c_B^2 (1/\Delta_T)$$

where γ_A and γ_B are the gyromagnetic ratios of the involved nulcei, $|\Psi_A(0)|^2$ is the electron density at the site of the nucleus A and c_A the coefficient of the contribution of the atomic orbital A to the σ MO. Δ_T is the triplet excitation

energy that measures the energy required to promote an electron from the singlet into the triplet spin state (parallel alignment):

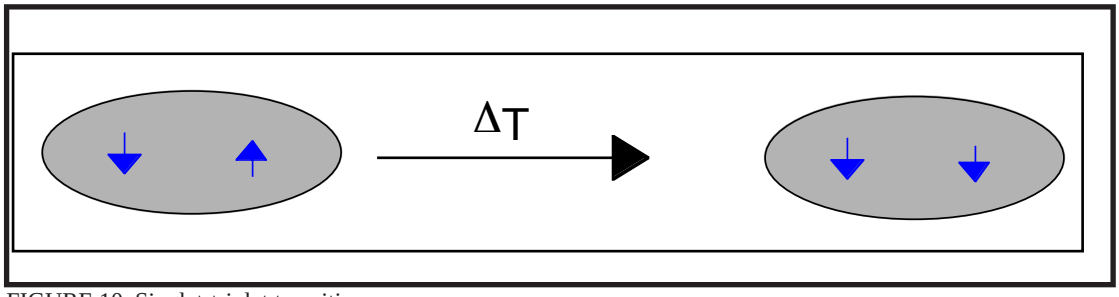

FIGURE 10. Singlet-triplet transition

The scalar coupling constant is usually given the symbol ^{n}J, in which n indicates the number of intervening bonds. As we will see later, the magnitude of coupling depends on the amount of overlap of the involved electron orbitals.

The s-character of orbitals depends heavily on the hybridization of the involved nuclei. This is very clear from the ^{1}J $^{1}H,^{13}C$ coupling constants which can be roughly categorized as:

- sp^3: 140 Hz
- sp^2: 160Hz
- sp: 250 Hz

The sp orbital has the highest content of s-character and hence gives the largest coupling.

The coupling also depends on the gyromagnetic ratios of the involved nuclei. When hydrogen is substituted by deuterium, the corresponding coupling to another proton is scaled by the factor $\gamma_D/\gamma_H = 1/6.514$. Therefore, the couplings are sometimes reported in form of the **reduced couplings**, which are defined as:

$$\kappa_{ik} = (J_{ik}/h)(2\pi/\gamma_i)(2\pi/\gamma_k)$$

2.1 Direct couplings (^{1}J):

In order to be able to detect scalar spin,spin couplings it is necessary that the two protons are not isochronous, meaning that they don't have the same chemical shift. The one-bond coupling constant usually has a positive sign.

2.2 Geminal couplings (^{2}J):

Geminal proton couplings largely depend on the hybridization of the involved carbon nuclei:

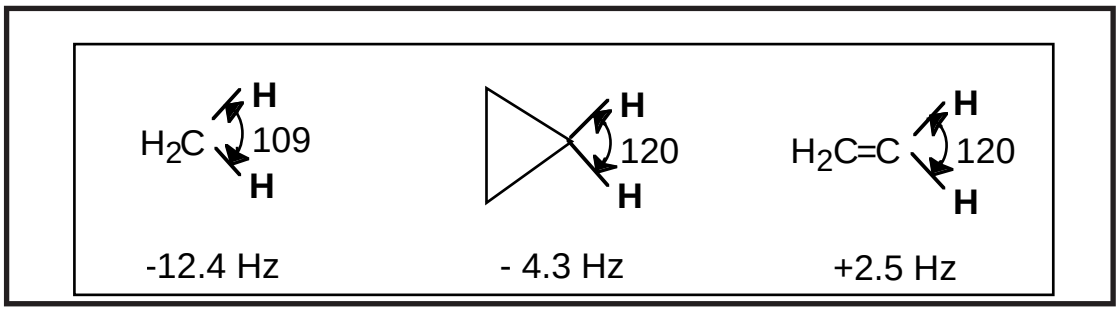

FIGURE 11. Various geminal couplings

To be able to observe these couplings the geminal bonded protons need to be diastereotopic in order to give separate proton frequencies.

2.3 Vicinal couplings (^{3}J):

Vicinal couplings display a characteristic dependence upon the involved dihedral angle:

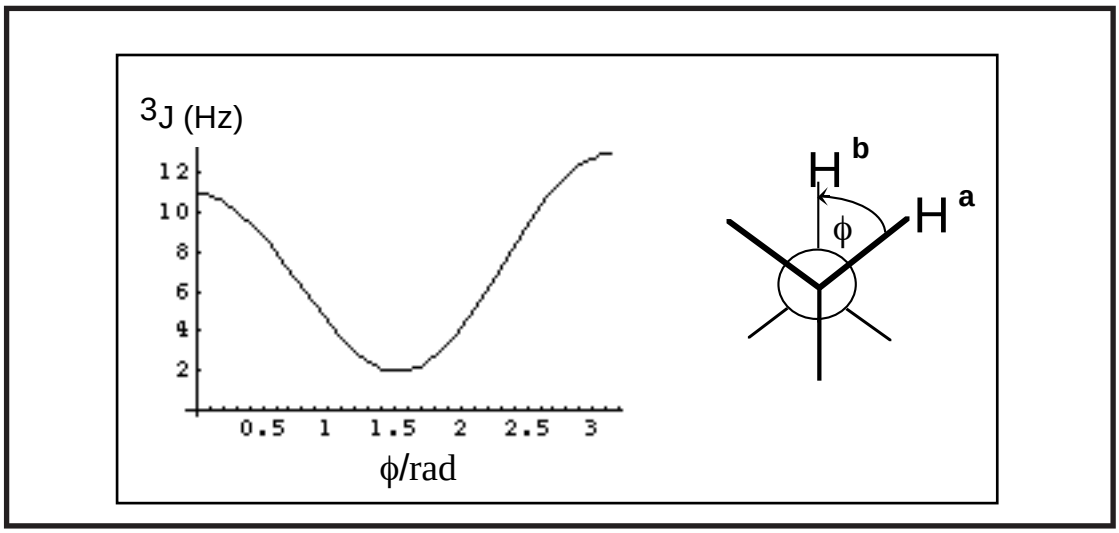

FIGURE 12. Left: Karplus curve, right: Definition of dihedral angles

according to the relation:

$$^3J = 7 - 1.0\cos\phi + 5\cos 2\phi$$

for protons.

For ^{1}H,^{13}C couplings a similar equation has been suggested:

$$^3J = 3.81 - 0.9\cos\phi + 3.83\cos 2\phi$$

This relationship, also known as the **Karplus relation,** has been successfully exploited to determine the stereochemistry of compounds. Of course, it

requires the dihedral angle to assume a certain value fixed over time. Therefore, rapid averaging of dihedral angles (rotatable bonds) leads to averaging of coupling constants, which for that case corresponds to the arithmetic mean from the mainly populated rotational states, e.g. gauche and trans rotamers. Open-chain aliphatic compounds therefore mostly display vicinal couplings of about 7 Hz.

For systems where the bond cannot be rotated (e.g. cyclic systems or macromolecules with defined secondary structure such as proteins), the coupling is very useful to determine the stereochemistry or derive structural constraints:

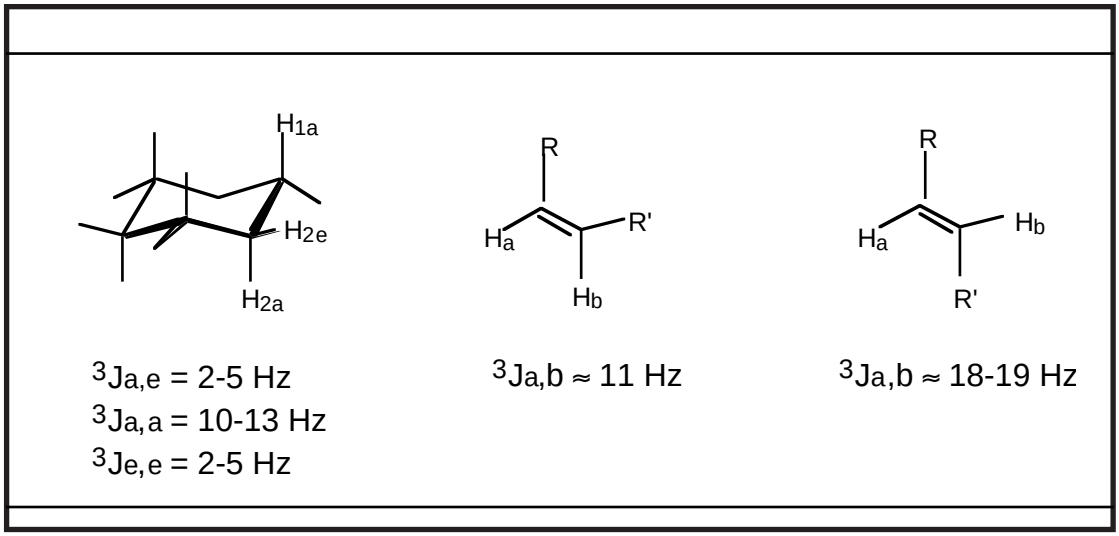

FIGURE 13. Vicinal couplings of systems with hindered rotation about C-C bonds

For example, in sugars the vicinal coupling between the anomeric proton and the neigbouring proton determines whether the sugar is α or β.

The reason for the dependence of the vicinal coupling on the dihedral angle is the follwoing: The scalar coupling is propagated via electrons. The angular dependence comes into play, because the dihedral angle determines how large the overlap of the molecular orbitals and thereby the efficiency of transfer is:

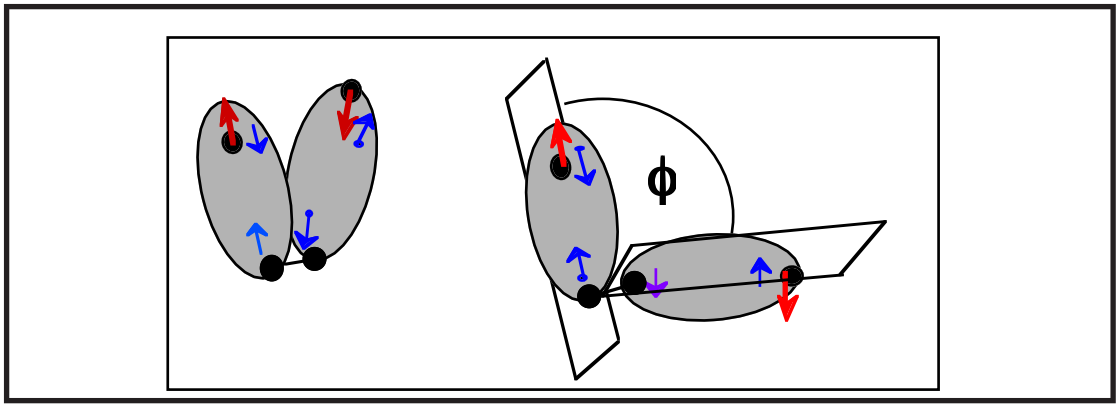

FIGURE 14. Overlap of adjacent orbiatals for ϕ=0° (left) and ϕ=90° (right).

Further effects on the vicinal couplings are:

- electron negative substituents decrease ^3J
- increasing HCC bond angles decrease ^3J
- increasing C--C bond lengths decrease ^3J

2.4 Long-range couplings:

^4J couplings are rarely observed. For saturated systems they require the atoms to be coplanar and in zigzag (W) conformation:

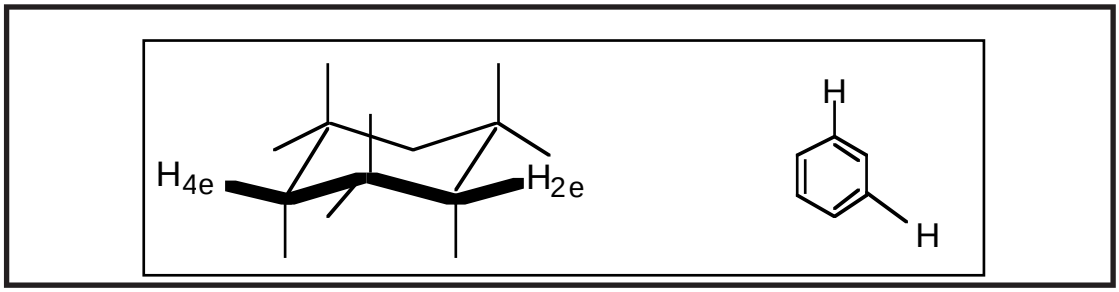

FIGURE 15. Systems with ^4J couplings.

2.5 Couplings involving π electrons:

In principle, π electrons cannot propagate scalar couplings because π orbitals have nodes at the position of the nuclei. Therefore, spin-correlation between σ and π electrons is required:

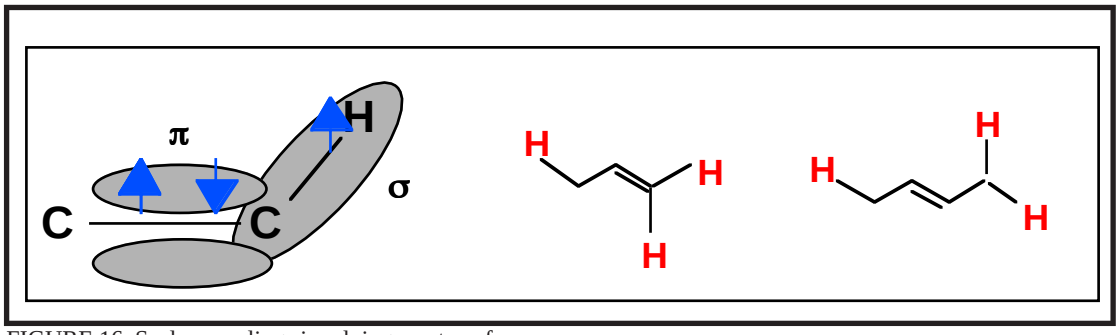

FIGURE 16. Scalar couplings involving σ,π transfers

Since π electron systems are highly delocalized, these interactions can be propagated over many bonds. The orientation of the double bond in ^4J couplings is not important, e.g. cisoid and transoid couplings are of similar magnitude.

2.6 The number of lines due to scalar spin,spin couplings:

In principle, each coupling doubles the numbers of lines. However, when couplings are of similar magnitude, some lines overlap. In the absence of geminal couplings (no diastereotopic protons) all couplings are usually due to vicinal

protons. In open-chain compounds single bond dihedral angles are rotationally averaged so that all vicinal couplings are around 7 Hz (*vide supra*)´. In this case the total number of lines of a single resonance due to the coupling with N neighbouring protons is N+1. In cyclic or structurally well-defined compounds where the couplings may be much different the total number is $2^{(N-1)}$.

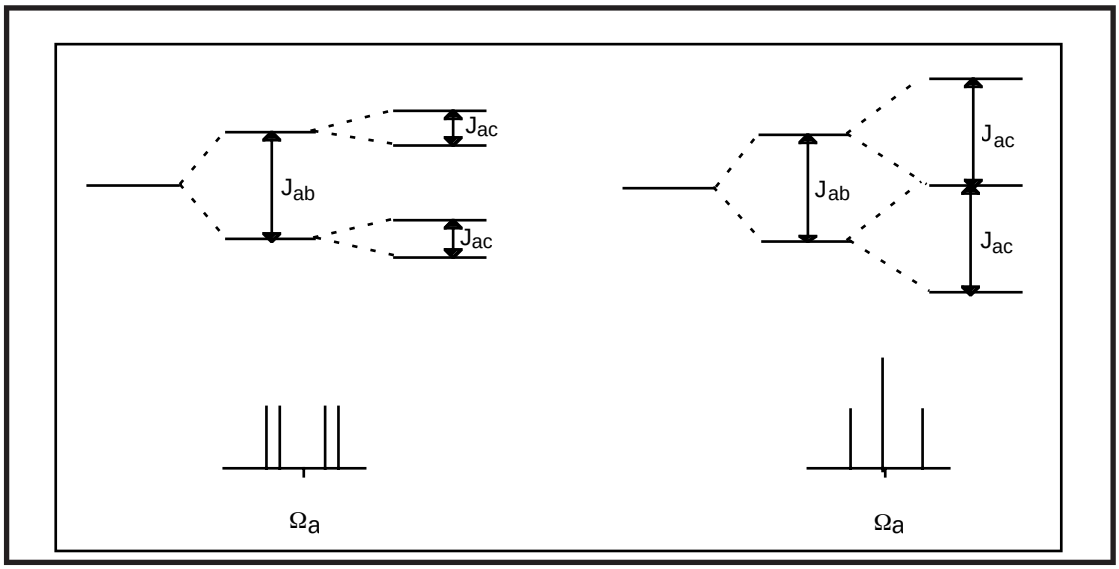

FIGURE 17. Coupling of a proton a with two other protons b and c for the case of different (left) or similar (right) couplings.

The intensities of the lines in the case of overlapping lines (similar magnitude of couplings) can be derived from the coefficient in the Pascal triangle:

Number of coupled nuclei		Number of lines	rel. intensities
I=1/2	I=1		
0		1 (singlet)	1
1		2 (doublet)	1:1
2		3 (triplet)	1:2:1
3		4 (quartet)	1:3:3:1
4		5 (quintet)	1:4:6:4:1
5		6 (sextet)	1:5:10:10:5:1
6		7 (septet)	1:6:15:20:15:6:1
	0	1 (singlet)	1
	1	3 (triplet)	1:1:1
	2	5 (quintet)	1:2:3:2:1
	3	7 (septet)	1:3:6:7:6:3:1

2.7 Strong coupling:

The rules for line multiplicities and intensities described above are only valid in the case of weak coupling. However, when the chemical shift difference is not very large compared to the scalar coupling constant ($\Delta\delta > 10$ J), these rules do not apply anymore. In the strong-coupling case spin properties are mixed. A practical consequence is that a resonance line cannot be referred to belong to a spin A or B. Whereas in the limit of weak coupling a spin-flip of spin A does not cause spin B to flip there is a probability to do so in the strong coupling case. In order to derive coupling constants or chemical shifts from strongly coupled spins these parameters may not be extracted from the spectrum but have to be derived from a simulation and comparison to the measured spectrum. For the case of two dublets due to two strongly coupled protons the inner lines are larger then the outer ones ("roof effect"). Thereby it is possible to decide which signals are coupled with each other.

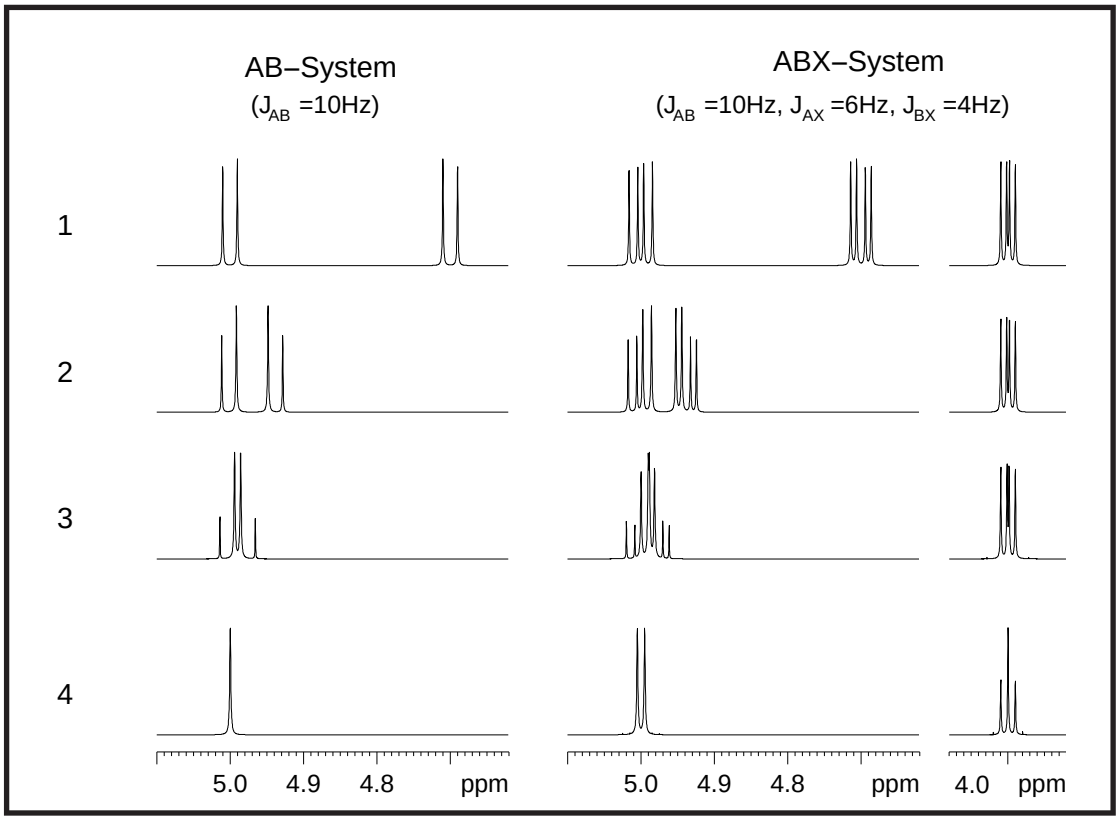

FIGURE 18. Second order effects depending on the chemical shift difference. The simulations were calculated using $\nu_A - \nu_B/J$=15(1), 3(2), 1(3) and 0(4). In the case of the ABX system the X-part is shown separately.

1. RELAXATION:

As stated in the first chapter thermal equilibrium is a state in which the population of α- and β-states corresponds to the Boltzmann distribution. Furthermore, the spins are uncorrelated in phase such that no transverse magnetization exists. However, when RF pulses are applied the state of the spins is pertubated away from equilibrium distributions. The process that brings the spins back to thermal equilibrium is called relaxation:

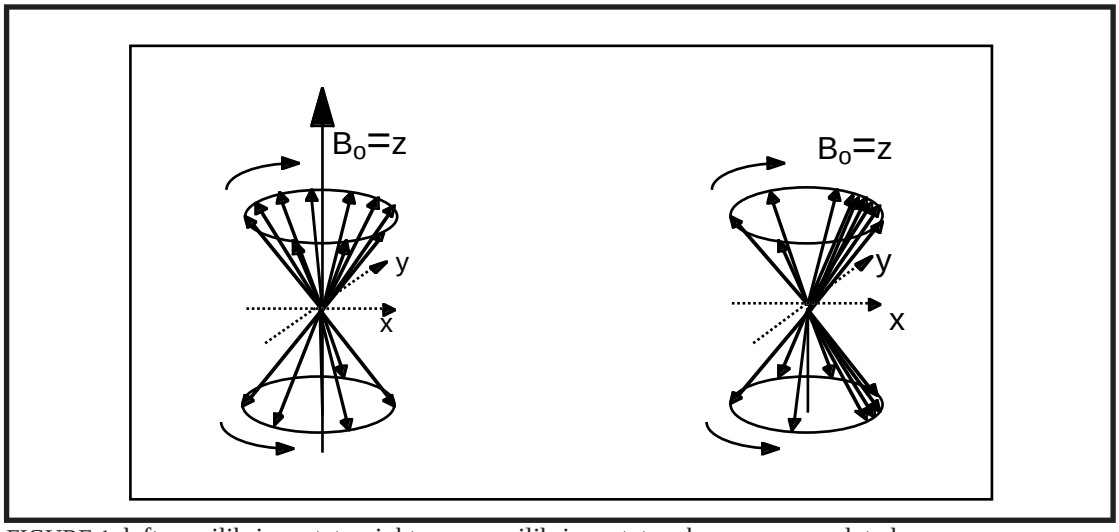

FIGURE 1. left: equilibrium state. right: non-equilibrium state, phases are correlated

It is important to note that a particular spin can be only in either the α- or the β-state. What relaxation describes is the behaviour of *magnetization* which is defined as the sum of the magnetic moments from all spins. However, to understand the mechanisms of relaxation we will look at the fate of individual spins.

Phenomenologically, relaxation is categorized into

1. **longitudinal relaxation** (or **T1 relaxation**) that describes the return of the z-component of longitudinal (z-)magnetization to its equilibrium value. The corresponding time constant of that process is called T1.
2. **transverse relaxation** (or **T2 relaxation**) that describes the decay of transverse (x,y) magnetization. Analogously, the corresponding time constant is called T2.

1.1 T1 relaxation:

The equilibrium distribution of α *vs.* β -state is governed by the Boltzman distribution:

$$\frac{\#(\alpha)}{\#(\beta)} = e^{-(E_\alpha - E_\beta)/kT}$$

Since α and β -states correspond to different energies changing the relative populations of these states changes the energy of the system. Therefore, T1 relaxation is an **enthalpic process**. The energy is transferred to or taken from other spins. The surrounding of spins is often called the lattice and hence T1 relaxation is often referred to as **spin-lattice relaxation**:

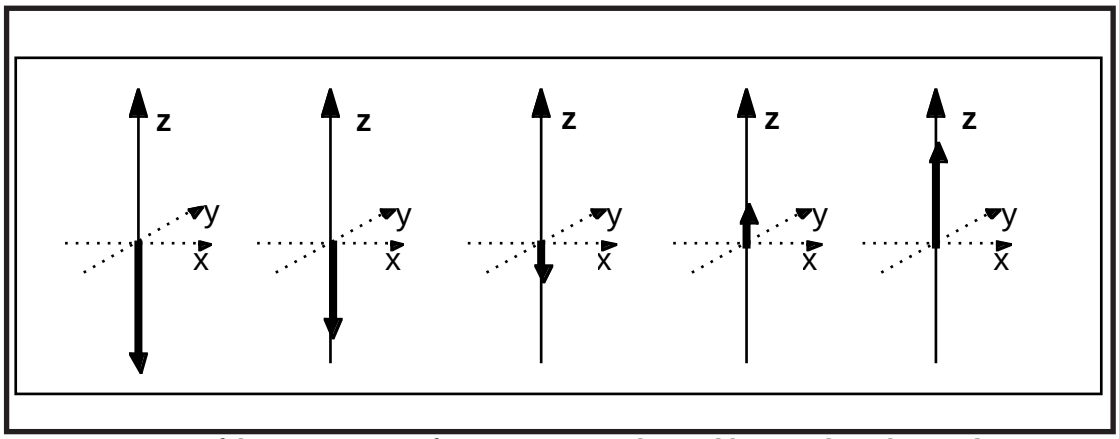

FIGURE 2. Return of the z-component of magnetization to the equilibrium value. The initial state may have been created through population inversion arising from an 180˚ pulse.

Note that the vectors shown in the figure above represent the magnetization vectors rather than magnetic moments from individual spins. Longitudinal magnetization decays exponentially according to

$$M_z(t) \quad = \quad M_z(t_0)\, e^{-t/T1}$$

The T1 relaxation time determines the pulse repetition rate, the delay that has to be inserted between individual scans. T1 times for protons are in the range of 0.5 to a few seconds. T1 times for quadrupolar nuclei ($I > 1/2$) can be rather short (ms range). Degassing the sample will remove paramagnetic oxygen which otherwise facilitates T1 relaxation. Therefore, degassing samples is useful when measuring small NOE effects.

1.2 T2 relaxation:

The transverse relaxation determines how fast phase coherence between spins is lost. Since dephasing in the spins does not cause any changes in the relative population of α– and β-state, it is not changing the energy of the system. T2 relaxation is merely a **entropic process**. It is often referred to as **spin,spin relaxation**:

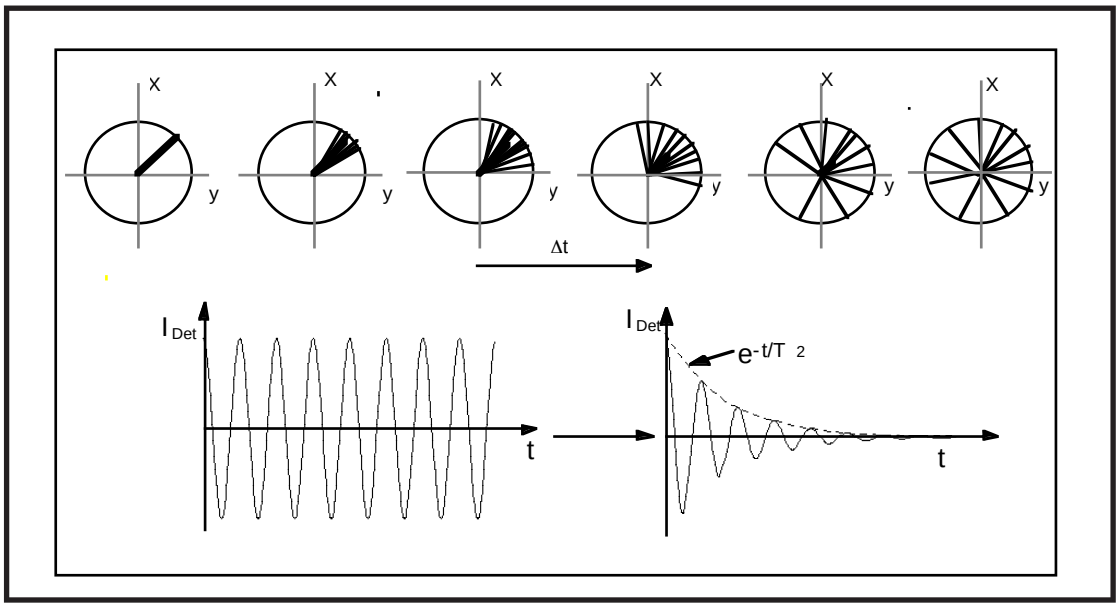

FIGURE 3. Top: Dephasing of transverse coherence leading to T2 relaxation. Lower: Influence of T2 relaxation on the appearance of the FID.

Once the transverse relaxation time T2 passed by transverse magnetization has decayed to 1/e of its original value:

$$M_{x,y}(t) = M_{x,y}(t_0)\, e^{-t/T2}$$

The transverse relaxation time determines the linewidths of the signals. The shorter T2 the broader the signals. The linewidth at half height of the signals can be expressed as:

$$\Delta\nu_{1/2} = \frac{1}{\pi T_2}$$

There is no reason to sample the signal for times much longer than T2 because only noise will then be added to the FID. The T2 time and hence the linewidth also determines the theoretically achievable resolution.

1.3 The mechanisms of relaxation:

In principle the spin system may return to equilibrium via stimulated relaxation (some kind of energy exchange process that initiates relaxation) or by spontaneous relaxation. It can be shown that the probability for spontaneous relaxation is far too low to account for it.

Mechanistically, relaxation is caused by additional fields that happen to have exactly the frequency that corresponds to the required transition. For example, T1 relaxation takes place if spins change from the α- to the β-state or vice versa.

The energy difference between these states correspond to a specific frequency

$$\Delta E = E_\alpha - E_\beta = h\nu$$

and this frequency matches to a field fluctuating at

$$\nu = \frac{\gamma B}{2\pi}$$

There are two major mechanisms by which these fluctuating fields are formed:

- dipole-dipole interaction between two different spins
- chemical shift anisotropy

Both processes are connected to the movement of spins in space due to overall tumbling of the molecules or due to internal motions.

Dipole-dipole induced relaxation:

Spin A close in space to spin B causes a (small) dipole moment at the nucleus B:

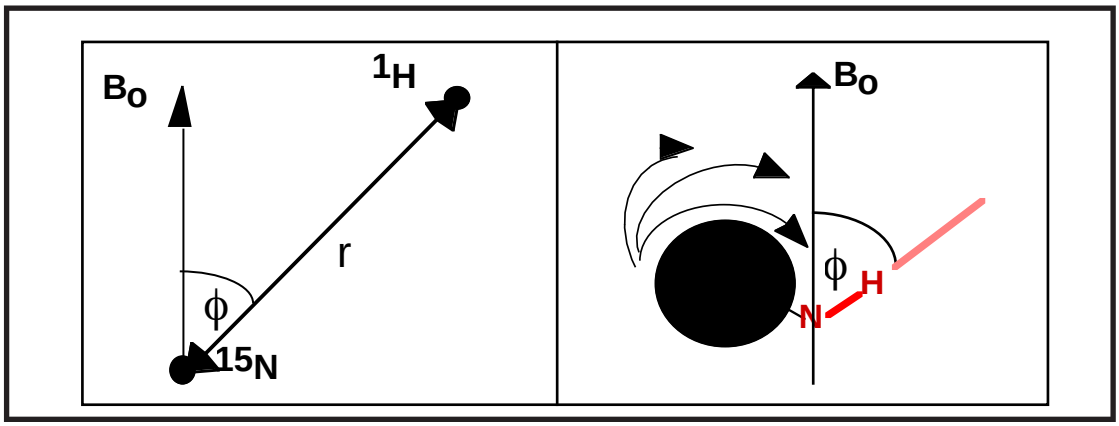

FIGURE 4. Left: definition of the vector connecting two spins and its orientation ϕ with respect to the external field. Right: Overall tumbling changes ϕ.

The induced local field can be expressed as:

$$B_{loc} = \frac{\mu\,(3\cos^2\phi - 1)}{r^3}$$

The magnitude of the induced field depends on both the distance of the two interacting nuclei and on the angle formed between the interatomic vector and the static field. Through molecule tumbling the angle ϕ permanently changes its magnitude causing a *fluctuating* field.

For protons that relax mostly through dipole,dipole interaction with other protons the transverse relaxation time T2 and thereby its linewidth is determined by a) how far the next protons are in space and b) the overall tumbling time of the molecule. It is often found that isolated protons (those that do not have other protons on the neighbouring carbons) display incorrect integrals in 1D proton spectra. This is due to the fact that T1 relaxation for these protons is

inefficient and therefore these protons do not have completely relaxed in between different scans. The line-broadening of signals due to slow overall tumbling is obvious from the linewidth of spectra from large proteins that display very broad lines.

The distance between geminal protons depends on the bond geometries but for all other protons it is determined by the structure. An important application therefore is the NOE effect, a method that depends on relaxation properties of spins and helps to elucidate the three-dimensional arrangement of protons (see next chapter).

1.4 Other relaxation mechanisms:

Any particular event that will cause a fluctuating field at the site of the nucleus may contribute to relaxation provided that it delivers spectral density at any of the possible NMR transitions.

1.4.1 Chemical shift anisotropy (CSA):

Non-spherical distribution of electron density (e.g. occurring for sp^2 hybridized carbon nuclei) will cause a fluctuating field upon rotation of the nucleus which serves as a efficient source for relaxation:

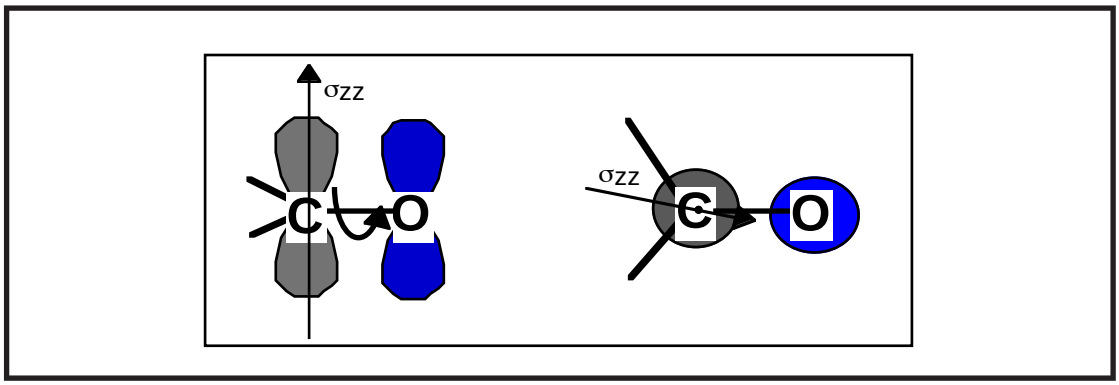

FIGURE 5. Dependence of electron shielding for carbonyl carbons on the orientation of the external field relative to the p_z orbital

The efficiency of CSA relaxation increases with the square of the magnetic field and is the major relaxation source for amide nitrogen nuclei at fields higher than 600 MHz. It is also the major relaxation source for non-proton bearing carbon nuclei such as carbonyl or olefinic carbons.

1.4.2 Scalar relaxation:

Relaxation may also be induced when the scalar spin,spin coupling to another nucleus fluctuates rapidly. This could be caused by

- chemical exchange of the coupled nucleus (**scalar relaxation of the first kind**)

- rapid T1 relaxation of the coupled nucleus (**scalar relaxation of the second kind**).

Scalar relaxation of the first kind is observed for protons coupled to quickly exchanging hydroxyl protons. Scalar relaxation of the second kind is frequently encountered for protons coupled to quadrupolar nuclei. An practical example is the case of nitrile carbons in which the carbon is mostly coupled to the quadrupolar ^{14}N nucleus and is usually significantly broadened. Scalar relaxation is much more likely to effect T2 than T1 relaxation times.

1.4.3 Quadrupolar relaxation:

Nuclei with a spin > 1/2 rapidly relax under the influence of a **electric field gradient**. T1 and T2 relaxation is very fast for these nuclei provided that the ligand environment of the nucleus is non-symmetrical. This is seen for ^{14}N, which gives a narrow resonance in the tetrahedral NH_4^+ ion but much broader lines in asymmetrical environment such as pyrrole.

1.4.4 Spin-rotation relaxation:

Rapidly rotating groups such as methyl groups induce a fluctuating field at the frequency of rotation. This effect is usually of minor importance.

1.4.5 Interaction with unpaired electrons:

The interactions can be either of dipolar or scalar nature. The effects are dramatic such that small contaminations with paramagnetic impurities may severely broaden the lines. Therefore, oxygen (which is paramagnetic,diradical) is often removed through thaw and freeze cycles to increase T1.

For ^{13}C NMR relaxation reagents like $Cr(acac)_3$ are added in very small quantities to bring the T1's down to about 1s (otherwise, carbonyl nuclei may have T1's of 20-30sec) to allow faster pulsing.

1.5 The motional properties:

In this section we will see how the dependence on the motional properties is expressed mathematically. The time-dependence of the motions is of prime importance since it determines the frequency at which the induced local fields fluctuate and therefore whether they may contribute to relaxation or not. In order to describe how the angle ϕ changes with time we use the **correlation function** $g(\tau)$:

$$g(\tau) = \overline{f(t)\, f(t+\tau)}$$

that describes how quickly a function changes with time. The following figure displays the correlation function for functions with no (left), little (middle) or

rapid (right) time dependence:

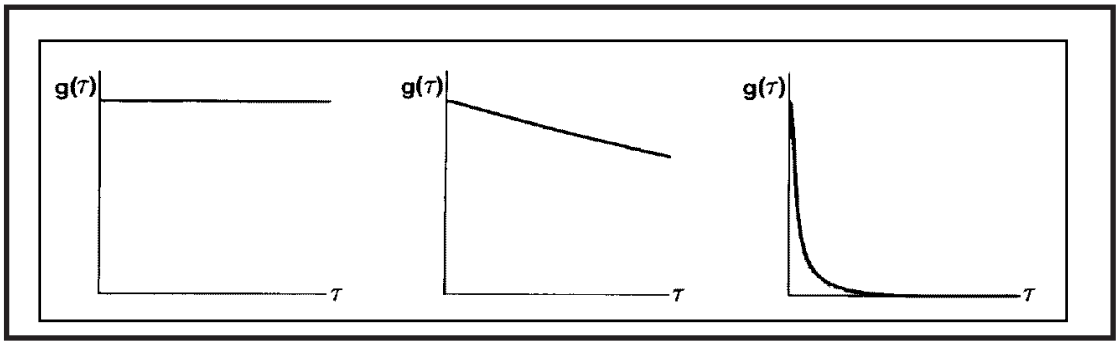

FIGURE 6. typical correlation functions for no decay (left), slow decay (middle) and fast decay (right.

Since the NMR signal decays exponentially (this can be derived from the line-shape which must be lorentzian for exponential decay), g(τ) is believed to be exponential:

$$g(\tau) = e^{-\tau/\tau_c}$$

τ_C is the **correlation time** which is defined to be the time required for a 360° rotation of the molecule. A very approximate formula valid for globular proteins in water is $\tau_C \approx 10^{-12}$ M (M = molecular weight in Dalton) but depends highly on temperature, shape etc.

We are not interested so much into the time it takes for a molecule to change its spatial arrangement but rather on the frequency with which these changes take place. Therefore, the **spectral densities**, which are the Fourier transform of the correlation function, are preferred. The spectral density J(ω) tells us how much power is available from the motion of the molecule to cause fluctuations at the frequency ω. It can be calculated as:

$$J(\omega) = \frac{2\tau_c}{1+\omega^2\tau_c^{\,2}}$$

The dependence of the spectral densities on the frequencies are shown in the figure below for large (left), medium-sized (middle) and small molecules (right). It is clear that the densities at low frequencies increase with increasing correlation times (larger molecules). This can be rationalized in the following way: The overall power from all frequencies (the integral under the spectral density function) must remain the same for all molecules. However, smaller molecules may rotate faster than larger molecules so that the highest possible frequency is lower for larger molecules.

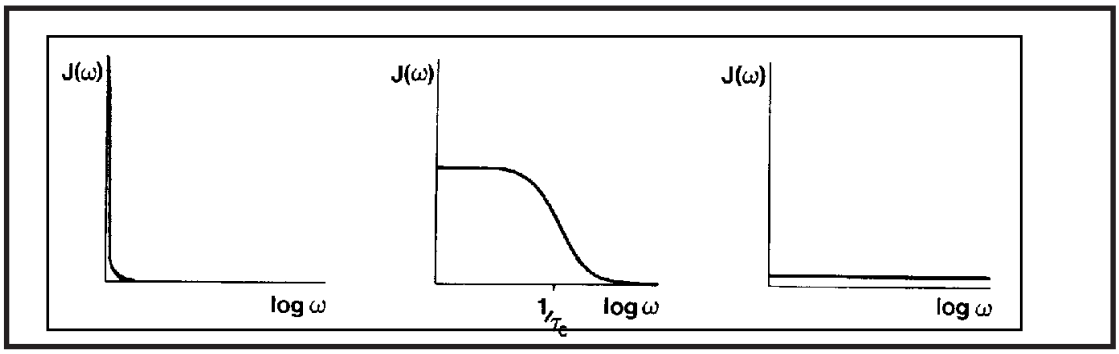

FIGURE 7. Spectral density functions for no decay (left), medium decay (middle) and fast decay (right).

The motional fate of a molecule can be described by the following scenario: A molecule rotates with a certain frequency. Then it hits another molecule and the rotation is slowed down or stopped. After the crash the molecule starts to rotate again until it has reached its highest possible frequency or has hit another molecule:

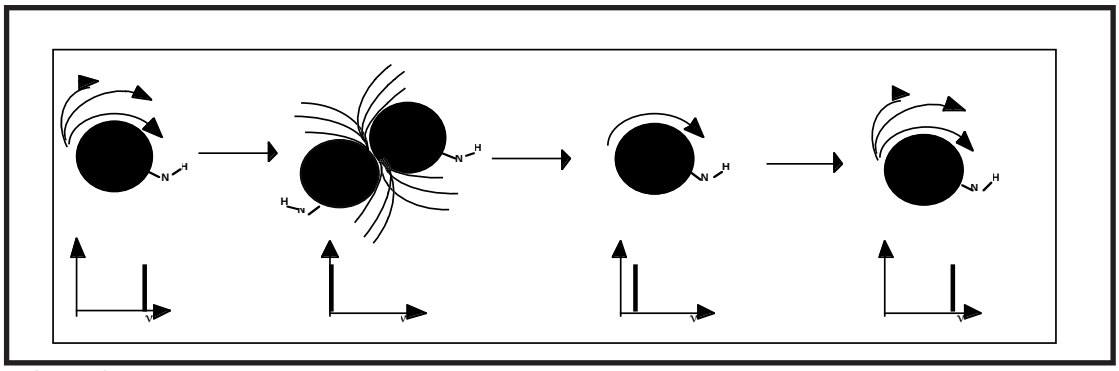

FIGURE 8.

Small molecules therefore posses a broad band of rotational frequencies whereas the larger molecules have more spectral density at the lower frequencies (in fact, the highest spectral density is at frequency zero). We will see later that the frequencies that match possible NMR transitions determine how quickly a nucleus may relax.

1.5.1 The dependence of the relaxation rates on the fluctuating fields in x,y or z direction:

An additional field in z-direction means that the spins additionally precess about the z-axis with the frequency of that field.In contrast, fields in x- or y-directions cause spins to flip from the α-to the β-state or vice versa.

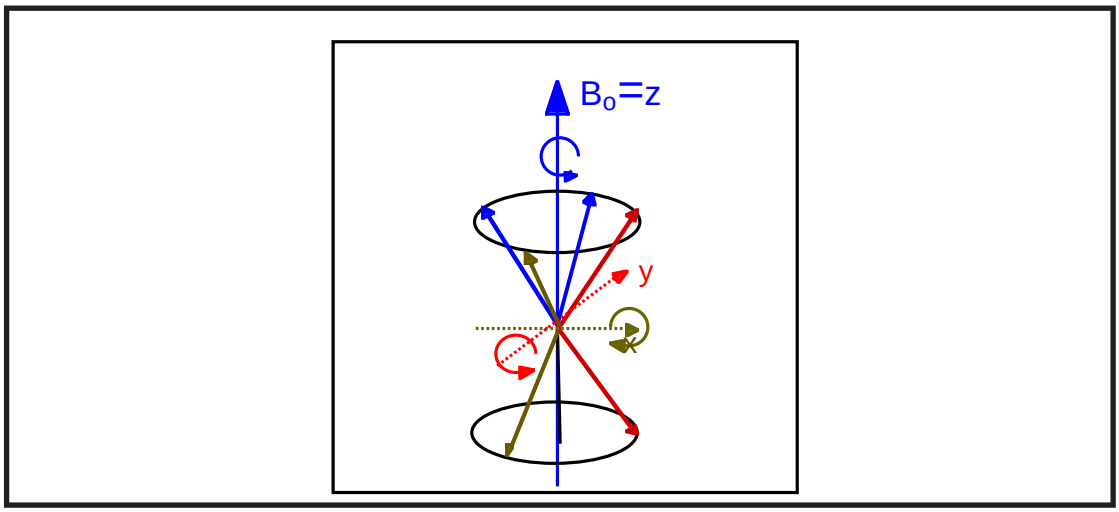

FIGURE 9.

The longitudinal relaxation time depends on the frequency of α- to β-state transitions and therefore on the fields along x or y:

$$\frac{1}{T_1} \propto \gamma^2 (\overline{H_x^2} + \overline{H_y^2})\, J(\omega)$$

In order to be effective these fields must precess with frequencies comparable to the larmor frequency about z. This is analogous to the case of the B_1 field which can only influence spins when the field precesses about the z-axis.
The transverse relaxation time is determined by the amount of dephasing of transverse magnetization. Obviously, fields along z change the precession frequency since they alter the strength of the static field (which is also along z):

$$\frac{1}{T_{2,x}} = \gamma^2 (\overline{H_z^2} J(0) + \overline{H_y^2} J(\omega))$$

$$\frac{1}{T_{2,y}} = \gamma^2 (\overline{H_z^2} J(0) + \overline{H_x^2} J(\omega))$$

This mechanism is represented by the field term along z in the equations above. Dephasing at J(0) is effective because if the z-field would fluctuate, say from the +z-direction to the -z-direction, the dephasing effect from it would be reversed and averaged out. It can therefore only be effective if that field stays in the +z direction and hence the spectral density at zero frequency is important. In addition, rotations about the x- or y-axis (causing α- to β-transitions) will reduce the lifetime of the state (lifetime broadening). This can be seen from the Heisenberg principle which states that the shorter the lifetime is the larger the uncertainty in energy is. The contribution of lifetime broadening to T2 is the same as to T1 since it uses the same mechanism and hence similar spectral densities are required.

1.6 Excurs: The Lipari-Szabo model for motions:

The Lipari-Szabo model (also sometimes referred to as the "modelfree" approach) factorizes the autocorrelation function into a correlation function for overall tumbling and one for internal motions:

$$g(t) = g_o(t) \bullet g_i(t)$$

The overall correlation is assumed to decay exponentially

$$g_o(t) = e^{-t/\tau_R}$$

The correlation function describing internal motions is described as

$$g_i(t) = S^2 + (1 - S^2)e^{-t/\tau_e}$$

The generalized order parameter S^2 describes the spatial restriction of the internal motion with respect to a molecule-fixed coordinate system. τ_e is the effective correlation time for that internal motion. A value of 1 means that a particular vetor does not move relative to the molecular frame and a value of zero indicates that movement of a vector is completely uncorrelated to overall tumbling which is the case for highly flexible loop regions in globular proteins for example.

The spectral densities in this model is expressed as:

$$J(\omega) = S^2(\tau_R / (1 + \omega\tau_R)^2) + (1 - S^2)\tau_e / (1 + \omega\tau_e)^2$$

The strength of the Lipari-Szabo interpretation is that it gives an impression about the relative "floppiness" of parts of the molecule in absence of any specific model about the exact nature of the internal motion. Assuming free diffusion in a cone the half-angle θ expressing the spatial restriction of the internal motion can be calculated as

$$S^2(\theta_{max}) = 0.5\cos(\theta_{max})(1 + \cos\theta_{max})^2$$

which translates for an S^2 of 0.4 into a half angle of 45°:

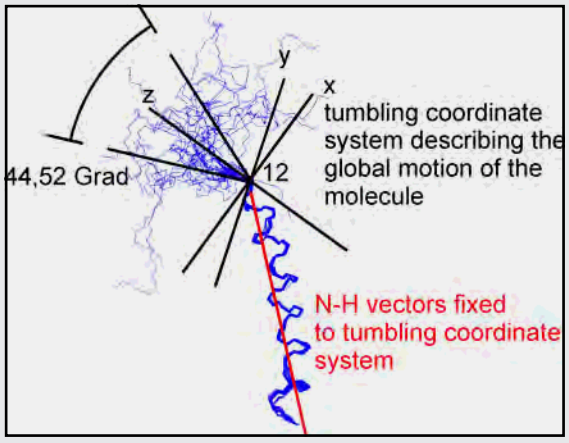

1.7 The nature of the transitions:

So far we have only been talking about a single spin changing his state due to interaction with the surrounding spins. A transition that involves a single spin going from the α- to the β-state is called a **single-quantum transition**:

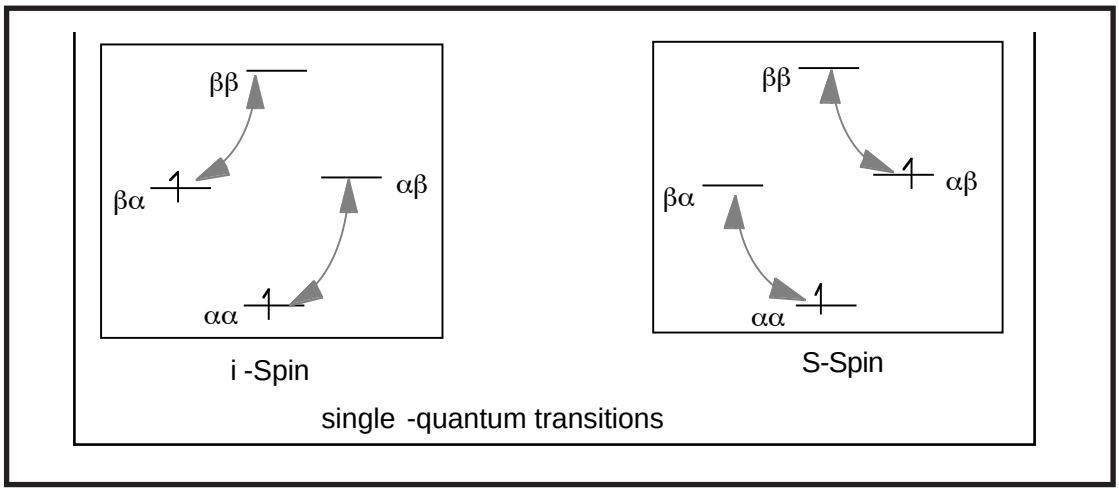

FIGURE 11. left: I-spin single quantum transitions. Right: S-spin single quantum transitions

Alternatively two spins may simultaneously go from the α- to the β-state (**double-quantum transition**). Furthermore one spin may go from the α- to the β-state and another one from the β- to the α-state in a correlated fashion **(zero-quantum transition**). The frequency for the double quantum transition corresponds to the sum of the frequencies of the individual spins whereas the zero-quantum frequencies are formed from the difference of their corresponding frequencies. For homonuclear spin systems the zero-quantum frequencies are very low (kHz range) and the double quantum frequencies very high.

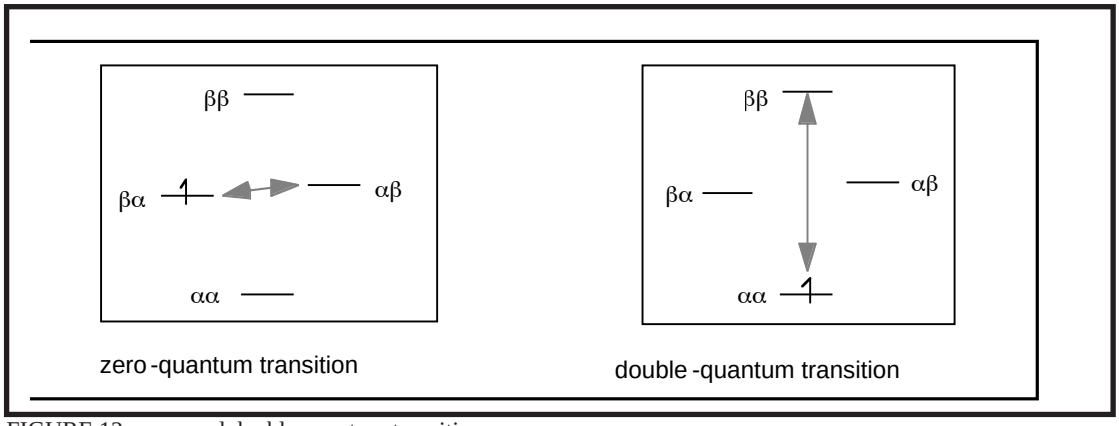

FIGURE 12. zero- and double quantum transitions

For T1 and T2 processes spectral densities at frequencies corresponding to different transitions are utilized. It can be seen from the figure below that for T2 relaxation spectral density at J(0) is important in contrast to T1 and NOE. As we have seen before J(0) steadily increases with increasing molecular size and for larger molecules such as proteins almost all spectral density is at J(0). Hence T2 times are very short for large molecules leading to very broad lines.

Note that the parameters in the figure below are given for ^{15}N relaxation data (the mechanism is dipolar relaxation with ^{1}H). For ^{1}H relaxation, the zero quantum frequencies (which are the difference of the chemical shifts) are in the 0-10 KHz range and therefore very close J(0) whereas for ^{15}N nuclei the zero-quantum frequencies are not so much away from the proton frequencies (MHz range).

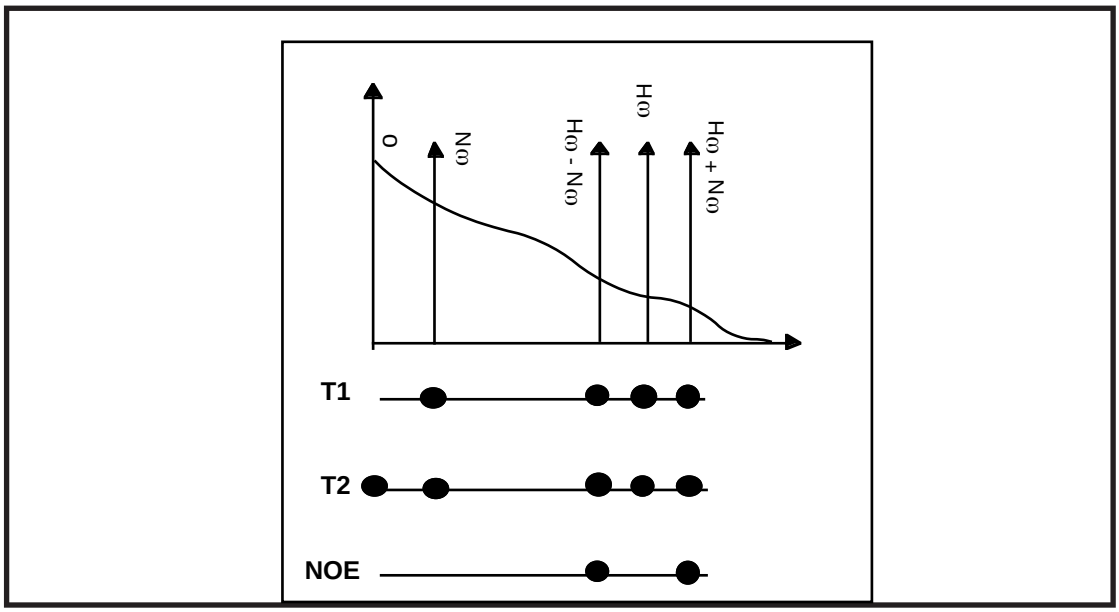

FIGURE 13. Dependence of T1, T2 and NOE upon spectral densities at various frequencies.

For ^{15}N magnetization, relaxation is mainly due to ^{1}H,^{15}N dipolar interactions and ^{15}N chemical shift anisotropy. It depends on spectral density of single quantum proton coherences, single quantum nitrogen coherences and hetero-nuclear (^{15}N,^{1}H) double and zero-quantum coherences:

$$\frac{1}{T_1} = R_N(N_Z) = \frac{\gamma_H^2 \gamma_N^2 \hbar^2}{4 r_{N,H}^6} \left\{ \begin{matrix} J(\omega_H - \omega_N) + 3J(\omega_N) + \\ 6J(\omega_H + \omega_N) \end{matrix} \right\} + \frac{\Delta^2 \omega_N^2}{3} J(\omega_N)$$

$$\frac{1}{T_2} = R_N(N_{x,y}) = \frac{\gamma_H^2 \gamma_N^2 \hbar^2}{8 r_{N,H}^6} \left\{ \begin{matrix} 4J(0) + J(\omega_H - \omega_N) + 3J(\omega_N) + \\ 6J(\omega_H) + 6J(\omega_H + \omega_N) \end{matrix} \right\} + \frac{\Delta^2 \omega_N^2}{3} \left\{ \frac{2}{3} J(0) + \frac{1}{2} J(\omega_N) \right\}$$

in which Δ denotes the chemical shift anisotropy of nitrogen. Note, that the rates of T1 and T2 relaxation differ in the contribution of J(0) for T2. Fore large molecules, J(0) contains almost all spectral density. Hence, T2 relaxation is very fast, and this is the principal reason why large molecules display very broad nmr lines.

The dependence of transverse and longitudinal relaxation upon the correlation time is shown in the next figure. T2 continuously gets shorter with increasing molecular size due to the increase in spectral density at J(0). T1 however passes a minimum. Following the point where spectral density at the zero-quantum frequencies decreases T1 is getting larger again. (T1 relaxation does not depend upon spectral density at J(0):

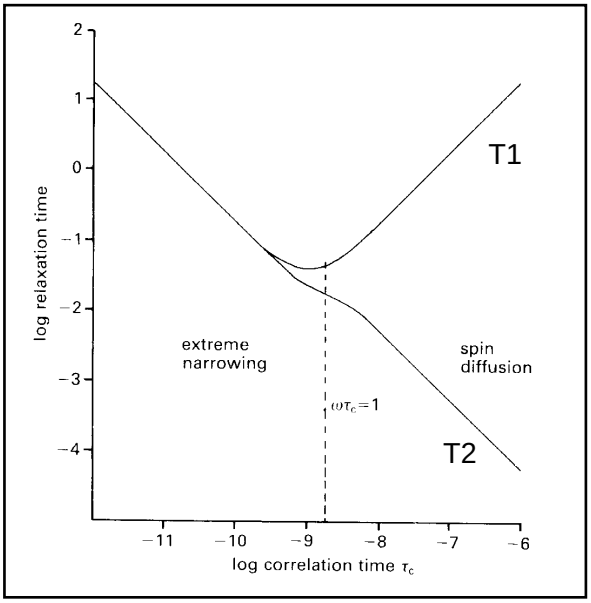

FIGURE 14. Dependence of T1 and T2 upon the overall tumbling time

1.8 Measurement of relaxation times:

T1 relaxation times are usually determined from the **inversion recovery** sequence: 180 deg pulse…delay…90 deg pulse…delay ..acquisition

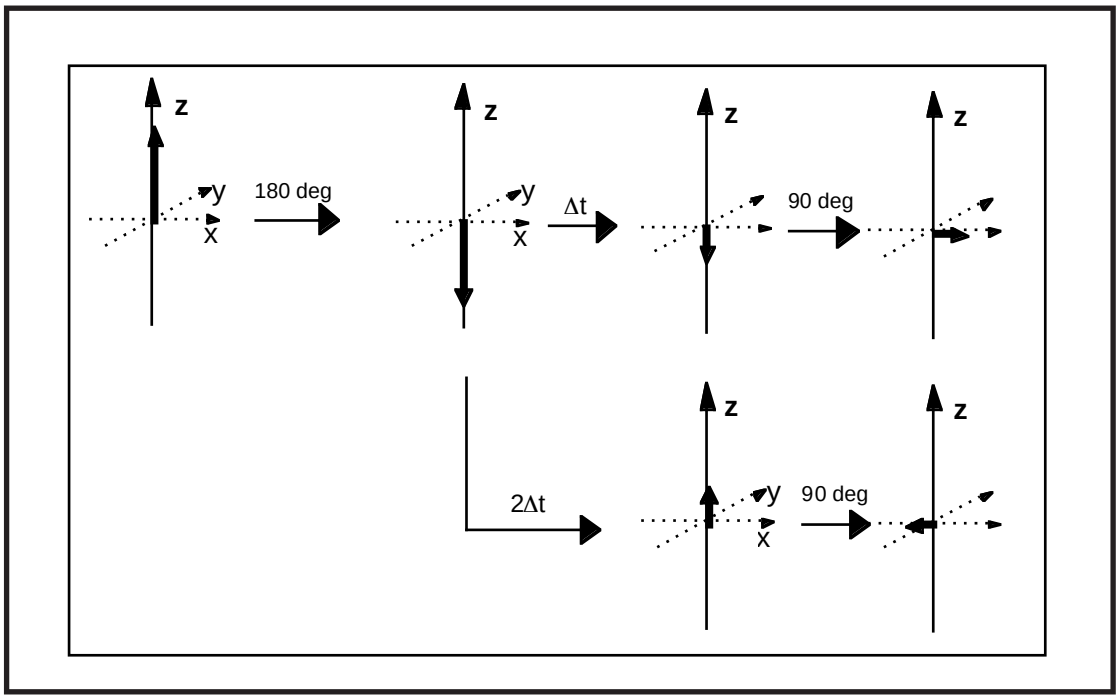

FIGURE 15. Inversion recovery.

In this sequence, magnetization is inverted by application of a 180 degree pulse. A delay follows during which T1 relaxation takes place bringing the -z magnetization back towards +z. Afterwards a 90 degree pulse along y turns the magnetization onto the x-axis into observable signal. The magnitude and sign of the x-magnetization at the end of the sequence depends on a) the T1 constant and b) the relaxation delay Δ.

Transverse relaxation time is determined from a **Carr-Purcell Spin echo**. In principle, one could simply measure the decay of transverse magnetization following a 90 degree pulse. However, inhomogeneity of the static field leads to accelerated transverse relaxation. Usually, one is not interested into the contribution from field inhomogeneity (this would mean that the transverse relaxation time would depend on the quality of shimming) and therefore the Carr-Purcell sequence that eliminates the additional T2 relaxation due to field inhomogeneity is applied:

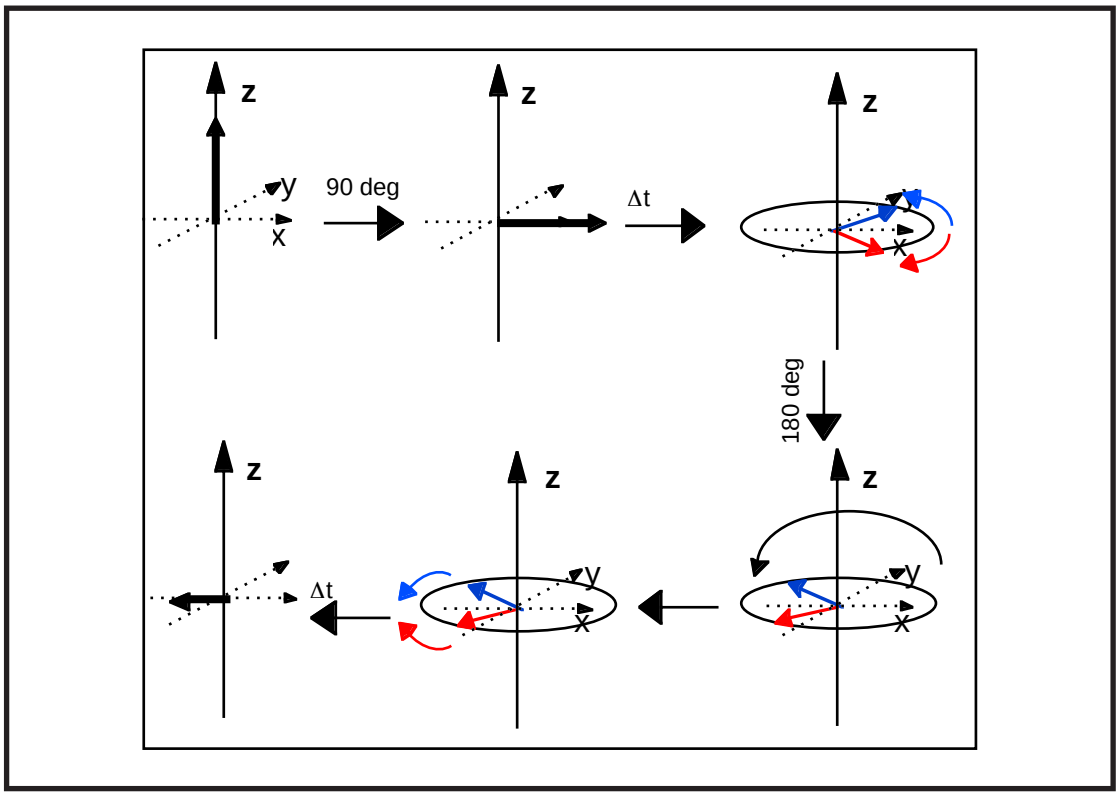

FIGURE 16. Carr-Purcell spin echo.

In this sequence 180 degree pulses are applied during the T2 relaxation delay equally spaced by delay periods. The effect of the 180˚ pulses is to refocus differential precession due to field inhomogeneity. The sequence is also referred to as an **spin-echo**.

For both experiments, the inversion recovery and the Carr-Purcell sequence a set of 1D (or 2D) spectra is recorded with different relaxation periods. The intensities of the remaining signal is measured and plotted against the relaxation delay. Mostly these plots yield decaying exponentials and by fitting procedures (least squares fit to the experimental data) it is possible to extract the time constant for the decay:

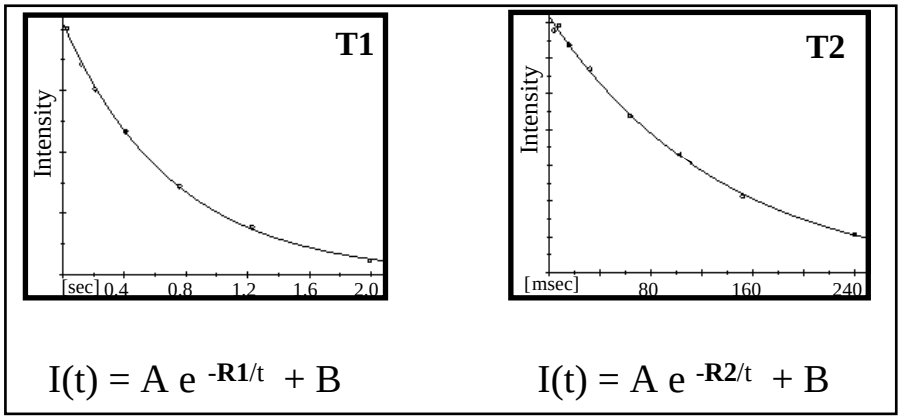

FIGURE 17. Analytical formula to describe the decay of longitudinal (left) and transversal (right) magnetization.

1. THE NUCLEAR OVERHAUSER EFFECT (NOE):

If one resonance A is irradiated, an increase (positive NOE) or decrease (negative NOE) of signal intensity of *other* resonances such as resonance C is observed when spin C is close in space to spin A:

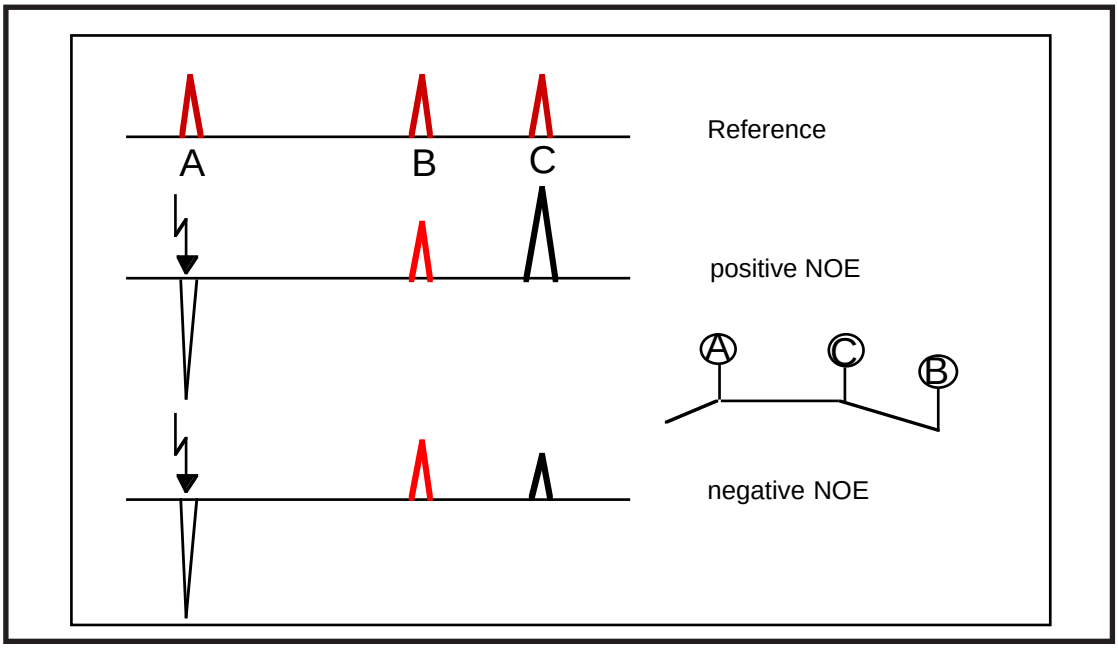

FIGURE 1. Irradiation of resonance A leads to a increase of peak intensity of the neighboring spin C (positive NOE) or to a decrease of peak intensity (negative NOE).

This phenomenon is called *nuclear Overhauser effect* or NOE. The NOE effect is *the* method for elucidation of 3D structural features and stereochemistry using NMR together with information from scalar spin,spin couplings. The NOE enhancement factor η is defined as

$$\eta = f_I\{S\} = \frac{\left(I - I^o\right)}{I^o}$$

in which I and I^o is the observed intensity of the resonance of spin I with and without irradiation of spin S, respectively. The efficiency through which the NOE is transferred from spin I to spin S depends strongly on the distance of the two protons involved and on the tumbling properties of the molecule:

$$\eta = f\left(\tau_c\, r^{-6}\right)$$

Because of the distance dependence, the NOE is the major tool for elucidation of stereo-chemistry of molecules in solution. The NOE depends on the relaxation rates of zero- and double quantum transitions:

$$f_I\{S\} = \frac{\gamma_S}{\gamma_I}\frac{\sigma_{IS}}{\rho_{IS}}$$

σ_{IS} is the **cross-relaxation rate**. Physically speaking, it characterizes the rate of

dipole-dipole transitions that give rise to the NOE. It can be expressed as:

$$\sigma_{IS} = W_{2QC} - W_{ZQC}$$

Therein, W_{2QC} and W_{ZQC} are the rates for double-quantum and zero-quantum transitions.

ρ_{IS} is the **longitudinal-relaxation rate**. It is the rate constant for direct dipolar relaxation of spin I by spin S. It corresponds to the rate of recovery of I-signal after selective inversion. In a two-spin system is ρ_{IS} equals to 1/T1. In multi-spin systems, however, dipolar relaxation with other spins contributes to 1/T1 and then ρ_{IS} is not equal to 1/T1. In the case of multispin systems

$$R_1 = \frac{1}{T1} = \rho_{IS} + \sum_x \rho_{IX} + \rho_I^*$$

ρ_{IX} corresponds to dipolar interaction with all other spins X and ρ^* to other relaxation mechanisms for spin I such as CSA. The important point to note here is that the magnitude of a NOE between two particular spins not only depends on their distance (and on the tumbling of the molecule) but also on the fact how many other protons are in close distance:

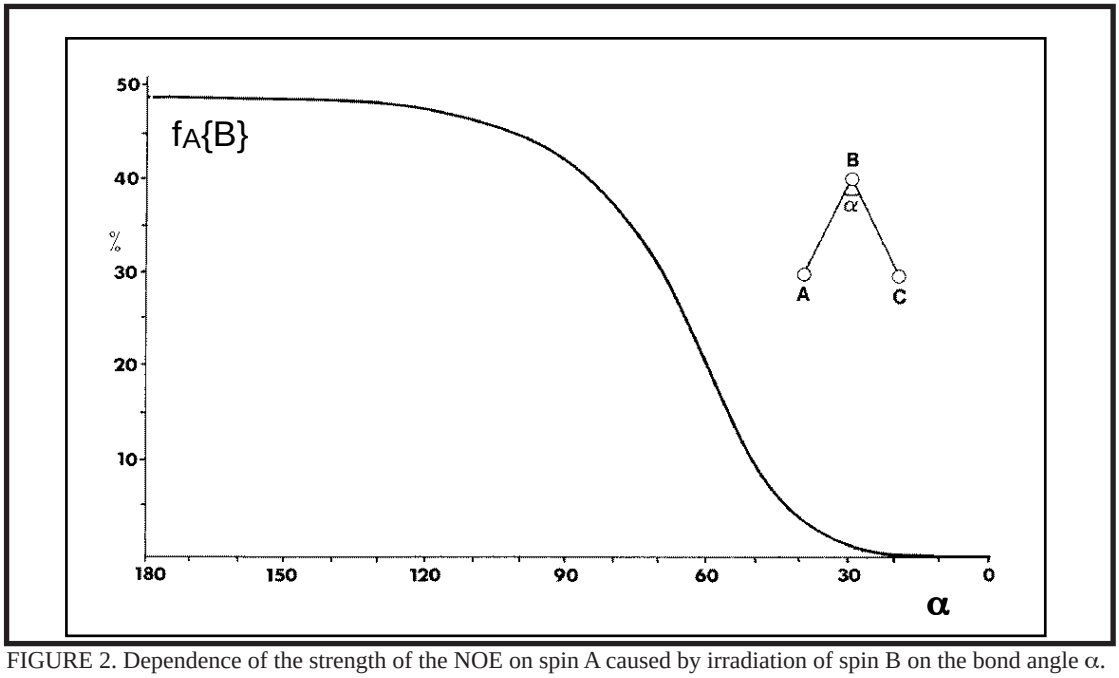

FIGURE 2. Dependence of the strength of the NOE on spin A caused by irradiation of spin B on the bond angle α.

This is nicely demonstrated in the figure above which shows the magnitude of the NOE between two protons A and B. The smaller the angle α the closer the third spin C is and the more efficient dipolar relaxation of spin A by spin C becomes thereby dramatically reducing the magnitude of the NOE between spins A and B. Note that the distance r_{AB} remained unchanged!

1.1 Experiments to measure NOEs:

In principle, a NOE enhancement can be triggered whenever the population of α- and β- states of a spin system are different from the equilibrium value. This can be accomplished by

- an inversion pulse (180 degree pulse) that inverts the relative populations of α- and β- states
- saturation of a resonance line that causes the corresponding α- and β- states to be equally populated.

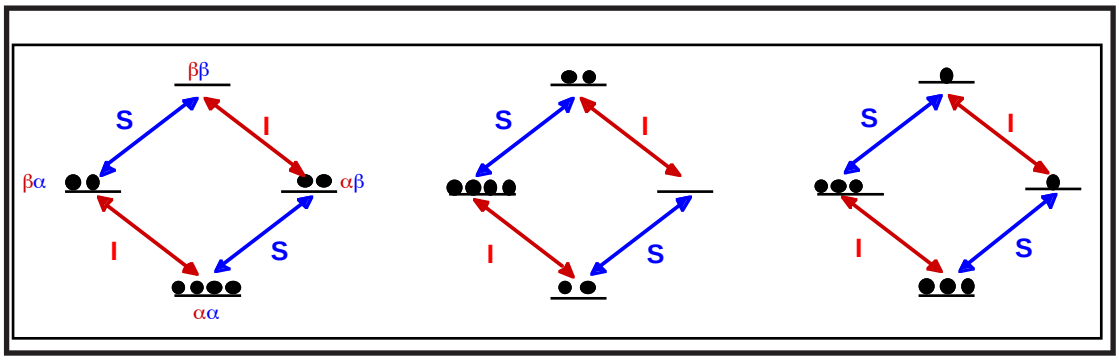

FIGURE 3. Left: Equilibrium population. Middle: Population after selective I-spin inversion pulse. Right: Population after saturation of the I-spin resonance.

Utilizing these two different means of disturbing the populations of spin systems the experiments for measuring NOEs can be categorized into the following

- the *steady-state* NOE experiment, in which a resonance is selectively irradiated with low power for a time τ_m sufficiently long to completely saturate the transition and propagate the NOE (approx. > 0.5s). A reference spectrum is recorded without irradiation and subtracted. The difference spectrum shows only signals which have received a NOE (that means, which have changed their intensity) and the irradiated resonance.
- the *transient* NOE. In this experiment a resonance is selectively inverted with a selective 180° pulse. After a delay τ_m for NOE buildup a 90° read pulse is applied and a 1D acquired. Again, one experiment with and one without the selective 180° pulse are subtracted from each other. The famous NOESY (or ROESY) is the 2D variant.

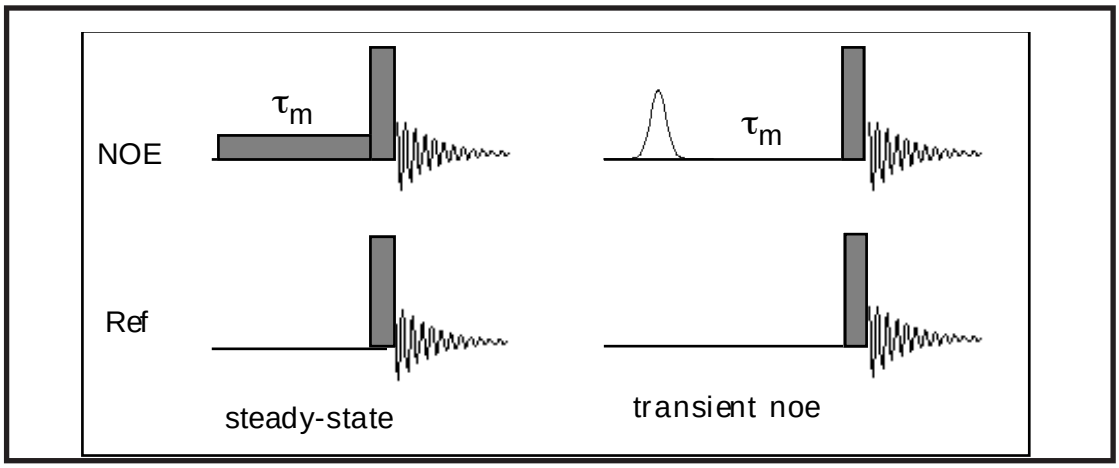

FIGURE 4. Pulse-schemes for measuring of steady state NOE (left) and transient NOE(right).

1.2 The steady-state NOE:

The steady state NOE depends on the geometry of all protons nearby, not only on those saturated and observed. The enhancement is:

$$f_I\{S\} = \eta_{\max}\frac{r_{IS}^{-6}}{r_{IS}^{-6}+\sum_x r_{IX}^{-6}} - \eta_{\max}\sum_x\left[\frac{f_X\{S\}r_{IX}^{-6}}{r_{IS}^{-6}+\sum_x r_{IX}^{-6}}\right]$$

In this equation the first term represents the **direct** contribution to the NOE. The magnitude due to the direct NOE is influenced by nearby protons because they have an influence on T1.

The second term in the equation above describes the **indirect** NOE transfer. The indirect transfer is a 3-spin effect. It is also called **spin-diffusion**. In spin-diffusion a relay spin that is close to both spins serves to transfer the NOE.

Depending on the correlation time and the sign of the NOE one distinguishes two cases:

1.2.1 Extreme narrowing (η_{max} >0):

- Most enhancements are positive but some can also be negative, depending on the geometry.
- T1 and T2 values are very similar.
- The lines are rather sharp (hence the name extreme-narrowing).
- The influence of the indirect effect is smaller but noticeable. This is shown in the figure below that displays the contribution due to the 3-spin effect depending on the angle α (extreme narrowing).

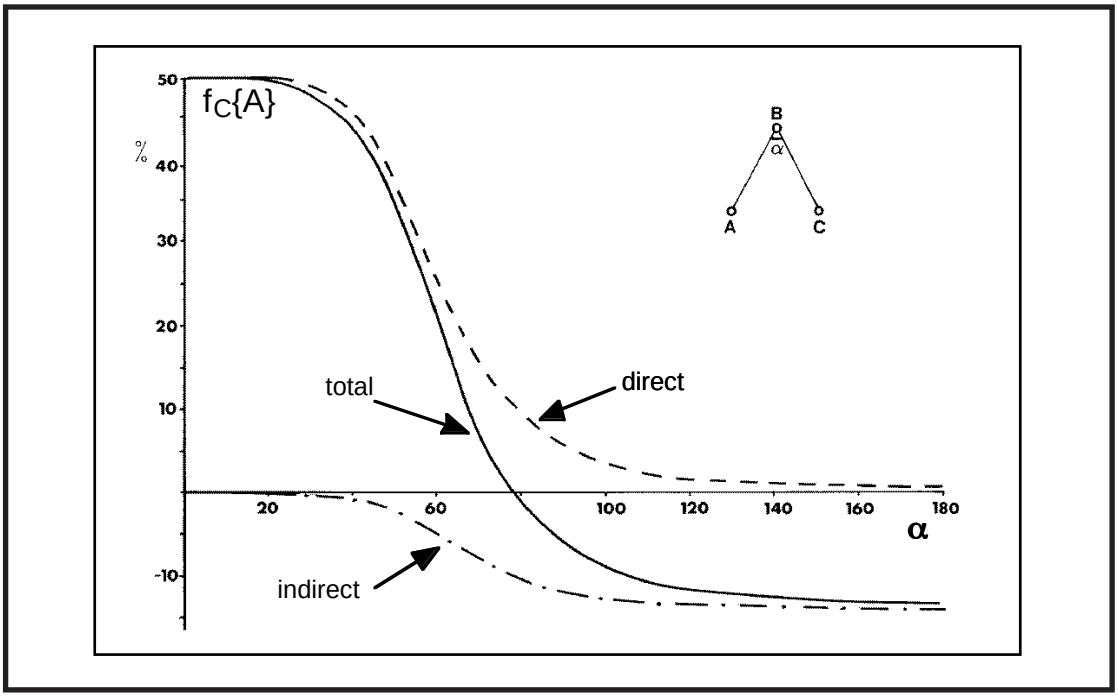

FIGURE 5. Contributions of direct and indirect (spin diffusion) effects to the overall NOE.

1.2.2 Spin-diffusion (η_{max} <0):

- In the negative NOE regime (large molecules), all enhancements are negative.
- The T2 values are very much shorter than T1.
- The lines are broad.

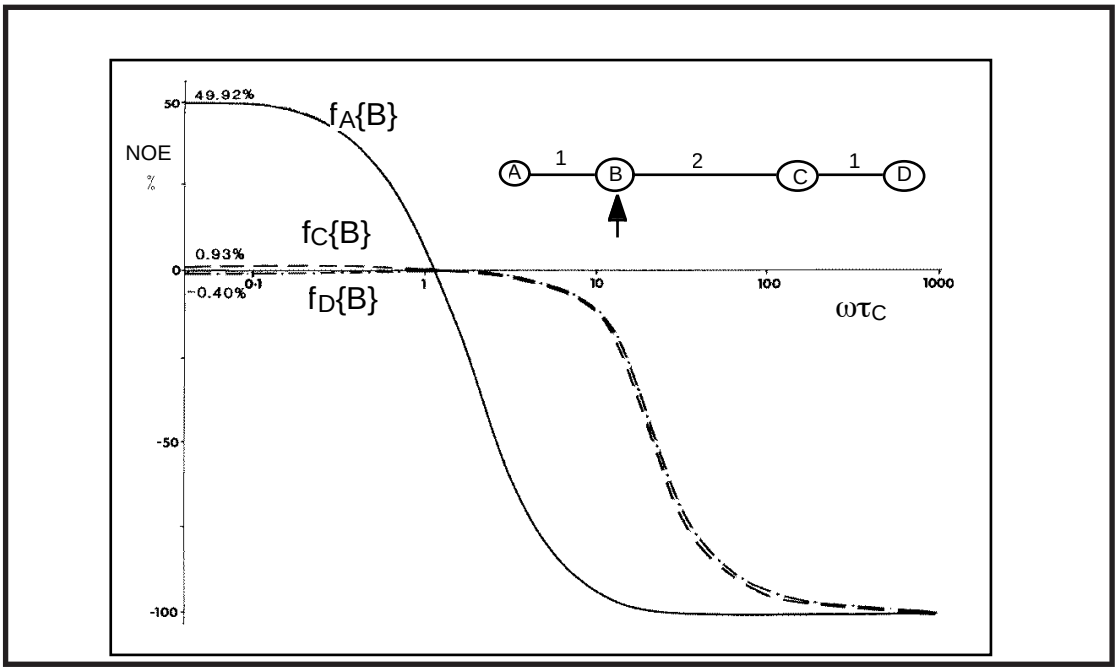

FIGURE 6. Steady-state enhancements depending on the correlation time for a four-spin system. The relative distances between spins A,B,C and D are 1:2:1 as indicated in the insert. Resonance B is irradiated.

Spin-diffusion is very effective and *steady-state NOE measurements are completely useless.* This is shown in the figure above. When the molecules have gained a certain size the spin-diffusion effect spreads the NOE out to all other protons (see the magnitude of the NOE for $\omega\tau_c > 100$*) respectable of what their distance to the irradiated proton is*!

In order to circumvent the problems associated with spin-diffusion the **truncated-driven NOE** has been used, in which the irradiation time is limited to short periods. In both regimes, the extreme narrowing and the spin-diffusion limit, enhancements are non-symmetrical due to possible relaxation leakage with a third spin:

$$f_I\{S\} \neq f_S\{I\}$$

1.3 The transient NOE:

In the transient NOE experiment a resonance is inverted by application of a selective 180 degree pulse or unselectively in a 2D experiment (NOESY). The NOE enhancement is:

$$f_I\{S\} = \frac{\sigma}{D}\left(e^{-(R' + D)\tau_m} - e^{-(R' - D)\tau_m}\right)$$

$$D = \frac{1}{4}\sqrt{(R_I - R_S)^2 + \sigma_{IS}^2} \qquad R' = \frac{1}{2}(R_I + R_{S)}$$

The transient NOE has some features that are remarkably different from the steady-state NOE:

- Enhancements are symmetrical

  $$f_I\{S\} = f_S\{I\}$$

  irrespective whether spin S has another proton close in space (which quenches the NOE in the steady state case dramatically).

- Using short mixing times NOE information is still useful in the spin-diffusion case. Spin-diffusion can be recognized from the buildup curves of the NOEs (a number of NOESY experiments are recorded with increased mixing times. Spin-diffusion cross peaks should show a characteristic induction phase).

- 1D transient and NOESY experiments give identical enhancements.

The following figure shows the transient NOE buildup upon irradiation of

Lys-56 NH of bovine phospholipase A_2 and observation of Ala-55 NH (N), Lys-56 β_1-H and β_2-H depending on the used mixing time for molecules in the extreme narrowing (τ_c = $3x10^{-11}$ or $3x10^{-10}$) or in the spin-diffusion limit (τ_c = $3x10^{-9}$ or $3x10^{-8}$):

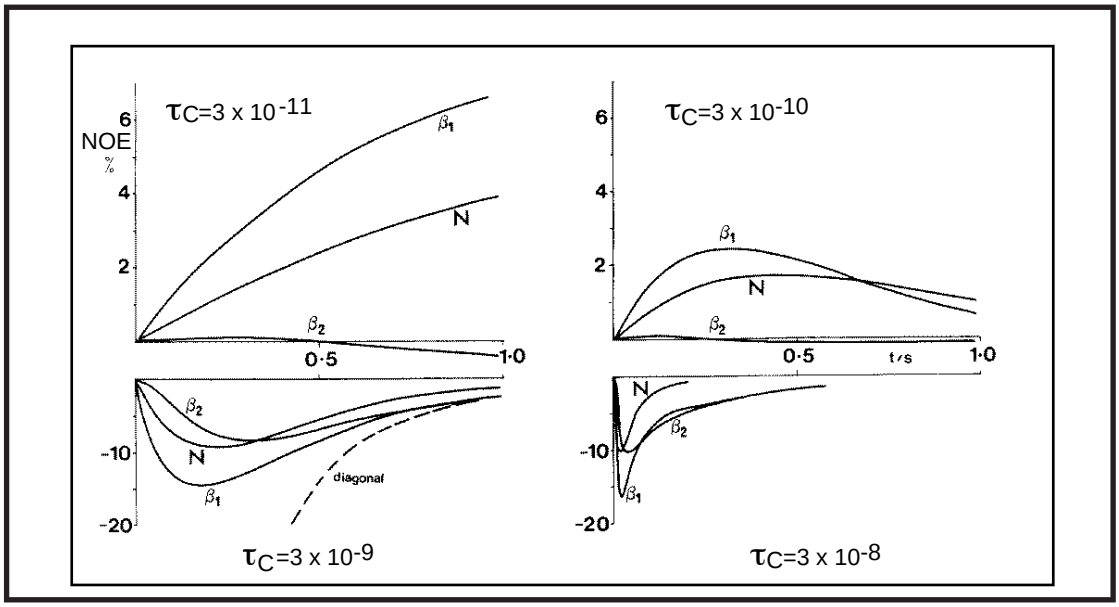

FIGURE 7. Strength of the spin-diffusion peak (β2) in dependence of the correlation time.

In the extreme narrowing the spin-diffusion peak β_2-H is of negligible intensity. In the spin-diffusion limit it can still be distinguished from the genuine NOE peaks at short mixing times. This is in contrast to the use of steady-state NOE's in that case.

1.4 The state of the spin system and the density matrix:

The density matrix describes the state of the spin-system. A one-spin system may be in the α or β state or may undergo a transition from the α into the β state (or vice versa). The density matrix contains the probabilities for a given state or transition and hence is a convenient way to simultaneously represent all possible states of a spin system. The density matrix contains diagonal elements which correspond to **populations**. These are states that do not undergo transitions. Off-diagonal elements are transitions. In thermal equilibrium all off-diagonal elements are zero.

A two-spin system may be in the $\alpha\alpha$, the $\alpha\beta$, the $\beta\alpha$ or the $\beta\beta$ state or may undergo transitions between them. The

$$\alpha\alpha \longrightarrow \alpha\beta \quad or \quad \alpha\alpha \longrightarrow \beta\alpha \quad or$$
$$\alpha\beta \longrightarrow \alpha\alpha \quad or \quad \beta\alpha \longrightarrow \alpha\alpha$$

transitions are called **single-quantum coherences**, since only one spin changes its state. Those are the only transitions which lead to observable signals during detection periods.

The **double quantum coherences**:

$$\alpha\alpha \longrightarrow \beta\beta \quad or \quad \beta\beta \longrightarrow \alpha\alpha$$

and the **zero-quantum coherences** (flip-flop transitions):

$$\alpha\beta \longrightarrow \beta\alpha \quad or \quad \beta\alpha \longrightarrow \alpha\beta$$

are not directly observable but play a very important role for the theoretical description of the nuclear Overhauser effect (NOE) because their efficiency determines the cross-relaxation rate. Double quantum transitions involve transitions where two spins flip the same way and in zero-quantum transitions the two spins undergo opposite flips. Double quantum coherences evolve with the sum of the chemical shifts of the comprising spins, zero quantum coherences evolve with the difference of their chemical shifts:

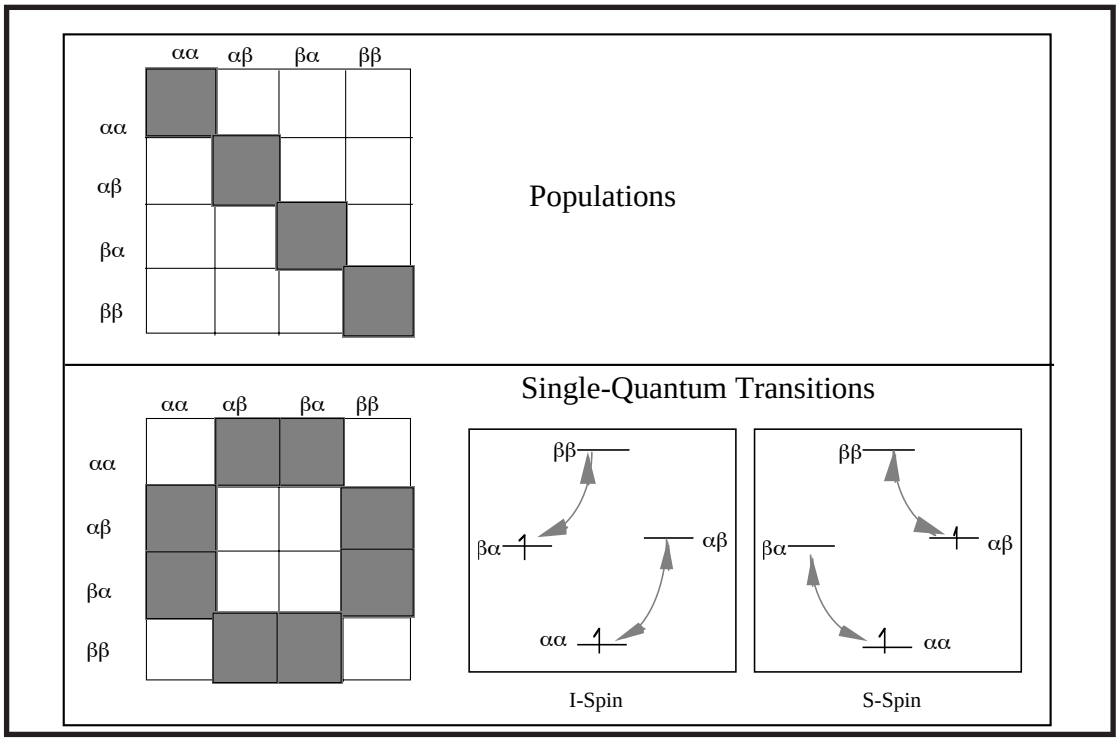

FIGURE 8. Occupied states of the density matrix (left) of populations and single-quantum transitions with corresponding transitions.

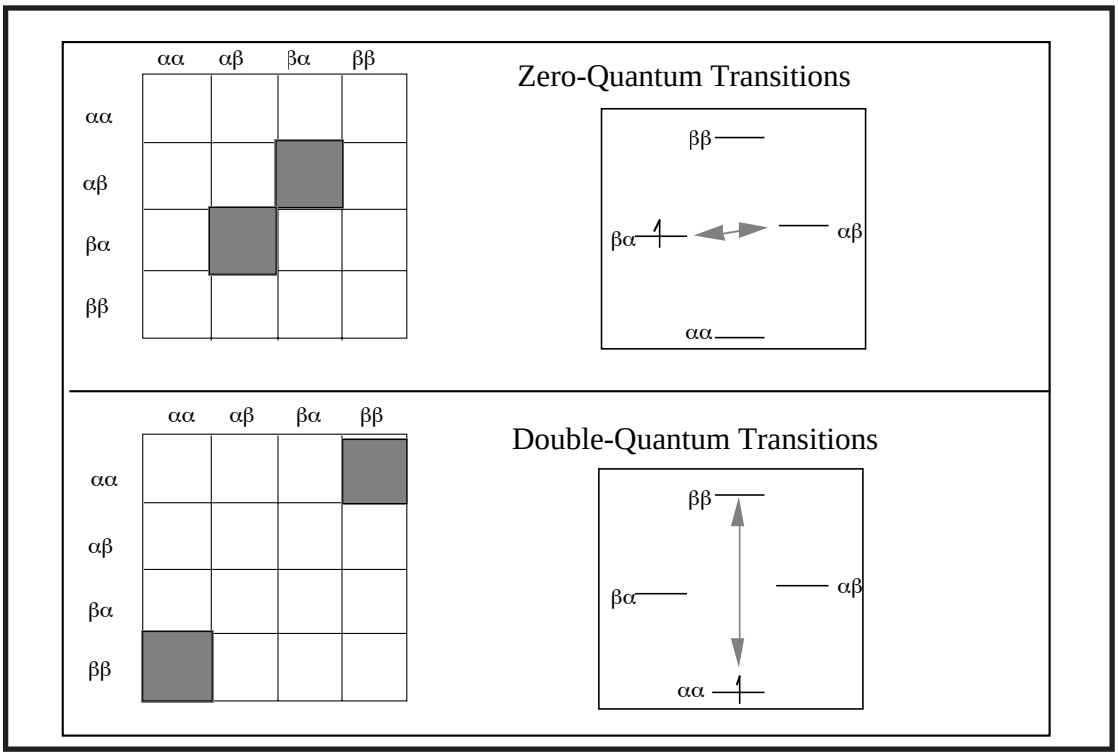

FIGURE 9. Occupied states of the density matrix (left) of zero- and double-quantum transitions with corresponding transitions.

1.5 The sign of the NOE:

The sign of the NOE can be positive (small molecules, extreme narrowing) or negative (large molecules, spin-diffusion limit). The dependence on the size of the molecule (to be more specific: on their correlation time) comes into play because the cross-relaxation rate is defined as:

$$\sigma_{IS} = W_{2QC} - W_{ZQC}$$

For proton,proton NOEs the zero-quantum frequencies are close to zero and the double-quantum frequencies are very high. As we have seen before large molecules have spectral density only at frequencies close to zero. Therefore, large molecules relax via zero-quantum transitions whereas small molecules mostly use double-quantum transitions, hence the change in the sign of the NOE:

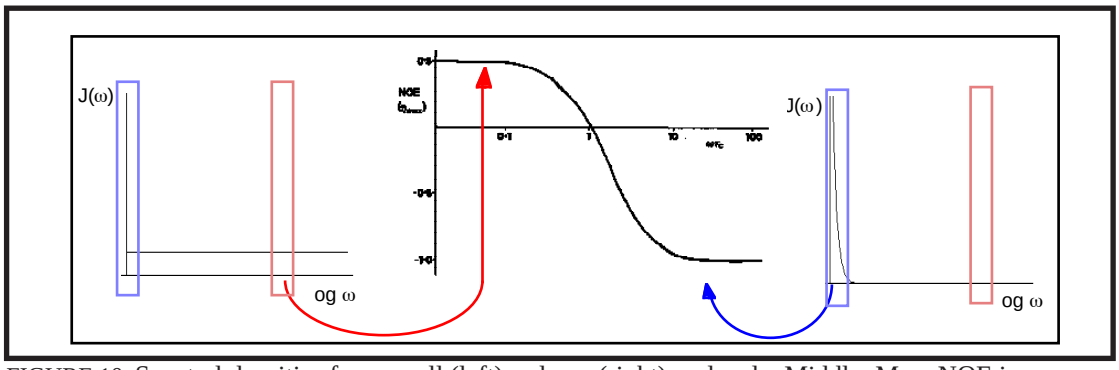

FIGURE 10. Spectral densities for a small (left) or large (right) molecule. Middle: Max. NOE in dependence of the correlation time.

This is the reason, why NOE spectra give very disappointing results for medium sized molecules (approx. 2000 m.wt. at RT). At this size efficiency of zero-quantum and double-quantum transitions is approximately the same and therefore the cross-relaxation rate (which is the difference between the two rates) is close to zero:

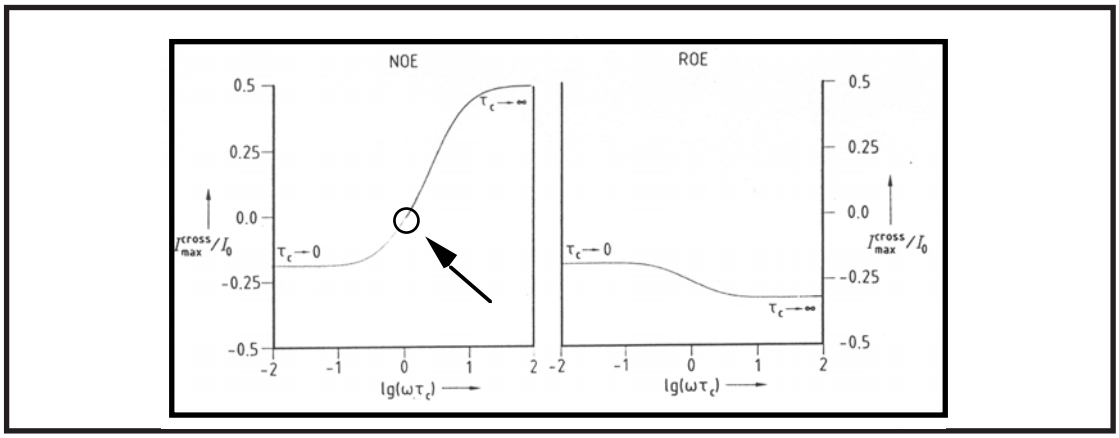

FIGURE 11. NOE and ROE dependence on the correlation time.

The absolute size of zero- and double-quantum transitions depends on the strength of the applied field. In the **rotating frame NOE** (ROE) experiment an additional field, the so-called **spin-lock** field, is applied along a transverse axis (x- or y-axis). In the ROE experiment magnetization therefore precesses about the x- (or y-) axis with a much lower frequency as the magnetization precesses about the z-axis in the NOE experiment. Because the B_1 field is much weaker (kHz range instead of MHz range), the zero- or double-quantum transitions have much lower frequencies, and hence relaxation always takes place via the

double-quantum transitions and no zero crossing is observed:

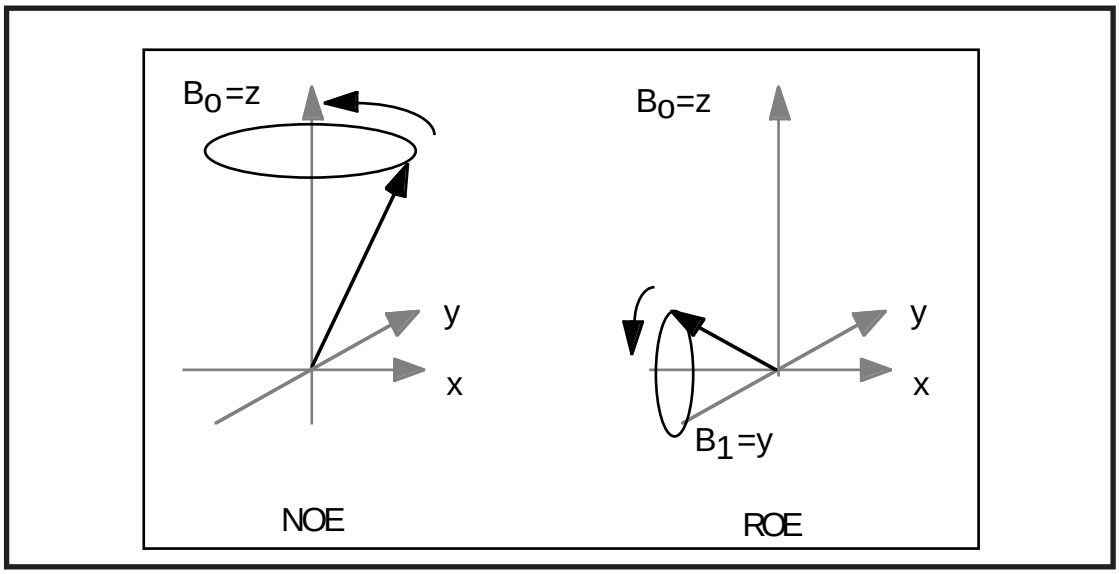

FIGURE 12. Axis of rotation during NOE (left) and ROE(right) buildup.

The ROE buildup is about 2.5 times faster than the NOE buildup and hence shorter mixing times can be used. However the spins relax with T1ρ during the spin-lock time (which is similar to T2) and hence the ROESY cannot be used for larger molecules due to rapid relaxation during the mixing time. In contrast, relaxation during the mixing time of a NOESY takes place with T1 which is long, even for large molecules.

1.6 Why only zero- and double-quantum transitions contribute to the NOE

In a two-spin system the transitions α_2->β_2 give rise to the spin-2 resonance and the transitions α_1->β_1 to the spin-1 resonance:

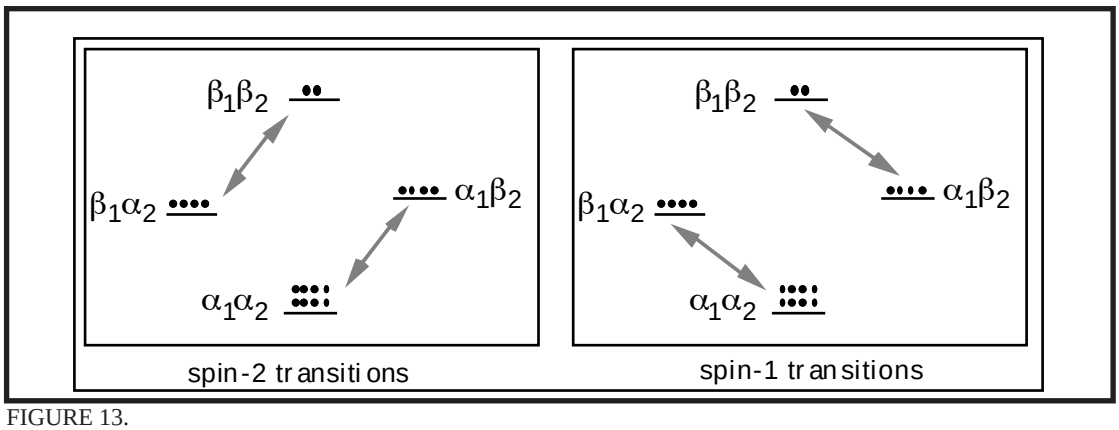

FIGURE 13.

Let us assume that we irradiate the resonance of spin 2:

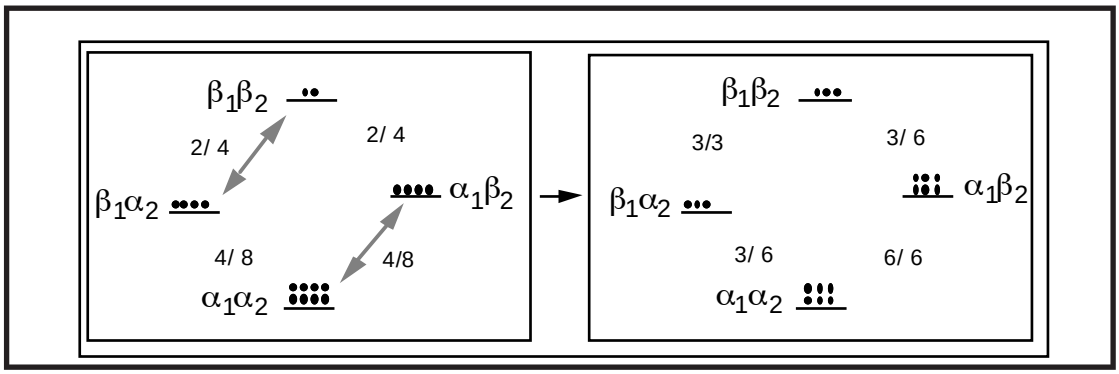

FIGURE 14.

Due to the irradiation the populations of the two states α_2 and β_2 are equalized. Now, this system tries to go back to the equilibrium state. It can do so via zero-, single- or double quantum transitions::

$$\alpha\alpha \longrightarrow \alpha\beta \quad or \quad \alpha\alpha \longrightarrow \beta\alpha \quad or$$
$$\alpha\beta \longrightarrow \alpha\alpha \quad or \quad \beta\alpha \longrightarrow \alpha\alpha \quad (SQC)$$
$$\alpha_1\alpha_2 \longrightarrow \beta_1\beta_2 \quad or \quad \beta_1\beta_2 \longrightarrow \alpha_1\alpha_2 \quad (DQC)$$
$$\alpha_1\beta_2 \longrightarrow \beta_1\alpha_2 \quad or \quad \beta_1\alpha_2 \longrightarrow \alpha_1\beta_2 \quad (ZQC)$$

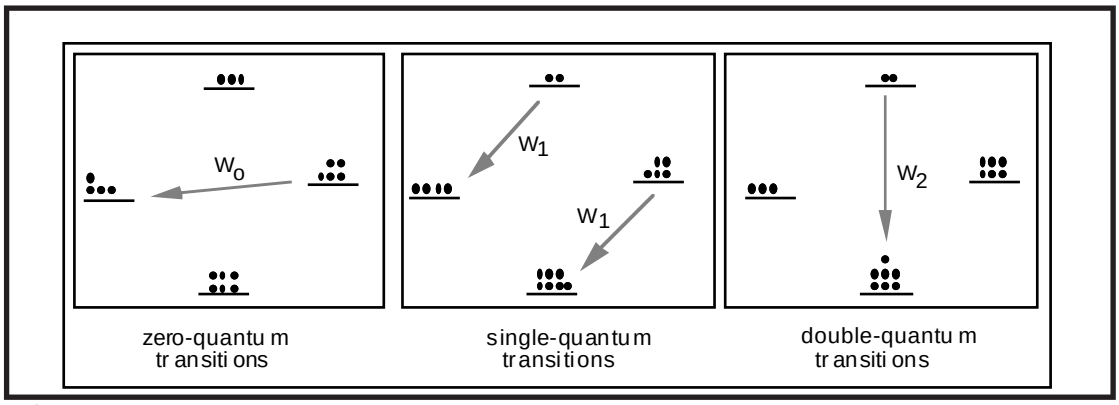

FIGURE 15.

However, because irradiation of the spin 2 resonances still keeps the populations of the two α_2 and β_2 states equal leading to $\beta_1\alpha_2 = \beta_1\beta_2$ and $\alpha_1\alpha_2 = \alpha_1\beta_2$. As can be seen from the following figure, only zero- and double-quantum transitions lead to a change of the intensity of the spin-1 transition (and hence to a NOE effect):

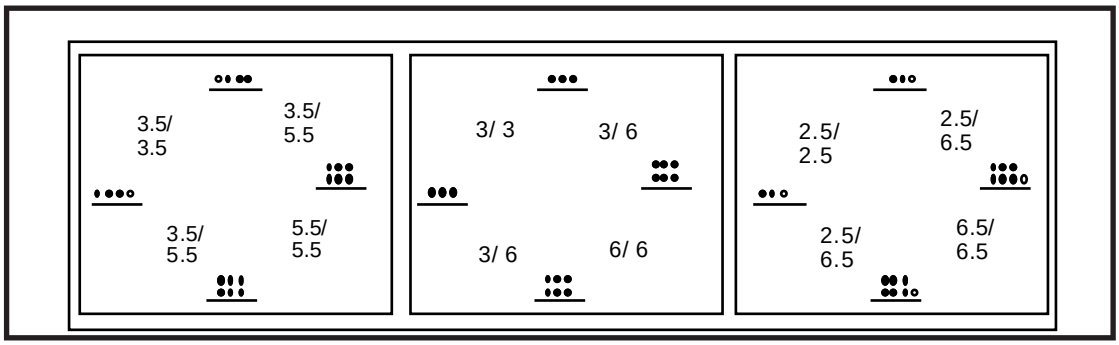

FIGURE 16. Populations after zero-quantum (left), single-quantum (middle) and double-quantum (right) transitions and subsequent restoring due to spin-2 irradiation.

1.7 Practical tips for NOE measurements:

- the conditions for measurement must be very stable
- (as always true for methods that rely on differences). Especially, the temperature must be stable. For the same reason, *never use spinning* for NOE measurements! Measuring over night or on weekends is preferred because of less traffic in the building. Optimize the lock power, adjust lock power just below saturation to give a strong lock signal.
- the mixing time has to be optimized for the molecule size, do not use too long mixing times in order to avoid spin diffusion.
- Avoid paramagnetic impurities!
- If very small effects should be measured, remove oxygen (degas the sample; oxygen is a biradical).
- The sample should be concentrated enough but not too concentrated (little lock signal).
- For observation of NOE's between methyl groups and other protons, irradiate the methyl group, because relaxation of methyl protons is mainly governed by the other methyl protons.
- Pay attention to the choice of the solvent. Use a solvent, that gives an intense lock signal (DMSO, acetone, rather not $CDCl_3$ or D_2O if possible), because than the lock is more stable. D_2O also has a large temperature shift of the solvent line, so that the lines easily shift when the temperature is not stable.
- If the NOE is very small, that means if the tumbling time is such that the NOE is near to the zero-crossing, going from a non-viscous solvent (acetone) to a viscous solvent (DMSO) or measuring at lower temperatures may increase the size of the NOE dramatically (note that at low temperatures the danger is high that the temperature is not stable).
- Use sufficiently long relaxation delays (3-5 times T_1).

Excurs I: The use of NOE data for structure calculation of peptides and proteins

NMR data can be used for structure calculations of proteins up to about 30 kDa presently. The method uses the fact, that the strength of the NOE between protons depends on their distance. The volume of the NOESY crosspeaks may be expressed as

$$V = \langle r^{-6} \rangle f(\tau_c)$$

The distance between the two protons may vary due to flexibility of the polypeptide chain. The NOE depends also on the correlation time.

The first step in the procedure is to assign the NOESY spectrum completely. Peaks are then integrated. The next step is to convert NOESY peak volumes into distances, a process known as “calibration”:

$$V = k / d^{4-6}$$

These distances will then serve as upper limits to constrain distances between different protons in the calculated structures. Due to the flexible nature of polypeptides no lower limits are used (except for disulfide bridges). The inherently different flexibility of different classes of protons in peptides (e.g. compare backbone atoms with methyl-groups) is taken into account by applying different calibration functions for them. Backbone atoms are calibrated with a r^{-6} dependence, whereas for NOE’s involving methyl protons a r^{-4} calibration will be applied. The constant k can be determined on the basis of known distances (e.g. the distance of sequential amide protons in helices is about 3Å). Additionally, scalar vicinal coupling constants may be used to constrain torsional angles.

To calculate structures from these upper limits and torsion angle constraints distance geometry algorithms have been used in the past. However, nowadays restrained molecular dynamics calculations are performed. In these calculations, Newtons equation of motion is integrated:

$$m_i \frac{d^2}{dt^2} r_i(t) = F_i(t) \qquad i = 1, \ldots, N$$

Thereby, the coordinate of a atom at time t can be calculated from the force acting on it. The force itself is expressed as the negative gradient of the potential energy. The potential energy function is the normal force field expanded by an additional term reflecting the nmr constraints:

$$U_{pot} = U_{forcefield} + U_{NMR}$$

During a structure calculation a number of (typ. 20-50) randomly chosen conformers is energy minimized under a simulated annealing protocol. The NMR constrains in the potential energy function will force the molecule to adopt a structure that is compatible with the NMR data. After the calculation the 20-50 separately energy-minimized conformers is superimposed for best fit. A resulting narrow structure bundle indicates good convergence of the calculation. This is mostly the case when enough NOE’s are present to define the structure. Flexible parts of the molecule usually will display less NOE’s are less well defined in the resulting structure bundle.

Excurs II: Use of dipolar couplings to yield structural constraints:

Orientations of structural elements with respect to each other (e.g. the relative orientation of two helices) is difficult to describe from NMR experiments. Usually, only a few NOE's between the two elements may be used. Any misassignment will lead to a large errors in the relative orientation.

Relatively newly, residual dipolar couplings have been used for describe orientations of parts of the molecule that are separated by a large distance. Dipolar interactions between two protons depend on the orientation of the vecto connecting the two atoms with respect to the external field

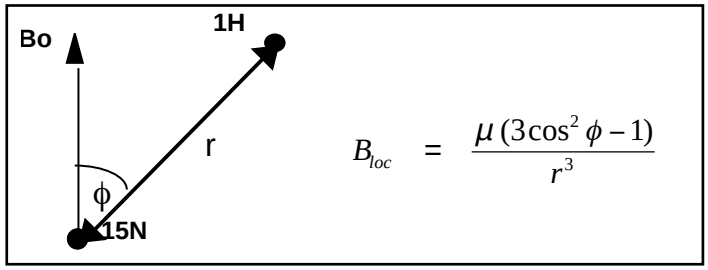

$$B_{loc} = \frac{\mu(3\cos^2\phi - 1)}{r^3}$$

Usually, these dipolar interactions are averaged to zero in solution due to rapid tumbling and therefore rapid changes in the angle f. However, Bax et al. could show, that it is possible to partially orient macromolecules in solutions containing bicelles (disk-shaped vesicles). These pospholipid vesicles orient in the magnetic field such that the membrane normal is perpendicular to the direction of the magnetic field. Marcomolecules in these solution are then partially oriented by simple steric reasons:

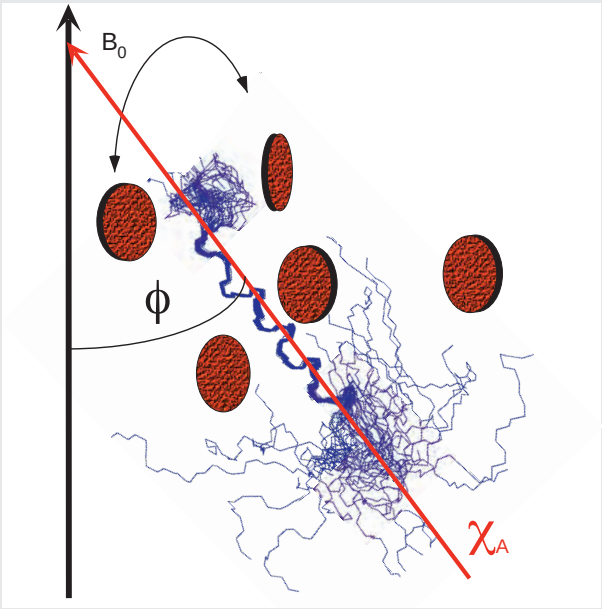

The dipolar coupling can be calculated as:

$$\delta_{dip} \propto S(B_0^2)\gamma_A\gamma_B r_{AB}^{-3} \bullet [\chi_A(3\cos^2(\phi - 1)) + \chi_B(\sin^2\phi\cos 2\phi)]$$

where c_A and c_B are the axial and rhombic alignment tensors and S the order parameter. Thereby, a reference frame for all protons (the alignment frame) is available and orientations are possible with respect to that frame irrespective of the number of intervening bonds. Thereby, parts of molecules that are far apart may be oriented relative to each other.

1. CHEMICAL OR CONFORMATIONAL EXCHANGE:

Let us assume that ethanol binds to a target molecule and dissociates of again:

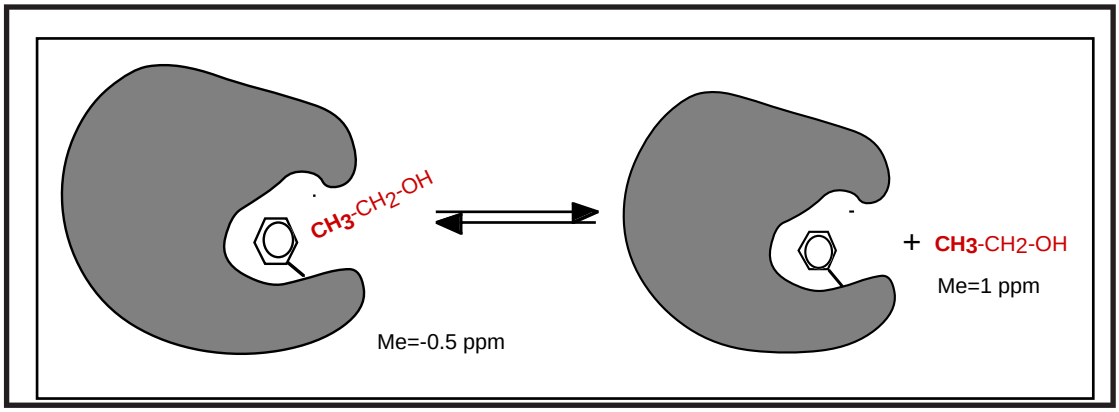

FIGURE 1. Binding of methanol to protein in the vicinity of a aromatic residue leads to strong shift of methyl signal

In such a situation the methyl group of ethanol has different chemical environments in the bound and in the free state. In the bound state it is under the influence of the ring current shift of a tyrosine residue for example, and therefore the chemical shift will be low-field shifted. In the free state the anisotropy effect due to the ring current shift has disappeared. Depending on the exchange kinetics the methyl signal will appear as a single or as two resonances with more or less exchange broadening. Three different states can be distinguished:

- **Slow exchange** (two sets of resonances with reasonable sharp lines)
- **Fast exchange** (a single, sharp line positioned somewhere between the two lines)
- **Intermediate exchange** (a single, very broad (or invisible) line.)

The underlying exchange process may also be chemical exchange, such as exchange between the hydroxyl protons and protons from dissolved water. Alternatively it could be conformational exchange. All these processes are frequently encountered in NMR.

1.1 Two-site exchange:

Let as assume the following reaction:

$$A \xrightarrow{k_{+1}} B$$

$$B \xrightarrow{k_{-1}} A$$

The lifetime of state A is:

$$\tau_A = 1/k_{+1}$$

and of state B is

$$\tau_B = 1/k_{-1}$$

The NMR parameters that characterize both states are a) the chemical shift, b) scalar spin,spin couplings and c) the linewidth (transverse relaxation time). The **NMR time-scale** is defined by the relation of the exchange rate with respect to the magnitude of the accompanying change in the corresponding NMR parameter:

	Exchange rates		
Time scale	**slow**	**intermediate**	**fast**
Chemical Shift	$k << \delta_A - \delta_B$	$k = \delta_A - \delta_B$	$k >> \delta_A - \delta_B$
Scalar Coupling	$k << J_A - J_B$	$k = J_A - J_B$	$k >> J_A - J_B$
Transverse Relax.	$k << 1/T_{2A} - 1/T_{2B}$	$k = 1/T_{2A} - 1/T_{2B}$	$k >> 1/T_{2A} - 1/T_{2B}$

The exchange time scale is defined by the separation of the two signals *relative to the exchange rate*. The ratio is influenced by

- increasing temperature accelerates the exchange reaction and therefore pushes the system into the fast exchange regime
- increasing static fields increases the line separation and therefore drives the system into the slow exchange regime.

The effect of chemical or conformational exchange on the chemical shift is shown below. Therein, a signal in the fast exchange regime is into the slow exchange regime pushed by decreasing the temperature or increasing the field strength. At the **coalescence temperature** a very broad line with a plateau is observed.

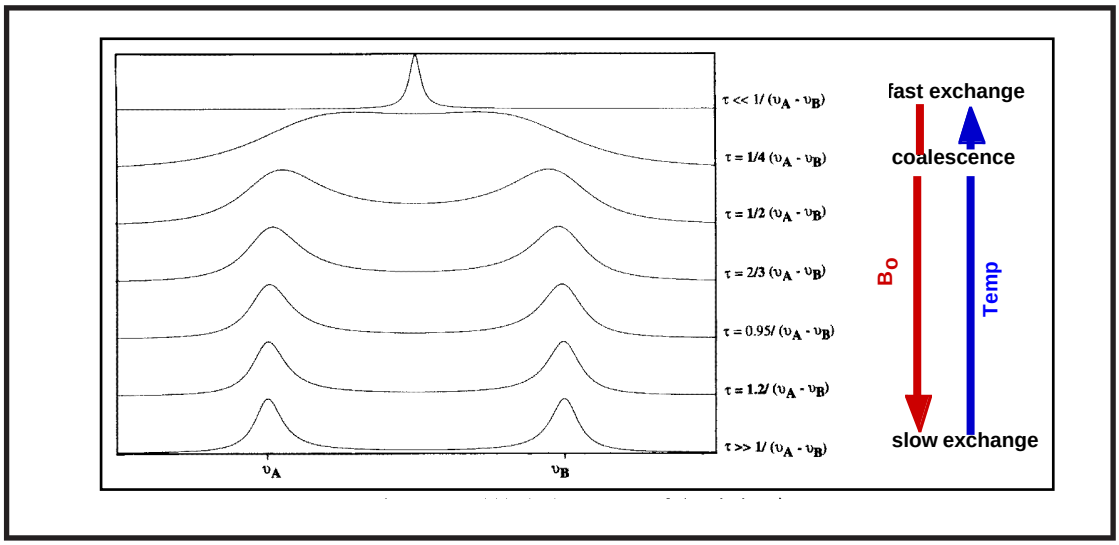

FIGURE 2. Appearance of two-site exchange spectra in dependence on the exchange rate. Top: Fast exchange, Bottom: Slow exchange, 2nd row from top: coalescence.

1.1.1 Fast exchange:

At fast exchange a single resonance line is observed at the frequency

$$\delta_{ave} = p_A\delta_A + (1 - p_A)\delta_B$$

It is obvious from the equation above that the resonance position of the averaged signal may not be simply the arithmetic mean of the resonance positions of the two slow-exchanging lines because the population of the two states has to be taken into account (usually a unknown).

The exchange reaction causes an additional contribution to the linewidth of

$$\Delta\nu_{1/2} = \frac{1}{2}\frac{\pi(\nu_A - \nu_B)^2}{k_{+1}}$$

Thereby, the faster the reaction or the smaller the frequency difference (provided that a single line is observed, fast exchange regime) the narrower the line. Such an increase in reaction rate can be accomplished via a temperature increase and a decrease in frequency separation by lowering the magnitude of the static field.

A similar situation exist with *averaging of couplings*:

$$J_{ave} = p_A J_A + (1 - p_A)J_B$$

An important example for averaging of couplings is found for hydroxyl protons of alcohols that exchange with solvent water protons. In the figure below, the boxed proton feels the vicinal proton to be in the α-state (left side). Through chemical exchange that proton is substituted by a proton that comes from water and is in the β-state. When the exchange is slow both lines of the doublet are visible but for the fast case only the average singlet will be observed. This mechanism has been termed **self-decoupling** and is the reason why OH protons in alcohols usually appear as (broad) singlets:

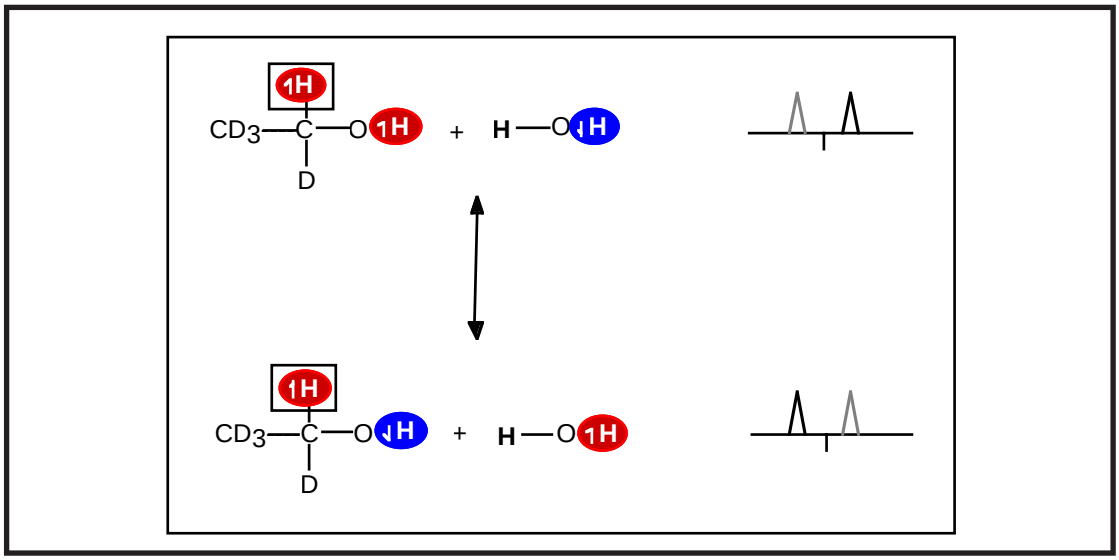

FIGURE 3. Exchange of the hydroxyl proton with a proton from water may lead to a change in the spin state of the OH proton. If this process is fast, only the avaraged line at the center without splitting due to coupling is visible.

1.1.2 The slow exchange limit:

When two separate signals are observed the *additional* contribution to the linewidth due to exchange is:

$$\Delta\nu = \frac{k_{+1}}{\pi}$$

Hence, temperature decrease or field increase will lead to a sharpening of the lines.

A typical example where both situations (slow and fast exchange) are simultaneously encountered is exchange of amide and hydroxyl protons of peptides with solvent in aqueous solution. At slightly acidic pH the amide protons give separate, sharp lines and the exchange rate is on the order of 1-10 sec^{-1}. In contrast, exchange between hydroxyl and water protons is so fast that the hydroxyl protons coincide with the water chemical shift and cannot be observed separately.

1.1.3 The intermediate case:

The lineshape of the signals changes upon passing from the slow into the fast exchange regime. A detailed investigation shows that it may be described as:

$$g(\nu) = \frac{2\tau_A(\nu_A-\nu_X)^2}{\left[\nu-\frac{1}{2}(\nu_A+\nu_X)\right]^2+\pi^2\tau_A{}^2(\nu-\nu_A)^2(\nu-\nu_X)^2}$$

The following figure shows calculated lineshapes for two signals 10 Hz apart (top trace) depending on the lifetime (which is the inverse of the reaction rate) or for two signals with 0.1sec lifetime depending on the frequency separation (given in Hz):

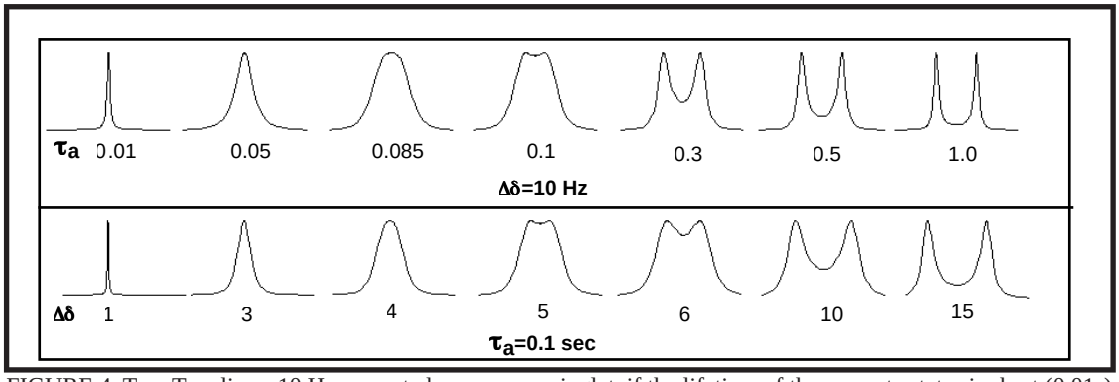

FIGURE 4. Top: Two lines, 10 Hz separated appear as a singlet, if the lifetime of the separate states is short (0.01s) or as two separate lines, when the lifetime is long (1s). Bottom: Calculated for a lifetime of 0.1 s with varying frequency separations (1-15 Hz).

At coalescence the lineshape is characterized by a flat top. The corresponding lifetime at coalescence is given by

$$\tau_A^c = \frac{\sqrt{2}}{\pi}(\nu_A-\nu_X)$$

Usually, one is not interested in recording spectra with exchange-broadened lines. You

can find out the proper measuring conditions by

- recording spectra at higher temperature
  ==>when the lines get sharper heat until the lines are sufficiently narrow. When that temperature cannot be reached (sample not heat-stable or solvent is volatile), record spectra at lower field.
- when the lines get broader upon temperature rise cool down or proceed at higher field.

If you cannot get spectra with reasonable sharp lines following this procedure it is worth trying to change the solvent which may have a dramatic effect.
The following figure shows 1D spectra (expansions) of chinin recorded at 300 and 600 MHz. It is obvious that by going from 600 to 300 MHz a considerable improvement in linewidths has been achieved. Often cyclic compounds display such dynamic behavior due to slow conformational interconversions.

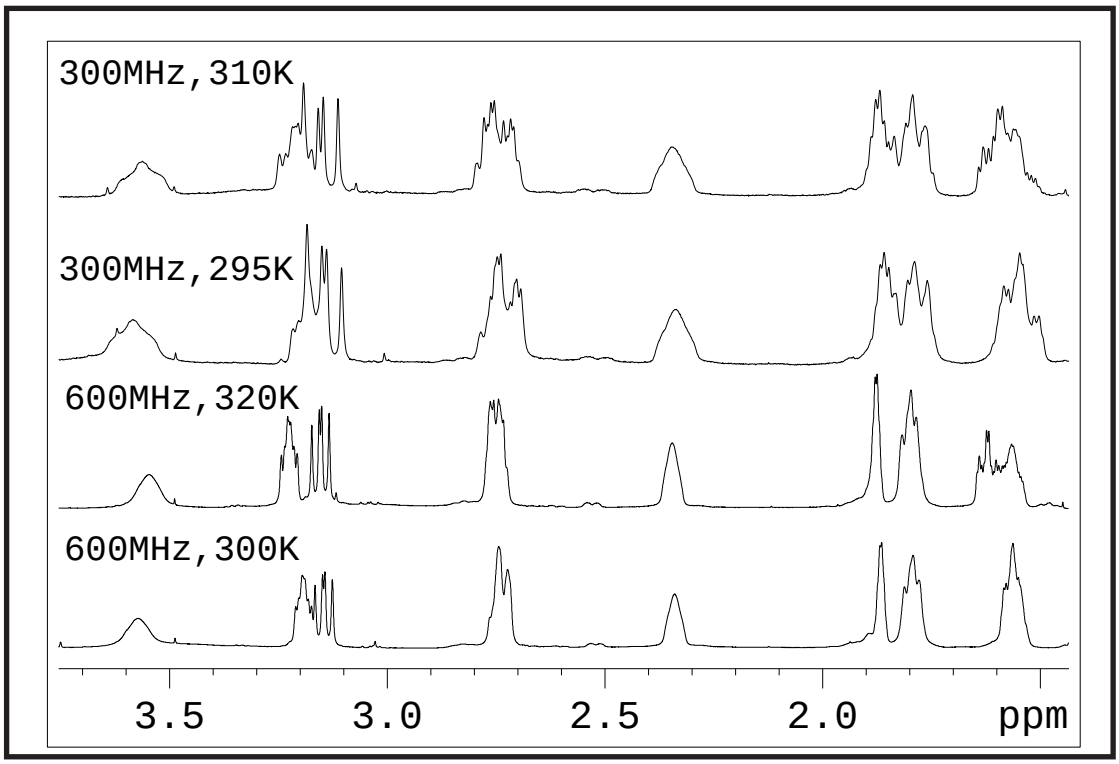

FIGURE 5. Appearance of spectra displaying exchange phenomena in dependence on the static field

1.2 Investigation of exchange processes:

1.2.1 EXSY spectroscopy:
The 2D EXSY experiment is in principle identical to the NOESY pulse experiment. However, the mixing time is usually chosen shorter, since the exchange rate is normally much faster than the cross-relaxation rate. Crosspeaks are due to exchanging (chemical

or conformational) protons.

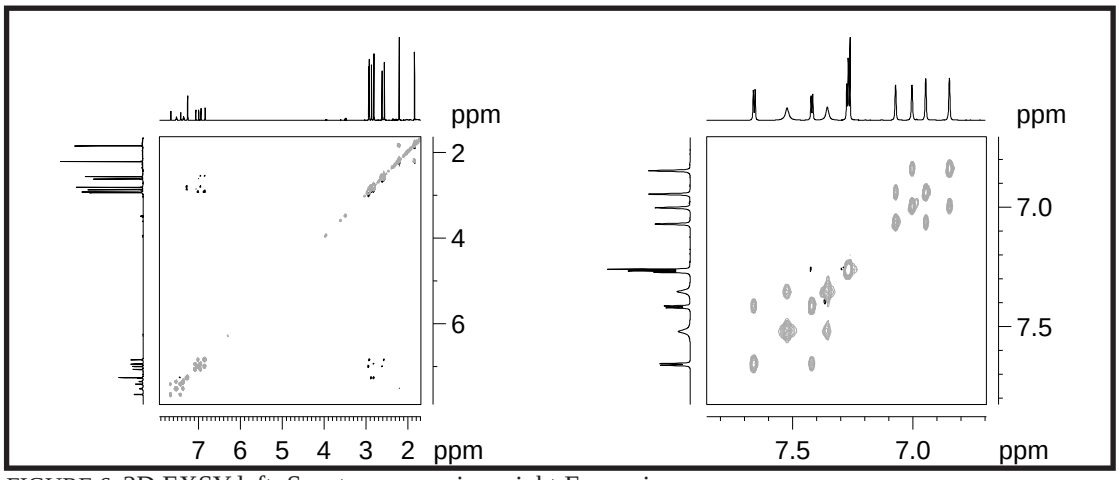

FIGURE 6. 2D EXSY:left: Spectrum overview, right:Expansion

1.2.2 Saturation transfer:

When a signal is inverted (e.g. by application of a selective 180 deg. pulse), it recovers with T1. However, other protons that are in exchange with the inverted or saturated resonance become also saturated or inverted:

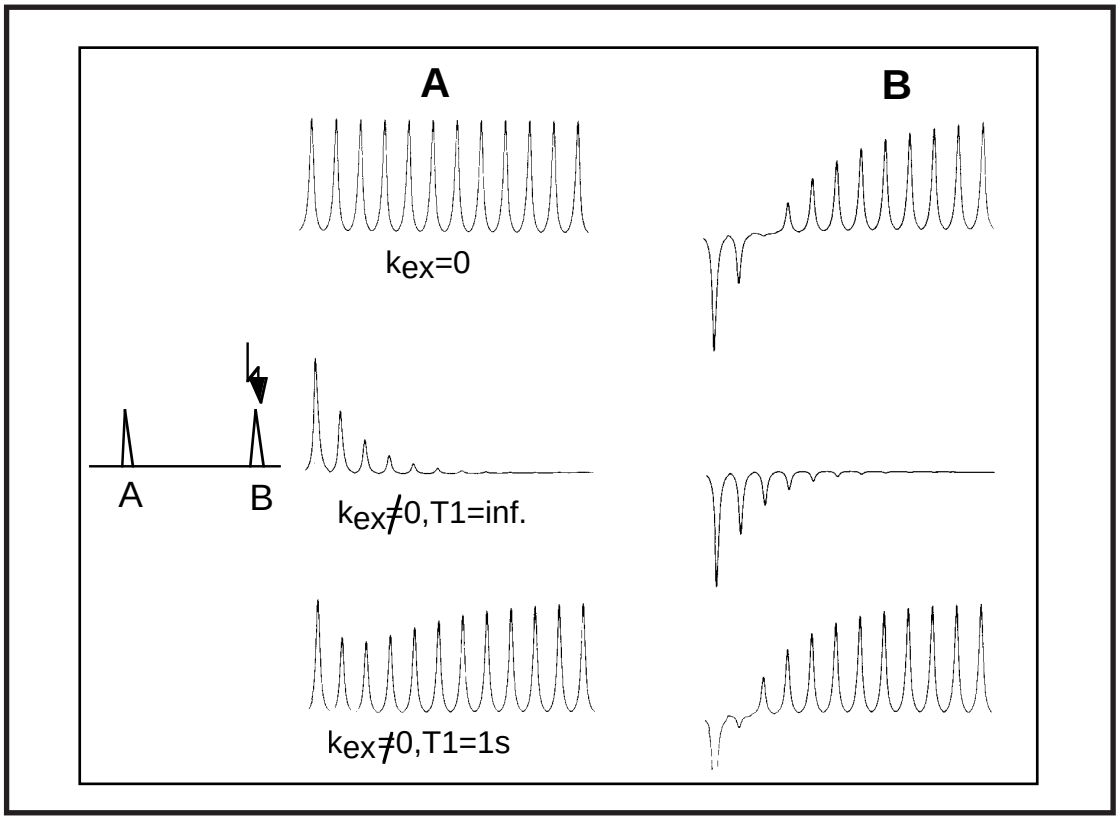

FIGURE 7. Single-line spectra of resonance A (left) and B (right)after various time increments. Top: No exchange. Middle:Exchange, infinitely long T1, bottom: exchange, T1=1s.

In this figure resonance B has been inverted. The signal is shown after successive time increments for resonance A (left) or resonance B (right). The top trace shows the case without exchange between A and B (no effect on A). The middle trace displays a dramatic effect on resonance A when exchange occurs. However, the longitudinal relax-

ation time T1 has been assumed to be infinity. In the lower trace the signal A recovers due to T1 relaxation.

A frequent case where saturation transfer occurs is through presaturation of solvent. Hydroxyl protons that exchange with the solvent (e.g. water) vanish from the spectrum or largely decrease in intensity when solvent presaturation is applied. From the rate of recovery the exchange rate can be calculated (provided T1 has been determined before).

1.3 Determination of activation parameters:

The observation of dynamic processes in NMR spectra allows to calculate parameters for the activation parameters of the exchange process. The activation energy for such a process can be calculated according to the Arhenius equation

$$E_a = -RT \ln K^{\#}$$

in which $K^{\#}$ is the equilibrium constant for the formation of the activated complex. This is related to the reaction rate k via

$$k = \kappa \frac{kT}{h} e^{-\Delta G^{\#}/RT}$$

Theory of thermodynamics states that

$$\Delta G^{\#} = \Delta H^{\#} - T\Delta S^{\#}$$

so that

$$k = \kappa \frac{kT}{h} e^{-\Delta H^{\#}/RT} e^{\Delta S^{\#}/R}$$

therein,

- κ is the transmission coefficient (usually 1)
- k the Boltzmann constant
- T the temperature
- h the Planck constant

A plot of ln(k/T) versus 1/T yields a line with slope (- $\Delta H^{\#}$/R) and intercept (23.76 + - $\Delta S^{\#}$/R).

In close agreement the activation energy can be estimated as

$$\Delta G^{\#} \approx RT_c \left(22.96 + \ln \frac{T_c}{\nu_A - \nu_B} \right) \quad [Jmol^{-1}]$$

1. THE PRODUCT OPERATOR FORMALISM (POF) FOR DESCRIPTION OF PULSE-EXPERIMENTS:

Simple one-dimensional NMR experiments may be conveniently described using the pictorial vector description. However, in order to more deeply understand two-dimensional NMR or multiple-quantum spectroscopy the product operator formalism is required.

The following events may happen during or after application of radiofrequency (RF) pulses:

- chemical shift precession
- evolution of scalar or dipolar couplings
- change of the state of the spins due to additional RF fields
- relaxation

In the following we will see how these events are described in the product operator formalism (POF). Truly speaking, the POF may only be used to describe spin systems in the *weak coupling* case (no second order effects). In the POF, precession and scalar coupling can be calculated in arbitrary order. If not necessary, relaxation effects are usually ignored but can be added easily.

In the POF calculations are done on magnetization, which is the ensemble property formed by adding up all dipole moments from separate spin, rather than on individual spins. The transformations due to shift precession or coupling are described as rotations in three-dimensional cartesian space:

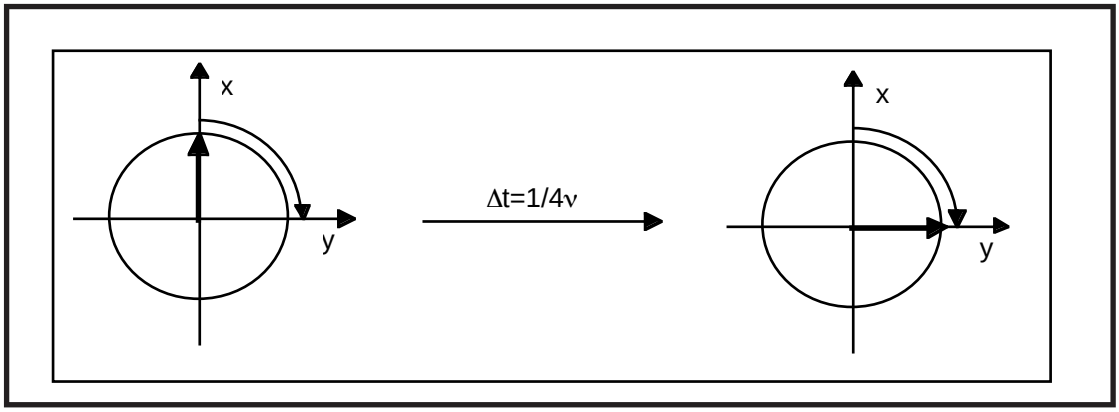

FIGURE 1. Rotation of a vector after a time 1/4ν

We have seen before that a continous rotation can be described as an harmonic oscillation and presents a superpostion of a sine- and cosine modulated function.

In the example given above a property aligned along the x-axis rotates about the z-axis onto the y-axis with a frequency ω. In the POF this will read as follows:

$$A_x \xrightarrow{\omega A_z} A_x \cos(\omega t) + A_y \sin(\omega t)$$

The symbol over the arrow indicates the axis and the frequency of rotation.

1.1 RF pulses:

Application of a RF field along the x-axis will rotate z-magnetization in the z,y plane:

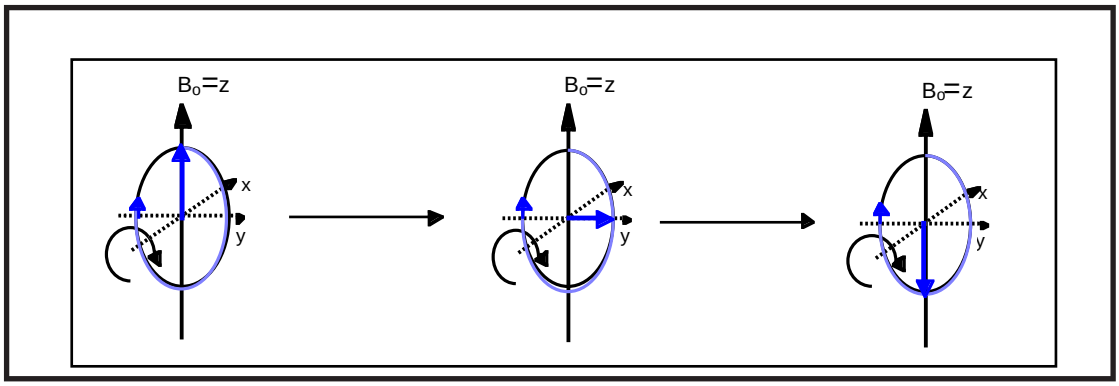

FIGURE 2. Rotation of z-magnetization about the -x-axis. This will achieve the following conversions: z -> y -> -z -> -y -> z

It is described as:

$$I_z \xrightarrow{\beta I_x} I_z \cos\beta - I_y \sin\beta$$

Of particular importance are rotations of 90 and 180 degrees. The frequency of rotation depends on the strength of the field. The field strength is expressed in terms of the frequency, which is the inverse of the time required for a 360˚ rotation.

$$\frac{\gamma B_1}{2\pi} = \frac{1}{PW(360°)}$$

The sign convention for rotations is that applying a field along the x-axis will rotate in *clockwise* sense (Field along y: Look down the y-axis and rotate clockwise, e.g. from z to -x)

1.2 Chemical shift precession:

After application of a 90˚ RF pulse spins are correlated in phase leading to a bunching of phases. The resulting magnetization vector rotates in the x,y plane

(transverse plane) with a certain angular velocity. After a certain amount of time it will have rotated by a specific angle depending on its offset frequency. Note that chemical shift evolution can only take place for *transverse* magnetization!

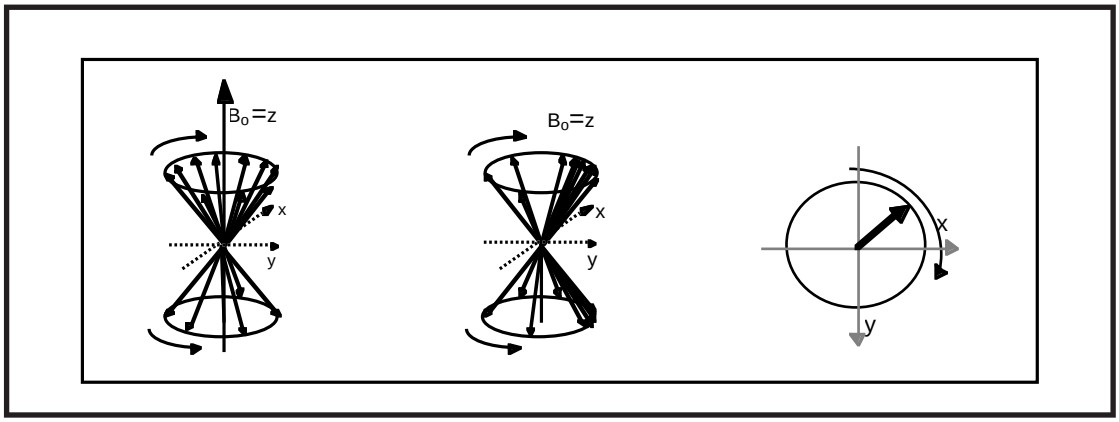

FIGURE 3. Left: Equilibrium state. Middle: State after 90 deg RF pulse. Right: Shift precession in the transverse plane.

Shift precession amounts to a rotation of the magnetization vector in the transverse plane.

$$I_x \xrightarrow{\omega I_z} I_x \cos(\omega t) + I_y \sin(\omega t)$$

The precession frequency is

$$\omega = 2\pi\delta$$

where δ is the offset from the transmitter frequency.

1.3 Scalar spin,spin coupling:

Due to the fermi-contact interaction spins that have a neigbouring spin in the α-state are of slightly different energy than those that have them in the β-state. Having different energies means that these two different kinds of spins precess with different frequencies because frequency and energy are related to each other. In a reference coordinate system that rotates with the center frequency of a dublet the downfield component will rotate with a frequency of +J/2 in one direction and the other component with –J/2 in the other direction. When both vectors are 180° out of phase the resulting term is

$$I_y S^{\alpha} + (-I_y) S^{\beta} = 2I_y (S^{\alpha} - S^{\beta}) = 2I_y S_z$$

This state is of particular importance for coherence transfer which is the crucial step for polarization transfer experiments (e.g. INEPT, DEPT) or the mixing

steps in 2D experiments. In the product operator formalism the transformation under scalar spin,spin coupling is described as:

$$I_x \xrightarrow{\pi J I_z S_z} I_x \cos(\pi J t) + 2 I_y S_z \sin(\pi J t) \xrightarrow{\pi J I_z S_z} -I_x$$

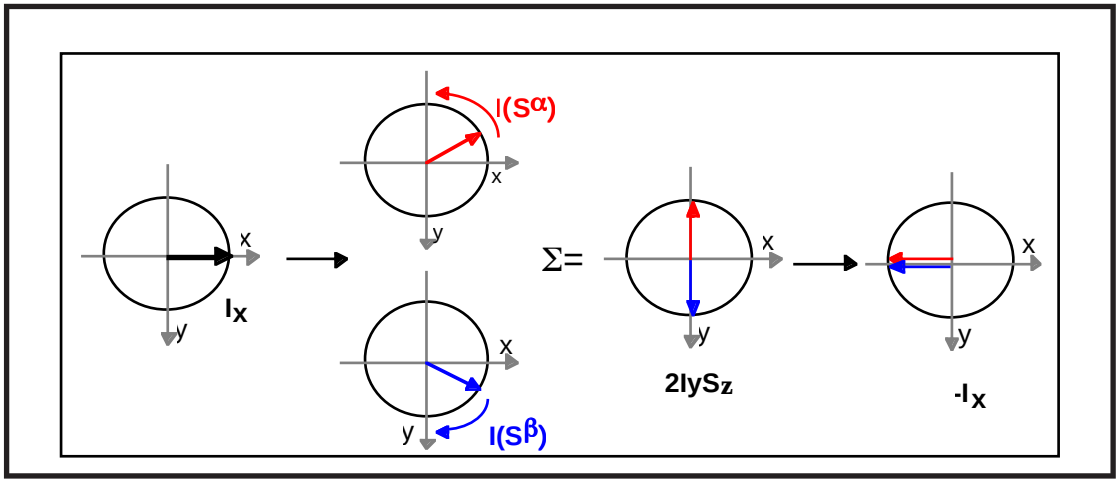

FIGURE 4. Vectorial representation of the states due to evolution of scalar couplings

A number of operators are frequently encountered during the calculations:

- I_x, $I_y$transverse x (or y) magnetization
- $I_z$longitudinal magnetization
- $2I_xS_z$antiphase I magnetization (or I magnetization antiphase w.r. to S)
- $2I_zS_z$longitudinal two-spin order
- $2I_xS_y$two-spin coherence (mixture of zero-and double-quantum
- coherence, multiple-quantum coherence)

Two operators that are both transverse cannot evolve scalar couplings amongst each other!

The product operators can be directly related to the appearance of signals. Scalar couplings do occur as in-phase splitting when the operator is

$$\mathbf{I_x cos(\pi J_{I,S} t)}$$

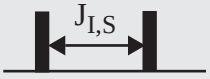

or as anti-phase splitting if the operator is

$$\mathbf{2I_yS_z sin(\pi J_{I,S} t)}$$

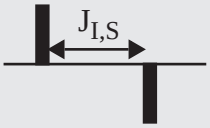

The operator $\mathbf{2IySzsin(\pi J_{I,S}t)cos(\pi J_{I,X}t)}$ leads to the following signal:

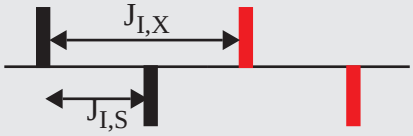

1.4 A simple one-dimensional NMR experiment:

A conventional one-dimensional experiment for recording proton spectra looks like the following:

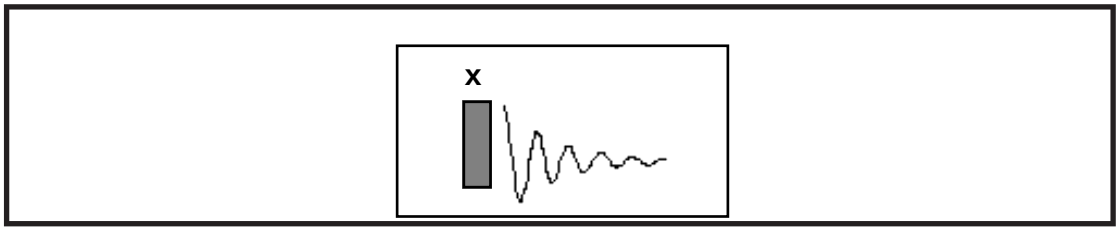

FIGURE 5. A simple 1D experiment consisting of a 90° pulse followed by sampling of the FID.

(In the following, 90 degree pulses are drawn as narrow, shaded rectangles, 180 deg. pulses as black, wider rectangles). A 90 degree RF pulse applied along the x-axis is immediately followed by data acquisition. Using the POF we can summarize the events for a 2-spin system. Usually, one starts with pure z-magnetization. The events are subsequently calculated:

- 90 degree x-pulse:

$$I_z \xrightarrow{90(I_x)} -I_y$$

- chemical shift evolution

$$-I_y \xrightarrow{\omega t I_z} -I_y\cos(\omega t) + I_x\sin(\omega t)$$

- scalar spin,spin coupling:

$$-I_y\cos(\omega t) + I_x\sin(\omega t) \xrightarrow{\pi Jt(I_zS_z)} -I_y\cos(\omega t)\cos(\pi Jt) + 2I_xS_z\cos(\omega t)\sin(\pi Jt) + I_x\sin(\omega t)\cos(\pi Jt) + 2I_yS_z\sin(\omega t)\sin(\pi Jt)$$

Note that chemical shift and scalar coupling may be calculated in arbitrary order (but not the effect of pulses and shift/coupling!).

During a pulse sequence all possible interactions have to be calculated which may lead to a huge number of terms. However, only a limited number of terms lead to detectable magnetization at the end and only those are of interest because they contribute to the signal:

- directly observable are only single operators that contain transverse terms (I_x,I_y, S_x, S_y..)
- antiphase magnetization (such as I_yS_z) evolves into in-phase magnetization ($-I_x$) if the corresponding coupling is resolved
- terms that contain more than one transverse operator are not observable and hence can be ignored *in the end* of the sequence

Certain terms that are of negligible intensity can be removed *during* the calculation thereby largely reducing the number of operators.

1.5 The effect of 180 degree pulses:

180 degree pulses are often used to

- refocus chemical shift
- refocus scalar couplings

When a 180 degree pulse is placed *in the centre* of a delay it will refocus chemical shift evolution of transverse magnetization (see left part of the following figure).

180 degree pulses will flip spins from the α- into the β-state:

$$I^{\alpha} \xrightarrow{180} I^{\beta} \qquad I^{\beta} \xrightarrow{180} I^{\alpha}$$

The effect of 180 degree pulses are summarized in the following figure:

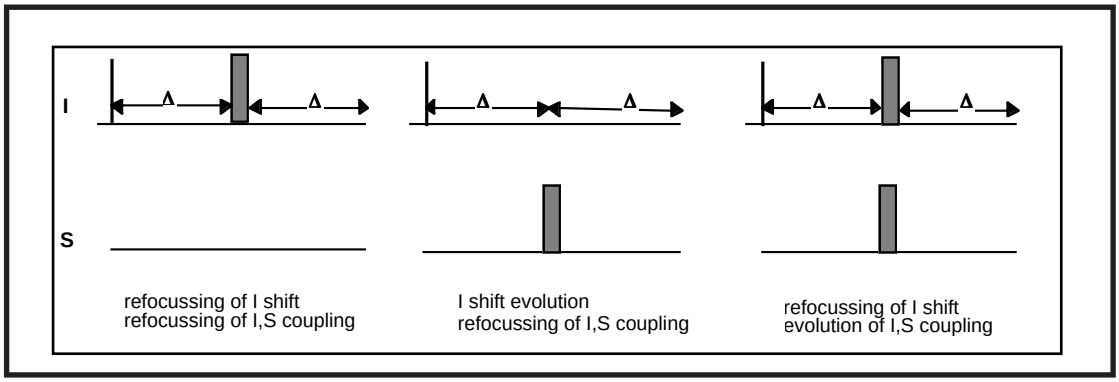

FIGURE 6. Effects of 180° pulse(s) on shift precession and evolution of scalar couplings

We have seen before that the two dublet lines arising from spin,spin coupling are due to different spins that have neighbouring spins in either the α- or the β-state. When this coupling partner is flipped from the α- into the β-state or vice versa the coupling evolution will be refocussed after a time that is the same as the one during which the system was allowed to evolve the coupling. In this context it is very important to distinguish two cases:

- both spins I and S experience the 180 degree pulse which is usually the case if they are both protons (homonuclear case)
- only one of the two nuclei experiences the pulse which is the case for a $^{1}H,^{13}C$ pair.

In the first case both spins are simultaneously flipped and no overall effect occurs. Only the latter leads to decoupling.

The refocussing of chemical shift can be described with the product operator formalism easily in the following way:

$$I_x \xrightarrow{\Delta} I_y \xrightarrow{180(x)} -I_y \xrightarrow{\Delta} I_x$$

and for evolution of heteronuclear scalar couplings:

$$I_x \xrightarrow{\Delta} 2I_yS_z \xrightarrow{180(S)} 2I_y(-S_z) \xrightarrow{\Delta} I_x$$

However, homonuclear scalar couplings are not refocussed since both spins are flipped:

$$I_x \xrightarrow{\Delta} 2I_yS_z \xrightarrow{180(I,S)} 2(-I_y)(-S_z) \xrightarrow{\Delta} -I_x$$

1.6 Coherence transfer:

Coherence transfer is the crucial step of

- polarization transfer experiments (INEPT,DEPT)
- multidimensional correlation experiments

In order to transfer coherence couplings must have been evolved. Antiphase I-spin coherence is then transferred into antiphase S-spin coherence:

$$I_x \xrightarrow{(\pi Jt)I_zS_z} I_x\cos(\pi Jt) + 2I_yS_z\sin(\pi Jt) \quad [1]$$

$$2I_yS_z \xrightarrow{90°(I_x)} 2I_zS_z \quad [2a]$$

$$2I_zS_z \xrightarrow{90°(S_x)} -2I_zS_y \quad [3a]$$

When the time t during which scalar coupling takes place is exactly equal to $(2J)^{-1}$ $\sin(\pi Jt)=\sin(\pi/2)$ and I-spin coherence has quantitatively been transformed into antiphase coherence. Note that in the homonuclear case steps [2] and [3] can be achieved with a single pulse. It is also important to realize that step [2] requires the phase of the 90° pulse to be x. Otherwise, multiple-quantum coherences are formed:

$$2I_yS_z \xrightarrow{90°(I_y)} 2I_yS_z \quad [2b]$$

$$2I_yS_z \xrightarrow{90°(S_x)} -2I_yS_y \quad [3b]$$

Through the coherence transfer step **transverse I-spin** magnetization has been transformed into **transverse S-spin** magnetization.

1.7 Polarization transfer:

Polarization transfer is a common building block in pulse-experiments to increase sensitivity. The sensitivity is proportional to the number of spins that can undergo a certain transition. We have seen before that this number depends on the relative populations of α- and β-states according to the Boltzmann distribution. The higher the energy gap between the two states the larger the population difference and hence the stronger the intensity of the signal.

^{13}C spectra are much lower in sensitivity because

- the natural abundance of ^{13}C is 1/100 of that of protons
- the energy separation between α- and β-states is $\gamma(^{13}C)/\gamma(^{1}H)=1/4$ and hence the number of transitions are much lower.

Polarization transfer is aimed at bringing the population difference from protons to carbons and hence increasing the sensitivity.

The prototype for the PT sequences is the INEPT experiment:

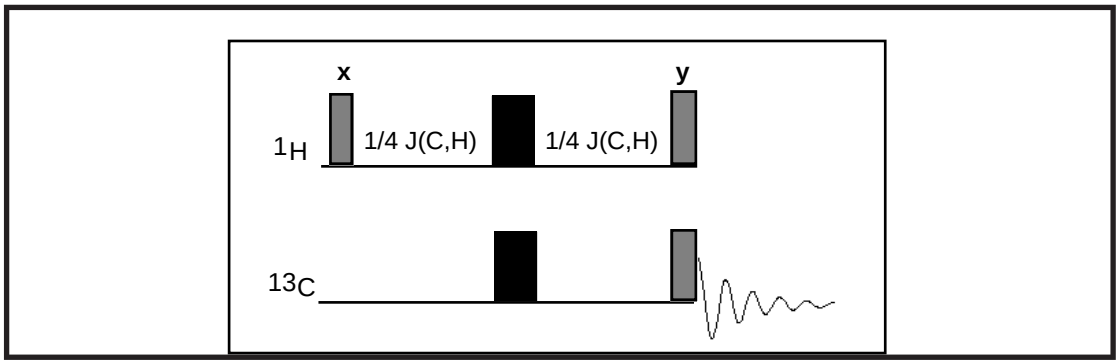

FIGURE 7. Pulse sequence for INEPT experiment (^{1}H,^{13}C polarization transfer).

Using the POF the INEPT sequence can be summarized in the following way:

$$I_z \xrightarrow{90°(I_x)} -I_y \xrightarrow{1/2J(I,S)} 2I_xS_z \xrightarrow{90°(I_y)} -2I_zS_z \xrightarrow{90°(S_x)} 2I_zS_y$$

In principle, one might be tempted to remove the 180° pulses on the proton and carbon channel. However, chemical shift evolution would then take place for protons transforming

$$2I_xS_z \xrightarrow{\omega t I_z} 2I_xS_z\cos(\omega t) + 2I_yS_z\sin(\omega t)$$

The second term would be transformed into non-observable multiple-quantum coherence through the cascade of the following two 90° pulses:

$$2I_yS_z\sin(\omega t) \xrightarrow{90°(I_y,S_x)} -2I_yS_y\sin(\omega t)$$

Therefore, we need a 180° pulse in the center of the proton delay. However, this

proton pulse would unfortunately decouple protons from carbons, and we do need the coupling evolution for the transfer. Hence, a 180° pulse on the carbon channel is additionally required in order to avoid decoupling.

The important achievement of the PT sequence is that the amount of antiphase carbon magnetization is proportional to the starting I-spin magnetization which is $I_z=(I^{\alpha}-I^{\beta})$. At the end of the PT sequence the amount of transverse cabon magnetization depends on the Boltzmann distribution of the proton levels which is much more favourable!

An experiment that has become even more popular than INEPT is the **DEPT** sequence. The DEPT experiment allows to record ^{13}C spectra that are **edited** with respect to the number of protons that are directly bonded to the carbons. Non-proton bearing carbons are missing in DEPT spectra. The editing is achieved through suitable choice of the length of the final proton pulse in the sequence. For β=135 degrees, methyl and methin carbons are positive and methylen carbons are negative. For β =90 degrees, only CH carbons are contained. The dependence of the signal intensity for CH_3,CH_2 and CH carbons on the proton pulse length is shown below:

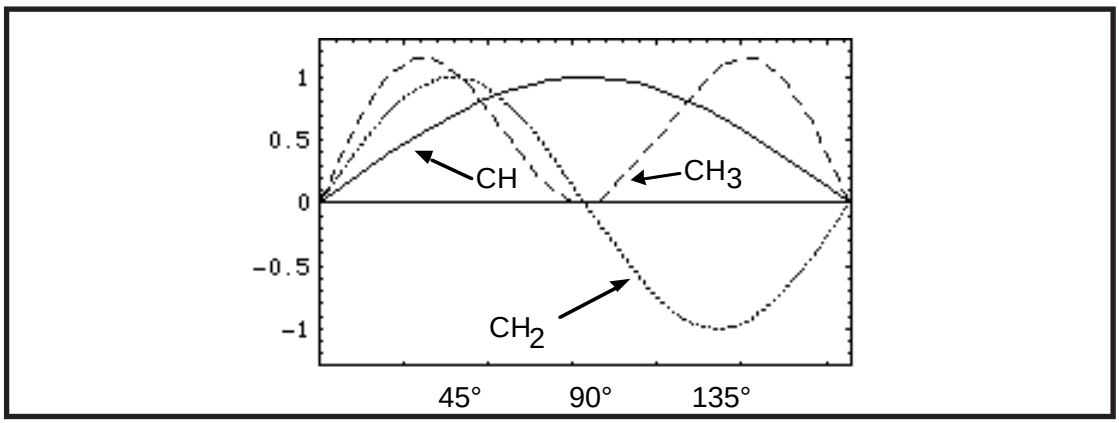

FIGURE 8. Transfer amplitudes for CH_n (n=1-3) groups in DEPT experiments in dependency of the flip angle of the final proton pulse.

Since CH and CH_3 carbons can usually be distinguished on the base of their chemical shifts, a DEPT-135 experiment is mostly sufficient but should be complemented by a DEPT-90 in case of ambiguities for CH_3/CH. The DEPT sequence relies on uniform ^1J (CH) coupling constants, a large variation of coupling constants leads to cross-talk in the edited spectra.

Of course, a double PT 2D experiment can be used to increase the senitivity

further such as the HSQC experiment:

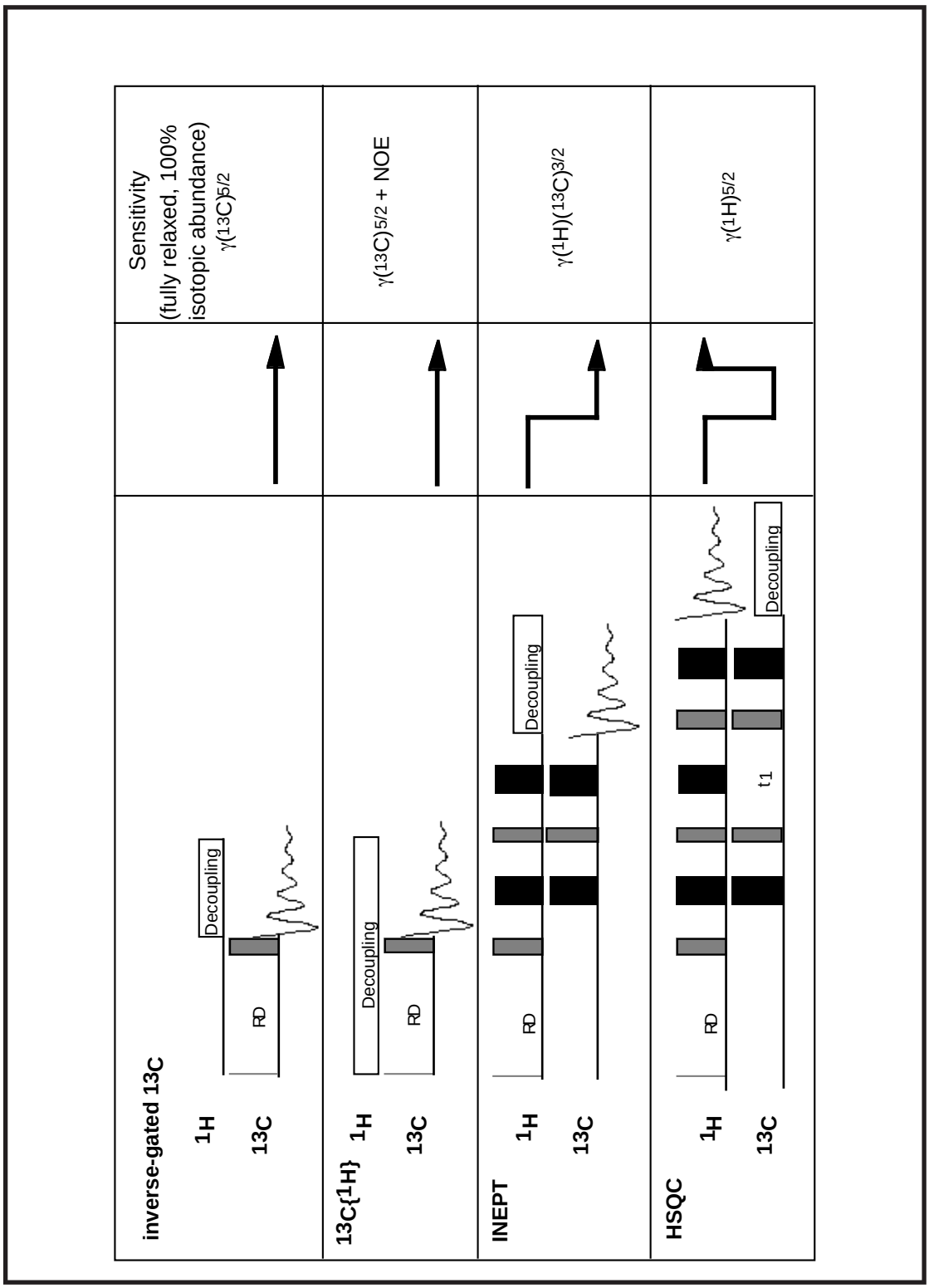

FIGURE 9. Comparison of sensitivity of carbon-detection experiments without PT (inverse-gated ^{13}C, $^{13}C\{^{1}H\}$), and with PT (INEPT) and with ^{1}H detection (2*PT, HSQC)

Excurs: The foundations of the product operator formalism:

The wavefunction for the state of a one-spin system can be formulated as

$$|\psi\rangle = c_1|\alpha\rangle + c_2|\beta\rangle$$

in which the coefficients c_1 and c_2 indicate to which extent the spin occupies the α or β state. $|\psi>$ is called a **state vector** and $|\alpha>$ and $|\beta>$ are the basis states. The basis states are orthogonal vectors in **Hilbert space** (a N-dimensional vector space for a system with N basis states with some special properties). The scalar product of the two vectors is defined as:

$$|\langle\psi|\psi\rangle|^2 = |c_1|^2 + |c_2|^2$$

which is the square of the length (norm) of the state vector ψ:

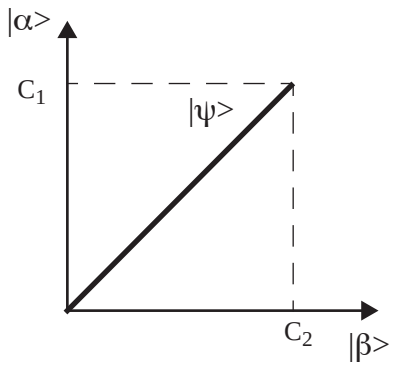

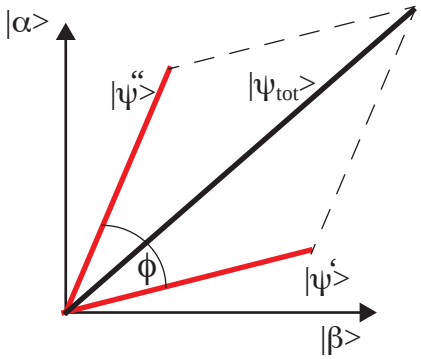

The length of the state vector $|\psi>$ is interpreted as the probability of finding the spin system in a particular state. The scalar product of two different states is

$$\langle\psi'|\psi''\rangle = \langle\psi'|\psi'\rangle + \langle\psi''|\psi''\rangle + \mathbf{2}\langle\psi'|\psi'\rangle^{\mathbf{1/2}}\langle\boldsymbol{\psi}''|\boldsymbol{\psi}''\rangle^{\mathbf{1/2}}\mathbf{cos\phi}$$

in which the component printed in bold indicates the amount of *interference between the two states*. $<\psi'|\psi''>$ is interpreted as the probability to go from state ψ' to ψ''. We can now define an operator A that transforms ψ'' into ψ':

$$|\boldsymbol{\psi}''\rangle = \mathbf{A}|\boldsymbol{\psi}'\rangle$$

Often in NMR these transformations are rotations in 3D space that do not change the length of the vectors (so-called “unitary transformations”) and the operator is a rotation matrix. Assume we have two state vectors, one describing the inital state of the spin system, one describing the final state:

$$|\psi_i\rangle = c_{1i}|\alpha\rangle + c_{2i}|\beta\rangle$$
$$|\psi_f\rangle = c_{1f}|\alpha\rangle + c_{2f}|\beta\rangle$$

To mathematically express the transformation we can arrange the state vector of the initial state as a column vector and the state vector ofthe final state in form of a row vector and write:

$$\begin{bmatrix} c_{1i} & c_{2i} \end{bmatrix} \begin{bmatrix} A_{11} & A_{12} \\ A_{21} & A_{22} \end{bmatrix} = \begin{bmatrix} c_{1f} \\ c_{2f} \end{bmatrix}$$

The time-evolution of the density matrix is described by the Liouville-van Neumann Equation:

$$\frac{d}{dt}\sigma(t) = -i[H, \sigma(t_0)]$$

in which H is the Hamiltonian describing the interaction (coupling, shift etc.). The commutator

$$-i[H, \sigma(t_0)] = -i(H\sigma - \sigma H)$$

The time evolution of the spin states can be expressed as:

$$C_q \xrightarrow{C_p} C_q$$

$$if \left[C_q, C_p\right] = 0$$

or

$$C_q \xrightarrow{C_p} C_q \cos\theta + i\left[C_q, C_p\right]\sin\theta$$

$$if \left[C_q, C_p\right] \neq 0$$

The basic rotations are:

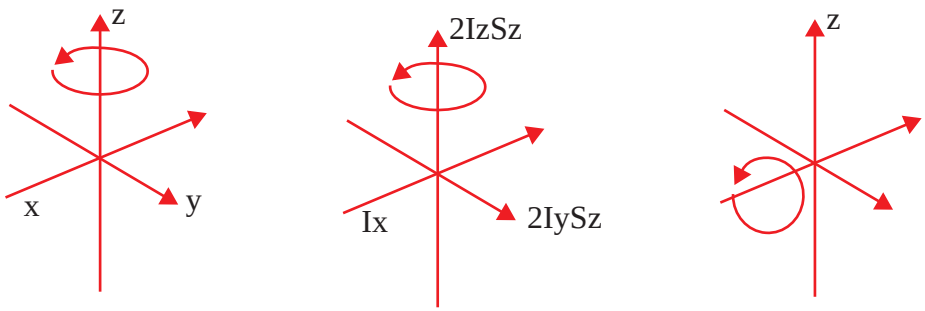

1. TWO-DIMENSIONAL NMR SPECTROSCOPY:

The introduction of two-dimensional NMR spectroscopy has largely increased the potential power of NMR as a tool for structure elucidation of larger molecules. It's main advantages are:

- dispersion of signals into two orthogonal dimensions and
- identification of correlations

The 2-dimensional NMR experiment is characterized by the introduction of a second frequency axis, which allows to *correlate* frequencies:

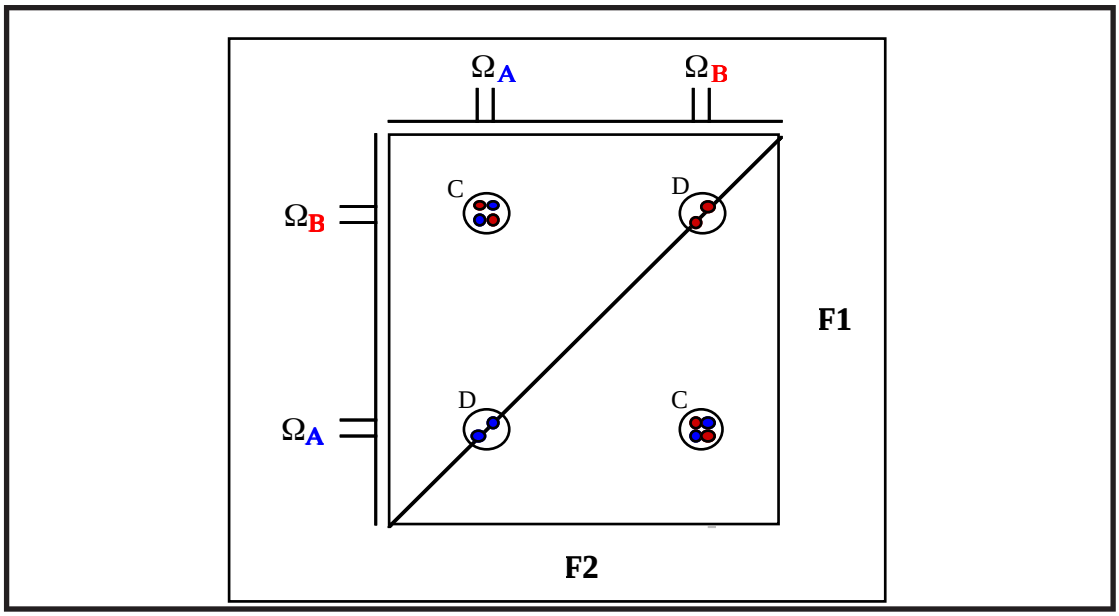

FIGURE 1. Appearance of homonuclear COSY spectrum with crosspeaks (C) and diagonalpeaks(D).

The two frequency domains are called the *direct* (F2) and the *indirect* (F1) frequency domains. Frequencies of signals in the direct dimension have been directly detected in the receiver coil, those of the indirect dimension were derived from the second Fourier transform of the amplitude modulated signals.

Homonuclear 2D spectra are usually symmetric about the diagonal. The diagonal contains the one-dimensional spectrum. Off-diagonal peaks at the frequency F2=Ω_A, F1=Ω_B are called *cross-peaks*, and they indicate the spins with frequencies Ω_A and Ω_B are correlated.

Two-dimensional experiments can be classified into certain groups:

- *homonuclear* correlated spectra that contain frequencies of similar nuclei in both dimensions (e.g. $^{1}H,^{1}H$ COSY, INADEQUATE)
- *heteronuclear* correlated spectra that contain frequencies of different nuclei (e.g. $^{1}H,^{13}C$ correlations) in different frequency dimensions.

Similarly experiments can be subdivided into

- *shift-correlated* 2D experiments, that link two spins via their chemical shifts (F2: chemical shift of spin A, F1: chemical shift of spin B for crosspeaks)
- *J-resolved* experiments, that separate chemical shift and J-coupling information in two orthogonal frequency dimensions (F2: chemical shift of spin A, F1: J-coupling of spin A).

Each pulse-sequence for a 2D experiment contains the basic elements

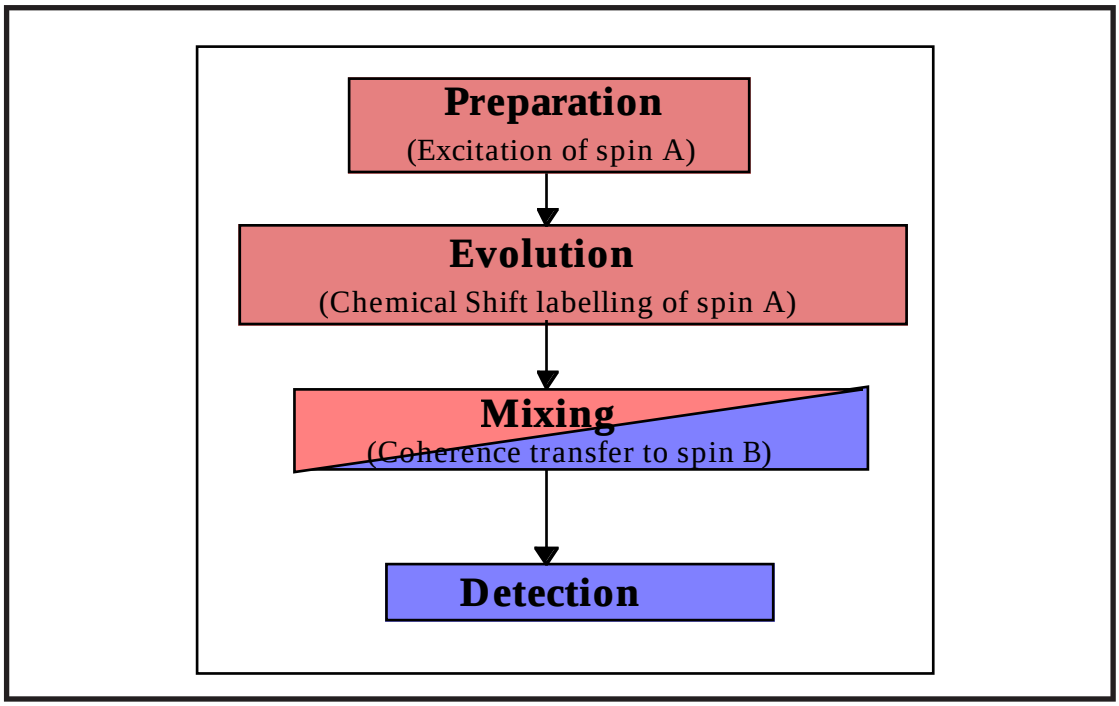

FIGURE 2. Building blocks of 2D experiment.

For the example of the F1=Ω_A, F2=Ω_B crosspeak the spin A is excited in the preparation period, then chemical shift labelled during the evolution period. Subsequently, magnetization is transferred from spin A to spin B in the mixing period. Finally, magnetization is detected on the spin B.

The 2D data matrix is recorded by performing a set of 1D spectra, in which a delay called the evolution time is systematically incremented. The signal of the spin B, which is detected, varies in amplitude from experiment to experiment,

and the modulation frequency of the signal intensity corresponds to the chemical shift of the spin A. The 2D spectrum is yielded from a two-dimensional Fourier transformation:

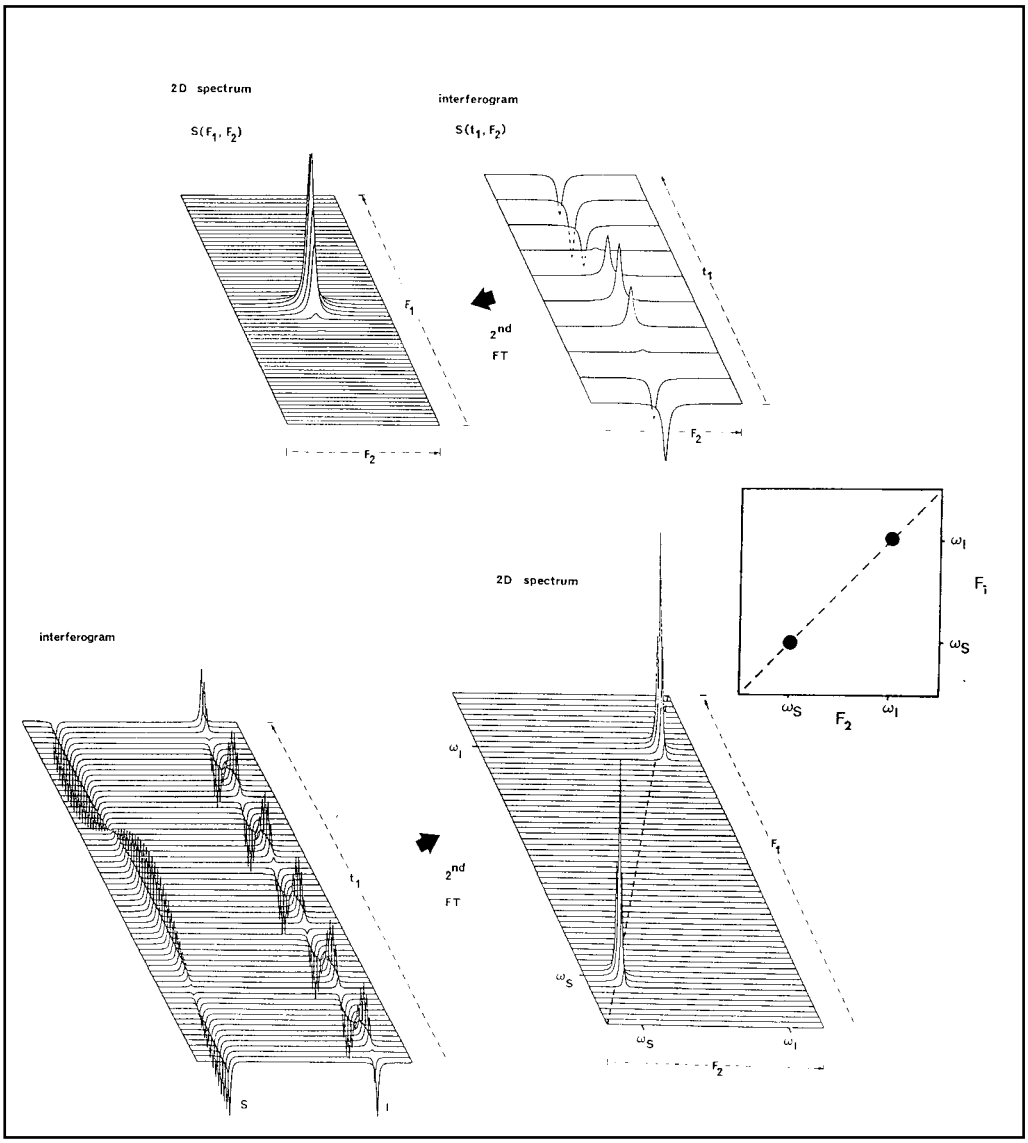

FIGURE 3. Translation of the amplitude modulation of a signal into the frequency of the indirect dimension through Fourier transform.

1.0.1 The preparation period:

In principle, the preparation period serves to create transverse coherences. In a proton,proton correlation experiment like the COSY, it is a simple 90 degree pulse for excitation. Some experiments that correlate carbon (or nitrogen) with proton frequencies use an initial INEPT polarization transfer from proton to carbon to increase sensitivity (dramatically). These experiments are the so-

called inverse-detection experiments. In the product operator formalism the preparation is described as

$$I_z \xrightarrow{90°x} -I_y$$

or in the case of inverse-detection experiments:

$$I_z \xrightarrow{90°(I_x)} -I_y \xrightarrow{\Delta-180(I,S)-\Delta} 2I_xS_z \xrightarrow{90°(I_y,S_y)} 2I_zS_x$$

1.0.2 The evolution period:

The evolution period is the pulse sequence element that enables frequency labelling in the indirect dimension. Usually, the corresponding time is called t1 in contrast to t2 in the direct detection dimension. Fourier transform of the t1-domain data yields the frequency dimension F1 and t2 corresponds to F2. In order to understand how frequency labelling in the indirect dimension is achieved, it is useful to recall how the frequencies in the direct dimension are sampled. The signal is sampled in *discontinuous* mode:

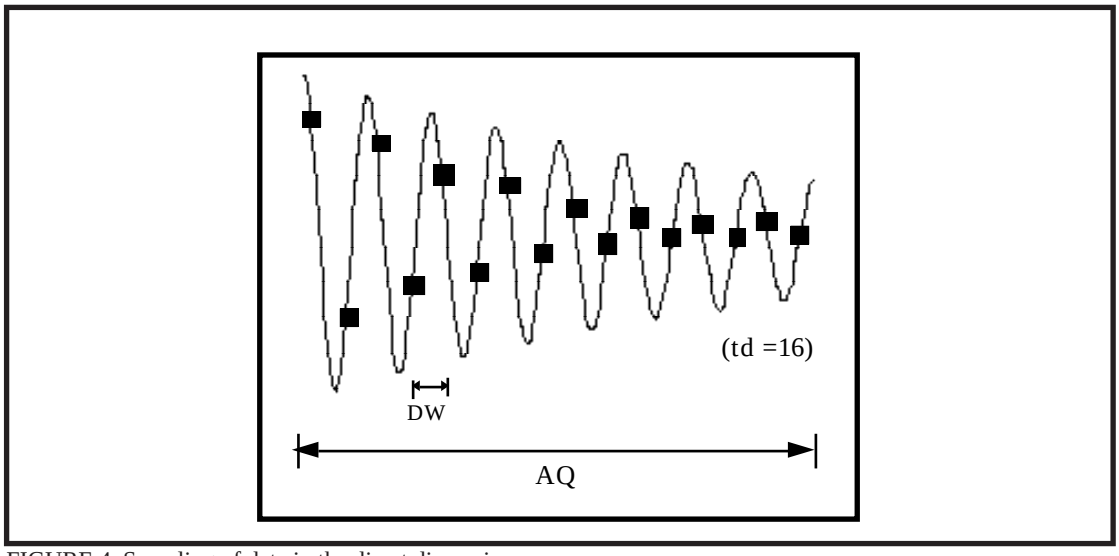

FIGURE 4. Sampling of data in the direct dimension.

Consecutive data points are separated by a dwell time. The length of the dwell time is related to the spectral width (SW, the width of the spectrum in Hz):

$$dw = \frac{1}{SW}$$

The resolution depends on the number of data points sampled and the spectral width (neglecting relaxation effects).

Frequency labelling in the indirect dimension is done analogously. However,

data points are taken in *separate* 1D experiments. During a 2D experiment *a series of 1D spectra* is recorded which differ by the fact that the evolution time has been systematically incremented from experiment to experiment. This is schematically shown in the figure on the following page for signals that lead to diagonal peaks (no magnetization transfer during the sequence). The signal precesses during t1. Depending on the length of the evolution period more or less of the magnetization will be turned onto the z-axis thereby modulating the intensity of the remaining signal. Since the evolution time is incremented systematically in successive FIDs the frequency in the indirect dimension is sampled analogously to the one of the direct dimension.

In the product operator formalism frequency labelling is described as:

$$I_x \xrightarrow{t_1} I_x \cos(\omega_I t_1) + I_y \sin(\omega_I t_1)$$

1.0.3 The mixing period:

The many 2D experiments differ in the way they transfer magnetization from spin A to spin B, that means in the construction of the mixing process. Possible transfer-sequences may rely on

- scalar couplings (COSY, TOCSY-type experiments)
- dipolar couplings (NOESY/ROESY type experiments)
- chemical exchanges (EXSY type experiments)

In product operator language the mixing for the COSY-type experiments is described as

$$2I_xS_z \xrightarrow{90°(I_y,S_y)} 2I_zS_x$$

Herein, transverse I-spin coherence is transferred into transverse S-spin coherence. Operators like I_xS_z evolve with the chemical shift of the spin I whereas operators like I_zS_x evolve with the shift of spin S. Because the mixing step separates the t1 and t2 periods, such a transfer step will lead to signals corresponding to crosspeaks after 2D FT. However, depending on the chemical shift evolution of the I spin in t1, the term just before the transfer step can also be I_yS_z(instead of I_xS_z). Application of a 90° pulse with phase y on the I and S spin will give I_yS_x, a mixture of double- and zero-quantum coherence, which cannot

be observed.

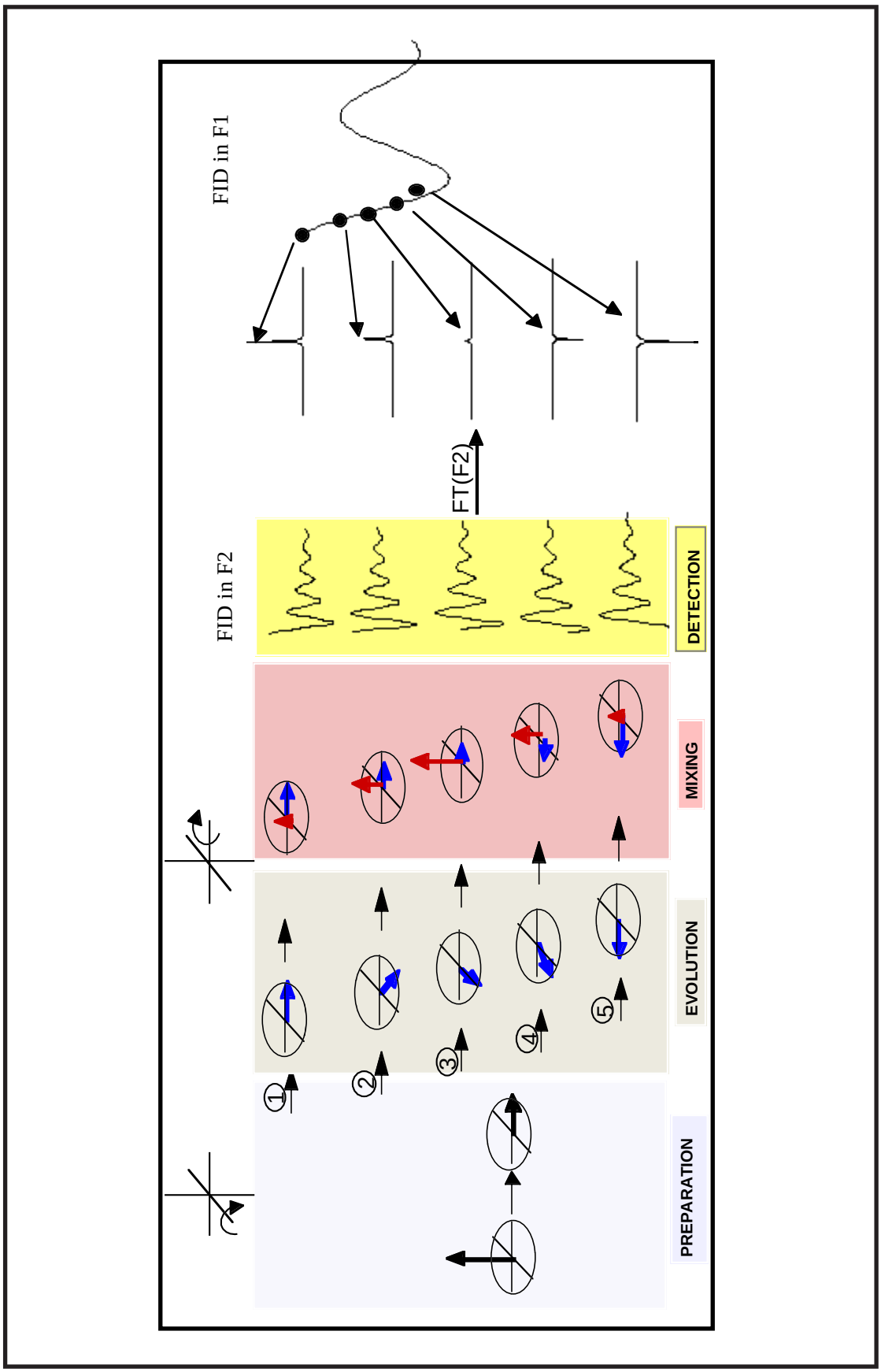

FIGURE 5. COSY-type mixing in the vector model

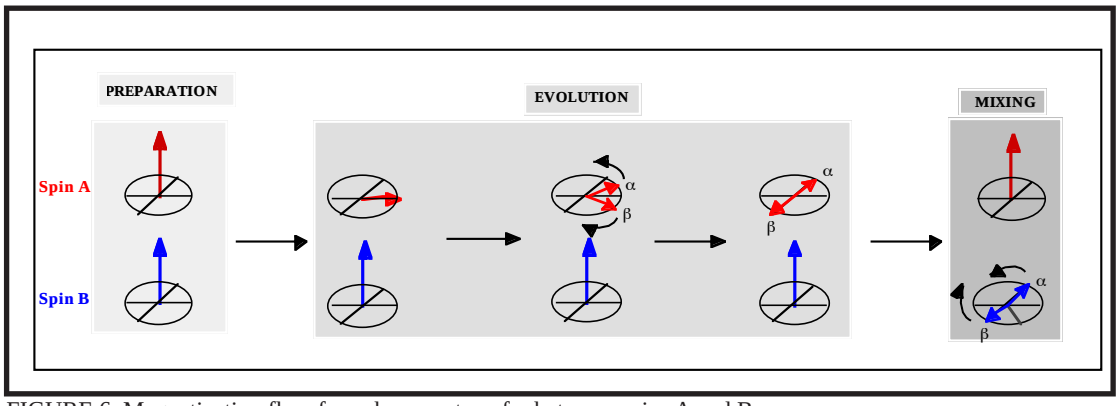

FIGURE 6. Magnetization flow for coherence transfer between spins A and B.

The TOCSY transfer is different in the way that *in-phase* magnetization is transferred at twice the rate:

$$I_x \xrightarrow{\text{"180°"}} S_x$$

For the NOESY mixing the description is

$$I_z \xrightarrow{\tau_m} (-)S_z$$

Some of the more advanced triple-resonance experiments mixing includes magnetization relay via many nuclei of possibly different nature.

1.0.4 The detection period:

The detection period simply comprises acquisition of the FID with or without heteronuclear decoupling.

1.0.5 Hetcor and inverse-detection experiments:

The heteronuclear correlation experiments (Hetcor, HMQC, etc.) are in principle of the COSY-type. However, the mixing pulse must be applied for both kinds of nuclei (^{1}H and ^{13}C) separately. Inverse detection experiments include an additional INEPT-type proton-heteronucleus polarization transfer step. Thereby, the sensitivity is increased according to

$$Int \propto \gamma_{ex} \gamma_{\text{det}}^{3/2}$$

In addition, faster pulsing is possible since the proton T1's are usually much

shorter than those of ^{13}C or ^{15}N.

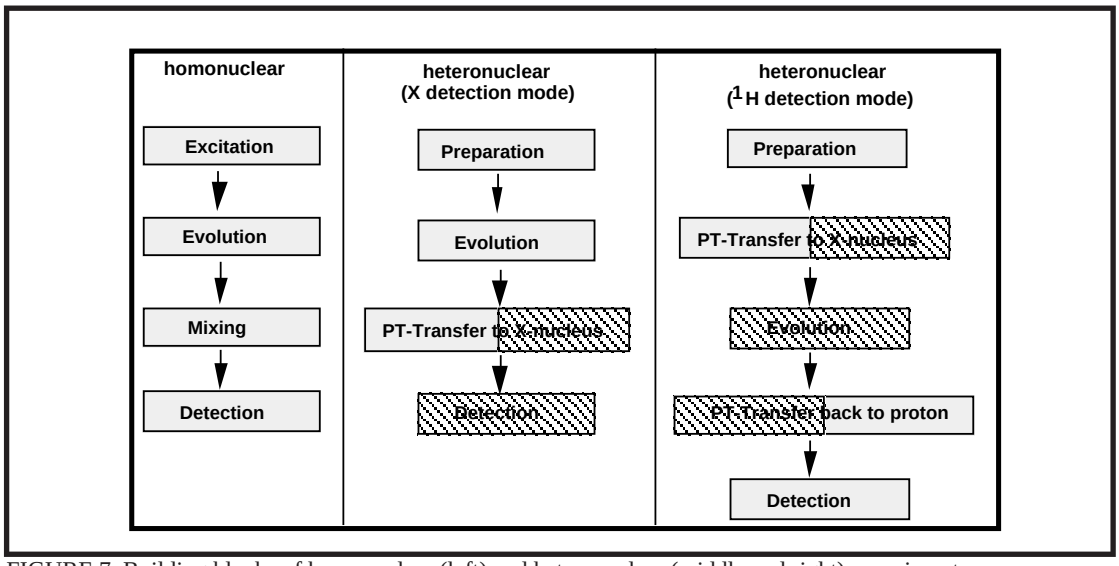

FIGURE 7. Building blocks of homonuclear (left) and heteronuclear (middle and right) experiments.

The prototype inverse detection experiment, the HSQC (heteronuclear single-quantum coherence) experiment is shown below. The experiment contains two polarization transfer (INEPT) steps.

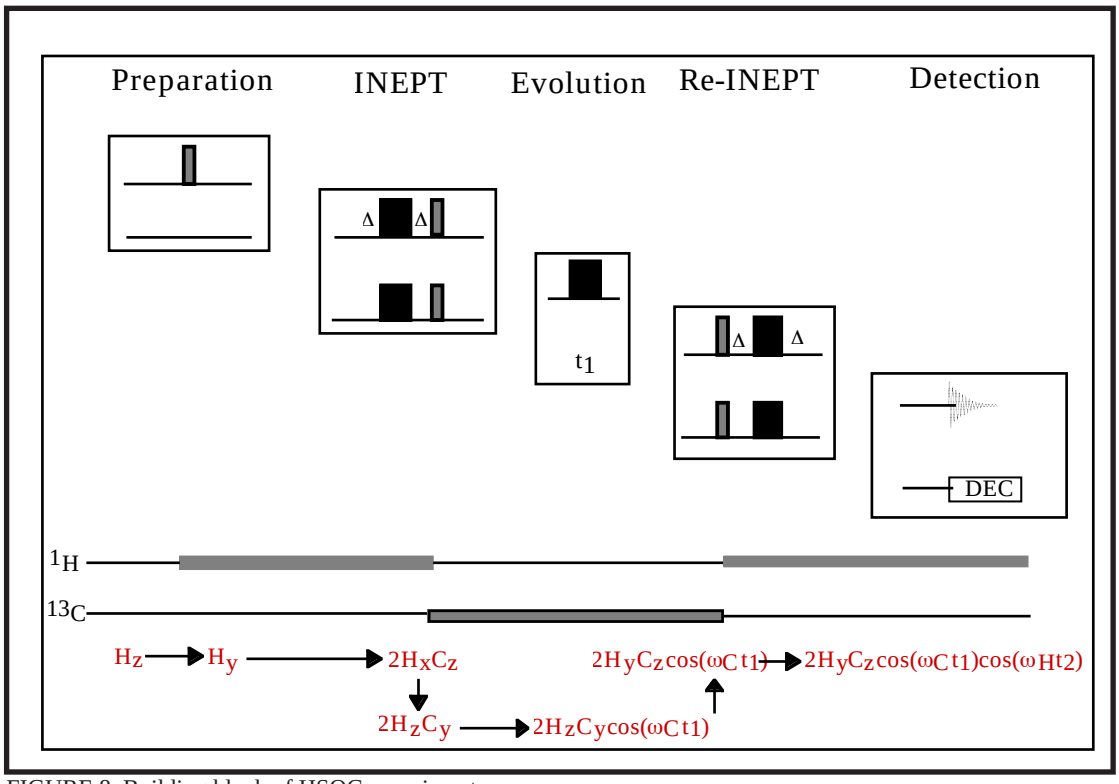

FIGURE 8. Building block of HSQC experiment.

1.1 Phasecycling:

A large problem in [^{13}C,^{1}H] spectra is suppression of protons bound to ^{12}C.

This is achieved through phase-cycling of the first 90° pulse on the carbon channel. The satellite lines (those proton lines, which belong to the ^{1}H-^{13}C fragment) are inverted when the phase of the first 90° carbon pulse is shifted by 180°. When the receiver phase is inverted too addition of the two FIDs leads to cancellation of the central proton line (the one that belongs to the ^{1}H-^{12}C fragment). Clearly, unstable measuring conditions will cause incomplete cancellation, and the centre signal will show up as t_1 noise:

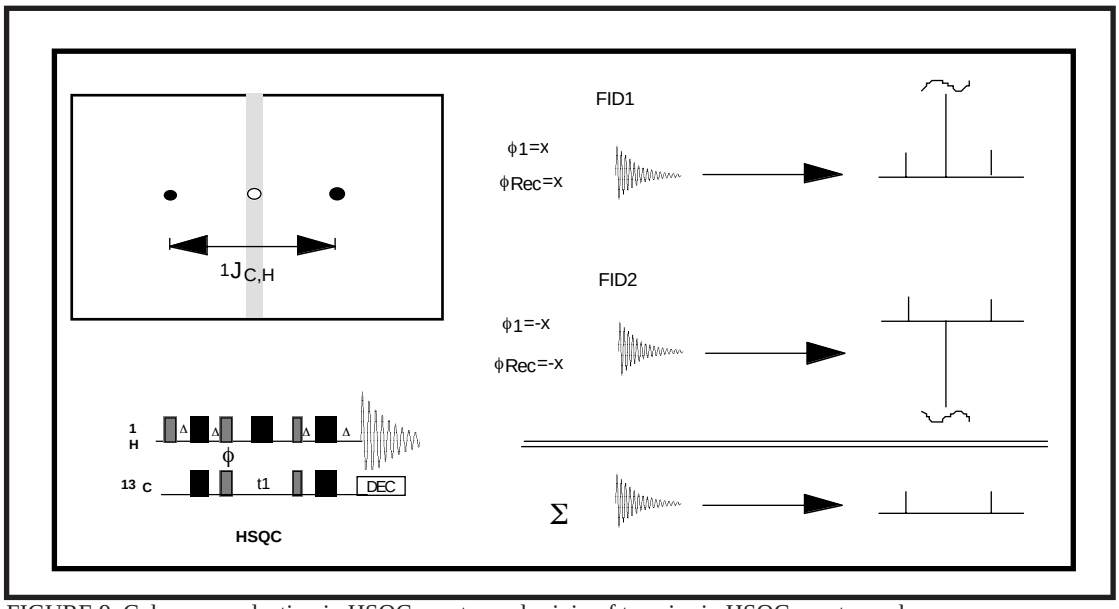

FIGURE 9. Coherence selection in HSQC spectra and origin of t_1 noise in HSQC spectra and

1.2 An Alternative: Pulsed Field Gradients

By applying pulsed field gradients the homogeneity of the external magnetic field is destroyed and spins with the same chemical shift are defocused to a degree which depends on their location in the probe. Usually the NMR spectroscopist spends a considerable amount of time to have maximum field homogeneity over the sample volume. By *detuning* the z-shim starting from a perfectly shimmed magnet a linear B_0 gradient is created along the sample axis so that spins in the upper part of the tube have higher frequencies than those at the bottom. If such a gradient would be applied during signal acquisition a broad signal corresponding to a wide range of frequencies would be observed instead of a sharp line. The crucial point is that the amount of *dephasing is proportional to the coherence level* of the spins at the time the gradient is applied. Double-quantum coherences are dephased by twice the amount than single

quantum coherences, zero-quantum coherences are not dephased at all. Usually at least two gradients are applied during the sequence. In the double-quantum filtered COSY experiment a gradient is applied during the time double-quantum coherence is exists. At the end of the sequence (when single-quantum coherences are existent) a read-out gradient is used of *half the strength* to refocus the gradient. The 2:1 ratio of the two gradients ensures that the desired coherence pathway has been selected:

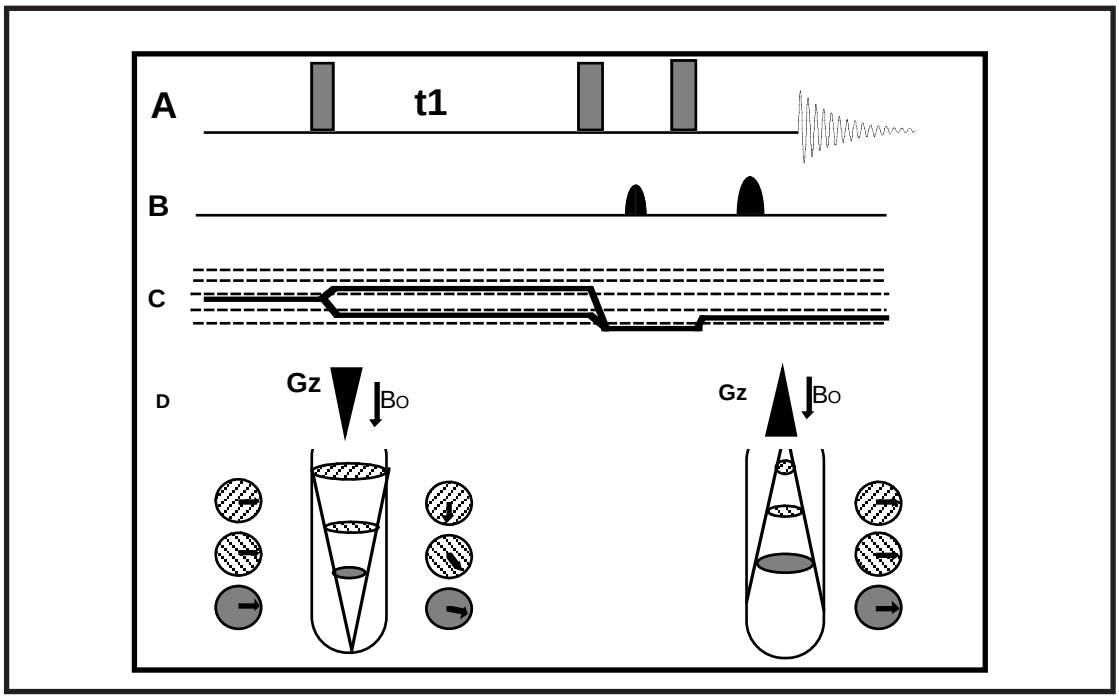

FIGURE 10. Effect of field gradients on isochronous spins at different locations in the probe. (A) DQF-COSY sequence with application of gradients (B); (C) selected coherence transfer pathway; (D) vector representation of isochronous spins during the experiment.

The change of the lamor frequency is proportional to the order of coherence p_i, the gyromagnetic ratio γ_i of the spin, the strength and sign of the applied *linear* field gradient pulse G_z, it's coordinate Z_i in the probe and the duration τ:

$$\Delta\upsilon \quad \propto \quad p_i \gamma_i Z_i G_z \tau$$

By applying a gradient of the same strength but opposite sign, coherences of the same order are rephased again. Alternatively, proton coherences can be labelled using a pulsed field gradient, and, after magnetization transfer to carbon-13, carbon single quantum coherences can be refocused by a gradient of opposite sign and appropriate strength. Since dephasing and rephasing is done within the same scan, no further scans are needed provided the S/N is sufficient. Because spectra are recorded without addition/subtraction of scans.

instrumental instabilities are less pronounced and therefore two-dimensional experiments tend to contain much less t_1 noise. Furthermore, solvent suppression is superior, no saturation transfer due to fast exchanging protons is possible and signals with identical chemical shifts to those of the solvent can easily be observed. Whenever dephasing and rephasing intervals are separated by a long delay, as is the case for NOESY or TOCSY experiments, diffusion leads to a significant loss of magnetization. A second disadvantage stems from the relatively long duration of gradients and the time required for re-establishing the homogenous field.

1.3 Hybrid 2D techniques:

Hybrid experiments are very similar to three-dimensional NMR experiments, in which the second time variable is kept constant. Classical examples are HMQC/HSQC experiments coupled with a subsequent TOCSY or NOESY (ROESY) transfer step. In these experiment, not only the direct (^{1}J(C,H) connectivities are observed, but also connectivies to other (mostly vicinal) protons of the proton spin system. This is especially helpful in case of overlap of proton frequencies. One obviously useful field for application lies in oligosaccharide NMR. For example, a [^{13}C,^{1}H] HSQC-TOCSY experiment correlates not only the anomeric proton with its carbon but also with the neighboring protons.

Obviously, the sensitivity of the correlations is reduced when compared with the HSQC experiment. For small molecules with small NOE enhancements, a HSQC-NOESY on natural abundance is very insensitive. In case of isotropic enrichment, such a HSQC-NOESY can be a rather sensitive experiment for larger molecules (those that give strong NOE enhancements).When the mixing time is limited (e.g. 12ms) coherence transfer in HSQC-TOCSY experiments is limited to neighboring protons. Then, information from such an experiment is similar to that of COSY spectra but signals are dispersed along the carbon dimension making it a very valuable experiments for (oligo)saccharides or peptides.

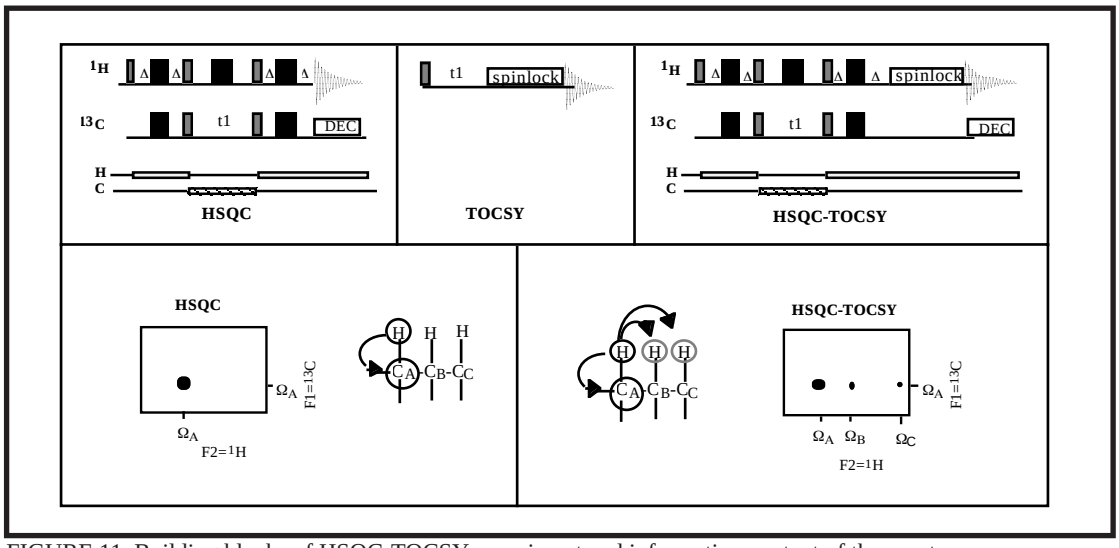

FIGURE 11. Building blocks of HSQC-TOCSY experiment and information content of the spectra.

1.4 Overview of 2D experiments:

homonuclear shift correlated spectra

via scalar couplings

(DQF)-COSY vicinal / geminal protons correlated

COSYlr COSY optimized for small couplings (long-range couplings)

INADEQUATE mostly used for carbon, carbon correlation experiments for nat. abundance samples.

relay-COSY COSY with additional relay step

TOCSY experiment with multiple proton relay, for long mixing times all protons within the same spinsystem are correlated

double-quantum spectroscopy identification of degenerate methylene protons

TQF-COSY identification of glycine residues in peptides

X-filtered Exp. normal 2D experiment, but only spins that have an additional coupling to a heteronucleus are displayed

via dipolar couplings

NOESY correlation via dipolar interaction

ROESY rotating frame analogue of the NOESY

exchange spectroscopy

EXSY correlates exchanging protons (chemical and conforma tional exchange)

heteronuclear shift correlated spectra via scalar coupling

^{13}C detected experiments

hetcor correlation of directly bonded protons and carbons

COLOC proton, carbon correlation via long-range (^{2}J, ^{3}J) couplings

^{1}H detected experiments

HMQC,HSQC correlation of directly bonded protons and carbons

HMBC proton, carbon correlation via long-range (^{2}J, ^{3}J) couplings

the following experiments include an additional TOCSY / NOESY / COSY transfer step:

H(S)MQC-TOCSY
H(S)MQC-NOESY
H(S)MQC-COSY

via dipolar couplings

HOESY correlation via heteronuclear dipolar interaction (via NOE)

Experiments for measurement of J-couplings

homonuclear j-resolved experiments
heteronuclear j-resolved experiments
ECOSY
HMQC-J

1.5 Original references for 2D experiments:

COSY:
Aue, W. P.; Batholdi, E.; Ernst, R. R. *J. Chem. Phys.* **1976**, *64*, 2229-2246.

COSY-DQF:
Piantini, U.; Sørensen, O. W.; Ernst, R. R. *J. Am. Chem. Soc.* **1982**, *104*, 6800-6801.
Rance, M.; Sørensen, O. W.; Bodenhausen, G.; Wagner, G.; Ernst, R. R.; Wüthrich, K. *Biochem. Biophys. Res. Commun.* **1983**, *117*, 479-485.

COSY-LR:
Bax, A.; Freeman, R. *J. Magn. Reson.* **1981**, *44*, 542-561.

E.COSY:
Griesinger, C.; Sørensen, O. W.; Ernst, R. R. *J. Chem. Phys.* **1986**, *85*, 6837.

TOCSY:
Bax, A.; Davis, D. G. *J. Magn. Reson.* **1985**, *65*, 355-360.
Braunschweiler, L.; Ernst, R. R. *J. Magn. Reson.* **1983**, *53*, 521-528.
NOESY:
Jeener, J.; Meier, B. H.; Bachmann, P.; Ernst, R. R. *J. Chem. Phys.* **1979**, *71*, 4546.
Wüthrich, K. *NMR of Proteins and Nucleic Acids*; 1st ed.; Wiley: New York, 1986.

INADEQUATE:
Bax, A.; Freeman, R.; Kempsell, S. P. *J. Am. Chem. Soc.* **1980**, *102*, 4849-4851.
Bax, A.; Freeman, R.; Frenkiel, T. A. *J. Am. Chem. Soc.* **1981**, *103*, 2102-2104.

ROESY:
Bothner-By, A. A.; Stephens, R. L.; Lee, J.-M. *J. Am. Chem. Soc.* **1984**, *106*, 811-813.
Bax, A.; Davis, D. G. *J. Magn. Reson.* **1985**, *63*, 207-213.

HMQC:
Bax, A.; Griffey, R. H.; Hawkins, B. L. *J. Magn. Reson.* **1983**, *55*, 301-315.
Müller, L. *J. Am. Chem. Soc.* **1979**, *101*, 4481-4484.

HSQC:
Bodenhausen, G.; Ruben, D. J. *Chem. Phys. Lett.* **1980**, *69*, 185-189.

HMBC:
Bax, A.; Summers, M. *J. Am. Chem. Soc.* **1986**, *108*, 2093-2094.

1. SOLID STATE NMR SPECTROSCOPY:

Solid-State NMR spectroscopy is increasingly being used for a number of reasons:

- it allows to probe properties in the solid state (-> material sciences)
- it enables to structural characterize insoluble compounds such as (synthetic) polymers
- it has *per se* no moleccular size limit and therefore is of advantage when looking at very large systems (e.g. membrane-proteins embedded in bilayers)

However, a number of additional interactions do appear that complicate spectra to an extend that they become essentially useless unless they are experimentally removed. Although similar interactions are also encountered in the liquid state they are averaged out due to rapid tumbling of the molecules. We will therefore shortly review basic interactions that are important for solid-state NMR applications. The typical range of various interactions is listed in the table below (from Ref. Williamson *et al.*):

interaction	nuclei	typical magnitude
chemical-shift range	^{1}H	~15 ppm
	^{13}C	~200 ppm
	^{15}N	~200 ppm
anisotropy of CSA	^{1}H	< 10 ppm
	^{13}C	< 140 ppm
	^{15}N	< 200 ppm
one-bond dipolar coupling	^{1}H-^{13}C	~22 kHz
	^{1}H-^{15}N	~20 kHz
	^{13}C-^{13}C	4.5 kHz
	^{13}C-^{15}N	2 kHz
	^{15}N-^{15}N	< 1 kHz

1.1 The chemical shift

It has been recognized very early on that the resonance frequency of a nucleus is influenced by the surrounding electrons. For nuclei with non-spherical electron distributions the shielding effect depends on the orientation of the electron cloud with respect to the static field B_0. For non-sp^3 hybridized carbons the anisotropy can be as large as 150 ppm and even larger values are encountered for heavier elements.

The chemical shift tensor **σ** denotes the tensor required to transform the B_o field vector into the vector B_{eff} representing the effective field:

$$\begin{bmatrix} Beff_x \\ Beff_y \\ Beff_z \end{bmatrix} = \begin{bmatrix} \sigma_{xx} & \sigma_{xy} & \sigma_{xz} \\ \sigma_{yx} & \sigma_{yy} & \sigma_{yz} \\ \sigma_{zx} & \sigma_{zy} & \sigma_{zz} \end{bmatrix} \otimes \begin{bmatrix} 0 \\ 0 \\ B_0 \end{bmatrix}$$

By suitable choice of the coordinate system the chemical shift tensor only contains the diagonal elements σ_{xx}, σ_{yy} and σ_{zz}. Such a system is called the *principal axis system* (PAS). For the shielding tensor the z-axis points into the direction of the largest electron density. The trace of the tensor (by convention $\sigma_{zz} \geq \sigma_{xx} \geq \sigma_{yy}$)

$$\sigma = (\sigma_{xx} + \sigma_{yy} + \sigma_{zz}) /3$$

denotes the *isotropic value* of the shielding tensor, is rotationally invariant and corresponds to the shift observed in isotropic solution.

The parameter δ is the *anisotropy* and reflects the deviation from *cubic* symmetry

$$\delta = \left(\sigma_{zz} - \frac{\sigma}{3}\right)$$

and η the *asymmetry,* which reflects the deviation from *axial* symmetry:

$$\eta = (\sigma_{xx} + \sigma_{yy}) /\delta$$

The orientation of the shift tensor is depicted below:

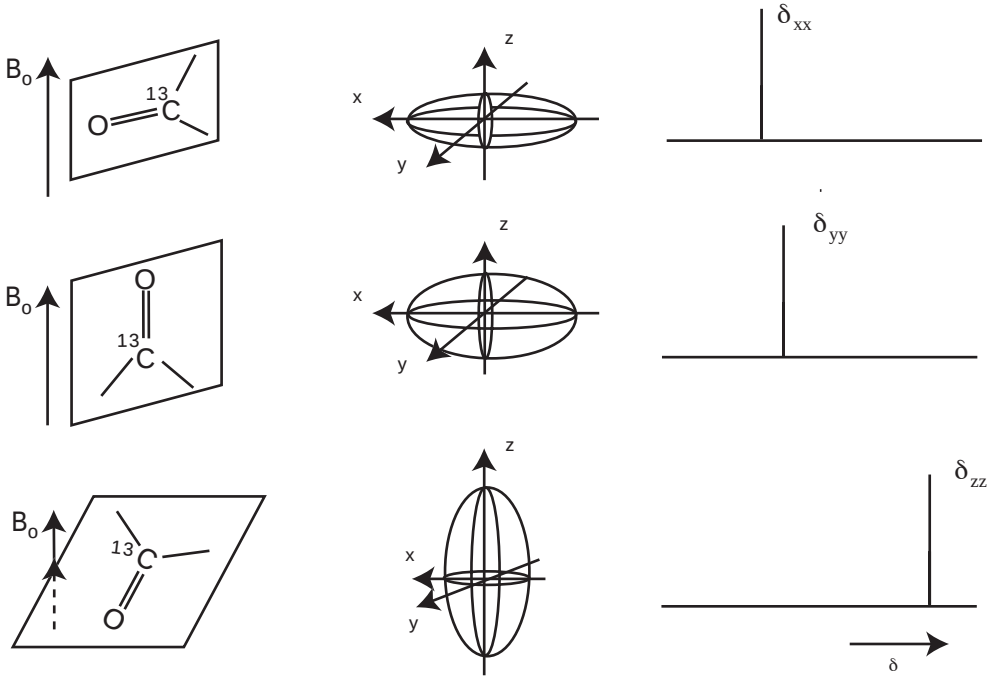

In a non-crystalline powder sample the nuclei are randomly oriented and the observed chemical shift tensor corresponds to the statistical average over all possible orientations. The powder lineshapes are characteristic for the magnitudes of anisotropy δ and asymmetry η. The examples depicted at the left correspond to axially symmetric ligand fields. For nuclei with cubic symmetry (e.g. ^{15}N in NH_4) even sharper signals are observed:

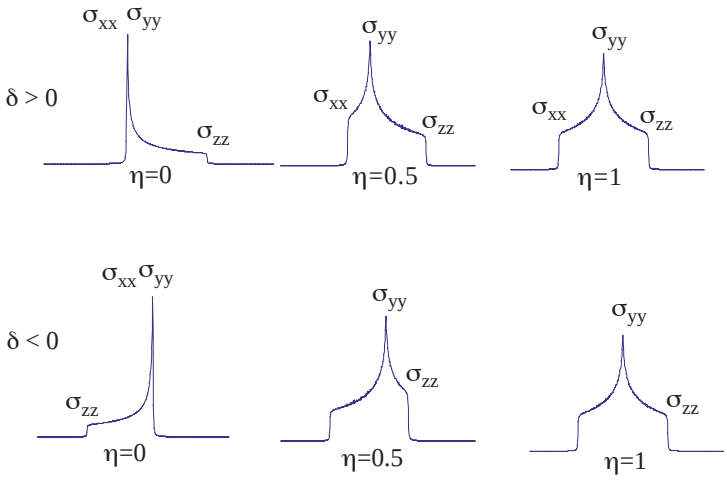

Note that in *crystalline* material orientations are non-random! Sample preparation is very important for solid-state NMR applications:

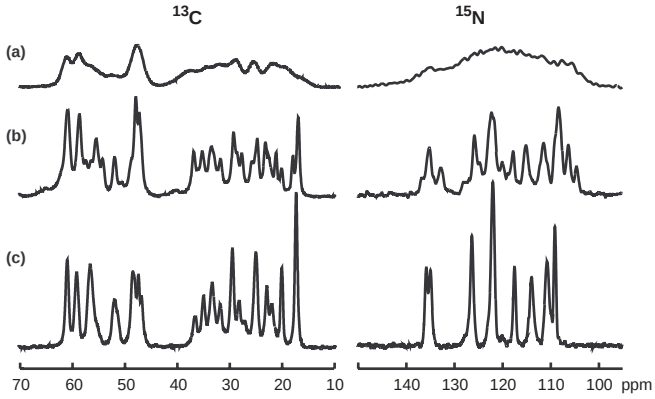

The figure above displays ^{13}C and ^{15}N MAS spectra of antamanide from a) lyophilized powder, b) and c) microcrystalline powder obtained by evaporation of solvent with different protocols (see ref. Williamson *et al.*). Structural disorder or inhomogeneity represents a major issue in solid-state NMR applications!

1.2 Dipolar couplings:

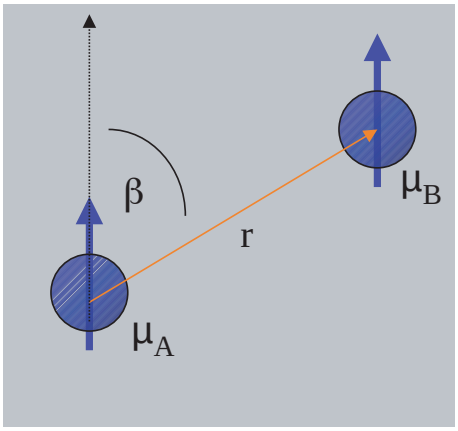

Dipolar couplings depend on the orientation of the vector that connects the two nuclei relative to the static field, on the separating distance and on the gyromagnetic ratios of the two nuclei involved.

For dipolar couplings the Hamiltonian is:
is *homonuclear* couplings

$\mathbf{H}_{IS} = -d\,(3\cos^2\beta - 1)\, I_Z S_Z$; $\quad d = (\mu_o/4\pi)\, \hbar\gamma_I\gamma_S/r_{IS}^3$

and for *hetereonuclear* couplings:

$\mathbf{H}_{II} = -d/2\,(3\cos^2\beta - 1)\, 3I_{1Z}I_{2Z} - I_1I_2$; $\quad d = (\mu_o/4\pi)\, \hbar\gamma_I^2/r_{II}^3$

In solution, dipolar couplings are averaged to zero due to rapid (rotational) motion of the molecules (but give rise to the important relaxation phenomena). In the solid state no such rapid rotation exists and hence the dipolar couplings give rise to line splittings which can easily exceed 10 kHz in magnitude. Because these dipolar couplings can be so large they are not only observed between direct neighboring nuclei but also longer-reaching interactions are encountered. Note that dipolar couplings have recently also been introduced into solution NMR by the use of weakly aligned systems for recording *residual dipolar couplings* (RDCs).

The scalar (J) couplings do not fundamentally differ from the quantities observed in isotropic (solution) phase. However, it is very important to remove heteronuclear scalar couplings to increase resolution (and hence sensitivity) in the spectra. RF irradiation schemes similar to those used to remove heteronuclear couplings in solution are applied. For spins with I≥1, quadrupolar couplings exist, but those will not be described here.

Solid-state NMR experiments fundamentally suffer from the additional dipolar interactions and from the chemical shift anisotropy. Due to the increased line-widths sensitivity is an important issue in SS-NMR, and the quantities required are usually much larger than for solution-state NMR.

1.3 Magic Angle Spinning (MAS)

The effects from chemical shift anisotropy and dipolar couplings lead to excessively broad lines. To a large extend this line-broadening can be removed by spinning the sample about the magic angle 54.74° (*magic-angle spinning*, MAS). For this angle the second-order legendre polynomial $(3\cos^2\beta-1)/2$, which describes the angular dependence in both the dipolar coupling as well as in the chemical shift Hamiltonians, vanishes. In MAS, the sample is placed in a cylindrical rotor which is rapidly spun (up to 30-50 kHz) about an axis that is tilted by 54° away from the direction of the static field. The tremendous line-narrowing effects due to MAS are displayed in the powder ^{13}C spectra of $^{13}C,^{15}N$ labeled glycine below (from ref. Williamson *et al.*):

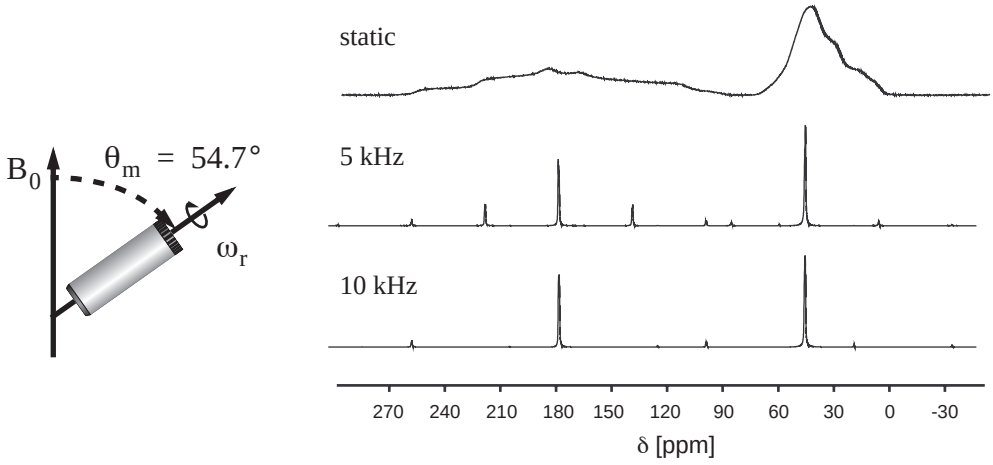

At the lower frequencies spinning sidebands fall into the spectral regions of interest. Upon rising the spinning frequencies those bands occur outside the spectral region. The broad lines observed in the powder spectrum collapse into rather sharp lines which occur at the position of the isotropic chemical shift.

Unfortunately spinning the samples at high frequencies does heat up the sample (tens of degrees!) and the heating effect must be removed by cooling the rotor appropriately.

1.4 Sensitivity Enhancement:

Solution-state NMR normally utilizes proton detection experiments due to the high gyromagnetic ratio of protons which makes this nucleus very sensitive. In SS-NMR applications proton detection is less favorable due to the large number of homonuclear dipolar interactions, and mostly carbon detection is used instead. Carbon, however, is a much less sensitive nucleus. Polarization-transfer techniques are therefore employed to

transfer the much more favorable proton polarization onto the carbon nuclei.[1]
Nowadays *Hartmann-Hahn Cross Polarization* (CP) is used. In this technique B_1 fields are simultaneously applied to the proton and carbon spins such that the precession frequencies of the two spins are approximately equal ($\gamma_H B_H \approx \gamma_C B_C$). Thereby, carbon polarization can be enhanced by up to a factor of four (γ_H/γ_C), and advantage can be taken from the much shorter T1 of protons (higher repetition rate).
The extend by which magnetization can be transferred to the heteronucleus by Hartmann-Hahn cross polarization transfer depends on the mixing time, but also on the distance between the nuclei. This technique may therefore be use to derive distance information of pairs of nuclei:

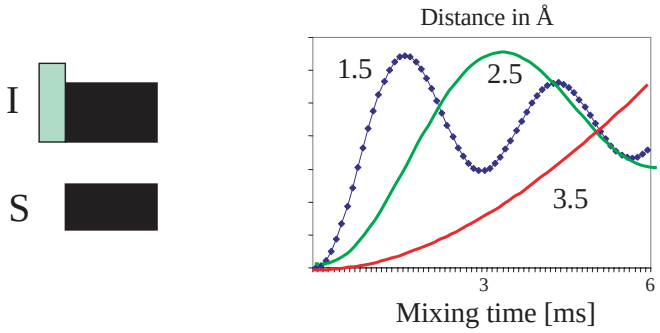

Fig. Left: Pulse sequence for hetero CP. Right: Signal buildup curves for various durations of mixing time and distances. A two spin system has been used and interactions other than dipolar couplings are neglected.

1.5 Recoupling techniques in SS-NMR:

Whereas magic-angle spinning (MAS) leads to significant line-narrowing in 1D spectra, the removed interactions need to be re-introduced in order to yield distance or (dihedral) angle information. One way to yield information on spin-interactions is to spin the sample more slowly and extract spin interaction parameters from spinning side-band amplitudes.
A more commonly technique used nowadays is to re-introduce spin-interactions by *recoupling* techniques. The basic idea behind recoupling techniques is that the averaging of spatial-dependent parameter such as dipolar couplings or chemical shift anisotropy under MAS can be removed if RF pulses are applied in rotor-synchronized fash-

1. Due to the four-fold higher γ of protons the energy difference between α and β-states is much larger for protons and hence the population difference is also larger.

ion:

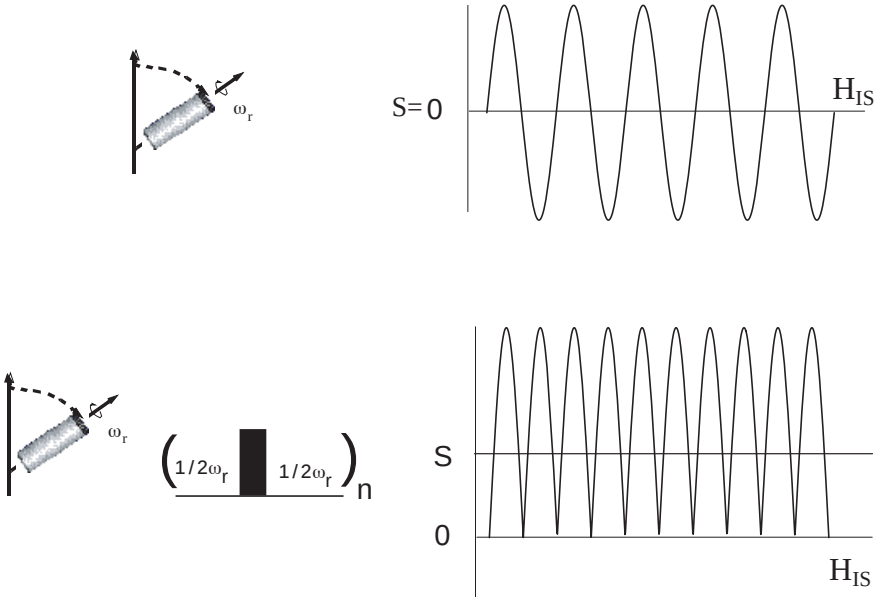

For heteronuclear dipolar recoupling *rotational echo double resonance* (REDOR) has been used. Herein, ^{15}N,^{13}C dipolar couplings are re-introduced during the mixing time leading to dephasing of the signal by the dipolar coupling. Note that during signal acquisition the dipolar couplings are removed by MAS so that narrow signals are sampled:

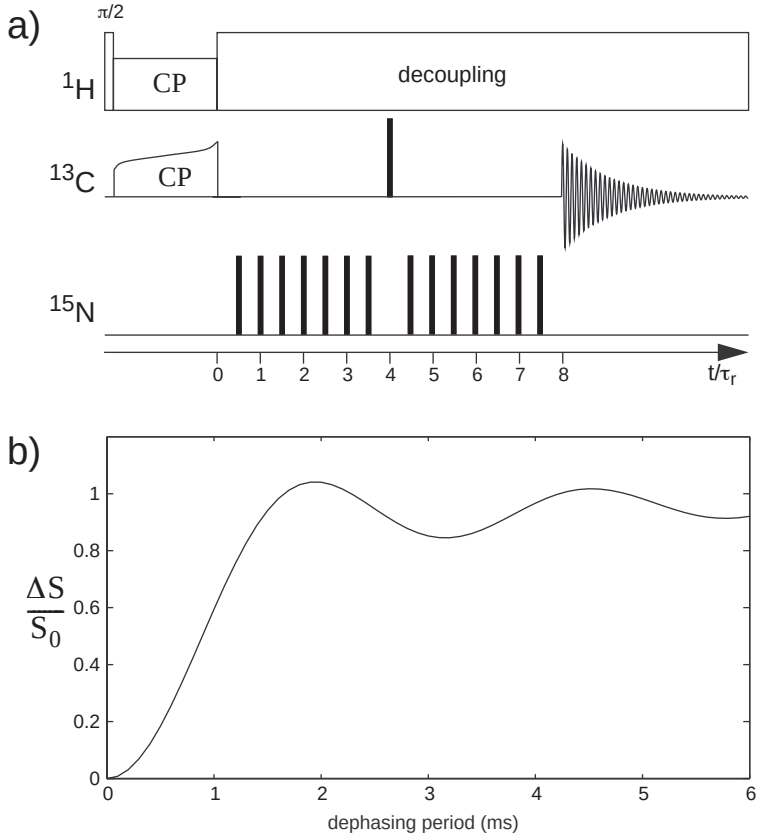

Fig.: a) REDOR pulse sequence for recording ^{13}C,^{15}N dipolar couplings. b) Relative signal intensity change against mixing time for a one-bond dipolar coupling (from ref. Williamson *et al.)*

Usually, a reference spectrum without the rotor-synchronized ^{15}N pulses is additionally acquired and the intensities in both spectra are compared. The curves reflecting signal intensity versus time depend on the magnitude of the heteronuclear dipolar couplings, which in turn depend on their distance, and precise values for these can be extracted from the data by comparison of the experimental data with simulations. Note that strictly speaking the RF pulses are applied to the spin-part of the dipolar Hamiltonian (I_zS_z) whereas MAS only influences the spatial part ($3\cos^2\theta$-1).

Homonuclear recoupling techniques have also been developed. Whereas its implementation is similar to the heteronuclear variants in principle, it is complicated by the fact that the spin-interactions need to be reintroduced *selectively.* (A transformation I_zS_z --> $I_z(-S_z)$ is easily accomplished for a heteronuclear pair of spin by just applying a 180° pulse to the S spin but usually difficult for homonuclear spin pairs which will both be flipped unless the 180° pulse is selective). Selectivity in the homonuclear recoupling techniques is achieved by adjusting a chosen property such as the spinning (rotor) frequency to the zero- or double-quantum frequencies of the spin pair of interest ($\omega_{zq}= \omega_a-\omega_b$, $\omega_{dq}=\omega_a$ *plus* ω_b). For example, in *rotational resonance* (R^2) the rotor frequency is set to a submultiple of the chemical shift difference. The dipolar coupling is then measured in form of an exchange experiment: A resonance A is selectively inverted and the exchange between the two sites is monitored:

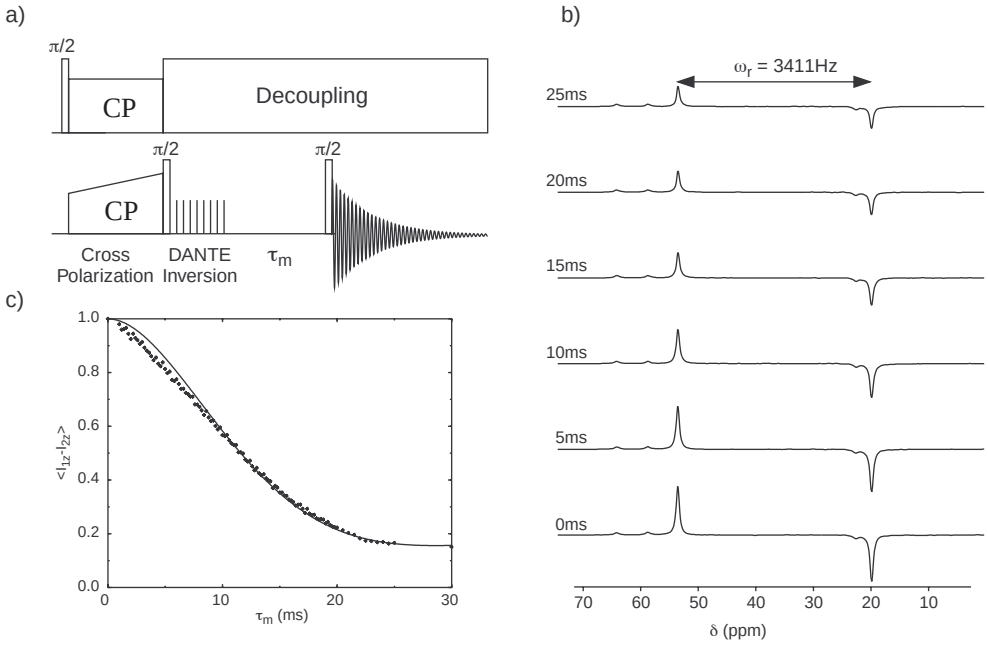

Fig.: a) Pulse sequence for a rotational resonance experiment. b) 1D spectra taken at various setting of the mixing time τ_m. Note the change in signal amplitude of the signal at 53 ppm after the resonance at 20 ppm has been selectively inverted. c) Change in intensity *vs.* mixing time.

The condition for rotational resonance is fulfilled only for one (or at least a very few) spin pairs.

Other techniques use double quantum transitions (HORROR, DREAM, DRAMA etc.), and largely utilize rotor-synchronized RF pulses.

J-couplings are much smaller and transfer times are much longer. In addition, all other interactions need to be sufficiently eliminated. Therefore, methods relying on scalar couplings are rather new and their use has been motivated by the fact that they allow to trace along covalent networks (spin systems) leaving less ambiguity in the assignment process.

1.6 SS-NMR of oriented samples:

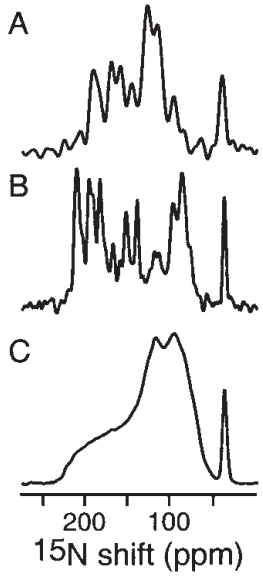

SS-NMR spectra are complicated by the fact that all kind of orientations with respect to the external field are possible. Some classes of molecules, e.g. crystalline materials or peptides/proteins embedded in phospholipid membranes, however, can be oriented either by deposition on glass plates or by magnetic alignment. Assuming a unique association with the membrane the nuclei therefore do not adopt all possible orientations with respect to the external field. This effect is demonstrated in the figure displayed on the left: The spectra were recorded on ^{15}N fd coat protein on unoriented lipid bilayers (C), magnetically-oriented lipid bicelles (A), and lipid bilayers oriented on glass plates (B) (taken from ref. Opella *et al.*).

It has recently become clear that the orientation of helices with respect to the membrane normal may be probed from a combination of chemical shift and the one-bond dipolar $^{15}N,^{1}H$ couplings in the so-called PISEMA spectra:

.

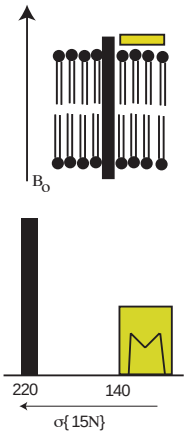

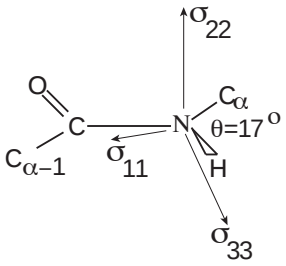

The figure above displays the chemical shift of a ^{15}N amide resonance in dependence of the orientation of the helix. In addition, the orientation of axes in the PAS are depicted. Peaks belonging to amide moieties from a single helix in PISEMA spectra occur at characteristic places, and the exact position and pattern can be rather easily related to the angle the helix makes with the membrane surface (and hence with the field):

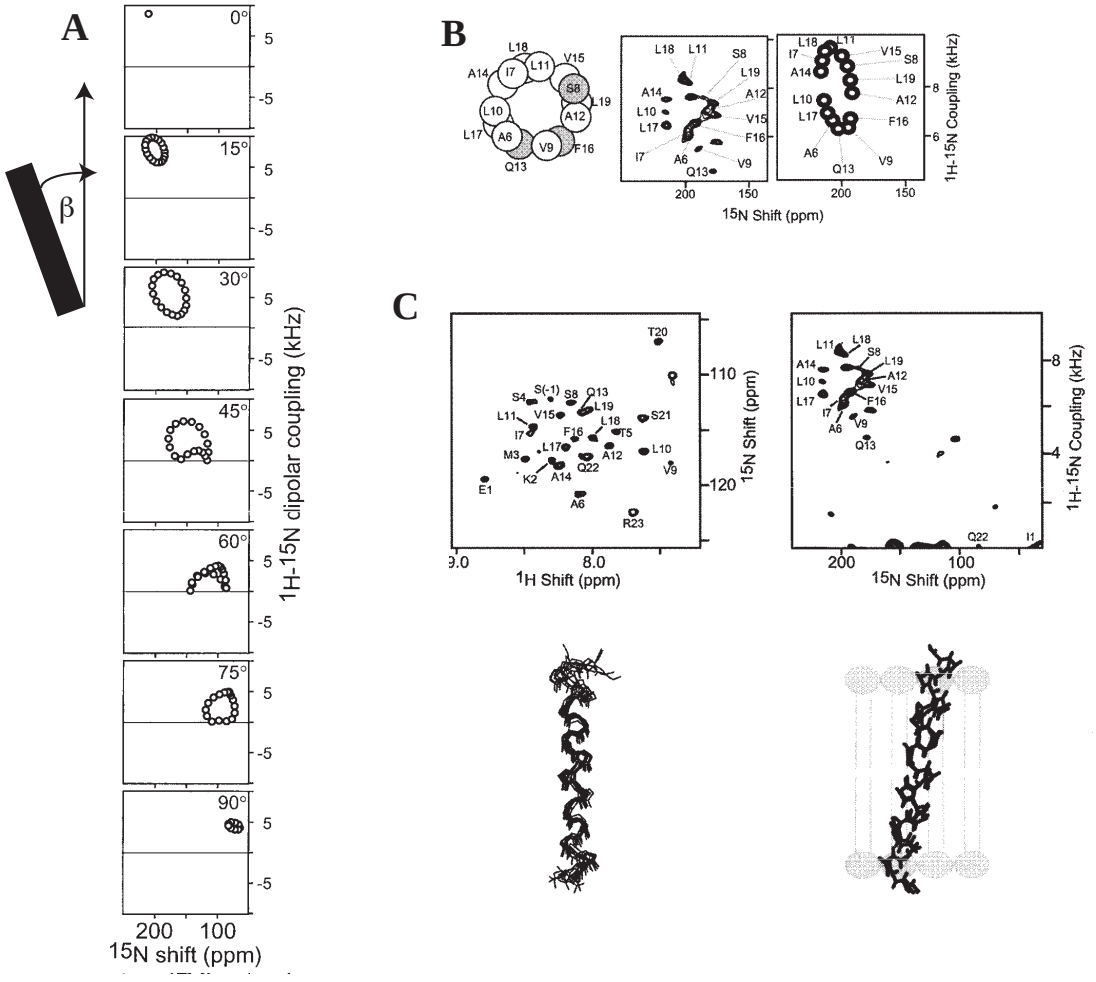

In the figure above, A) displays peak position for various angles the helix makes with

the membrane-normal. In B) experimental peak positions are assigned to the helical wheel positions for ^{15}N labeled AchR M2 peptide (a channel-forming peptide) in oriented bilayers and compared to a simulated PISEMA spectrum calculated for a tilt angle of 12°. In C) typical PISEMA spectra are displayed for the AchR M2 peptide (right) together with the HSQC spectrum recorded in solution on the DPC-micelle-bound form.

1.7 Labeling strategies for solid-state NMR applications:

The easiest (and most often used) remedy to reduce the vast number of interactions in the solid state is the use of selectively labeled material, in which NMR active isotopes (^{13}C,^{15}N) are only introduced at specific sites.

Whereas selectively labeled small molecules usually need to be synthesized from suitable precursors, peptides can be subsequently labeled at cysteine sites with methyliodide. Alternatively, biosynthetic routes to prepare alternatingly labeled peptides (only every second position is labeled) or selectively at methyl position have been developed.

Assigning polypeptides from uniformly labeled material still presents a major challenge. For that purpose a series of triple-resonance experiments relying on transfer pathways similar to those used for solution studies have been suggested.

Another common problem is that signals are inherently broadened due to the structural disordered in non-crystalline solids. Hence, microcystalline solids are usually required and much attention needs to be paid to sample preparation.

References:

- P.T.F. Williamson, M. Ernst, B.H. Meier: MAS Solid-State NMR of Isotropically Enriched Biological Samples in BioNMR in Drug Research, Ed. O. Zerbe, Wiley 2003.
- R. Tycko, Biomolecular Solid State NMR: Advances in Structural Methodology and Applications to Peptide and Protein Fibrils, *Annu. Rev. Phys. Chem.* (2001), **52**, 575-606.
- D.D. Laws, H.-M. Bitter, A. Jerschow, Solid-State Spectroscopic Methods in Chemistry, *Angew. Chem.* (2002), **41**, 3096-3129.
- S.J. Opella, C. Ma, F.M. Marassi, Nuclear Magnetic Resonance of Membrane-Associated Peptides and Proteins, *Meth. Enzymol.* (2001), **339**, 285-313.